LIBRARY
TECHNICAL REPORT SECTION
NAVAL POSTGRADUATE SCHOOL
MONTEREY, CALIFORNIA 93940

NPS-59SL76021

NAVAL POSTGRADUATE SCHOOL

Monterey, California

VORTEX SHEDDING AND RESISTANCE IN HARMONIC FLOW ABOUT SMOOTH AND ROUGH CIRCULAR CYLINDERS AT HIGH REYNOLDS NUMBERS

BY

TURGUT SARPKAYA

2 FEBRUARY 1976

Approved for public release; distribution unlimited.

PREPARED FOR:

NATIONAL SCIENCE FOUNDATION, WASHINGTON, D. C. 20550.

FEDDOCS
D 208.14/2:NPS-59SL76021

NAVAL POSTGRADUATE SCHOOL
Monterey, California

Rear Admiral Isham Linder
Superintendent

J. R. Borsting
Provost

VORTEX SHEDDING AND RESISTANCE IN HARMONIC FLOW ABOUT SMOOTH AND ROUGH CIRCULAR CYLINDERS AT HIGH REYNOLDS NUMBERS

This report presents the results of an extensive experimental investigation of the in-line and transverse forces acting on smooth and rough circular cylinders placed in oscillatory flow at Reynolds numbers up to 700,000, Keulegan-Carpenter numbers up to 150, and relative roughnesses from 0.002 to 0.02. The drag and inertia coefficients have been determined through the use of the Fourier analysis and the least squares method. The transverse force has been analysed in terms of its maximum, semi-peak-to-peak, and root-mean-square values. In addition, the frequency of vortex shedding and the Strouhal number have been determined. The results have shown that (a) for smooth cylinders, all of the coefficients cited above are functions of the Reynolds and Keulegan-Carpenter numbers, particularly for Reynolds numbers larger than about 20,000; (b) for rough cylinders, the force coefficients also depend on the relative roughness k/D and differ significantly from those corresponding to the smooth cylinder; and that (c) the use of the 'frequency parameter' $D^2/\nu T$ and the roughness Reynolds number $U_m k/\nu$ allow a new interpretation of the present as well as the previously obtained data and the establishment of model laws for oscillatory flow about cylinders at supercritical Reynolds numbers.

The work reported herein has been supported by the National Science Foundation through Grant No. AG-477.

SECURITY CLASSIFICATION OF THIS PAGE *(When Data Entered)*

REPORT DOCUMENTATION PAGE

READ INSTRUCTIONS BEFORE COMPLETING FORM

1. REPORT NUMBER: NPS-59SL76021	2. GOVT ACCESSION NO.
3. RECIPIENT'S CATALOG NUMBER	
4. TITLE *(and Subtitle)*: VORTEX SHEDDING AND RESISTANCE IN HARMONIC FLOW ABOUT SMOOTH AND ROUGH CIRCULAR CYLINDERS AT HIGH REYNOLDS NUMBERS.	5. TYPE OF REPORT & PERIOD COVERED: Interim Report Sept. 74 - February 1976
	6. PERFORMING ORG. REPORT NUMBER
7. AUTHOR(s): TURGUT SARPKAYA Distinguished Professor of Mechanical Engineering	8. CONTRACT OR GRANT NUMBER(s): National Science Foundation Grant No: AG-477.
9. PERFORMING ORGANIZATION NAME AND ADDRESS: Naval Postgraduate School Monterey, California 93940	10. PROGRAM ELEMENT, PROJECT, TASK AREA & WORK UNIT NUMBERS
11. CONTROLLING OFFICE NAME AND ADDRESS: National Science Foundation Washington, D. C. 20550	12. REPORT DATE: 2 February 1976 13. NUMBER OF PAGES: 189
14. MONITORING AGENCY NAME & ADDRESS *(if different from Controlling Office)*	15. SECURITY CLASS. *(of this report)*: Unclassified 15a. DECLASSIFICATION/DOWNGRADING SCHEDULE

16. DISTRIBUTION STATEMENT *(of this Report)*

Approved for public release; distribution unlimited.

17. DISTRIBUTION STATEMENT *(of the abstract entered in Block 20, if different from Report)*

18. SUPPLEMENTARY NOTES

19. KEY WORDS *(Continue on reverse side if necessary and identify by block number)*

Oscillating flow, Wave forces, Drag and inertia coefficients, Smooth and rough cylinders in harmonic flow.

20. ABSTRACT *(Continue on reverse side if necessary and identify by block number)*

This report presents the results of an extensive experimental investigation of the in-line and transverse forces acting on smooth and rough circular cylinders placed in oscillatory flow at Reynolds numbers up to 700,000, Keulegan-Carpenter numbers up to 150, and relative roughnesses from 0.002 to 0.02. The drag and inertia coefficients have been determined through the use of the Fourier analysis and the least-squares method. The transverse force (lift) has been analysed in terms of its maximum, semi-peak-to-peak, and

DD FORM 1 JAN 73 1473 EDITION OF 1 NOV 65 IS OBSOLETE
S/N 0102-014-6601

SECURITY CLASSIFICATION OF THIS PAGE *(When Data Entered)*

root-mean-square values. In addition, the frequency of vortex shedding and the Strouhal number have been determined.

The results have shown that: (a) for smooth cylinders, all of the coefficients cited above are functions of the Reynolds and Keulegan-Carpenter numbers, particularly for Reynolds numbers larger than about 20,000; (b) for rough cylinders, the force coefficients also depend on the relative roughness k/D and differ significantly from those corresponding to the smooth cylinder; (c) the use of the 'frequency parameter' $D^2/\nu T$ and the roughness Reynolds number $U_m k/\nu$ allow a new interpretation of the present as well as the previously obtained data and the establishment of model laws for oscillatory flow about cylinders at supercritical Reynolds numbers.

TABLE OF CONTENTS

I. INTRODUCTION - 11

II. FORCE COEFFICIENTS AND GOVERNING PARAMETERS - - - - - - 13

A. CONCEPT - 13

B. IN-LINE FORCE - - - - - - - - - - - - - - - - - - - 13

C. TRANSVERSE FORCE (LIFT) COEFFICIENTS - - - - - - - 19

D. GOVERNING PARAMETERS - - - - - - - - - - - - - - - 21

III. EXPERIMENTAL EQUIPMENT AND PROCEDURES - - - - - - - - - 30

A. OSCILLATING FLOW ABOUT A BODY AT REST VERSUS OSCILLATING BODY IN A FLUID OTHERWISE AT REST - - 30

B. THE U-SHAPED OSCILLATING FLOW TUNNEL - - - - - - - 34

C. CIRCULAR CYLINDERS - - - - - - - - - - - - - - - - 38

D. FORCE MEASUREMENTS - - - - - - - - - - - - - - - - 40

E. DATA ACQUISITION SYSTEM - - - - - - - - - - - - - 42

F. ACCELERATION, ELEVATION, OR VELOCITY MEASUREMENT - 43

G. DATA REDUCTION - - - - - - - - - - - - - - - - - - 45

H. BLOCKAGE AND LENGTH-TO-DIAMETER RATIO EFFECTS - - 46

IV. RESULTS AND DISCUSSIONS - - - - - - - - - - - - - - - - 49

A. IN-LINE FORCE COEFFICIENTS FOR SMOOTH CYLINDERS - 49

B. TRANSVERSE FORCE COEFFICIENTS FOR SMOOTH CYLINDERS 56

C. COMMENTS ON MORISON'S EQUATION - - - - - - - - - 63

D. IN-LINE FORCE COEFFICIENTS FOR ROUGH CYLINDERS - - 67

E. TRANSVERSE FORCE COEFFICIENTS FOR ROUGH CYLINDERS 72

V. CONCLUSIONS - 75

FIGURES - 77-148

APPENDIX A - IN-LINE FORCE DATA FOR SMOOTH CYLINDERS - - - - - 149-164

APPENDIX B - TRANSVERSE FORCE DATA FOR SMOOTH CYLINDERS - - - - 165-175

APPENDIX C - DISCRETE VORTEX REPRESENTATION OF VORTEX SHEDDING 176-180

LIST OF REFERENCES - 181-183

INITIAL DISTRIBUTION LIST - 184-189

LIST OF FIGURES

Figure

1. C_d versus K for various values of β, (Keulegan-Carpenter data [6]) - - - - - - - - - - - - - - 77

2. C_m versus K for various values of β, (Keulegan-Carpenter data [6]) - - - - - - - - - - - - - - 78

3. C_d versus K for various values of Re, (Keulegan-Carpenter data [6]) - - - - - - - - - - - - - - 79

4. C_m versus K for various values of Re, (Keulegan-Carpenter data [6]) - - - - - - - - - - - - - - 80

5. Schematic drawing of the U-shaped vertical water tunnel - 81

6. A general view of the U-shaped vertical water tunnel - - - 82

7. Butterfly valve assembly - - - - - - - - - - - - - - - - - - 83

8. Rack and pinion drive system - - - - - - - - - - - - - - - - 84

9. Force transducer - 85

10. Assembled force transducer - - - - - - - - - - - - - - - - 86

11. In-line force and acceleration traces - - - - - - - - - - - 87

12. Transverse force and acceleration traces - - - - - - - - - - 87

13. C_d versus K for β = 497 - - - - - - - - - - - - - - - - - 88

14. C_d versus K for β = 784 - - - - - - - - - - - - - - - - - 89

15. C_d versus K for β = 1107 - - - - - - - - - - - - - - - - - 90

16. C_d versus K for β = 1985 - - - - - - - - - - - - - - - - - 91

17. C_d versus K for β = 3123 - - - - - - - - - - - - - - - - - 92

18. C_d versus K for β = 4480 - - - - - - - - - - - - - - - - - 93

19. C_d versus K for β = 5260 - - - - - - - - - - - - - - - - - 94

20. C_d versus K for β = 8370 - - - - - - - - - - - - - - - - - 95

21. C_m versus K for β = 497 - - - - - - - - - - - - - - - - - 96

22. C_m versus K for β = 784 - - - - - - - - - - - - - - - - - 97

23. C_m versus K for β = 1107 - - - - - - - - - - - - - - - - - 98

24. C_m versus K for β = 1985 - - - - - - - - - - - - - - - - - - 99
25. C_m versus K for β = 3123 - - - - - - - - - - - - - - - - - - 100
26. C_m versus K for β = 4480 - - - - - - - - - - - - - - - - - - 101
27. C_m versus K for β = 5260 - - - - - - - - - - - - - - - - - - 102
28. C_m versus K for β = 8370 - - - - - - - - - - - - - - - - - - 103
29. C_f(mes) versus K for β = 497 - - - - - - - - - - - - - - - - 104
30. C_f(mes) versus K for β = 784 - - - - - - - - - - - - - - - - 105
31. C_f(mes) versus K for β = 1107 - - - - - - - - - - - - - - - - 106
32. C_f(mes) versus K for β = 1985 - - - - - - - - - - - - - - - - 107
33. C_f(mes) versus K for β = 3123 - - - - - - - - - - - - - - - - 108
34. C_f(mes) versus K for β = 4480 - - - - - - - - - - - - - - - - 109
35. C_f(mes) versus K for β = 5260 - - - - - - - - - - - - - - - - 110
36. C_f(mes) versus K for β = 8370 - - - - - - - - - - - - - - - - 111
37. C_d versus K for particular values of Re and β - - - - - - - 112
38. C_m versus K for particular values of Re and β - - - - - - - 113
39. C_f(mes) versus K for particular values of β - - - - - - - - 114
40. C_d versus Re for constant values of K - - - - - - - - - - - 115
41. C_m versus Re for constant values of K - - - - - - - - - - - 116
42. C_m versus C_d for various values of K - - - - - - - - - - - 117
43. C_L(max) versus K for β = 497 - - - - - - - - - - - - - - - 118
44. C_L(max) versus K for β = 784 - - - - - - - - - - - - - - - 119
45. C_L(max) versus K for β = 1107 - - - - - - - - - - - - - - - 120
46. C_L(max) versus K for β = 1985 - - - - - - - - - - - - - - - 121
47. C_L(max) versus K for β = 3123 - - - - - - - - - - - - - - - 122
48. C_L(max) versus K for β = 4480 - - - - - - - - - - - - - - - 123
49. C_L(max) versus K for β = 5260 - - - - - - - - - - - - - - - 124

50. C_L(max) versus K for various values of K and β - - - - - - 125

51. C_L(max) versus Re for various values of K - - - - - - - - - 126

52. Relative frequency of vortex shedding as a function of the Reynolds number and Keulegan-Carpenter number - - - - - 127

53. Transverse force and acceleration traces showing the irregularity of the transverse force at relatively high Keulegan-Carpenter numbers - - - - - - - - - - - - 128

54. Transverse force and acceleration traces and fractional shedding of vortices at K = 13 - - - - - - - - - - - - - - 129

55. Asymmetry in the in-line force and the comparison of measured and calculated forces - - - - - - - - - - - - - - 130

Special comments about Fig. 55 and computer output - - - - 131-133

56. (a) Strouhal number versus K for β = 497 - - - - - - - - - 134

(b) Strouhal number versus K for β = 1985 - - - - - - - - - 134

57. C_d versus K for β = 4072 and k/D = 1/360 - - - - - - - - - 135

58. C_m versus K for β = 4072 and k/D = 1/360 - - - - - - - - - 136

59. C_d versus Re for various relative roughnesses, (K = 50) - - 137

60. C_m versus Re for various relative roughnesses, (K = 50) - - 138

61. In-line force and acceleration traces for harmonic flow over a rough cylinder - - - - - - - - - - - - - - - - - - 139

62. C_d versus $U_m k/\nu$ for various relative roughnesses - - - - - 140

63. C_L(max) versus K, (rough cylinder) - - - - - - - - - - - - 141

64. C_L(max) versus K, (rough cylinder) - - - - - - - - - - - - 142

65. C_L(max) versus K, (rough cylinder) - - - - - - - - - - - - 143

66. C_L(max) versus K, (rough cylinder) - - - - - - - - - - - - 144

67. C_L(max) versus K, (rough cylinder) - - - - - - - - - - - - 145

68. C_L(max) versus K, (rough Cylinder) - - - - - - - - - - - - 146

69. C_L(max) versus K for various values of k/D and β - - - - - 147

70. Strouhal number versus K for a particular rough cylinder- - 148

NOMENCLATURE

A	amplitude at the test section
A_1	amplitude at the free surface
C_a	added-mass coefficient, C_m-1
C_d	drag coefficient through Fourier analysis
C_{dls}	drag coefficient through least squares method
$C_f(spp)$	semi-peak-to-peak force coefficient
$C_f(mes)$	measured maximum force coefficient
$C_L(max)$	maximum transverse force coefficient
$C_L(rms)$	root-mean-square of the normalized transverse force
C_m	inertia coefficient, $C_m = C_a + 1$, through Fourier analysis
C_{mls}	inertia coefficient through least squares method
D	effective diameter
E	$F_m - F_c$
F	force
F_c	calculated force
F_d	drag component of the force
F_i	inertial component of the in-line force
F_m	measured in-line force
f_r	relative frequency, $f_v T$
f_v	frequency of the transverse force
g	gravitational acceleration
H	see Fig. 5
K	Keulegan-Carpenter number, $U_m T/D = 2\pi A/D$
k	roughness height, k/D = relative roughness
L	length of cylinder

Re	Reynolds number, $U_m D/\nu$ (also referred to as the diametral Reynolds number)
Re_k	roughness Reynolds number, $U_m k/\nu$
St	Strouhal number, $f_v D/U_m = f_r/K$
T	period of oscillation
t	time
U	instantaneous velocity
U_m	maximum velocity
V	velocity in steady flow
w	width of the test section
β	frequency parameter, $D^2/\nu T$
η	a coefficient, see Eq. (31)
θ	$2\pi t/T$
λ	error parameter, see Eq. (15)
λ^*	error coefficient, see Eq. (16)
ν	kinematic viscosity
ρ	density of water
σ	goodness-of-fit parameter, see Eq. (17)
ϕ	phase angle

ACKNOWLEDGMENTS

The work described in this report represents part of a research program supported by the Engineering Division of the National Science Foundation through Grant No. AG-477. This support is gratefully acknowledged.

The writer is indebted to the many people whose co-operation made this investigation possible. The tunnel was constructed by the Gabilan Iron and Machine Co. of Salinas, California. Messrs. J. McKay, K. Mothersell, and T. F. Christian built the instrumentation. Messrs. N. J. Collins, S. Onur, and S. Evans, all graduate students at the Naval Postgraduate School, assisted with the experiments and data evaluation. The computer time was donated by the Naval Postgraduate School.

This report is dedicated to Garbis H. Keulegan and John S. McNown as a token of friendship.

I. INTRODUCTION

The work reported here is part of a wider research program undertaken at the Naval Postgraduate School to study the characteristics of periodic flow past bluff bodies. It was prompted in part by the current practical interest in ocean and wind engineering and in part by the need for more basic hydrodynamic data on flow-induced forces on structures.

Much of the present knowledge on time-dependent forces acting on bluff bodies in general and on circular cylinders in particular has been obtained by means of model tests in wave channels or in wind- or water tunnels at Reynolds numbers generally two to three orders of magnitude smaller than prototype Reynolds numbers. These model tests have relied heavily on the so-called Morison formula expressing the force as the sum of a velocity dependent term known as the drag and an acceleration dependent term known as the inertia force. This formula became a focus for research devoted primarily to the determination of the appropriate drag and inertia coefficients and gave rise to large quantities of data. There has been a growing awareness that the coefficients obtained at relatively low Reynolds numbers may not be applicable at higher Reynolds numbers, that the transverse forces acting on the elements of offshore structures may be as much or more important than the in-line forces given by the Morison formula, and that the initial or growing roughness may significantly alter the forces acting on the structure. This awareness is more of practical than academic interest for the margins of error previously tolerated are no longer acceptable.

In view of the foregoing considerations, the present research program was undertaken with two main objectives: (a) to identify the physical mechanisms and parameters responsible for the correlation or scatter of the force-transfer coefficients; and (b) to furnish data, obtained under

carefully controlled laboratory conditions, about the in-line and transverse forces acting on smooth and rough circular cylinders in a sinusoidally oscillating fluid at relatively large amplitudes and Reynolds numbers.

This report does not deal with ocean waves, non-harmonic fluid oscillations, wave and current combination and its consequences, diffraction effects, free-surface and/or wall-proximity effects, fluid elasticity or hydroelasticity of flexible or flexibly supported cylinders in harmonic fluid motion and with the interference effects between neighboring structural elements.

Furthermore, no attempt is made to offer a chronological and/or critical survey or a 'state of the art' appraisal of the fluid loading on cylinders or offshore structures. Fairly complete accounts in the context of wave forces are given by Wiegel [1], Hogben [2], and Grace [3], where an extensive list of references can be found. Only those works which have a direct bearing on the evaluation and/or discussion of the present data will be reviewed in some detail wherever appropriate.

II. FORCE COEFFICIENTS AND GOVERNING PARAMETERS

A. CONCEPT

A completely satisfactory analysis of the resistance in unsteady separated flow has escaped the concentrated efforts of many researchers. No theoretical model can, at the moment, predict the complete force and flow characteristics of a periodic flow about a circular cylinder. In the absence of such an analysis, the most serious difficulty lies in the description of the time-dependent force itself. Other difficulties arise in the description and interpretation of the history of the motion and of the effect of vortices. One approximate and physically meaningful way around these difficulties is to assume, following Stokes' classic analysis of the oscillating pendulum, that the total time-dependent in-line force may be expressed as a sum of a velocity-square dependent drag and an acceleration-dependent inertial force, each with a suitably-averaged force coefficient. This then is the basis of the so-called Morison's equation [4].

B. IN-LINE FORCE

Data reduction for the forces in-line with the direction of oscillation is based on Morison's equation and three different analysis of the force records, namely, Fourier analysis, least squares, and a modified least-squares method.

The in-line force which consists of the drag force F_d and the inertia force F_i is assumed to be given by [4]

$$F = F_d + F_i = 0.5C_d LD\rho |U|U + 0.25\pi\rho LD^2 C_m dU/dt \qquad (1)$$

in which C_d and C_m represent respectively the drag and inertia coefficients and U the instantaneous velocity of the ambient flow. The fact that C_d and C_m are history dependent may be demonstrated with a rather instructive example. Consider an impulsive change superposed on an already established viscous flow pattern. Just prior to the impulsive change, the drag coefficient is given by its steady state value at the corresponding Reynolds number. Sears, as reported by Rott [5], has shown that "the initial motion following the impulsive change of the boundary conditions consists of the superposition of the velocity pattern existing just before the change and the inviscid flow velocity pattern due to the impulsive boundary values (together with the corresponding infinitely thin wall vortex sheets)". In other words, at the initial instants of the impulsive change C_d is equal to its steady state value and $C_m = 2$. As time progresses neither C_d nor C_m remains the same and changes with the changes in the flow, ever dominated by the past history and ever affected by the gross features of the current state.

For an oscillating flow represented by $U = -U_m \cos\theta$, with $\theta = 2\pi t/T$, the Fourier averages of C_d and C_m are given by Keulegan and Carpenter [6] as

$$C_d = -\frac{3}{4}\int_0^{2\pi} \frac{F_m \cos\theta}{\rho U_m^2 LD} d\theta \tag{2}$$

and

$$C_m = \frac{2U_m T}{\pi^3 D}\int_0^{2\pi} \frac{F_m \sin\theta}{\rho U_m^2 LD} d\theta \tag{3}$$

in which F_m represents the measured force. Evidently, C_d and C_m are the first two terms in a complete series expansion of the normalized force in terms of the odd integers in sines and cosines. Additional coefficients

in the series may be calculated in a manner similar to that done by Keulegan and Carpenter [6]. An equally satisfactory and somewhat simpler procedure is to use these two coefficients to evaluate the difference between the measured and calculated forces as a function of the appropriate parameters. The use of such a procedure is preferred herein for two reasons. Firstly, previous studies by Keulegan and Carpenter [6] and Sarpkaya [7] have shown that C_d and C_m as given by equations (2) and (3) are the most significant ones and sufficient to represent the measured force adequately. Secondly, the Fourier analysis, as cited above, assumes the symmetry of both the measured force and the imposed fluid motion, i.e. $F(\theta) = -F(\theta+\pi)$. As will be discussed later, this is not always true and that a perfectly uniform harmonic motion about a symmetrically situated cylinder can give rise to an asymmetric flow and unexpected single vortex formation in certain ranges of the governing parameters. This in turn results in an asymmetry in the measured force. Obvious consequences of this asymmetry are that the maximum force in a cycle is not equal to the mean of the maximum forces (semi-peak-to-peak value) and that the mean value of the transverse force is not necessarily zero.

The method of least-squares consists of the minimization of the error between the measured and calculated forces. Letting F_m represent the instantaneous measured force and F_c the force calculated through the use of equation (1), and writing

$$E^2 = (F_m - F_c)^2 \tag{4}$$

and $dE^2/dC_m = 0$ and $dE^2/dC_d = 0$, one has

$$C_{dls} = -\frac{8}{3\pi}\int_0^{2\pi} \frac{F_m \left|\cos\theta\right| \cos\theta}{\rho D L U_m^2} d\theta \tag{5}$$

and

$$C_{mls} = C_m \tag{6}$$

Evidently, the Fourier analysis and the method of least-squares yield identical C_m values and that the C_d values differ only slightly.

The error between the measured and calculated forces, particularly in the neighborhood of the maximum forces, may be further minimized by choosing the square of the measured force as the weighting factor in the least-square analysis. Thus writing,

$$E^2 = F_m^2(F_m - F_c)^2 \tag{7}$$

and $dE^2/dC_d = 0$ and $dE^2/dC_m = 0$, one has

$$C_{dff} = \frac{2}{\rho DLU_m^2} \frac{f_5 f_3 - f_4 f_2}{f_4 f_1 - f_3 f_3} \tag{8}$$

and

$$C_{mff} = \frac{T^2}{\pi^3 \rho LAD^2} \frac{f_5 f_1 - f_3 f_2}{f_4 f_1 - f_3 f_3} \tag{9}$$

in which A and T represent respectively the amplitude and period of the oscillation and L the length of the cylinder. The functions f_i are given by

$$f_1 = \int_0^{2\pi} F_m^2 \cos^4\theta d\theta \quad , \quad f_2 = \int_0^{2\pi} F_m^3 \cos\theta \left|\cos\theta\right| d\theta$$

$$f_3 = \int_0^{2\pi} F_m^2 \sin\theta \left|\cos\theta\right| \cos\theta \, d\theta \, , \quad f_4 = \int_0^{2\pi} F_m^2 \sin^2\theta \, d\theta \, , \quad f_5 = \int_0^{2\pi} F_m^3 \sin\theta \, d\theta \tag{10}$$

Equations (8) and (9) may be shown to reduce to equations (5) and (6) by replacing F_m^n in equations (10) by F_m^{n-2} and carrying out the necessary integrations in which F_m does not appear.

It is recognized that C_m and C_d are only time-invariant averages and

are not constant throughout the cycle. This report will not deal with the instantaneous values of these coefficients.

In addition to those cited above, the following coefficients are of special interest.

The semi-peak-to-peak value of the calculated maximum force in a cycle, denoted by $C_f(spp)$, in terms of the drag and inertia coefficients C_d and C_m is given by

$$C_f(spp) = C_d + \frac{\pi^4 C_m^2}{4 C_d K^2} \qquad K \geq 10 \qquad (11)$$

in which $K = U_m T/D = 2\pi A/D$ and U_m, T, and D represent respectively the maximum velocity in a cycle, the period of the sinusoidal oscillation, and the diameter of the cylinder. Thus, $C_f(spp)$ is a measure of the calculated maximum force.

Measured maximum force coefficient, denoted by $C_f(mes)$, is defined by

$$C_f(mes) = \frac{\text{maximum of the measured force in a cycle}}{0.5\rho DLU_m^2} \qquad (12)$$

As will be noted later, $C_f(mes)$ is not necessarily equal to either $C_f(spp)$ or to a similar coefficient obtained through the use of the semi-peak-to-peak value of the measured force.

Another important characteristic of the calculated and measured forces is their root-mean-square (rms) values. The rms value of the calculated force, denoted by $C_f(rms)$, may be shown, through the use of equation (1), to reduce to

$$C_f(rms) = \sqrt{\frac{3}{8} C_d^2 + \frac{\pi^4 C_m^2}{2K^2}} \qquad (13)$$

The rms value of the measured force, denoted by $C_f(arms)$, is calculated in the usual manner by numerically evaluating the integral given by

$$C_f^2(arms) = \frac{1}{T}\int_0^T \frac{F_m^2}{(0.5\rho LDU_m^2)^2}\, dt \tag{14}$$

Evidently, $C_f(rms)$ and $C_f(arms)$ should have comparable magnitudes for identical values of the governing parameters.

It has been evident for quite sometime that equation (1) does not represent the measured force to the same degree of accuracy for all values of the governing parameters. It is, therefore, necessary to define and evaluate suitable coefficients expressing the difference between the measured and calculated forces. For this purpose three new coefficients have been defined. The first is the per cent error defined by

$$\lambda(\theta) = \frac{F_m - F_c}{F_m(max)} \tag{15}$$

in which F_m represents the measured force, F_c the force calculated through the use of equation (1), and $F_m(max)$ the maximum of the measured force in a cycle.

The second error coefficient is defined by

$$\lambda^* = \frac{F_m(max) - F_c(max)}{F_m(max)} \tag{16}$$

Evidently, the maximums of the measured and calculated forces do not occur at the same t/T because of the difference between the calculated and measured phase angles. Thus, it should be emphasized that $F_c(max)$ in equation (16) represents the maximum of the calculated force, as its definition clearly implies, and not the calculated force at t/T at which

the measured force reaches its maximum. Consequently, the maximum of $\lambda(\theta)$ (which may or may not result either from the difference between the maximum of the measured force and the force calculated at the same t/T or from the difference between the calculated maximum force and the measured force at the same t/T) is not equal to λ^*.

Even though $\lambda(\theta)$ is some measure of fitness, its perusal is practically impossible for it represents about 50 values per cycle and about 30,000 values for the set of data presented herein. Thus, a simpler measure of the goodness-of-fit is needed. For this purpose, the following definition is adopted

$$\sigma = 100 \sqrt{\frac{\frac{1}{T}\int_0^T (F_m - F_c)^2 \, dt}{\frac{1}{T}\int_0^T F_m^2 \, dt}} \qquad (17)$$

and evaluated for each run.

C. TRANSVERSE FORCE (LIFT) COEFFICIENTS

This particular component of the total force has been continuously recorded and analyzed in as much detail as possible for several reasons. Firstly, its amplitude could, under certain circumstances, be as large as that of the in-line force. Secondly, the transverse force could give rise to fluid-elastic oscillations in wavy flows and to fatigue failure. Thirdly, even the small transverse oscillations of the body distinctly regularizes the wake motion, alter the spanwise correlation, and change drastically the magnitude of both the in-line and transverse forces.

In the present study no attention is given to structural movement and/or response and the test cylinders are held in position with imperceptibly small motions as will be described later. Thus, in the

following we will be concerned only with the transverse force coefficients for rigid cylinders in uniform harmonic motion.

The transverse force may be analyzed in various ways. Some of these are listed below:

a. the ratio of transverse forces to in-line forces. The reference forces may be taken as their maximums (maximum peak values, irrespective of the phase angle between them), as their average maximums (mean peak values, particularly for wave basin studies), or as their rms values. Such a ratio may be useful in providing gross design information;

b. in terms of a Fourier series in which the coefficients for all the harmonics of the transverse force will have to be evaluated through the use of the experimental data;

c. in terms of the transverse force coefficients for each harmonic through the use of the definition

$$C_{Ln} = \frac{F(\text{maximum of the n-th harmonic of the transverse force})}{0.5\rho DLU_m^2} \tag{18}$$

d. in terms of a maximum lift coefficient defined by

$$C_L(\max) = \frac{\text{maximum peak of the transverse force}}{0.5\rho DLU_m^2} \tag{19}$$

e. in terms of the mean or semi-peak-to-peak value of the transverse force as

$$C_L(\text{spp}) = \frac{\text{semi peak-to-peak value of the transverse force}}{0.5\rho DLU_m^2} \tag{20}$$

f. in terms of the rms value of the transverse force as

$$C_L(\text{rms}) = \frac{\text{rms value of the transverse force}}{0.5\rho DLU_m^2} \tag{21}$$

Finally, the frequency of the transverse force may be analyzed in terms of frequencies of each harmonic and/or in terms of a spectrum analysis.

Other force coefficients based on velocities such as those corresponding to maximum in-line force rather than to maximum velocities will not be cited here in order not to confuse an already sufficiently complex subject.

In the present study, the transverse force is evaluated in terms of $C_L(\max)$ and $C_L(\text{rms})$. In addition, the frequency of the force oscillations are determined in terms of the governing parameters. No attempt was made to separately analyze the amplitudes of the harmonics of the transverse force.

D. GOVERNING PARAMETERS

A simple dimensional analysis of the flow under consideration (uniform harmonic motion about a circular cylinder placed with its axis normal to the flow) shows that the time-dependent force coefficients and error functions may be written as

$$\frac{F(\text{in-line or transverse force})}{0.5\rho DLU_m^2} = f(U_mT/D\ ,\ U_mD/\nu\ ,\ t/T) \qquad (22)$$

$$= f(K\ ,\ Re\ ,\ t/T)$$

and

$$\lambda(\theta) = g(K\ ,\ Re\ ,\ t/T) \qquad (23)$$

Evidently, U_mT/D may be replaced by $2\pi A/D$ or simply by A/D.

Equation (22), combined with equation (1), assuming for now that the latter is indeed valid, yields

$$C_d = f_1(K\ ,\ Re\ ,\ t/T) \qquad (24)$$

$$C_m = f_2(K , Re , t/T) \tag{25}$$

There is no simple way to deal with equations (24) and (25) even for the most manageable time-dependent flows. The evaluation of the instantaneous values of C_d and C_m in a manner similar to that done by Keulegan and Carpenter [6] is not always valid for the assumption of the coefficients C_d and C_m each having equal values at $\theta_1 = \pi/2 + \alpha$ and $\theta_2 = \pi/2 - \alpha$, where α is an angle less than $\pi/2$, or at $\theta_1 = 3\pi/2 + \alpha$ and $\theta_2 = 3\pi/2 - \alpha$ or at $\theta_1 = \pi + \beta$ and $\theta_2 = \pi - \beta$, where β is an angle less than π, does not always hold true. This is because of the single-vortex shedding phenomenon noted earlier and the resulting asymmetry in the in-line force. This aspect of the problem requires a stability analysis of the vortex motion in harmonic flow about cylinders.

Another and perhaps the only other alternative is to eliminate time as an independent variable in equations (22) through (25) and consider suitable time-invariant averages of the force coefficients. Thus, one has

$$\left\{ \begin{array}{l} C_d \\ C_m \\ C_d(\text{rms}) \\ . \\ . \\ \lambda^* \end{array} \right\} = f_i(K , Re) \tag{26}$$

Even the equation (26), as simple and idealized as it is, gives rise to many questions: Do the averaged coefficients really depend on both K and Re?; are K and Re the most suitable governing parameters?; can one obtain meaningful conclusions by plotting the data for a given coefficient

with respect to, say, K and connecting points having equal Re or vice-versa?; how should the experiments be conducted so that equation (26) yields manageable plots?; which of the two parameters, if any, has a more pronounced effect on the force coefficient under consideration?; why has there been considerable scatter [1] in the field data when plotted with respect to either K or Re?; are there ranges of K and Re in which the effect of one is obscured by a reasonable correlation of the force coefficients with the other? These and similar questions have been raised by many investigators and attempts were made to establish suitable correlations. The state of the art is such that the past conclusions and conjectures can be critically scrutinized only through the acquisition of reliable data obtained under controlled laboratory conditions with relatively simple and hopefully two dimensional harmonic flow situations. The purpose of such an effort is by no means to remove the need for actual full scale experience. In fact, it is to encourage full scale experiments and to enable those concerned to interpret and better understand the factors effecting the force-transfer functions.

Let us now return to equation (26) and to the discussion of the selection of the most suitable parameters. Past experience [6, 7] has shown that the force coefficients are primarily functions of K at relatively small Reynolds numbers and that the effect of viscosity is obscured by the excellent correlation between K and the force coefficients. Again previous efforts and the reasoning based on dimensional analysis have shown that there is an undeniable effect of the Reynolds number. Thus means have to be devised to delineate the effect of both K and Re or some other viscosity dependent parameter.

It appears, for the purposes of equation (26), that the Reynolds number is not the most suitable non-dimensional parameter involving viscosity even

though in most other flow situations "Reynolds number is the liveliest of all the non-dimensional parameters". The primary reasons for this are that the effect of viscosity is relatively small and that the maximum velocity U_m appears in both $K = U_m T/D$ and $Re = U_m D/\nu$.

Simple rules of dimensional analysis state that one obtains the maximum amount of experimental control over the dimensionless variables if the original variables that can be regulated each occur in only one dimensionless product. Thus, if U_m is easily varied experimentally, then U_m should occur in only one of the independent dimensionless parameters. With this hint in mind, let us reconsider equation (26) and replace Re by $Re/K = D^2/\nu T$. This parameter shall be called the 'frequency parameter' and denoted by β so that

$$\beta = D^2/\nu T \tag{27}$$

Evidently, for a series of experiments conducted with a cylinder of a given diameter D in water (of uniform and constant temperature) undergoing harmonic oscillations with a constant period of T, β is held constant. Then the variation of a force coefficient with K may be plotted for constant values of β. Subsequently, one can easily recover the Reynolds number from

$$Re = K\beta \tag{28}$$

and connect the points, on each β = constant curve, representing a given Reynolds number for suitably selected values of the Reynolds number. Such a procedure eliminates the difficulty of trying to draw contours of constant K, or constant Re, or constant C_d or C_m in plots of C_d or C_m versus K or Re, or K versus Re.

Suffice it to note that the smooth cylinder data reported herein shall be analyzed according to the relationship

$$C_i(\text{a coefficient}) = f_i(K\ ,\ \beta) \tag{29}$$

and the Reynolds number will be used in the manner described above. The power of this new plotting procedure (new as far as the wave force analysis is concerned) will become apparent later.

A few words about the frequency parameter β is necessary before proceeding further. It is often encountered in the analysis of periodic flows. For example, the exact solution of the flow in a pipe due to a periodic pressure gradient shows that [8] the velocity distribution is a function of β, among other parameters. The stability characteristics of such flows are also determined by β as shown by Sarpkaya [9]. Additional discussion of the role played by β will be presented in connection with the discussion of results.

Let us now re-examine a set of data previously obtained by others [6] partly to illustrate the use and significance of K and β as the governing parameters and partly to take up, as early as possible, the question of the effect of Reynolds number on the various force coefficients.

The data given by Keulegan and Carpenter [6] may be represented by 12 different values of β. The drag and inertia coefficients for each β are plotted in Figs. 1 and 2 and connected with straightline segments. The individual data points are not shown in order to keep the figures relatively clean. A careful examination of these figures reveals several important facts: (a) in Fig. 1, the data corresponding to $\beta = 2935$, which fall in the region where the drag forces are small relative to the inertial forces, show peaks and valleys which may or may not be due to the experimental errors; (b) the data corresponding to $\beta = 141$ appear to be out of place relative to those corresponding to $\beta = 97$ and $\beta = 217$; (c) in both figures the range of K for each β is relatively narrow; and that (d) the identification of the individual data points in terms of the cylinder diameter, as was done by Keulegan and Carpenter, irrespective of the β values gives

the impression of a scatter in the data and invites one to draw a mean drag curve through all data points. Such a temptation is further increased by the fact that the data for each β span over only a small range of K values. Evidently, the drawing of such a mean curve eliminates the dependence of C_d and/or C_m on β and hence on Re.

Also shown in Figs. 1 and 2 are points representing four selected Reynolds numbers. The K values for each Re and β were calculated from $K = Re/\beta$ and are shown in Table-I together with the run numbers (used by Keulegan and Carpenter) and cylinder diameters. Note that for runs 34 through 38, $\beta \simeq 217$ and D = 0.75 inches, and for runs 90 through 93, $\beta \simeq 141$ and D = 0.75 inches. The difference in β values for the same cylinder stems from the fact that the two sets of experiments were conducted at different water temperatures. Similar comparisons may be made between runs 20 through 24 and 82 through 85, and between runs 39 through 41 and 86 through 89. In fact, this is the reason why 9 cylinders used by Keulegan and Carpenter yield 12 different β values.

The points corresponding to the suitably selected Reynolds numbers (re = 10,000, 15,000, 20,000, and 25,000) are reproduced in Figs. 3 and 4 and connected, as carefully as possible, with smooth curves. These figures show, within the range of Re and K values encountered in the data of Keulegan and Carpenter, that (a) C_d depends on both K and Re for all values of K and decreases with increasing Re for a given K; (b) C_m depends on both K and Re for K larger than approximately 15 and decreases with increasing Re; and that (c) the dependence of C_d on Re as well as on K for $K > 15$ is more significant than the apparent dependence of C_d on Re for $K < 15$ and of C_m on Re for $K > 15$. The reason for this is that the experimental errors in C_m for $K > 15$ (where the inertial force is relatively small) and in C_d for

TABLE-I

Run No.	Diameter in inches	β	K for Re= 10,000	K for Re = 15,000	K for Re = 20,000	K for Re = 25,000
1- 9	3.00	2935	3.4	5.1	6.8	8.5
10-14	2.50	2106	4.8	7.1	9.5	11.9*
15-19	2.00	1360	7.4*	11.0	14.7	18.4*
78-81	1.75	987	---	----	----	----
20-24	1.50	796	12.6	18.8	25.1	31.4*
82-85	1.50	701	14.3	----	----	----
25-29	1.25	560	16.9*	28.2	34.6	44.6*
30-33	1.00	387	25.8*	38.8	51.7	----
34-38	0.75	217	46.1	69.1	----	----
90-93	0.75	141	----	----	----	----
39-41	0.50	97	103.1	----	----	----
86-89	0.50	78	----	----	----	----

* Points plotted with a small extrapolation of the β lines beyond the limits of the data given by Keulegan and Carpenter [6].

$K < 15$ (where the drag force is relatively small) are likely to be large. Notwithstanding this fact, Figs. 1 through 4 show unmistakably the dependence of C_d and C_m on both K and Re and help to put to rest the long standing controversy regarding the dependence or lack of dependence of the Keulegan-Carpenter data on the Reynolds number. These figures also show the importance of β as one of the governing parameters in interpreting the data, in interpolating the K values for a given Re, and in providing guide lines for further experiments as far as the ranges of K and β are concerned.

The foregoing is not the first attempt to show the role played by viscosity.* The previous attempts have all been based on drawing mean lines through bands of Reynolds numbers or relative amplitudes or K values. Thirriot, Longree, and Barthet [10] have classified the drag coefficient by bands of Reynolds numbers and plotted them as a function of A/D. This plot then yielded two other plots in which C_d is plotted as a function of Re for constant values of A/D. One of the plots is for $A/D < 1.6$ and the other for $A/D > 2$. Such plots do show the dependence of C_d on Re as well as on K but they are not as unambiguous as those presented herein.

Thirriot et al. [10] did not deal with the inertia coefficient either in Keulegan-Carpenter data or in their own experiments. Isaacson [11] replotted Keulegan-Carpenter data by drawing K = constant lines through bands of K values in a plot of C_m versus Re. This plot shows, as we have shown in Fig. 4 that, C_m decreases with increasing Re for a given K.

---

* This writer, working with John S. McNown and Garbis H. Keulegan in 1957, found among many plots and cross-plots of Keulegan's data some indication of the effect of viscosity. But the plots were never as clear and definitive as the ones presented herein 18 years later!

As we shall see later, this conclusion as well as the data which it is based on appears to be incorrect.

Thirriot et al. [10] have oscillated cylinders in a tank of still water and carefully recorded all of the experimental difficulties. They have found that their own data, like those of Keulegan and Carpenter, show a dependence on both Re and K. Thirriot et al.'s data are not given in a tabulated form. Thus, no attempt is made here to replot them through the use of the parameters K and β. One of the most important findings of Thirriot et al. was the existence of a second maximum in C_d for very small values of K or A/D, (e.g. at Re $\simeq 1.25 \times 10^4$ the maximums occur at K $\simeq$ 18 and at K $\simeq$ 4). The second maximum at K = 4 is about 60% lower than the first maximum. Thirriot et al. [10], having underlined the experimental difficulties encountered with the free surface, cylinder supports, oscillating mechanism, etc., did not elaborate further on their data and chose to give "des résultats à l'état presque brut."

It was noted earlier in connection with the discussion of Fig. 1 that the Keulegan-Carpenter data for β = 2935 show some irregularity which may or may not be due to the experimental errors. It is noted that for β = 2935, C_d rises to a maximum of 1.23 at K = 4.3 and then decreases to 0.91 at K = 5.2 and so on. This maximum occurs at a Reynolds number of 1.25×10^4 and is about 56% of the maximum value of C_d for Re = 12,500 (see Fig. 3). It may be concluded tentatively, on the basis of the strong similarity between these values and those noted above in Thirriot et al.'s data, that the rapid changes in Keulegan-Carpenter data for β = 2935 are not due to experimental errors and do indeed reflect the true changes in C_d. We will return to the discussion of this point later in connection with the discussion of the data obtained in the present investigation.

III. EXPERIMENTAL EQUIPMENT AND PROCEDURES

A. OSCILLATING FLOW ABOUT A BODY AT REST VERSUS OSCILLATING BODY IN A FLUID OTHERWISE AT REST

Mathematically, there is no difference between the two situations. As stated by Batchelor [12], "The equation of motion of a fluid in the moving frame is therefore identical in form with that in an absolute frame provided we suppose that the fictitious body force $-f_o$ (assuming a non-rotating frame) per unit mass acts upon the fluid in addition to the real body and surface forces". "$-f_o$ is simply the apparent body-force that compensates for the translational acceleration of the frame." In other words, the inertia coefficient C_m for the fluid accelerating about a body at rest is equal to $C_m = 1 + C_a$ where C_a is the added mass coefficient. For an ideal fluid flow (or for the initial instants of an impulsive change in the velocity of a real fluid) about a cylinder, one has $C_m = 2$ and $C_a = 1$. The transverse force remains unaffected since there is no additional net lift on any body element aligned in the transverse direction [11].

Experimentally, there are significant differences between the difficulties encountered in the two situations. In fact, the selection of one situation over the other has to be based on an extremely careful consideration of all the known and anticipated difficulties, errors to be tolerated, forces to be measured (in-line and/or transverse), the purpose of the investigation, etc. Let us now consider some of these difficulties.

1. Advantages and disadvantages of oscillating the body:

   a. The effect of waves and free surface disturbances in the test basin created by the oscillating body are difficult to assess;

   b. The supporting or driving arms can cause additional disturbances

and time-dependent forces which are not easy to eliminate or estimate;

c. Vibration of the entire system, particularly at low frequencies of oscillation, is unavoidable. Consequently, one has to draw smooth lines over the recorded forces or use suitable electronic filters;

d. The inertial force due to the mass of the oscillating body has to be subtracted from the total force either electronically by mounting an image cylinder and force transducer system above the test body or by carrying out the experiments once in air and once in water. This may be possible where either the drag or the inertial force is large. However, in the region of governing parameters where both are important, a small error in the phase angle can lead to large errors in the coefficients.

e. It may be difficult to give a perfectly repetetive or harmonic motion to the body at high velocities because of the possible changes in the speed of the driving motor due to the changes in the forces acting on the body;

f. It is quite difficult to measure simultaneously or independently both the in-line and transverse forces. Mercier [13] who measured both the in-line and transverse force by oscillating a circular cylinder had considerable difficulties in assessing the degree of accuracy of his measurements even at relatively small Reynolds numbers. In fact Mercier noted that "The forces in-line with the oscillation are strongly dependent on the inertia force associated with the model and apparatus, which accounts for about three-fourths of the total force for small amplitudes of motion and about half for large amplitudes." "In view of this, it is considered difficult and imprecise to attempt to derive hydrodynamic force information for this component from the oscillograph records", and that "data analysis of oscillator test results must be done with the utmost care because of the

unavoidable large inertia tare." As noted earlier, Thirriot et al. [10] have encountered similar difficulties in evaluating the drag component of the in-line force. They were not concerned with the inertial component of the in-line force and the transverse force. In spite of these difficulties, however, both Thirriot et al. and Mercier have been reasonably successful in determining the force coefficients for most of the cases studied by them.

Hamann and Dalton [14] oscillated the cylinder in a fluid at rest and encountered various difficulties which are aptly described by them. They had to use both low-pass and high-pass filters before feeding the signals to the amplifier-recorder system. This, in turn, caused phase shift and it had to be determined through indirect means. It became clear to them that a real picture of the force on the oscillating cylinder could be obtained only after the values from the recordings had been corrected by the dynamic component and were brought into correct relation with the recorded position signal.

g. The advantages of oscillating the body are that one can independently vary the Reynolds number and the amplitude and that one determines, after subtracting the inertial force due to the mass of the oscillating body, the fluid induced forces and hence C_d and C_a instead of C_d and $1+C_a$ since no pressure gradient exists in the fluid otherwise at rest. Thus, the added mass coefficient can be determined more directly provided that all of the difficulties cited above can be overcome with sufficient ease and accuracy to justify the achievement of a slightly better accuracy in C_m or C_a. As far as this writer is concerned, the difficulties outlined above are next to impossible to overcome particularly for oscillations in the higher Reynolds number range. Furthermore, the

efforts devoted merely to the determination of the in-line force without due regard to the transverse force meet the problem under consideration only half way. It is now clear that one must consider a rather large transverse force as well as an in-line force in the design of structures subjected to wave forces. It is further clear that the oscillations of the transverse force and the fatigue which could be caused by them may be the most important design criteria. Past experience shows that it is difficult to obtain reliable transverse force data by oscillating the body in a fluid at rest or in motion.

2. Advantages and disadvantages of oscillating the fluid about a body at rest:

a. If the fluid is allowed to oscillate harmonically at its natural frequency in a U-shaped tunnel [7], or in a wave basin [6] then the frequency of oscillation is fixed. Consequently, the Reynolds number cannot be varied independently. However, the frequency parameter β, introduced in this report, can be kept constant while varying K. The power of this procedure has already been demonstrated by re-analyzing the data provided by Keulegan and Carpenter. Thus, the constancy of the period is no longer a disadvantage.

b. The fluid may also be oscillated by a piston in a large water tunnel at desired amplitudes and frequencies. Such a system will have to be extremely complex for large Reynolds numbers. Even then it may not be free from the difficulties described in connection with the oscillating body.

c. If the oscillating fluid involves a free surface, one has to deal with the fact that the free surface is inherently unstable, particularly when the acceleration is directed towards the liquid as shown by Taylor [15]

and Benjamin and Ursell [16]. Hence, for a fluid oscillating in a U-shaped tunnel or wave basin, the free surface is unstable in a down motion. It turns out that this instability is not a serious problem and in fact, a very easy one to deal with.

B. THE U-SHAPED OSCILLATING FLOW TUNNEL

Experiments carried out [7] in the initial phases of the study with small smooth cylinders at low Reynolds numbers have proved the versatility and usefulness of a U-shaped oscillating-flow apparatus. Thus, in an attempt to achieve larger Reynolds numbers, it was only natural to construct a larger U-shaped tunnel.

Among the various designs considered, the one shown in Fig. 5 was finally selected for construction. A photograph of the completed and fully-instrumented structure is shown in Fig. 6. It consists of 11 modules for ease of construction, transportation, and final assembly. Each module is made of 3/8 inch aluminum plates reinforced with 1/2x4x18 inch flanges welded to the plates. The modules were assembled with the help of an air drying silicon rubber between the flanges of two adjacent modules and one inch steel bolts placed 6 inches apart. The inside of each module was precision machined so that the largest misalignment was 0.04 inches.

Prior to the description of its instrumentation and operation, a few words are necessary about the general shape of the tunnel. The cross-section of the two legs is 6 ft by 3 ft whereas that of the test section is 3 ft by 3 ft. This selection was dictated by several considerations such as the available ceiling height, pressures to be encountered and hence the structural and economic considerations, desire to obtain an actual amplitude or velocity of oscillation at least twice that of the free surface, period of oscillation, Reynolds number and the relative amplitudes

desired, possible separation of the flow at the corners, natural damping of the oscillations, and the magnitude and the frequency of the forces to be encountered. The length of the 3 ft by 3 ft horizontal section was chosen larger than twice the actual amplitude to insure fully developed uniform flow at the test section. Finally, the two corners of the tunnel were carefully streamlined to prevent separation. The design proved to be more than adequate for no separation was encountered, and the desired amplitude and frequency of oscillations have been achieved.

The auxiliary components of the tunnel consisted of plumbing for filling and emptying of the tunnel, butterfly-valve system, and the air supply system. The plumbing consisted of simple piping for hot and cold water (55° to 120° F), heat exchanger, several pumps, and a filter.

The butterfly-valve system (mounted on top of one of the legs of the tunnel) consisted of 4 plates, each 18 inches wide and 36 inches long. A one inch steel shaft was placed at the axis of each valve plate. Aluminum housings supported both ends of the shaft with self-aligning ball bearings. A 6 inch gear was attached to one end of each shaft which extended beyond the bearing. All four valve plates were then aligned and driven by a simple rack-and-pinion system. The rack was actuated by an air-driven piston with the help of a three-way valve connected to the air-supply system.

The valves, in their closed position, completely sealed the top of one of the legs of the tunnel (see Figs. 7 and 8). The top of the other leg was left open. Initially, the butterfly valves were closed and air was admitted to that side of the tunnel to create the desired differential water level between the two legs of the tunnel. Then the valves were opened quickly with the help of a pneumatically-driven three-way control

valve. This action set the fluid in the tunnel in oscillatory motion with a natural period of T = 5.272 seconds. Subsequent oscillations were maintained either by closing and opening the valves with a suitable period, in perfect synchronization with the oscillation of water, or by simply letting the butterfly valves remain open. A series of experiments starting with the largest amplitude and cylinder diameter was conducted through the use of both methods. The following important conclusions have been reached. Firstly, the damping of the motion is such that the amplitude of oscillation decreases about 0.13 inches per cycle for the largest amplitude and about 0.06 inches per cycle for amplitudes smaller than about half the maximum. In other words, the amplitude decreases 0.4% per cycle for the maximum amplitude and about 0.2% per cycle for smaller amplitudes. In fact, an oscillation beginning with an amplitude of 30 inches damped to an oscillation with an amplitude of 2 inches over a period of 45 minutes, after about 500 cycles of oscillation. Thus, over a period of 4 complete cycles of oscillation at any mean amplitude, the amplitude, velocity, and the acceleration of the fluid changed about 1%. On the other hand, experiments with forced oscillation about the natural frequency of oscillation of the fluid have shown that the amplitude cannot be maintained to an accuracy better than 1% and that one must contend with some high frequency oscillations, however small, superposed on the acceleration trace due to the cyclic operation of the butterfly valves.

Following the observations cited above, experiments were carried out with non-forced oscillations and the results were compared from time to time with those obtained with forced oscillations. The advantages of the method adopted became apparent very quickly. Firstly, the oscillations were so smooth that there was no need for filters between the transducer outputs and the recording system. Secondly, one test, over a period of

about an hour, showed the evolution of the in-line and transverse forces for all possible values of K for a given β.

1. Velocity Distribution at the Test Section

There was no easy way to check the uniformity of the velocity distribution at the test section. This could have been done by recording the velocity at various points along a vertical and horizontal line at the test section through the use of a hot-film anemometer and comparing the velocity traces and the amplitudes of velocities at the corresponding times. Such a method was seriously considered but the difficulties to be encountered led to its abandonment. Instead, it was decided to measure and compare the pressure gradients along the top and side walls of the tunnel at the test section. A differential pressure transducer was connected to two pressure taps placed one foot on either side of the test section, on all three sides of the tunnel. The outputs of all transducers (each calibrated properly so as to yield the same millivolts of signal for the same static differential pressure) were recorded simultaneously. The signals which were in fact measurements of the instantaneous acceleration of the fluid, were almost identical and did not differ more than 0.5% for all amplitudes of oscillation. This procedure has shown that the instantaneous pressure gradient or acceleration along the three faces of the tunnel were identical.

The above method of measurement of the instantaneous acceleration was also applied to two other sections, one 4 ft to the left and one 4 ft to the right of the test section, in order to check the uniformity of the instantaneous acceleration distribution in the approach flow. Repeated experiments with representative amplitudes of oscillation have shown that the instantaneous as well as maximum acceleration along the top and side

faces of the tunnel do not differ more than 0.5%. The foregoing two sets of experiments were taken as an indication of the uniformity of the acceleration distribution and hence of the velocity distribution both in the test section and away from the test section.

C. CIRCULAR CYLINDERS

Seven circular cylinders with diameters ranging from 6.5 inches to 2 inches were used. The cylinders were turned on a lathe from aluminum pipes and polished to a mirror-shine surface. The resulting surface texture was as smooth as possible as verified by microscopic inspection. There is no doubt that it was hydrodynamically smooth also. The length of each cylinder was precisely 35-15/16 inches. This allowed 1/32 inch gap between the tunnel wall and each end of the cylinder. As will be noted later, the cylinder was prevented from moving towards one or the other wall by means of small O-rings attached to the end of the force transducers. A double-ball precision bearing (SKF-2303-J) with an approximately 0.6 inch bore was inserted into the ends of the cylinder in 3 inch long housings which sealed the cylinder air tight. The outer face of each bearing was flush with the end of the cylinder.

Same cylinders were also used as rough cylinders with various types of distributed surface roughnesses. Some of the cylinders were roughened with sand. For this purpose, sand was sieved and applied on the cylinder surface with air-drying epoxy paint. The second type of distributed surface roughness was obtained through the use of commercially available sand paper purchased from the 3M company. The sand papers were carefully wrapped around the cylinders and glued with the same epoxy paint. The thickness of the various papers, together with the glue, varied from about 0.03 inch to 0.05 inch. The Reynolds numbers were calculated by adding

to the diameter of the smooth cylinder twice the paper and paint thickness plus one half the hight of the roughness element. Evidently, the thicknesses involved were rather small relative to the size of the cylinders used and the difference between the Reynolds numbers calculated as above and those based on the smooth cylinder diameter were quite small and certainly within the range of experimental errors.

The third type of distributed surface roughness was obtained through the use of commercially available polistyrene beads of uniform diameter, glued to the cylinder surface as described above.

The following tables summarize the characteristics of the cylinders used.

Smooth cylinders:

Dimater in iches	D/w^*	L/D	$D^2/\nu T$
6.475	0.18	5.52	5259.9 and 8370
5.975	0.17	5.99	4480.2
4.990	0.14	7.17	3123.2
3.978	0.11	8.99	1985.2
2.970	0.082	12.05	1106.6
2.500	0.069	14.31	783.8
1.991	0.055	17.97	497.2

* w is the width or hight of the test section, w = 3 ft.
  L = w = 3 ft.

Rough cylinders:

Diameters of the cylinders used before roughness is applied:

D = 6.475"	5.975"	4.990"	3.978"	2.970"	2.500"	1.991"

Relative roughness k/D used for each cylinder:

k/D ≅ 1/50	1/180	1/360	1/500

Temperatures used for each D and k/D:

F° = 55	65	75	85	100	120

D. FORCE MEASUREMENTS

Two identical force transducers, one at each end of the cylinder, were used to measure the instantaneous in-line and transverse forces. The basic transducer was purchased from the BLH Electronics, Inc. under the trade name of Type LBP1 and catalogue No. 420271. The important dimensions of the transducer are shown in Fig. 9. The gage had a capacity of 500 pounds with an overload capacity of 200%. The deflection of the gage under a 500 pound load was 0.01 inches. For the largest cylinder used and the amplitude of oscillation tested, the maximum load was about 100 pounds and the deflection of the cantilever end of the gage was less than 0.002 inches.

A special housing was built for each gage so that it can be mounted on the tunnel window and rotated to measure either the in-line or the transverse force alone. Figure 10 shows the entire gage assembly.

The bellows which protected the strain gages had to be water proofed in such a manner that they would not adversely affect the operation of the gages when subjected to about 20 ft water pressure at temperatures

65 F° to 165 F°. For this purpose, the bellows were filled completely with a liquid silicon rubber (Dow Corning 3140 RTV coating) without bringing the rubber into contact with air during the filling operation. Then the ends of the bellows were sealed air tight with special clamps. The silicon rubber remained in its original liquid form throughout the operation of the gage.

The cylinders were placed in the test section by retracting the gages from their housing and then pushing them into the bearings mounted at each end of the cylinders. As noted earlier, the O-rings placed on the cantilever end of each gage prevented the test cylinders from moving side ways towards one or the other wall and helped to set exactly 1/32 inch space between the cylinder and the tunnel wall. The cylinders were free to rotate, as they should be, at the application of a slight torque by hand.

After mounting the first cylinder, the exact angular position of the gages within their housing had to be determined and set with a pin so that the gages measure either only the in-line or the transverse force. For this purpose, a 200 Pound load was hung on the cylinder with a lubricated nylon rope. The in-line force (acting in the horizontal direction) was observed on the amplifier-recorder system. Then the gage was rotated in small increments until the in-line force was exactly zero. A final check was made by measuring the outputs of the gages with a precision voltmeter. Then the position of each gage was marked and set with a pin. Finally, four bolts were placed on the gage housing to hold the gages rigidly in position. Removal of these bolts and the pin allowed the rotation of the gages for exactly 90 degrees. Then the bolts and a new pin were placed in position. In this manner the gages were capable of measuring either

the in-line or the transverse force without a cross-talk between the two forces. At times both gages were used to measure only the in-line or only the transverse force.

The calibration of each gage was accomplished by hanging loads in the middle of the cylinder after setting both gages to sense only the transverse force (here in the vertical direction). The directional sensitivity of the gages was also checked by applying identical loads upwards on the cylinders with the help of a hook-cantilever arm attached to the top of the tunnel outside the test section. Repeated calibrations have shown that (a) the gages were absolutely linear up to 500 pounds; (b) the gages yielded the same signal for loads applied either upward or downward; and that (c) the gages, together with the electronic system to which they were attached, were capable of sensing loads as small as 0.02 pounds, (this corresponded to a 1 mm deflection on a 50 mm wide recorder paper).

The natural frequency of vibration of the cylinder-gage assembly in water was found to be in excess of 100 Hertz for all cylinders tested. This frequency was several times larger than the largest vortex shedding frequency encountered.

E. DATA ACQUISITION SYSTEM

It was deemed desirable to have both analog and digital outputs of the in-line and transverse force versus elevation. For this purpose, the output of the force transducers were first fed to an 8 channel carrier-amplifier-recorder system. The output of the 8-channel system was then fed to two two-channel amplifier-recorder systems. One of the recorders gave a simultaneous recording of the in-line force versus elevation. The other recorder gave a simultaneous recording of the transverse force versus elevation. The force signals from the 8-channel recorder were branched

off to two DC amplifiers and then to a Varian computer for analog-to-digital conversion. Also fed into the Varian computer were the signals received from other pressure transducers which did not require further amplification after leaving the 8-channel recorder. The analog output of the 8-channel recorder and the digital output of the Varian computer were calibrated for a series of loads applied on the force gages and pressure transducers. Frequently, both the analog and digital data for a given test have been evaluated to check the consistency of the data acquisition system. As will be amplified later, the analog data have been read at every 0.1 seconds which corresponded to every 6.8285 degrees in a cycle. The digital sampling rate was set at either 10 samples/second/channel or at 20 samples/second/channel.

F. ACCELERATION, ELEVATION, OR VELOCITY MEASUREMENT

It is because of the extreme importance of the accurate measurement of the instantaneous values of these quantities that they are discussed here separately.

Firstly, it should be noted that the measurement of the amplitude of either the acceleration, or elevation, or the velocity is more or less a matter of interpretation of the signal received from the appropriate transducer in light of one of the following expressions

$$U_m = 2\pi A/T \quad , \quad a_m = (dU/dt)_m = (2\pi/T)^2 A = 2\pi U_m/T$$

in which T is constant and equal to 5.272 seconds for the experiments reported herein.

Three transducers were used to generate three independent DC signals, each proportional to the instantaneous value of one of the quantities cited above. The first one consisted of a six feet long platinum wire

stretched vertically in one leg of the tunnel. The output of the capacitance-wire bridge was connected to the 8-channel recorder as noted above. The response of the wire was found to be perfectly linear within the range of oscillations encountered. The wire was capable of yielding a measurable signal for changes in water elevation as small as 1/32 inches. Such a sensitivity was not, however, always desirable for the small instabilities previously noted on the water surface gave rise to small oscillations in the analog recorders. The effect of such instabilities were practically eliminated by placing the wire along the axis of a 1 ft diameter and 8 ft long thin plastic pipe.

The second method consisted of the measurement of the instantaneous acceleration by means of a differential-pressure transducer connected to two pressure taps placed horizontally 2 ft apart and 4 ft to one side of the test section. The output of the transducer was connected to the 8-channel recorder and then to the Varian computer. The instantaneous acceleration was then calculated from $\Delta p = \rho s \, dU/dt$ where Δp is the differential pressure, s the distance between the pressure taps, and dU/dt is the instantaneous acceleration of the fluid. The effect of the pressure drop due to the viscous forces over the distance s was calculated and found to be negligible.

The third method again consisted of the measurement of the differential pressure between two pressure taps. The two taps were placed symmetrically on the two legs of the tunnel at an elevation H = 50 inches below the mean water level about which the fluid oscillated (see Fig. 5). Applying Bernoulli's equation for unsteady flow between each pressure tap and the instantaneous level of water, one can easily show that twice the amplitude of the free surface oscillation (virtual amplitude) is given by

$$A = 2A_1 = (\Delta p/\gamma)/[1 - (2\pi/T)^2 H/g] \qquad (30)$$

in which g, γ, and T are constants and H is kept constant. Thus, the signal of this transducer yielded the virtual amplitude or the maximum velocity in each cycle. It was entirely free from noise or small free surface effects. Before each series of experiments a static calibration of the transducer was obtained by applying known differential pressures to the transducer. As noted before, the calibration was not only consistent but also perfectly linear. The transducer did not have to be dynamically calibrated for it had a fequency response in excess of several hundred Hertz.

All three methods cited above were used to monitor the oscillations. The results were most gratifying and yielded the amplitude, velocity, or acceleration to an accuracy of about 1% of the amplitude of each of these variables. These comparisons as well as the perfectly sinusoidal character of the traces speak for the suitability of the unique test facility used in this investigation, (see Figs. 11 and 12).

G. DATA REDUCTION

The in-line and transverse forces were reduced from both the 2-channel recorder traces and the Varian-computer output. Furthermore, the frequency or frequencies of the transverse-force oscillations were recorded for each run.

Experiments were repeated at least five times for each cylinder. Only two of such runs were evaluated, however, because of the enormity of the effort involved in data reduction. Initially, at least three runs were evaluated and it was found that the differences in the results obtained from a set of three runs were always less than 5%.

The tabulated data were punched on IBM cards and combined with a computer program to evaluate all of the coefficients previously discussed. Some of the coefficients and the corresponding governing parameters are presented in Appendix-A in tabular form. Tables for raw data for each Re and K are not presented due to space limitations (about 2000 pages).

H. BLOCKAGE AND LENGTH-TO-DIAMETER RATIO EFFECTS

Attempts to achieve as high Reynolds numbers as possible in conducting wind-tunnel and water-tunnel experiments invariably give rise to wall-interference effects which, of course, influence whatever measurements are made. There are several blockage correction formulas for steady flows which might be used so that the wall-interference effects on the calculated force coefficients might be minimized. Unfortunately, none of these formulas could be used in the present study for no one has demonstrated that the blockage effects in oscillatory flows are identical to those experienced in steady flows.

The blockage ratio D/w and the length-to-diameter ratio L/D, for the cylinders used in the present study, were previously tabulated. For comparison, it should be noted that in the cylinder experiments of Achenbach [17] and in some of the experiments of Fage and Falkner [18] the blockage ratios were o.166 and 0.185 respectively. Guven et al. [19] used cylinders with a blockage ratio of 0.178. The length-to-diameter ratio in Fage and Warsap's [20] experiments was 20.2 or 7.88, depending on the diameter of the two cylinders they used, as compared to 3.33 in the experiments of Achenbach [17] and 3.08 in the experiments of Guven et al. [19].

It is generally observed that values of C_d are smaller for cylinders

with larger length-to-diameter ratio. Furthermore, the wake of the cylinder, near the cylinder ends, is supplied with high pressure fluid from the front and as a result smaller values of C_d are expected since the base pressure is increased over the value it would otherwise attain. Thus the presence of gaps and the larger L/D ratios could result in lower drag coefficients. In the subcritical range of Re, however, these effects appear to be negligible. In fact Morsbach [21] found that in the subcritical range there is no effect of length-to-diameter ratio.

In the present experiments, the gap cannot be eliminated by extending the cylinder into a cylindrical cavity within the two windows supporting the gages and the cylinder because of the fact that several cylinders of different diameters were used. It would have been too costly to build a pair of windows for each cylinder. It is believed that the very small gap-to-diameter ratios encountered plus the cantilever end of the gage extending into the cylinder minimized the supply of high pressure fluid into the wake of the cylinder during part of the cycle.

Returning to the discussion of the blockage effect it must be emphasized that the formulas used for steady flow correction effects cannot be applied to oscillating flows and that there is not a unique blockage correction for the entire period of the harmonic flow. This is evident from the fact that within a given cycle the fluid undergoes varying accelerations and velocities and the wake width, momentum deficiency, and the wake pressure change accordingly. Thus, a blockage correction made for the instant of maximum velocity is not applicable to the instant at which the maximum acceleration occurs.

In view of the fact that there are no previous investigations, a series of experiments had to be conducted to determine the role of blockage in the

flow under consideration. For this purpose a differential-pressure transducer was connected to two pressure taps on the same side of the tunnel wall. One of the taps was placed on the wall directly above the axis of the test cylinder. The other tap was placed 30 inches to one side of the first tap along a line parallel to the flow. A series of experiments was carried out with the 6.475 inch cylinder and the differential pressure was recorded and compared with the differential pressure obtained from the acceleration transducer. Furthermore, to simplify the comparison both transducers were calibrated so as to render exactly the same output under identical calibration loads. The results have shown that the two differential pressures were nearly identical during the entire cycle and that they were certainly within 3% of each other. This somewhat surprising result is a clear indication of the fact that the blockage effect in harmonic flows is negligible at least for D/w ratios less than 0.18. Although no special attempt was made to interpret the lack of blockage effect in such flows it is believed that the presence of vortices on both sides of the cylinder together with the high periods of acceleration and velocity render the flow relatively more uniform at short distances away from the cylinder in the test section. Therefore, for the reasons cited above no blockage-effect corrections were applied to the data presented here. It might be of interest to note that had the flow been assumed steady and had the maximum velocity for the largest cylinder and the Reynolds number were used to calculate a blockage-effect correction through the use of one of the existing formulas, one would have found a correction of about 6% in the drag coefficient.

IV. RESULTS AND DISCUSSIONS

A. IN-LINE FORCE COEFFICIENTS FOR SMOOTH CYLINDERS

The drag, inertia, and the maximum-force coefficients are presented in Figs. 13 through 20, 21 through 28, and 29 through 36, respectively, as a function of K for constant values of β. In each figure, the Reynolds number increases with increasing K in accordance with $Re = K\beta$. Thus, one can determine K in each figure for a given Re and examine the variation of any one of these coefficients with the Reynolds number. For this purpose, the mean lines drawn through the data shown in Figs. 13 through 20 have been reproduced in Fig. 37. Similar plots for the inertia and the maximum force coefficients are shown in Figs. 38 and 39 respectively. Also shown in Figs. 37 through 39 are the constant Reynolds number lines obtained through the use of $K = Re/\beta$. Evidently, there is a remarkable correlation between the force coefficients, Reynolds number, and the Keulegan-Carpenter number. The smoothness of the constant Reynolds number lines is another indication of the consistency of the data from one cylinder to another.

Figures 37 through 39 show that C_d, C_m, and C_f(mes) do not vary appreciably with Re for Re smaller than about 20,000 and help to explain the conclusions previously reached by Keulegan and Carpenter [6] and Sarpkaya [7]. These figures also show that the drag, inertia, and the maximum force coefficients would have appeared to have had considerable scatter when plotted with respect to K had their variation with Re been ignored. Same could be said for a plot with respect to Re in which the dependence of the coefficients on K is ignored.

Figure 37 shows that there appears to be a second maximum in the drag coefficient for small values of Re and K (see for example β = 1985 line).

The presence of such a second maximum has previously been noted by Thiriot et al. [10] as discussed earlier. Figure 37 also shows that the drag coefficient goes through a minimum and then increases with increasing K for large values of β (see β = 8370 line).

The data similar to those given in Figs. 37 and 38 are also plotted as a function of the Reynolds number for constant values of K in Figs. 40 and 41. These figures dramatically show that C_d decreases with increasing Re to a value of about 0.5 (dependent on K) and then begins to increase slowly with further increases in Re and reaches a value of about 0.62 at Re = 7×10^5.

A comparison of the variation of C_d with Re for steady and harmonic flows shows that the transition in C_d in harmonic flow starts at lower Reynolds numbers and spans over a larger range of Reynolds numbers. In fact, it may be said that harmonic flow about a cylinder is in a continuous state of transition. The said comparison also shows that C_d for harmonic flow is about twice that for steady flow at both the lower end of the Re values (say Re = 10,000) and at the Reynolds numbers at which the drag coefficients go through their corresponding minimum values.

The inertia coefficient C_m increases with increasing Re, reaches a maximum, and then gradually approaches a value of about 1.75. It will be recalled that the Keulegan-Carpenter data indicated an opposite trend. It is believed that the Keulegan-Carpenter data for C_m are not quite reliable for K > 15.

The foregoing discussion of the force coefficients raises several questions which may be explained only partially on the basis of the observations with steady flows. Some of these questions are: why does the transition begin sooner and span over a larger range of Reynolds numbers;

why does the added mass coefficient C_a, ($C_a=C_m-1$), become negative for certain values of K and Re (see Fig. 41); is there a unique relationship between C_m and C_d; etc. It is a well-known fact that the occurrence of drag crisis in steady flow about a cylinder depends on the length and scale of turbulence in the ambient flow, blockage and the legth-to-diameter ratio of the cylinder, the vibration amplitude and frequency of the test body, surface roughness, and on other particularities of the wind- or water-tunnel in which the experiments are performed. In fact, it is for this reason that the minimum value of the drag coefficient in steady flow is widely scattered. Since the formation of laminar separation bubbles are largely responsible for the low values of C_d, one could state that the formation and the extent of the separation bubbles are very sensitive to the factors cited above. A priori, one would expect the same to occur in harmonic flow about a cylinder. During a given cycle, the flow at both sides of the cylinder contains a number of vortices and large scale turbulence. Thus, it is natural to assume that they would give rise to a larger time-averaged drag coefficient and to earlier transition.

The effect of the growth and motion of vortices on the increase of the drag coefficient relative to that for the steady flow needs further discussion. It has been shown that [22] the variation of the characteristics of vortices in the neighborhood of a cylinder strongly affects the lift, drag, and the inertia coefficients. It has also been shown by Sarpkaya [23] that the drag in the initial stages of an impulsively started flow about a circular cylinder can exceed its steady value by as much as 30%. These findings are relevant to the present study in a qualitative sense. During the periods of high acceleration in harmonic flow, vorticity is slow to diffuse and therefore accumulates rapidly in the close vicinity of the cylinder. Although the

growing vortex soon reaches unstable proportions and separates from its shear layer, the growth of the vortices are so rapid that the vortices become much larger than their quasi-steady-state size before they separate from their shear layers. This would ordinarily lead to a larger drag force. However, the maximum drag does not occur at the time of maximum acceleration or maximum velocity. Evidently, at the initial stages of acceleration, the vortices in the downstream side of the cylinder are not yet fully grown. Furthermore, the convection of the vortices shed in the previous cycle towards the cylinder help to reduce the pressure on the upstream side of the cylinder and prevent the drag force from reaching large values. As the velocity increases, the vortices on the upstream side move towards the top and bottom of the cylinder and loose their influence on the pressure distribution on the upstream face of the cylinder. The vortices on the downstream side of the cylinder, now fully grown and ready to shed, give rise to a large drag force. By the time the velocity reaches its maximum, the vortices coming from the upstream side are fully carried away and the vortices which are now shed from the downstream side of the cylinder are further convected downstream partly by the action of the other vortices existing in the flow and partly by the base flow itself. Thus, the drag force begins to decrease by the time the velocity reaches its maximum. The role played by the vortices becomes most pronounced on both the drag and inertia coefficients if the duration of flow in one direction is not too long (e.g. $A/D = 2$). In this case, the variation of the drag and inertia coefficients are further complicated by the locking of the vortices to the cylinder and fractional eddy shedding as will be discussed later.

The number of vortices shed in each cycle and the intensity of turbulence depend on the relative motion of the fluid and the Reynolds number.

Furthermore, there are as many as four separation bubbles in a given cycle during certain fractions of the cycle. Thus, in a given cycle the flow may start in one direction as a subcritical flow with boundary layers separating in a laminar state. As the flow speed or the instantaneous Reynolds number increases, the flow may enter a critical state and give rise to separation bubbles. However, the disturbances surrounding the cylinder (turbulence and vortices) may easily and often locally disrupt the separation bubbles (one or both). When this happens the flow may be affected over a considerable length of the cylinder and the base pressure along the span is no longer uniform. Such phenomena have been carefully noted by Bearman [24] in connection with steady flows. If the flow continues in the same direction with ever increasing instantaneous Reynolds numbers, the separation bubbles may completely disappear and part of the boundary layer may become turbulent. In other words, the flow enters a post-critical or transcritical state. The foregoing discussion helps to show that the time-averaged drag and other coefficients reflect only in a very crude way the state of an extremely complex time-dependent flow. For a given K and Re, the flow may be covering both subcritical and critical states or subcritical, critical, and transcritical states, or all of the states from subcritical to supercritical. The extent of each state depends on both K and Re (for smooth cylinders). Evidently, the transition starts at lower Reynolds numbers (anything that disturbs the boundary layer gives rise to an earlier transition provided that the Reynolds number is sufficiently high) and thus spans over a wider range of Reynolds numbers. The transition must depend on both K and Re since these two parameters in some way classify the events that occur in a given cycle.

The minimum value of C_d in harmonic flow is larger than that in steady flow and varies more gently around the [redacted] Reynolds numbers at which it

occurs. Its magnitude is explainable partly in terms of the formation, growth, and decay of vortices and partly in terms of the overall turbulence. Altogether these disturbances serve as a triggering agent such as the artificial roughness on a smooth cylinder in steady flow. The gradual variation of C_d with Re in the neigborhood of Re = 300,000 is understandable if we consider the fact that C_d is only a time-invariant average and that it reflects an integrated average of the various states of flow occurring in a given cycle. Lastly, the scatter in C_d in the drag-crisis region appears to be less than that encountered in steady flow due to the already stated fact that C_d in harmonic flow is an averaged value over a cycle.

The foregoing serves to partly explain how much more complex the flow is about a vertical pile subjected to ocean waves. With waves, assuming that they are unidirectional and there are no currents, the fluid has both a horizontal and vertical velocity component, the Keulegan-Carpenter number and the Reynolds number increase towards the free surface, and the flow varies from subcritical to supercritical state in a given cycle not only at a given depth but also along the pile. Furthermore, the flow at a given depth is not identical to plane harmonic flow at the same K and Re because of the influence of the prevailing flow states at the lower and higher depths and because of the vertical component of velocity. Furthermore, it is apparent that the differences between the wave flow and harmonic flow depend on the depth at which the measurements are made. The flow is more likely to behave like harmonic flow where the wave characteristics along the pile vary very slowly (at greater depths). If the foregoing is combined with free-surface effects, diffraction and aperiodic nature of the waves, and the effect of currents, one begins to understand the reasons for the scatter in the field data and cannot help but wonder why the drag and

and inertia coefficients obtained with harmonic flows work as well as they do in the design of the offshore structures.

It has previously been noted that the inertia coefficient shown in Fig. 41 may, for certain values of Re and K, be smaller than unity or the added mass coefficient may become negative. There is nothing mathematically or phenomenologically profound about it. The added mass coefficient, according to one definition, is a measure of the additional force needed to accelerate or decelerate the fluid particles exterior to the body undergoing a time-dependent motion. The time-average of this force in harmonic flow may simply become negative. According to another definition, the added mass is a measure of the mass drifted along the direction of flow [25]. The magnitude and relative direction of such a drift vary with time in a given cycle in harmonic flow and its average may be in a direction opposite to the direction of positive acceleration. Thus, a negative time-averaged added mass coefficient for certain ranges of K and Re means that the total drift mass during the period of flow deceleration is larger than that during the period of acceleration.

The relationship between C_m and C_d has been of special concern [26] and will be re-examined here. A plot of C_m versus C_d shows that there is not a unique relationship between them, independent of K and Re. The said relationship may be shown to depend either on K or Re (see Fig. 42). A similar plot may be prepared by maintaining Re constant at suitably selected values and plotting C_m versus C_d corresponding to the same value of K.

The maximum force coefficient (see Fig. 39) shows that in the drag dominated region of the flow the constant β lines are very similar to those shown in Fig. 37 for the drag coefficient. In the inertia dominated region, the maximum force coefficient is nearly independent of Re and increases with decreasing K.

All of the coefficients plotted in the figures cited above have been obtained with the Fourier analysis. A careful examination of the similar coefficients obtained through the use of the least-squares and modified least-squares methods have shown that they do not differ more than one or two percent from those obtained with the Fourier analysis. In fact, the inertia coefficients obtained with the Fourier analysis and the method of least squares are exactly the same, as noted earlier. For this reason and partly for sake of brevity, the coefficients obtained with other methods have not been plotted.

The error parameters λ^* and σ are tabulated in Appendix-A. In general, they show that the correspondence between the measured and calculated forces is very good except for K values in the neighborhood of 12. This may be partly due to the oscillations induced by the shedding of vortices in the in-line force. This important point will be taken up again following the discussion of the transverse force.

No attempt was made to plot the error parameters as a function of Re and/or K to establish relationships similar to those done for the force coefficients. Evidently, the inclusion of additional terms in the Morison equation to account for the lift-induced oscillations in the in-line force can improve the correspondence between the measured and calculated forces in the neighborhood of K = 12. Even without such an improvement, it appears that the Morison equation represents the measured force fairly accurately.

B. TRANSVERSE FORCE COEFFICIENTS FOR SMOOTH CYLINDERS

Vortex shedding and the resulting alternating force in steady flow have been studied extensively. In spite of the considerable interest, however, the transverse force or the lift force in harmonic flows received very little

attention. Recently, it became clear from the observations of the oscillations of long piles and strumming of cables that the lift forces are important not only because of their magnitude but also because of their alternating nature, which under certain circumstances may lead to the phenomenon known as the lock-in or vortex synchronization. This phenomenon may cause failure due to fatigue and increased in-line force. Obviously, the total instantaneous force acting on the structure is increased by the lift force and modified by the oscillations of the body. This increase refers to the vectorial sum of the in-line and transverse forces and not to the aforementioned oscillations in the in-line force due to vortex shedding.

Some of the previous studies include those carried out by Chang [27], Bidde [28], Wiegel and Delmonte [29], Mercier [13], and Sarpkaya [7, 30]. Bidde [28] dealt primarily with the ratio of the transverse force to in-line force in wavy flows and concluded that the lift force behaviour is primarily dependent on K rather than Re and that the predominant lift frequency is twice the wave frequency. Bidde's data are difficult to interpret because of the fact that the Reynolds number and the Keulegan-Carpenter number were calculated in terms of some average values, that the force measured was the total force on the complete length of the pile, and that the submerged end of the vertical cylinder was completely free to generate a complex three-dimensional flow and influence the vortex shedding.

Wiegel and Delmonte [29] extended Bidde's work and used the Keulegan-Carpenter number based on the wave-surface kinematics. They have in general confirmed Bidde's conclusions except for the fact that the lift frequency was irregular and varied from about 1.3 to 6 times the wave frequency.

Sarpkaya [7] measured the transverse force on cylinders in plane harmonic flow at relatively low Reynolds numbers and found that the maximum

lift coefficient is primarily a function of K and that it can acquire large magnitudes near K = 15. This work was subsequently extended to cylinders in the vicinity of a plane wall [30].

Isaacson [11] measured the lift force on vertical cylinders in wavy flows within a Keulegan-Carpenter number range of about 0 to 25 for intermediate depth waves. The Reynolds number range covered was from about 100 to 5000. Isaacson concluded on the basis of his and others' work that lift is dependent both on Re and K and that the dependence of lift on K is considerably stronger and tends to obscure the weaker dependence on Re. He also argued that for higher ranges of K the predominant lift frequency must increase with K. Isaacson's dissertation [11] contains a great deal of discussion of the lift force which the reader may find both interesting and useful in perusing the data presented herein.

Some of the data obtained in the present study with smooth cylinders are plotted in Figs. 43 through 49 in terms of $C_L(\max)$ and K for constant values of β, (see also Appendix-B). The random nature of the lift force is evident from the scatter in the data. Nevertheless, the variation of $C_L(\max)$ with K is unambiguous and permits one to draw mean lines through the data as shown in Fig. 50. Evidently, $C_L(\max)$ reaches its maximum value in the neighborhood of K = 12 and decreases rapidly with increasing K. Furthermore, $C_L(\max)$ decreases, for all values of K, with increasing β.

The minimum value of K at which lift or the asymmetry in the vortices develop is, by the very nature of vortices, extremely sensitive to the experimental conditions. Our observations show that the onset of lift depends not only on K and Re but also on noise and vibrations external to the tunnel. In certain runs, lift will first disappear for long periods of time

when K drops to about 6 and then will reappear, for no apparent reason, for one or two cycles and then disappear again. Suffice it to say that the asymmetry may be assumed to begin in the range of K values from 4 to 6. Attempts to further narrow down this range of K require a statistical approach. The concept used here is similar to that used in the determination of the intermittency factor and the critical Reynolds number in pipe flows. Evidently, it is not the highest value of K at which the symmetry of the vortices can be maintained with extensive care but the lowest value of K below which asymmetry cannot be initiated in spite of the magnitude of external disturbances. A careful analysis of all the lift traces have shown that there is a 90% chance that the asymmetry will occur at K = 5. At K = 4, there is only a 5% chance that the asymmetry will appear for very short periods of time. It should be noted in passing that the determination of the lowest value of K for the onset of asymmetry is of more than academic interest not only in connection with ocean structures but also with bodies of revolution flying at high angles of attack.

All of the transfer force data for smooth cylinders are summarized in Fig. 51 in terms of C_L(max) and Re for constant values of K. This figure may be divided into three regions as far as the dependence of C_L(max) on K and Re is concerned. For Re smaller than about 20,000, C_L(max) depends primarily on K as previously shown by Sarpkaya [7]. In the Reynolds number range from about 20,000 to 100,000, C_L(max) depends, to varying degrees, both on Re and K. Above a Reynolds number of about 100,000, the dependence of C_L(max) on Re and K is quite negligible and certainly obscured by the scatter in the data (see Figs. 43-49). However, the magnitude of C_L(max) relative to C_f(mes) is not negligible. For very large values of Re and K, C_L(max)/C_f(mes) approaches 0.20.

The r.m.s. values of the transverse force exhibit the same functional dependence as the peak values. The plots of the r.m.s. values are not reproduced here for sake of brevity but may be plotted by the reader using the data presented in Appendix-B.

Aside from its magnitude, the most important feature of the transverse force is its frequency of oscillation. For this reason the frequency ratio f_r (the ratio of the frequency of the alternating force f_v to the frequency of oscillation f of the water in the tunnel) has been evaluated for each run, rounded to the nearest whole number, and tabulated in Appendix-B together with the Strouhal number defined by $St = f_v D/U_m = f_r/K$. The data so obtained have been plotted in various ways such as f_r versus K, f_r versus Re, etc. It became clear that the only plot through which meaningful conclusions may be reached is the one shown in Fig. 52. Individual data points are not shown since they may be found in Appendix-B. In Fig. 52, a point on each line represents the maximum value of K for a given Re and f_r. In other words, a line such as $f_r < 4$ means that the alternating force does not contain frequencies larger than $f_r = 4$ for K and Re values in the region to the left of the line. Intermediate values of f_r such as $f_r = 3, 5,$ etc. are not shown to keep the figure relatively simple.

Several facts are of special importance and will be discussed in detail. Firstly, Fig. 52 begins with K = 5. As noted earlier, there is an occasional vortex shedding for K values between 4 and 5. Secondly, each $f_r = N$ line does not represent an absolute line of demarcation between the frequencies N-1 and N+1. Occasionally, a frequency of N+1 will occur on the N-1 side of the N line, and vice versa. A plot of the tabulated data will bear out this fact. Fourthly, the frequency of vortex shedding is not a pure multiple of the flow oscillation frequency (see Figs. 53 and 54). At first this

would appear anomalous but a closer examination of the behaviour of the vortices shows that a fractional value of f_r is perfectly understandable. Evidently, f_r, as an integer, is a measure of the number of vortices actually shed during a cycle. However, all of the vortices are not fully developed or completely shed. Leaving aside, for the purpose of this work, the detailed discussion of what is meant by shedding, let us simply adopt the definition that those vortices which do not break away from their shear layers before the flow is reversed are partially developed and result in incomplete vortex shedding. Thus, the fractional part of f_r indicates an incomplete shedding. The occasional shedding of one of these not-fully-grown vortices gives rise to an observation noted earlier, i.e., for a transverse force condition where the fractional part of f_r is fairly large (say f_r = 3.45), the vortex will shed, for one reason or another, and yield an f_r value of 4 for a set of Re and K values for which f_r is normally equal to 3. This becomes particularly true for f_r in the neighborhood of 3 and also for large values of K and Re where the oscillations of the transverse force become quite irregular. The significance of the foregoing relative to the in-line force will be taken up separately.

Flow visualization with hydrogen bubbles has revealed a related phenomenon, namely, the single eddy shedding or non-alternating vortex shedding at a preferred location. The numerous photographs are not reproduced here but will be discussed in general terms. The vortices are not always shed alternatingly from the top and bottom of the cylinder. For small values of K, two vortices begin to develop at the start of the cycle in one direction but the vortices do not acquire the same strength due to various reasons. As the flow reverses, the larger of the vortices is swept past the cylinder but the weaker one dissappears partly due to turbulent diffusion of vorticity and partly due to laminar diffusion which

is proportional to $\exp(-\beta)$. The consequences of this single shedding are that the in-line force becomes asymmetrical (see Fig. 55 where $F(\theta) \neq -F(\theta+\pi)$) and the vortex which is swept away plays an important role in the formation of new vortices when the flow reverses its direction once again. In other words, the dominant vortex establishes, by its sense of rotation, a preferred location for the generation of a new dominant vortex. Such vortices remain close to the cylinder and give rise to larger lift forces not only because of their proximity to the cylinder but also because of their apparently larger strength (accumulation of vorticity). It has been shown by Sarpkaya [31] that in an impulsively started flow the weakest and the strongest vortices form at the start of the motion and that the strength of the dominant vortex is considerably larger than that of a vortex shed in the later stages of the motion. A similar phenomenon seems to be occurring in harmonic flow. Isaacson [11] and Namork [32]* noted observations similar to those cited above. A computer simulation of the single vortex shedding through the use of the discrete vortices is presented in Appendix-C. The details of the analysis will not be presented here. A description of the method and its application to the flow past an inclined plate may be found in [31].

The Strouhal number defined as $St = f_v D/U_m = f_r/K$ is tabulated in Appendix-B together with the lift coefficients and f_r. Several facts become apparent from the perusal of this data and of their plotting with

---

* The author is grateful to Dr. M. M. Zdravkovich of the University of Salford for bringing this work (done under his direction) to his attention.

respect to K or Re (see Figs. 56a and b). Firstly, the Strouhal number does not remain constant at 0.2 as in steady flow for the Reynolds numbers under consideration. Secondly, St depends on both K and Re. Similar conclusions may be reached by calculating f_r/K along each line shown in Fig. 52. However, for Re smaller than about 50,000 and f_r larger than about 3, the upper limit of the Strouhal number is about 0.2 (in Fig. 52, one has f_r/K = 4/21, 6/30, 8/40, 10/52, 15/82, etc. at the lower end of each f_r line). Rance [33] claimed that St remained nearly constant at 0.2 and showed no variation with either K or **Re***. Finally, it is noted that at large values of Re the Strouhal number increases to about 0.3. This is consistent with the measurements made in steady flow at transcritical and supercritical Reynolds numbers [34].

C. COMMENTS ON MORISON'S EQUATION

The occurrence of relatively large lift forces, single vortex shedding, asymmetry in the in-line force, and the negative added-mass coefficient, all in the range of K values from 10 to 20, are directly related to the occurrence of relatively larger differences between the measured and calculated forces in the same range of K values. Thus, it is only natural that not only the limitations of the Morison's equation but also the reasons for them be discussed in some detail.

It should be stated at the onset that it is rather surprizing that Morison's equation holds as well as it does even in a range of K values where the vortex shedding is most sensitive to external disturbances.

---

* Rance's definition of Re is based on the velocity prevailing at the instant at which the maximum force occurred. He used only the maximum forces to determine C_d by assuming C_m = 2.

It appears that the mechanism responsible for the larger differences between the measured and calculated forces in the neighborhood of K = 15 is the vortex- or lift-induced oscillations in the in-line force.

In the disturbance-sensitive region of vortex formation the onset of asymmetry and the subsequent growth and shedding of single or alternating vortices have profound effects not only on the measured in-line force but also on the coefficients calculated. Morison's equation assumes that the in-line force F is an odd harmonic function, i.e., $F(\theta) = -F(\theta+\pi)$, for a flow represented by $U = -U_m \cos\theta$. Furthermore, the Fourier-averaged coefficients are derived on the basis of this assumption. Thus, the drag and inertia coefficients calculated through the use of an in-line force trace for which $F(\theta) \neq -F(\theta+\pi)$ are not quite correct. Furthermore, they are not equal to the corresponding coefficients which could have been calculated by considering only part of the measured in-line force in the range $0 < \theta < \pi$ or $\pi < \theta < 2\pi$ and assuming the remaining half to be its odd harmonic or mirror image shifted by T/2 or π. Evidently, had one used only that portion of the measured force for which the maximum value of $|F|$ is larger, and assumed the remaining portion to be given by its mirror image in calculating the force coefficients, one would obtain better agreement between the measured and calculated forces. Thus, it is clear that part of the reason for the larger differences between the measured and calculated forces is due to the use of the force-coefficient expressions which are derived by assuming the in-line force to be given by an odd harmonic function. In the range of K values from about 10 to 20, particularly for relatively low values of Re, this assumption is not quite correct as evidenced by the experiments (see Fig. 55).

The reason for the asymmetry in the magnitude of the in-line force

and differences between the measured and calculated forces is primarily the fractional shedding of vortices and vortex-induced oscillations in the in-line force. It is a well-known fact that in steady flow the vortex shedding causes a gradient of fluctuating pressure across the body. This, in turn, gives rise to periodic force fluctuations in the in-line direction on bodies with curvature or on plane surfaces not parallel to the ambient flow. These fluctuations have twice the lift frequency and can cause an as much as 40% fluctuation in the mean drag coefficient with somewhat lower values occurring in the supercritical range. Evidently, the physical movement of a pile in the in-line and/or transverse direction can significantly change the mean as well as the oscillating component of the force. Leaving aside this possibility, the instantaneous value of the 'steady drag' coefficient may be written as

$$C_d = \bar{C}_d + \eta C_L \sin(2\pi f_v t + \phi) \tag{31}$$

in which C_L is the lift coefficient appropriate to the particular Reynolds number and ηC_L represents the amplitude of the drag oscillations. Note that there is a phase angle, even in steady flow, between the occurrences of maximum lift and the maximum fluctuation in the drag force.

In harmonic flow, the fully grown vortices move back and forth about the cylinder and do not necessarily shed alternatingly. Thus, it is quite possible that the oscillations in the in-line force due to eddy shedding are relatively larger than those in steady flow. The magnitude of these oscillations may be expressed in a manner similar to that suggested above for the steady flow. Thus, we have

$$2\,\Delta F = \eta C_L \rho L D U_m^2 \cos(2\pi f_r t/T - \phi) \tag{32}$$

Evidently, one can consider the additional harmonics of the lift force by summing the above expression over all harmonics. This is not necessary at this stage of the discussion. As to the value of f_r to be used, it should be remembered that it is the fractional shedding of vortices that gives rise to the largest asymmetry in the in-line force. Thus, f_r should be taken equal to 3, 5, 7, etc. It turns out that f_r varies from 2 to 3 in the range of K values from 10 to 20 with considerable fractional shedding and this is the region where λ^* is largest. Thus, it is sufficient to consider only the correction due to $f_r = 3$. Morison's equation may then be written as

$$F/(0.5\rho DLU_m^2) = (\pi^2 D/U_m T)C_m \sin\theta - C_d|\cos\theta|\cos\theta - \eta C_L \cos(3\theta - \phi) \qquad (33)$$

in which C_m and C_d are assumed to be the usual Fourier averages, calculated using the actual in-line force data. For smooth cylinders C_L is Reynolds number dependent and varies from unity to 3 in the range of K from 10 to 20. Sample calculations through the use of the appropriate values of C_L and ϕ with $\eta = 0.2$ have shown that the above correction considerably reduces the difference between the measured and calculated in-line forces and phase angles. These calculations will not be reproduced here for their purpose was simply to demonstrate that the eddy-induced in-line oscillations can account for most of the error in the predictions of the Morison's equation in the range of K values from 10 to 20. Even without such a correction, Morison's equation predicts remarkably well the measured force provided that the kinematics of the flow field is known accurately.

It is noted in passing that the 'remainder function' introduced by Keulegan and Carpenter [6] is another means of correcting the predictions of the Morison's equation. It is not, however, related to vortex shedding in the manner described above.

D. IN-LINE FORCE COEFFICIENTS FOR ROUGH CYLINDERS

Experiments with artificially-roughened cylinders are an order of magnitude more complex and time consuming than those with smooth cylinders partly because of the number of cylinder-roughness combinations to be tested at various temperatures and partly because of the increase in the number of governing parameters.

The governing parameters for the smooth-cylinder results have been taken as K and β or Re and the in-line force coefficients have been expressed in terms of some time-invariant averages. With rough cylinders, one or more additional parameters are needed to express the effect of roughness. Ordinarily, the average roughness height k is taken as the additional independent variable and normalized with respect to the diameter of the cylinder. Such a simple procedure particularly for a flow as complex as the one discussed herein raises the question as to what is meant by roughness. The question is further complicated by the increase of the diameter. One may, for example, ask: What is the effective diameter and the effective roughness of a 3 ft diameter pile on which there is a 6 inch marine growth? Evidently, one would like to devise roughness parameters with which model laws or the similarity of roughness can be established. This cannot be done with a parameter k/D alone without taking into consideration the packing, size distribution, and shape of the grains used to obtain the roughness. To overcome some of these problems and to simplify the experiments, one can attempt to define an equivalent roughness height k_s as in Schlichting [8]. Such a definition may be perfectly useful for steady flow in channels and pipes but it may not be the solution for the unsteady flow over a cylinder where the characteristics of the boundary layer are changing along the cylinder and at a point with time.

In this case, one may need to express a roughness-length parameter based on the boundary layer characteristics in an effort to characterize the overall roughness geometry. It is evident that one-parameter characterization of roughness is quite limited. However, the experiments necessary to obtain one or two equivalent roughness parameters are extremely time consuming. Leaving aside, for the time being, the investigation of the roughness characterization in time-dependent flows, we will, in the present investigation, use the roughness height k as the characteristic length.

All cylinders have been carefully coated with roughness elements and inspected with a microscope to determine the height of the grains above the epoxy surface. Furthermore, photographs of the rough surface were taken with a camera attached to the microscope in order to compare the packing of the grains from one surface to another. Such photographs have shown that the grains were fairly uniformly distributed and closely packed. It is hoped that such qualitative descriptions of the rough surface will, with further research, be transformed into quantitative parameters.

Fully aware of the limitations of the use of one-parameter roughness characterization, the force coefficients are assumed to be given by

$$(C_d, C_m, C_L, \text{etc....}) = f_i(Re, K, k/D) \qquad (34)$$

or

$$= f_i(\beta, K, k/D)$$

The complexity of the experiments with rough cylinders now become clearer. If we assume that one would like to see the effect of a given relative roughness on C_d as the Reynolds number is increased say from

10,000 to 500,000, one has to maintain K constant. Alternatively, one can carry out the experiments with a given cylinder and roughness element for all values of K at a given water temperature. Then increase the temperature, repeat the experiments, and raise temperature again. Such a procedure yields an as much as 100% increase in the Reynolds number but it is not sufficient to cover the entire range of the Reynolds numbers. This difficulty is overcome by using other cylinders with the same relative roughness. Then the entire set of experiments are repeated with a different relative roughness. This procedure, however time consuming, is still preferable to oscillating a cylinder of a given relative roughness at various amplitudes and frequencies because of the difficulties encountered with severe vibrations.

The volume of the data obtained in the manner just described does not lend itself to simple reporting. A decision has been made to report only the data for a given cylinder and relative roughness and the summary of the entire data for only one Keulegan-Carpenter number. This procedure will prove to be sufficient to show the role played by roughness in harmonic flow.

Figures 57 and 58 show the variations of C_d and C_m with K for a given value of β and k/D. Also shown in these figures are the mean of the same coefficients for the smooth cylinder with identical β values. The effect of roughness is quite clear. For large values of K, the drag coefficient for the rough cylinder is larger than that for the smooth cylinder and does not vary appreciably with K. The inertia coefficient is considerably lower than that for the smooth cylinder. It too does not appreciably vary with K for sufficiently large values of K. It is through the use of such plots that the results shown in Figs. 59 and 60 have been obtained for C_d and C_m as a

function of Re for K = 50 and k/D = 1/50, 1/180, 1/360, and 1/500. The results do not appreciably depend on K for K larger than about 25.

Figures 59 and 60 show that the effect of roughness on the resistance to harmonic motion is quite significant. The entire motion becomes relatively more drag dependent. In other words, the phase angle between the occurrence of the maximum force and the maximum velocity considerably decreases relative to that for the smooth cylinder, at the same K and Re values (see Fig. 61). As will be seen shortly, this also indicates larger lift forces.

Figure 59 shows the occurrence of an earlier transition for a given roughness. In fact, for relatively small Reynolds numbers, the drag coefficient goes through a drag crisis and then following the transition of the entire boundary layer to turbulence, both the drag and the inertia coefficients acquire nearly constant values.

Why does roughness increase the drag coefficient and decrease the inertia coefficient? This is not an easy question to answer. One may look into the behavior of steady flow over a rough cylinder with an awareness of the additional complexities due to the unsteadiness of the harmonic flow. Roughness in steady flows (see, e.g. Schlichting [8]) precipitates the occurrence of drag crisis by causing earlier transition in the boundary layers and gives rise to a minimum drag coefficient which is larger than that obtained with a smooth cylinder. Following the disappearance of the separation bubbles and the transition of the entire boundary layer to turbulence, the separation points situate themselves in such a manner that the drag coefficient rises to a new value of about 0.9 at supercritical Reynolds numbers [8, 19, 34]. Thus the rise of the drag coefficient with roughness in harmonic flow over a cylinder is not too surprising even though there are no fixed separation points at supercritical Reynolds numbers.

In harmonic flow the entire boundary layer cannot be turbulent at all times. As K or the relative duration of flow in one direction increases, the entire front half of the boundary layer may become turbulent for a period of time spanning over the maximum velocity. This would preclude a turbulent reattachment of the boundary layer as in the case of smooth cylinders where the boundary layer is either not yet fully turbulent or turbulent only for a very brief period of time. This action will maintain the separation point at a more-or-less fixed position for the time period during which the boundary layer is turbulent. This, in turn, should give rise to an in-line force trace which is considerably flatter at its maximum , with a peak at about the time of maximum velocity, (see Fig. 61). The decrease of the phase angle almost always leads to smaller inertia coefficients. An alternative explanation of the decrease of the inertia coefficient is that the increase in C_d is nearly always accompanied by a decrease in the inertia coefficient (see Fig. 42).

The reason for the experiments with rough cylinders is, of course, more than the desire to examine the effect of relative roughness on C_d, C_m, and C_L. It is prompted essentially by an attempt at artificially increasing the Reynolds number to supercritical regime by means of surface roughness. Recent experiments [19, 35] with steady flow over rough cylinders have shown that (a) a change in flow regime takes place at a roughness Reynolds number Vk/ν of about 200 independently of the diametral Reynolds number; (b) a correct surface roughness condition provokes supercritical flow for $Vk/\nu > 200$, (the condition that must be respected is $k/D < 0.0022$); (c) a smooth cylinder is not a special case but behaves as if it had a roughness of $k/D = 3.5 \times 10^{-5}$; and that (d) the apparent diametral Reynolds number is increased by a factor of $k/3.5 \times 10^{-5}D$ for a cylinder of diameter D and surface roughness k. The importance of these conclusions is self evident for

supercritical Reynolds number simulation for flow about circular cylinders. In order to carry over these ideas to harmonic flow about rough cylinders, the data given in Fig. 59 were replotted in Fig. 62 as a function of $U_m k/\nu$ for various values of k/D. A similar plot for C_m has been prepared but will not be presented here. Also shown in Fig. 62 are the mean lines corresponding to steady flow data as compiled by Szechenyi [35]. Figure 62 shows that a change in the flow regime takes place at a roughness Reynolds number of about 130 and that the drag coefficient approaches values between 0.9 and 1.0 for k/D smaller than about 0.002. Evidently, the change in the flow regime occurs at higher values of $U_m k/\nu$ with increasing k/D. Of special interest for simulation purposes, however, is the smaller relative roughnesses.

The magnitude of the apparent increase in the diametral Reynolds number can be estimated by fitting the curve obtained for smooth cylinders for K = 50 onto the rough cylinder results shown in Fig. 62. Working back from the resulting values of $U_m k/\nu$ on the abscissa, this procedure gives an effective relative roughness between 0.0004 and 0.0006 for the 'smooth cylinder'. In other words, the presence of surface roughness (for K larger than about 25 and k/D smaller than about 0.003) is roughly equivalent to an increase in the diametral Reynolds number by a factor $k/5 \times 10^{-4} D$ for a cylinder of diameter D and surface roughness size of k. Further exploration of these ideas will be extremely useful in model tests and in the simulation of supercritical Reynolds numbers.

E. TRANSVERSE FORCE COEFFICIENTS FOR ROUGH CYLINDERS

The representative data for C_L(max) are presented in Figs. 63 through 68 as a function of K for various values of k/D and β. At first it would

appear that these data cannot be related to each other because of the variation of k/D and β. A closer examination of these figures reveals the very interesting fact that C_L(max) does not vary with either k/D or β. If there is some variation with these parameters, it is certainly masked by the scatter in the data. In fact, by plotting the entire data on one graph (see Fig. 69), one observes that the difference in C_L(max) from one β or k/D to another β or k/D for a given K is no more than the scatter of C_L(max) in any one plot for the same K. Furthermore, in comparing Figs. 63 through 68 with Fig. 50, one observes that a mean curve drawn through the entire rough cylinder C_L(max) data nearly coincide with the maximum of the smooth cylinder data. In other words, C_L(max) for rough cylinders is independent of Reynolds number for the roughness ratios larger than about 0.002 and is nearly identical to those for the smooth cylinder at relatively low Reynolds numbers. Thus, it may be concluded that C_L(max) for rough cylinders depends only on K (within the range of the parameters used) and constitutes the upper limit of the transverse force data for smooth cylinders. A similar conclusion may be tentatively arrived at for the drag and inertia coefficients by comparing Figs. 40 with 59 and 41 with 60. In other words, the drag and inertia coefficients for rough cylinders approach those obtained with smooth cylinders at relatively low Reynolds numbers. This is perhaps why the smooth cylinder drag data form the upper envelope and the inertia coefficient the lower envelope to the corresponding data obtained in the ocean, as noted by Wiegel [1].

The frequency of vortex shedding and the Strouhal number have been examined in a manner similar to that for the smooth cylinder. The results have shown that not only C_L(max) but also f_r is independent of Reynolds number within the range of parameters encountered. In other words, the

constant f_r lines for K > 15 are vertical lines in a plot of Re versus K. These lines have satisfied the relationship of $f_r/K = St = 0.22 \pm 0.02$ for K larger than about 15. A plot of Re versus f_r/K for smooth cylinders could not have reduced to such a single line.

The minimum value of K at which the onset of asymmetry was observed was slightly lower than that for the smooth cylinder. At high Reynolds numbers there is a 90% chance that the asymmetry will develop at K = 4.6. The Strouhal number between K = 5 and K = 15 varied from 0.45 to 0.15 and there was considerable single shedding of vortices. At about K = 15, the Strouhal number jumped from 0.15 to 0.27 and then decreased quickly to 0.22 at K = 20, (see Fig. 70). The jump for all rough cylinders occurred between K = 12 and 15 regardless of the Reynolds number or β. It is evident that the facts noted above greatly simplify the experimentation with rough cylinders.

The power of prediction of the Morison's equation for harmonic flow over rough cylinders has been examined in a manner similar to that for the smooth cylinders. The comparison of the measured and calculated in-line forces for all values of K, Re, and k/D has shown that Morison's equation predicts the measured force through the use of the Fourier-averaged coefficients with an accuracy equal or better than that for the smooth cylinders.

Finally, as regards physical applications of the foregoing data, the following points need mention:

a. The drag and inertia coefficients have been obtained only for harmonic flow over smooth and rough cylinders. Factors such as wave nonlinearity, variation of the characteristics of waves with depth, free-surface effects, flexibility of piles, currents superposed on waves,

proximity effects of adjacent piles, etc. have not been considered. Some or all of these factors may be important in the design of structures in the real ocean environment.

b. The ratio of the transverse force to in-line force is not negligibly small. At high Reynolds numbers, it has a value of about 0.2 for smooth cylinders. For rough cylinders, it varies from about 0.15 to 0.25 with decreasing roughness. Consequently, the transverse force should be taken into consideration in calculating the total force acting on the pile.

c. Roughness increases not only the in-line force on a cylinder of given diameter but also the effective diameter of the cylinder. In oceans where such roughness is likely to accumulate, the effective diameter and the effect of apparent roughness on the in-line and transverse forces should be carefully considered. In this regard, it would be difficult to predict the practical limitations of the data presented herein, and the matter is best left to be settled by carrying out experiments in the field.

d. It appears from the foregoing that a pile designed with a safety factor of 2 using $C_d = 0.6$ and $C_m = 1.5$ with no regard to roughness and the transverse forces may not in fact enjoy that safety partly because of the effect of transverse forces, partly because of the effects of roughness and increased diameter, and partly because of the probable fatigue of the structure.

V. CONCLUSIONS

The results presented herein warrant the following conclusions:

a. For smooth cylinders, the drag, lift, and the inertia coefficients depend on both the Reynolds number and the Keulegan-Carpenter number;

b. For rough cylinders, the same coefficients become independent of the Reynolds number about a critical value and depend only on the Keulegan-Carpenter number and the relative roughness;

c. Correct artificial roughness may be used to provoke and simulate supercritical flow in model tests in steady as well as oscillatory flows;

d. For both smooth and rough cylinders, the relationship between the drag and inertia coefficients is not unique and depends on the particular value of the Keulegan-Carpenter number;

e. The transverse force is a significant fraction of the total resistance and must be considered in the design of structures;

f. The Strouhal number for smooth cylinders varies with the Reynolds and Keulegan-Carpenter numbers. For rough cylinders, it is essentially constant;

g. The results reported herein and the conclusions arrived at are applicable only to cylinders in harmonic flow with zero mean velocity. The force coefficients for harmonic flow with a mean velocity superposed on it may differ significantly from those reported herein;

h. It is hoped that the data presented will accentuate the need for actual full scale experiments and enable those concerned to interpret and better understand the factors affecting the force-transfer coefficients in the ocean environment.

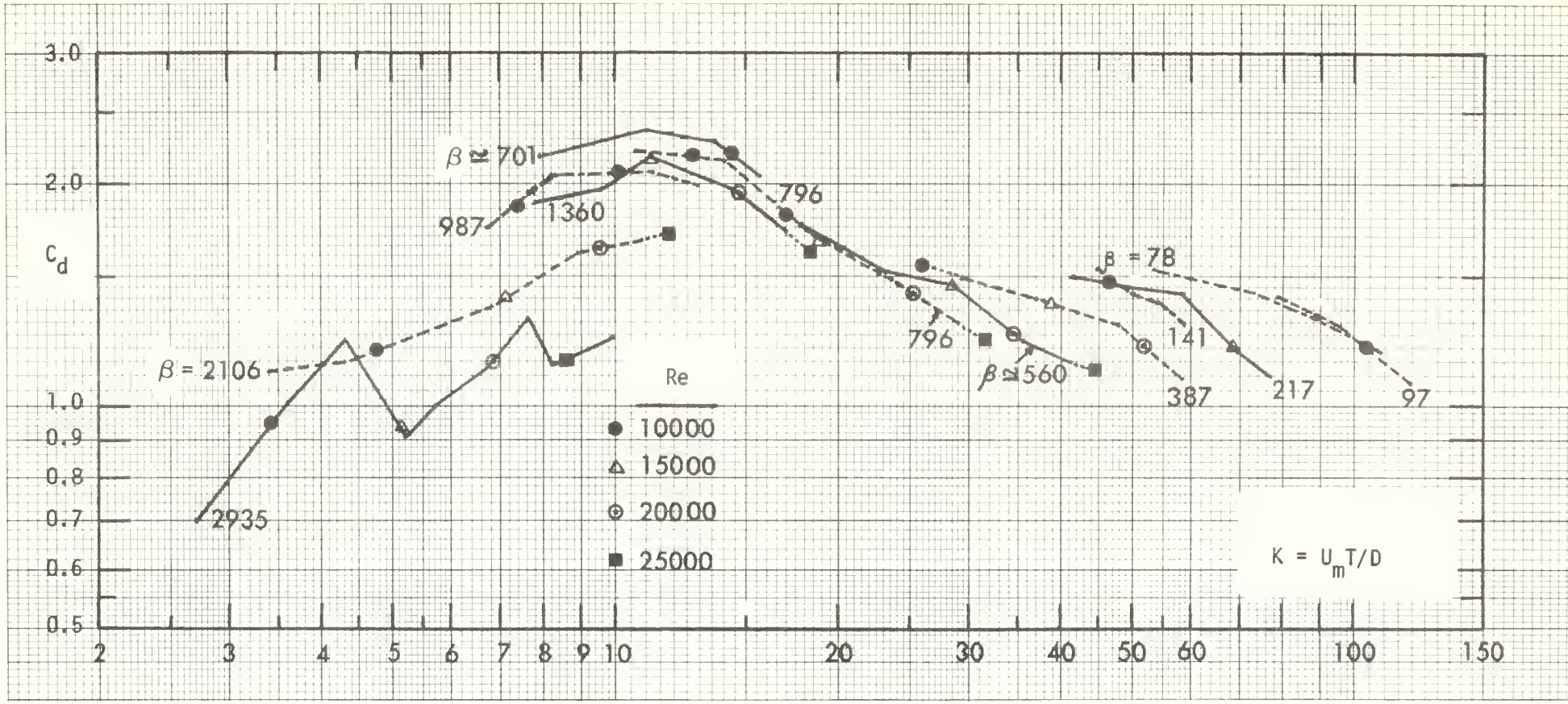

Fig. 1 C_d versus K for various values of β, (Keulegan-Carpenter data [6]).

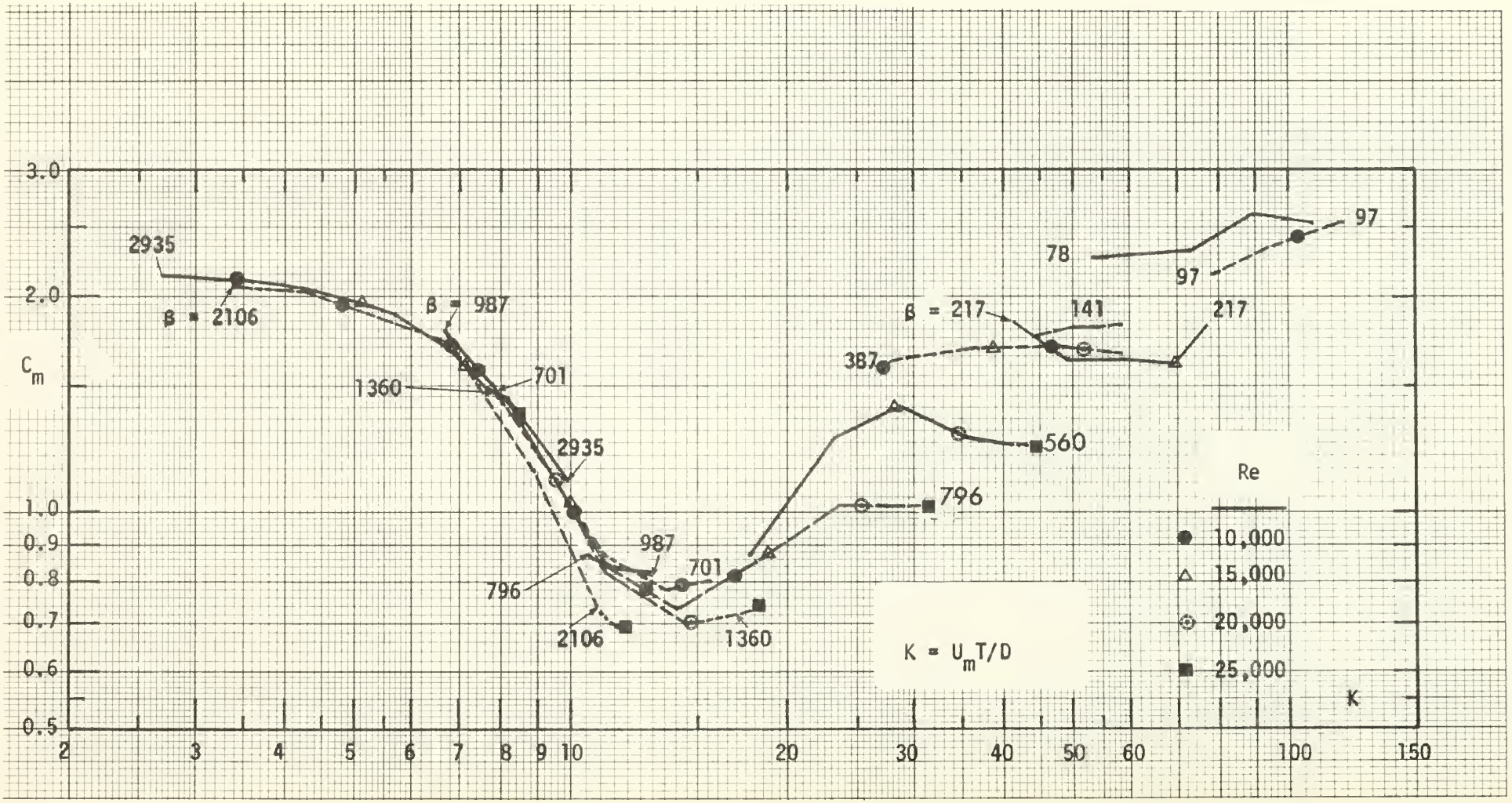

Fig. 2 C_m versus K for various values of β, (Keulegan-Carpenter data [6]).

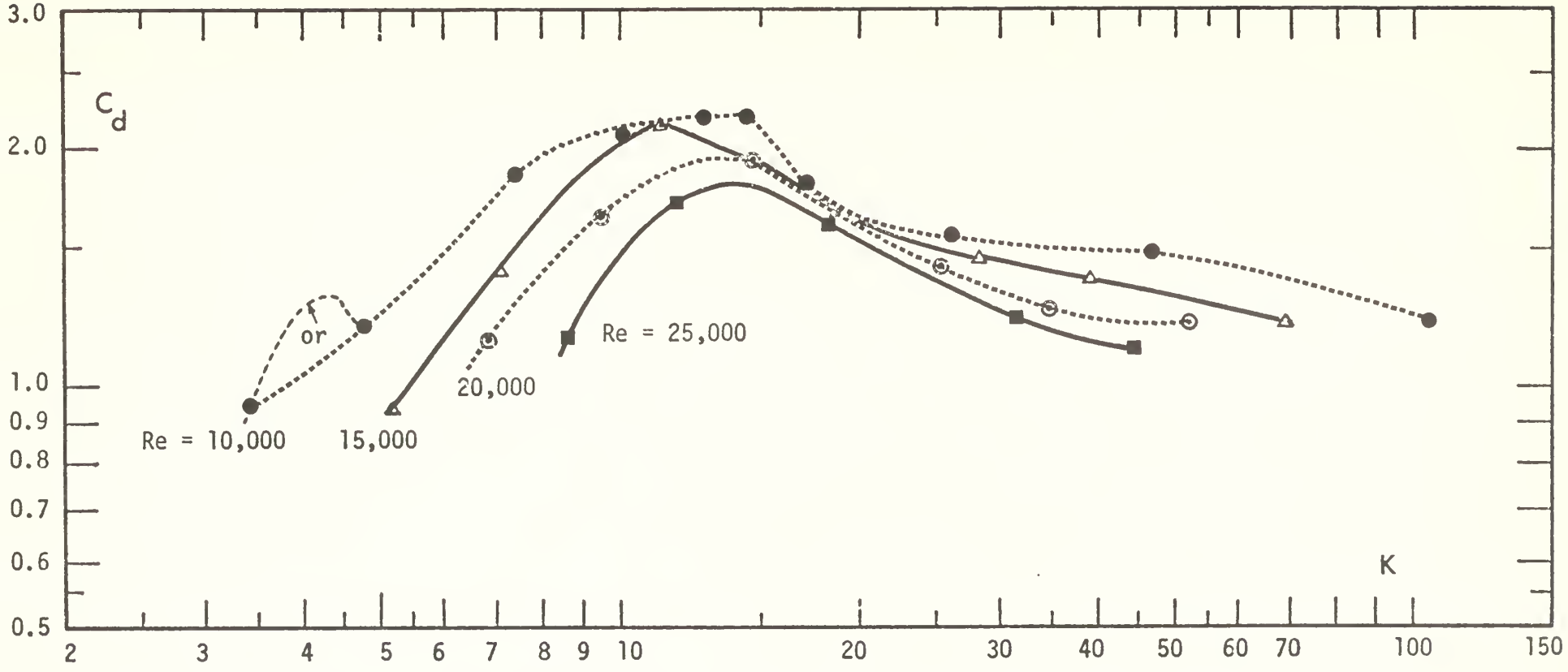

Fig. 3 C_d versus K for various values of Re, (Keulegan-Carpenter data [6])

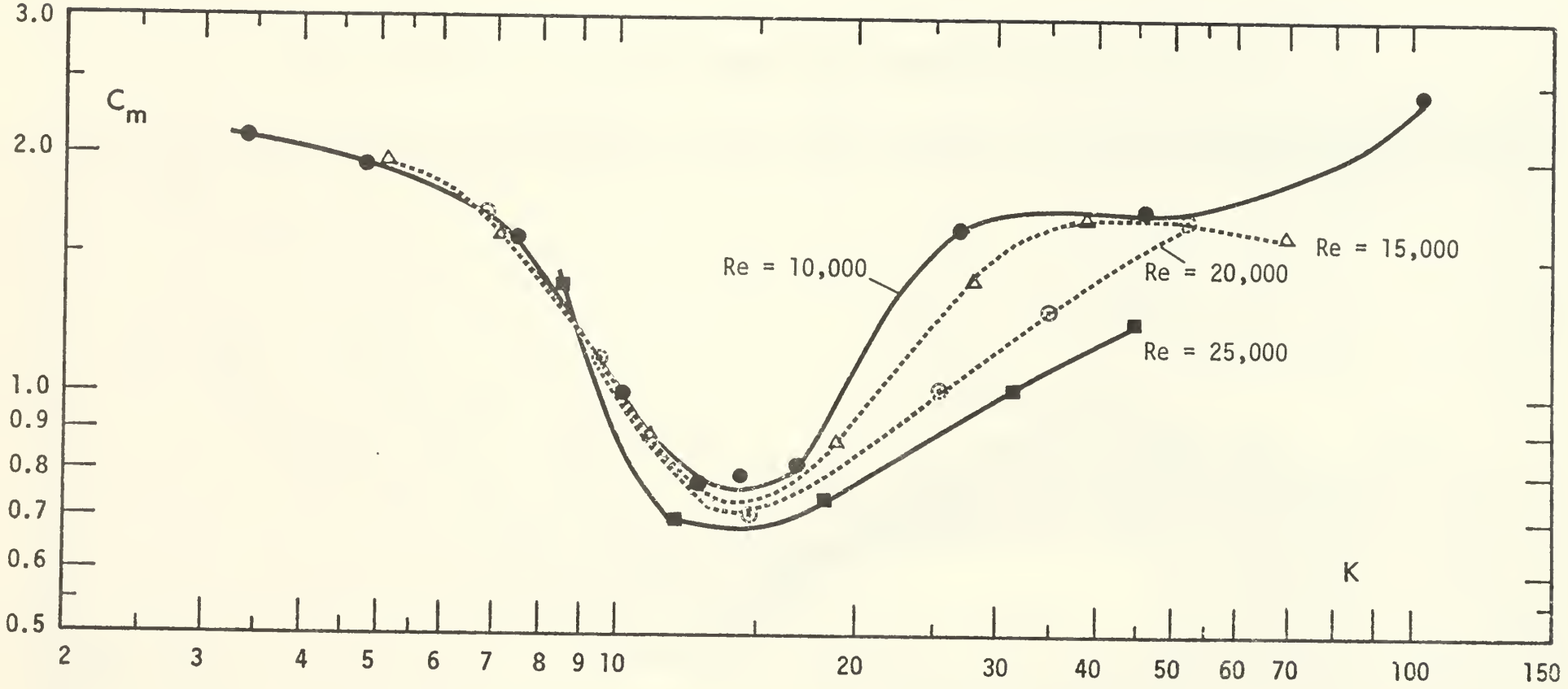

Fig. 4 C_m versus K for various values of Re, (Keulegan-Carpenter data [6])

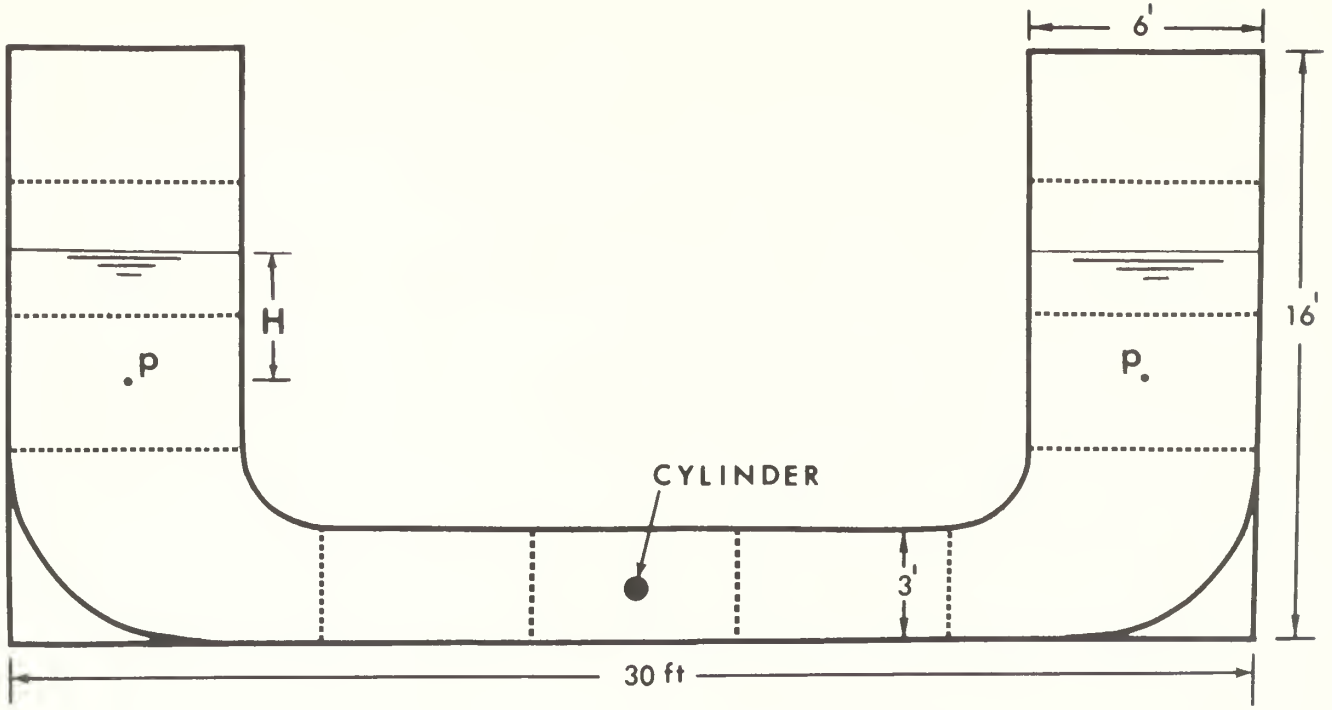

Fig. 5 Schematic drawing of the U-shaped vertical water tunnel.

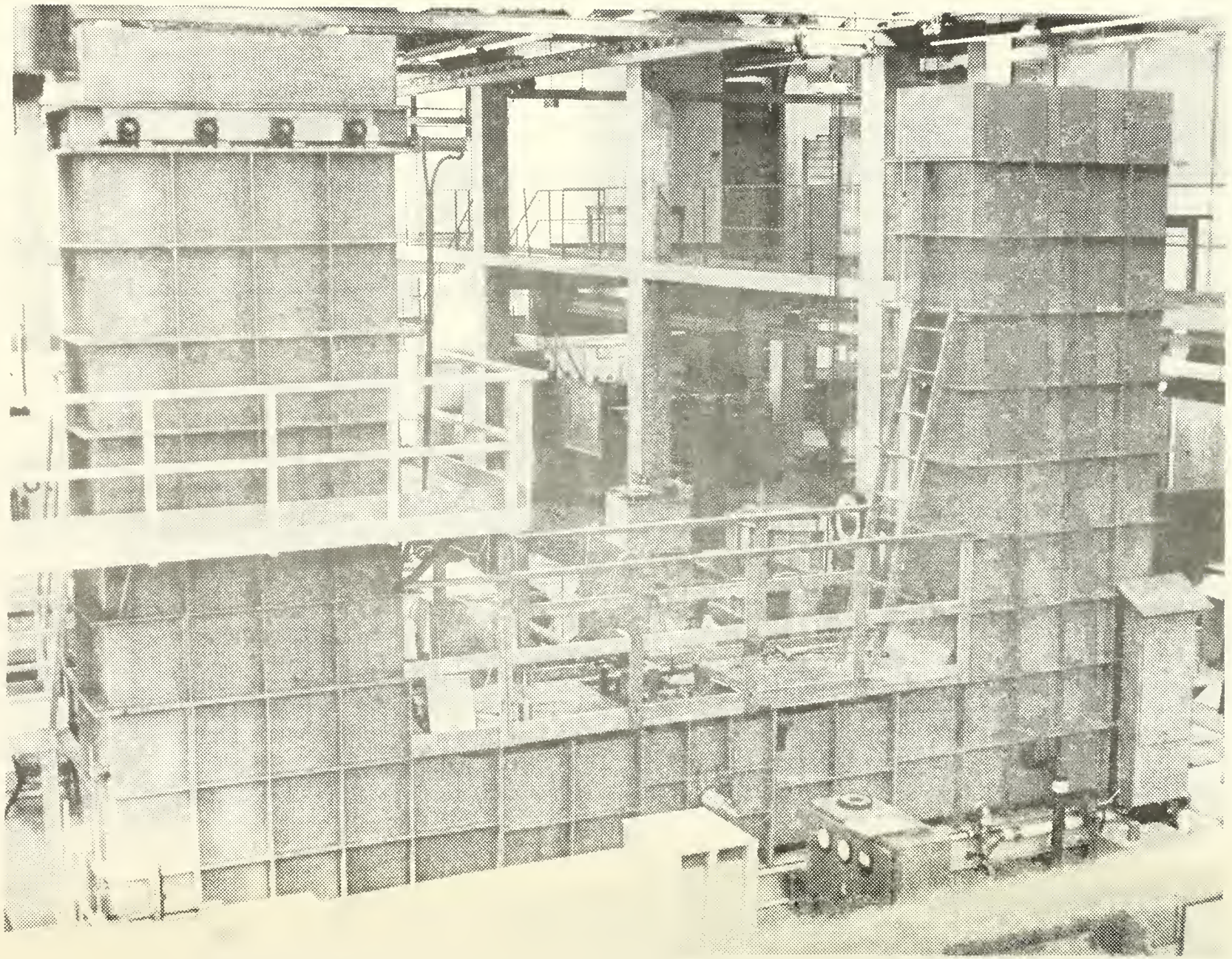

Fig. 6 A general view of the U-shaped vertical water tunnel

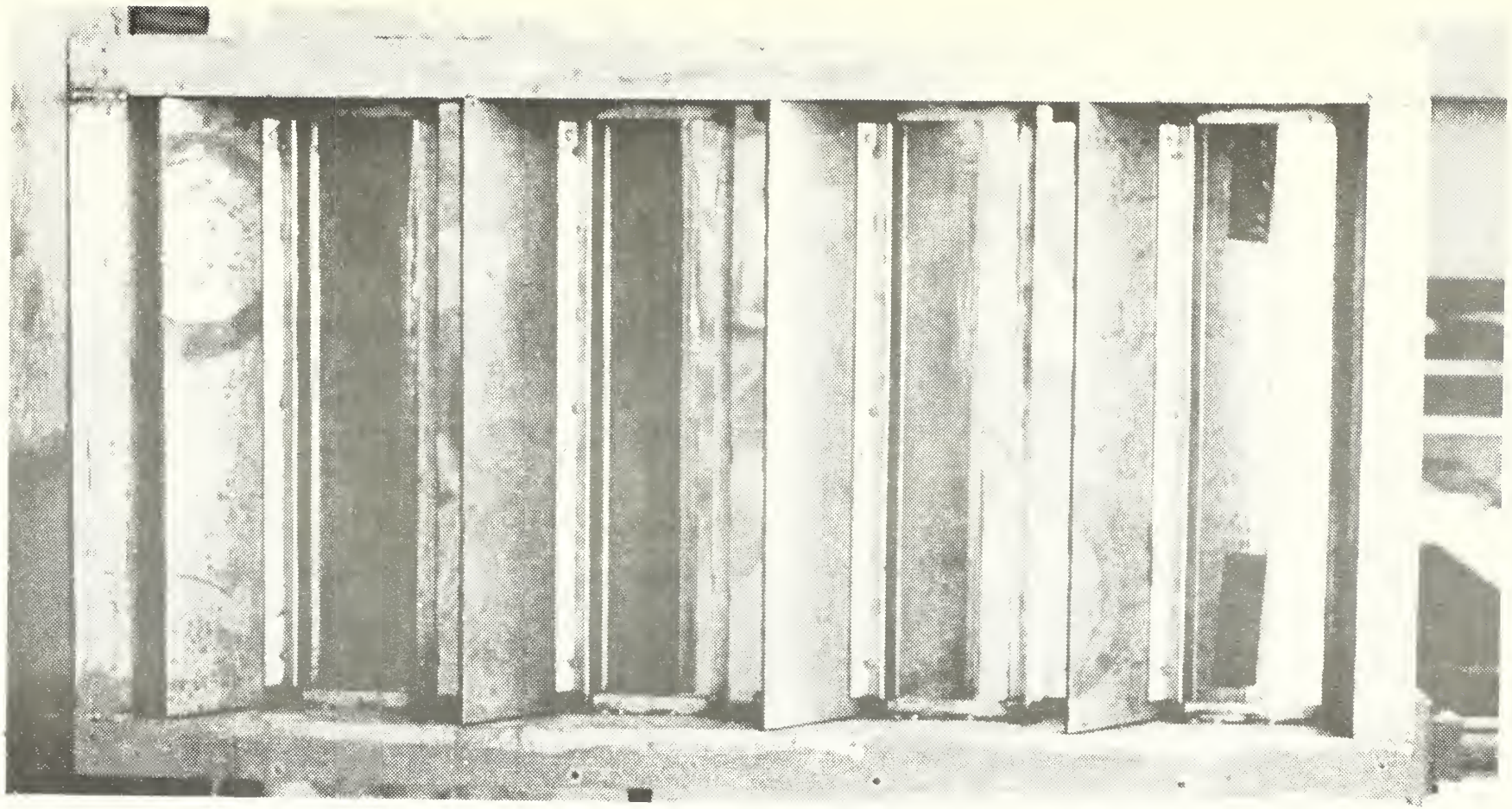

Fig. 7 Butterfly-valve assembly

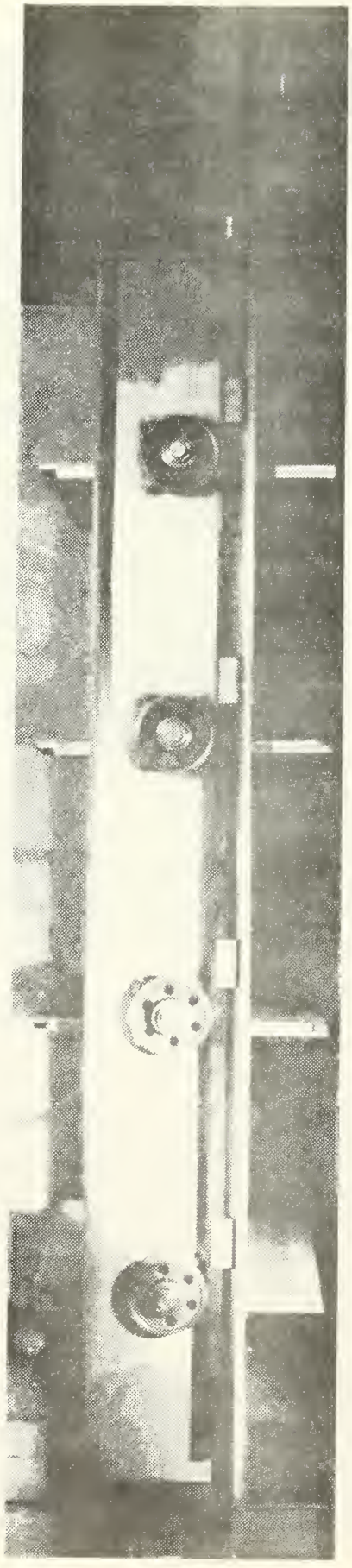

Fig. 8 Rack and pinion drive system

CAP. (LBS)	100	250	500	1000	1250
CAT. NO.	425185	420270	420271	420272	420269

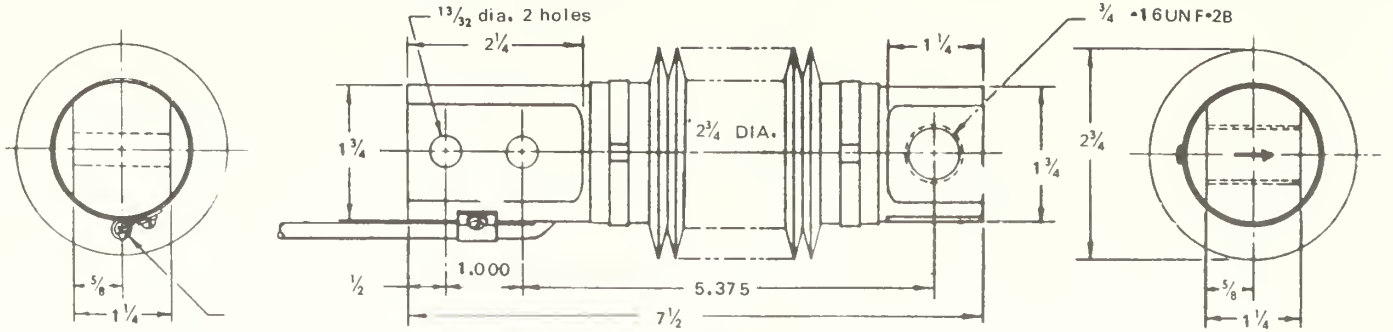

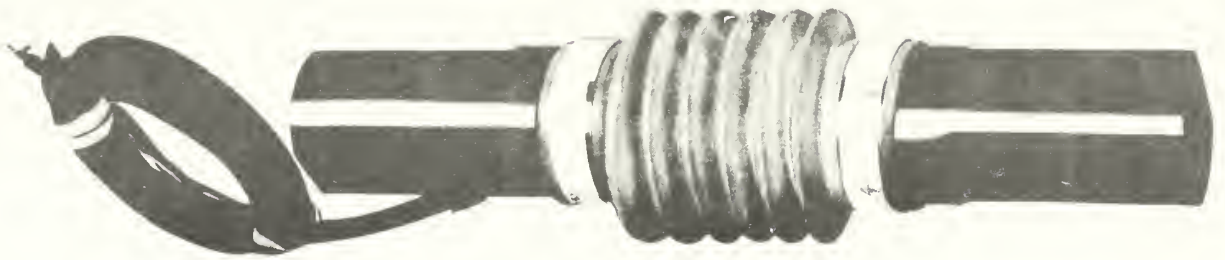

Fig. 9 Force transducer

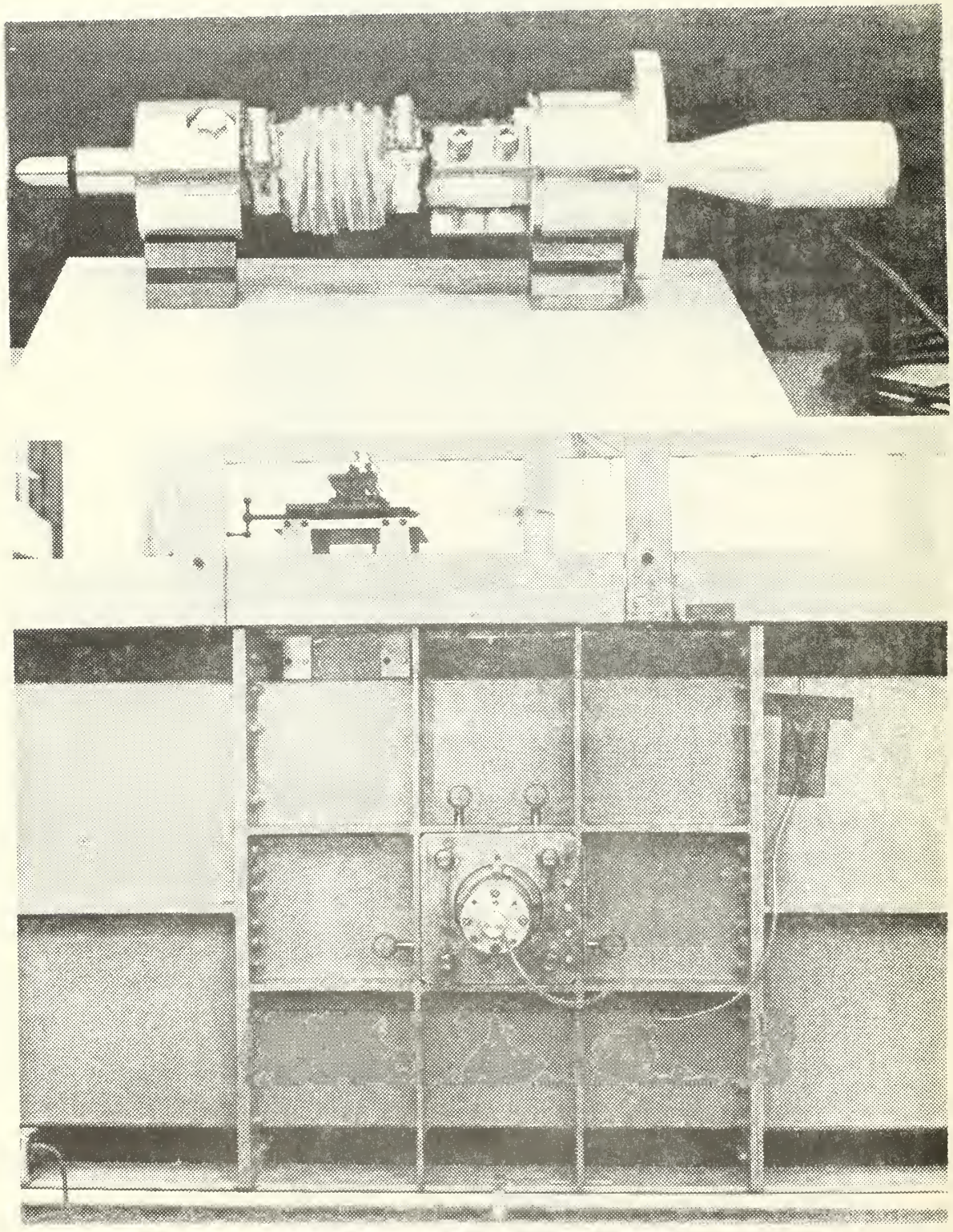

Fig. 10 Assembled force transducer

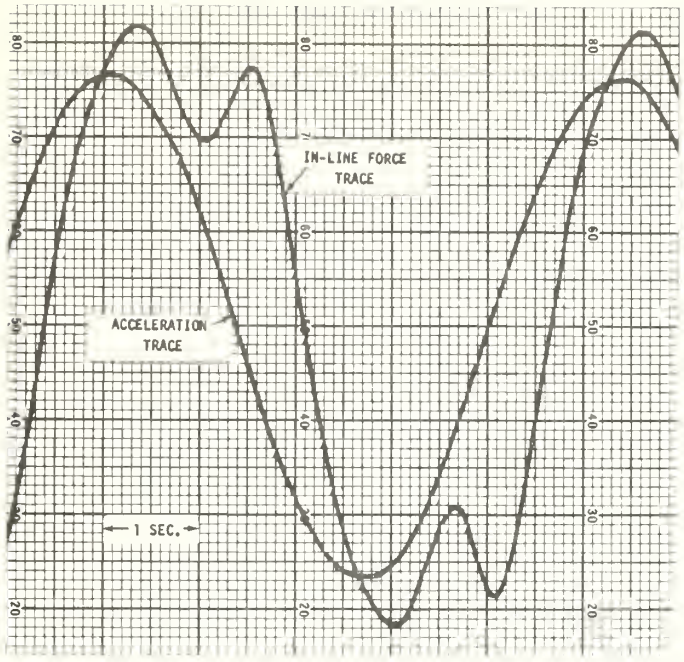

Fig. 11 In-line force and acceleration traces

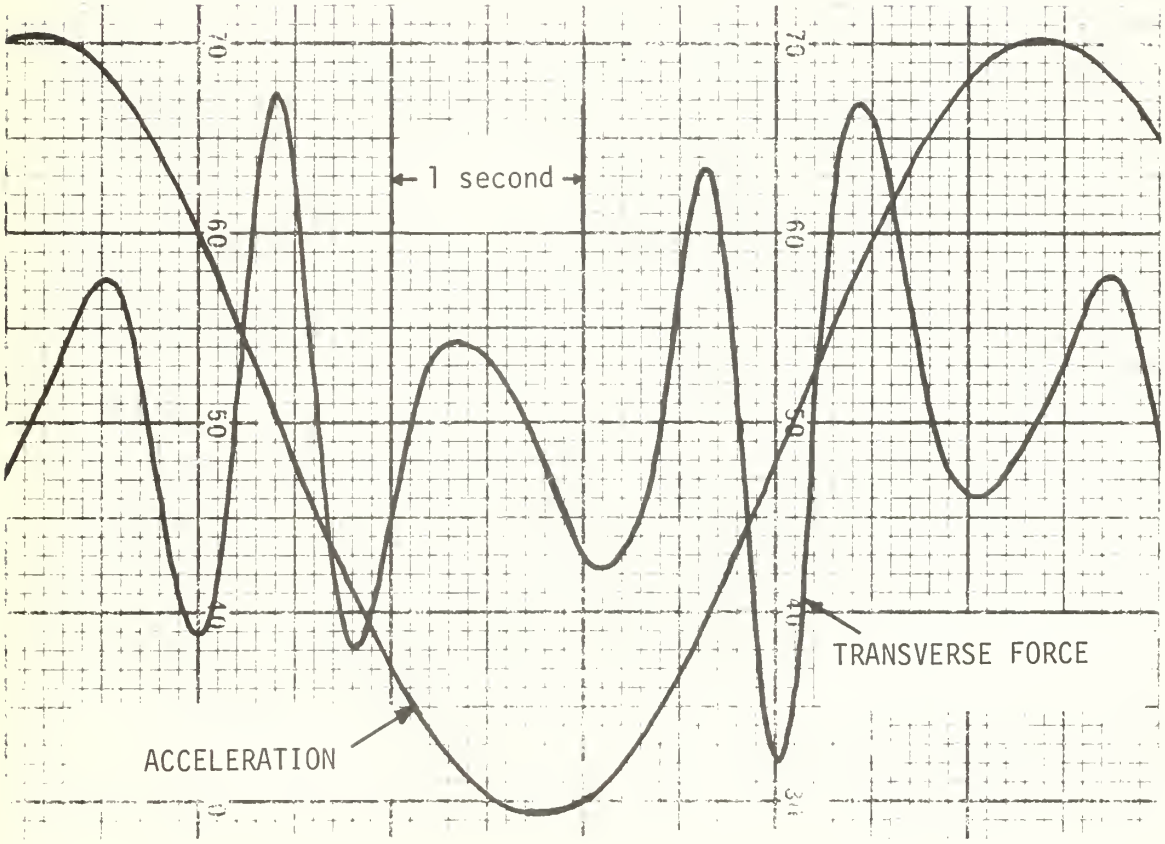

Fig. 12 Transverse force and acceleration traces

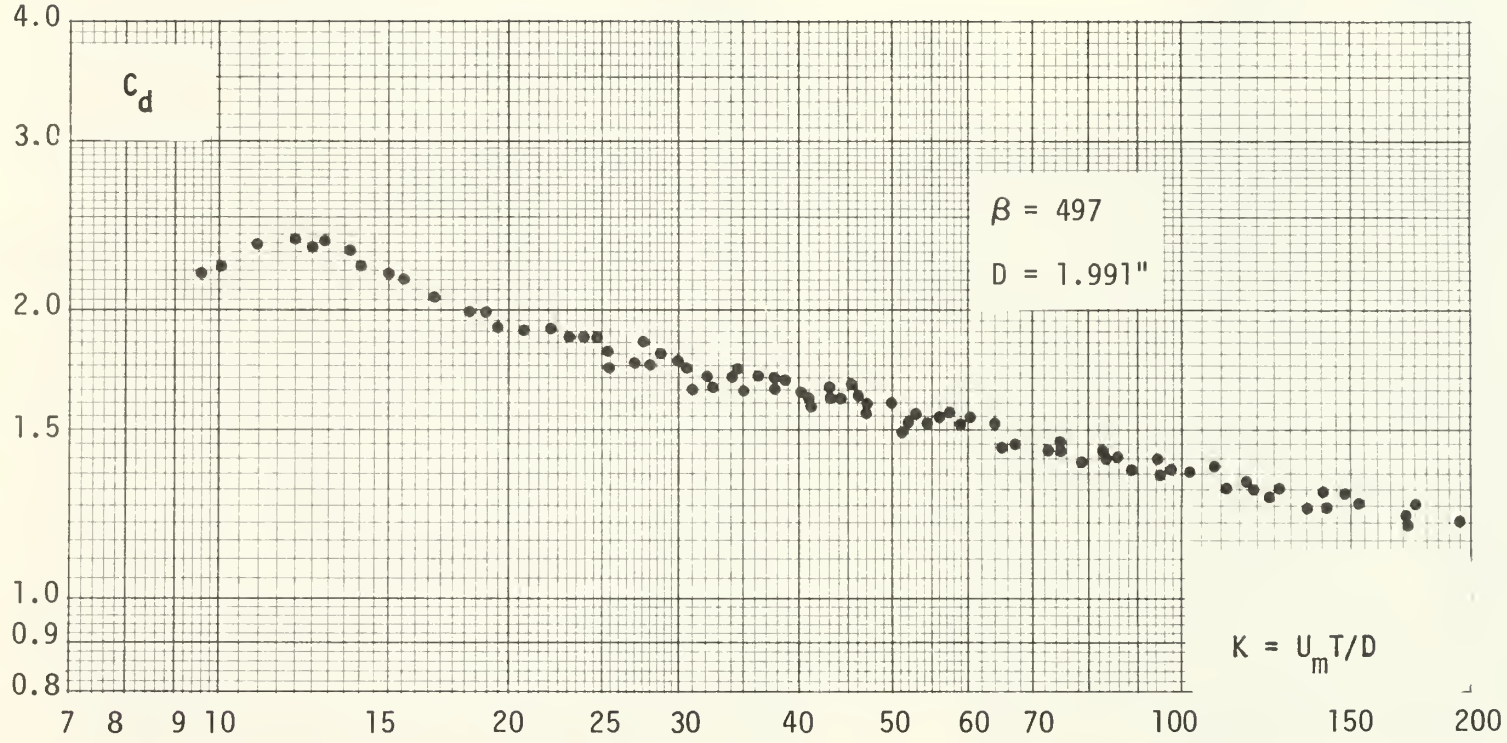

Fig. 13 C_d versus K for β = 497

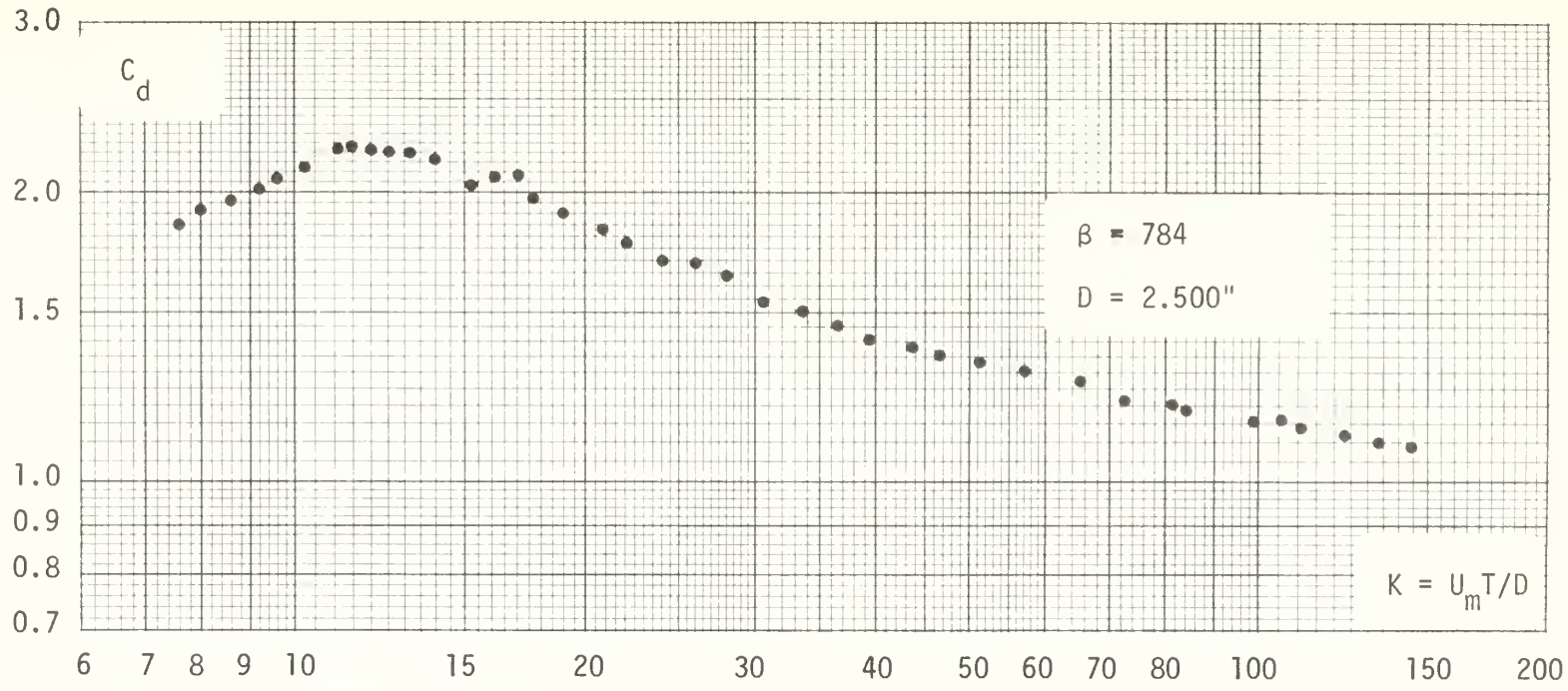

Fig. 14 C_d versus K for β = 784

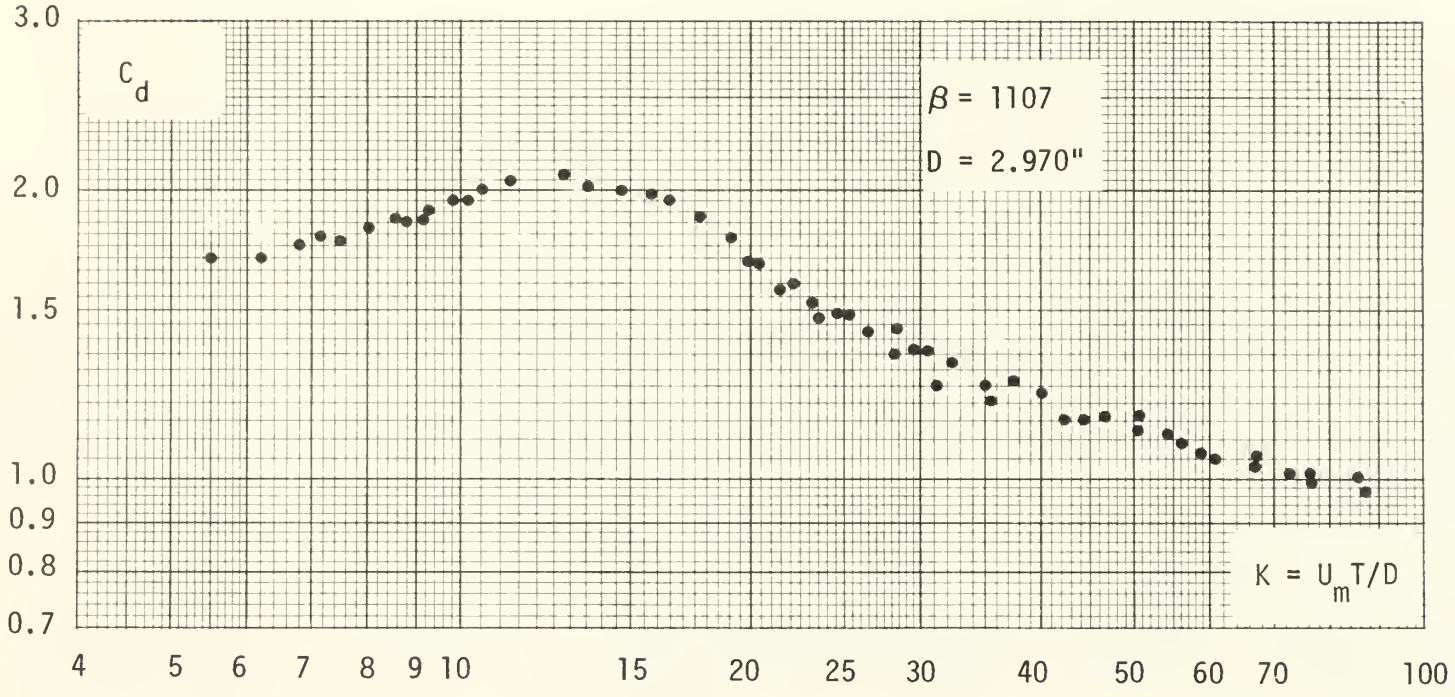

Fig. 15 C_d versus K for β = 1107

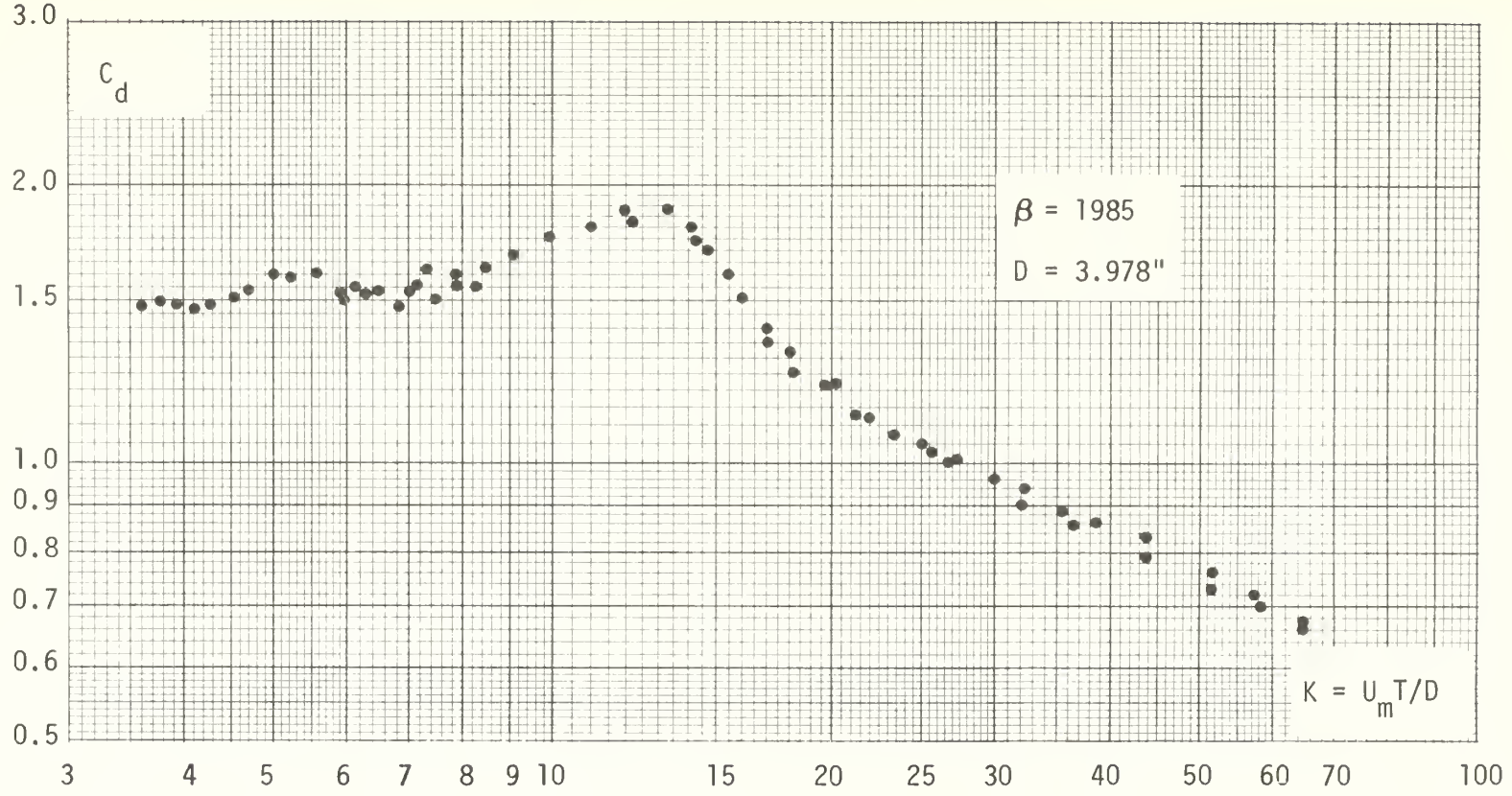

Fig. 16 C_d versus K for β = 1985

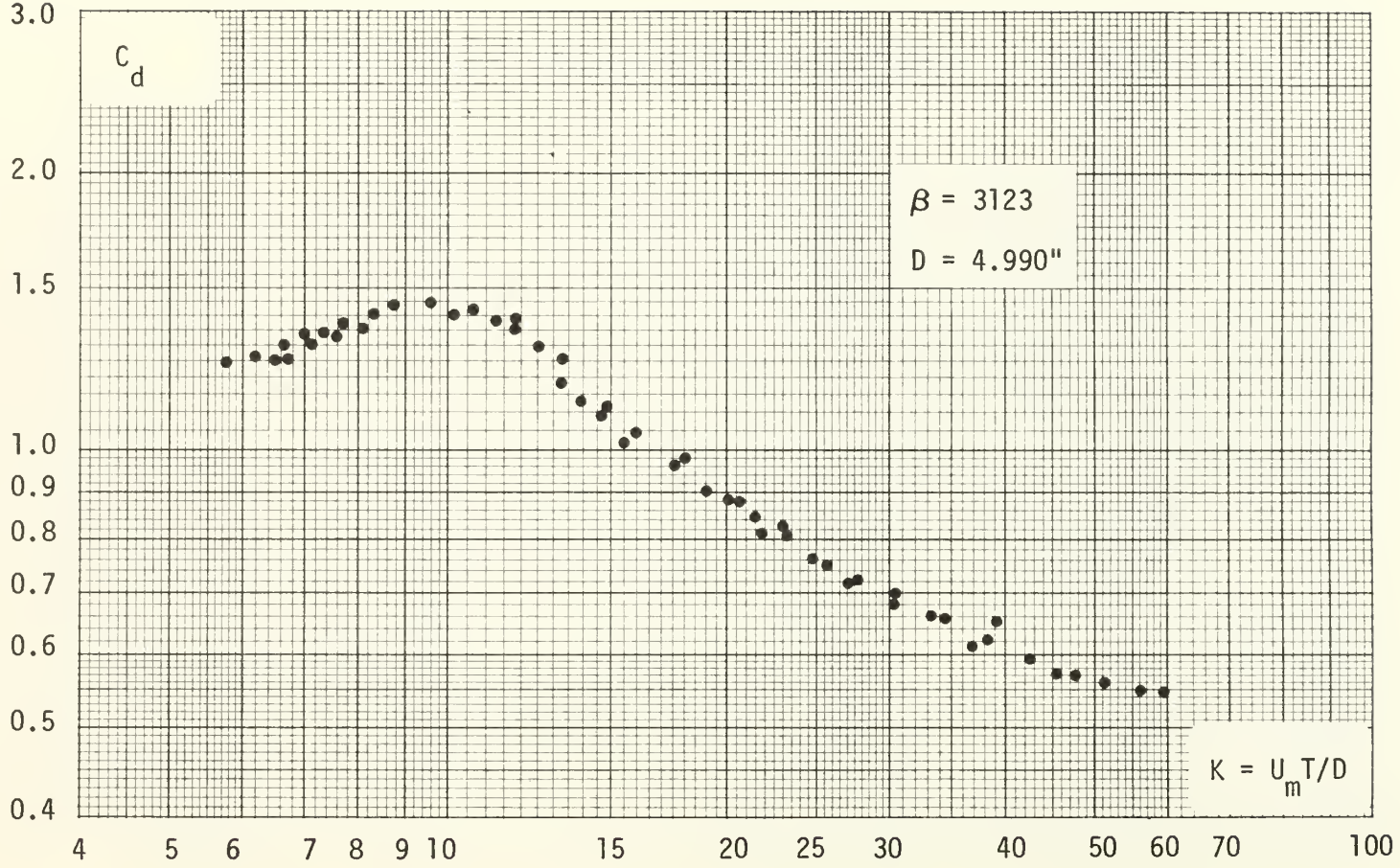

Fig. 17 C_d versus K for β = 3123

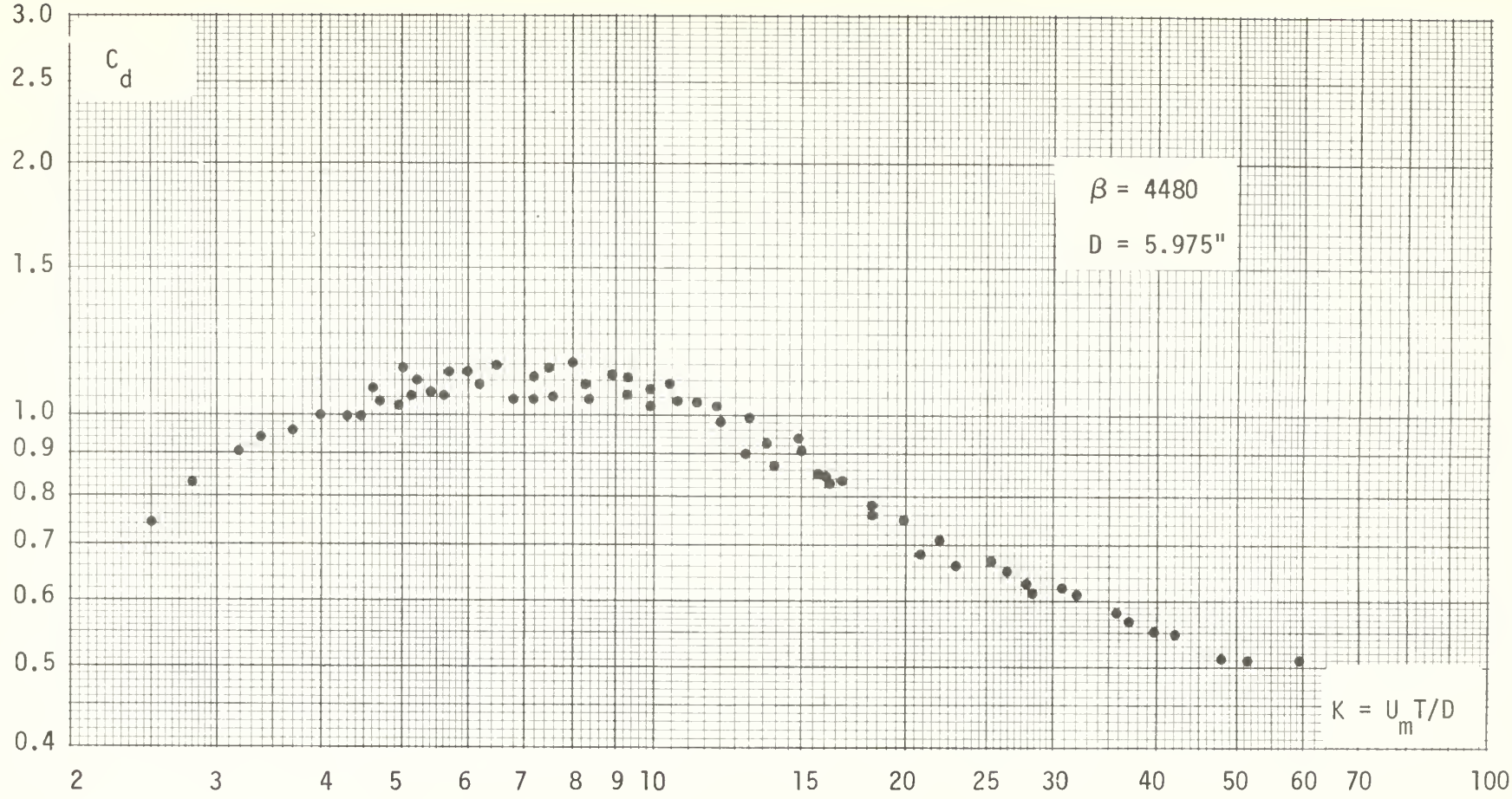

Fig. 18 C_d versus K for β = 4480

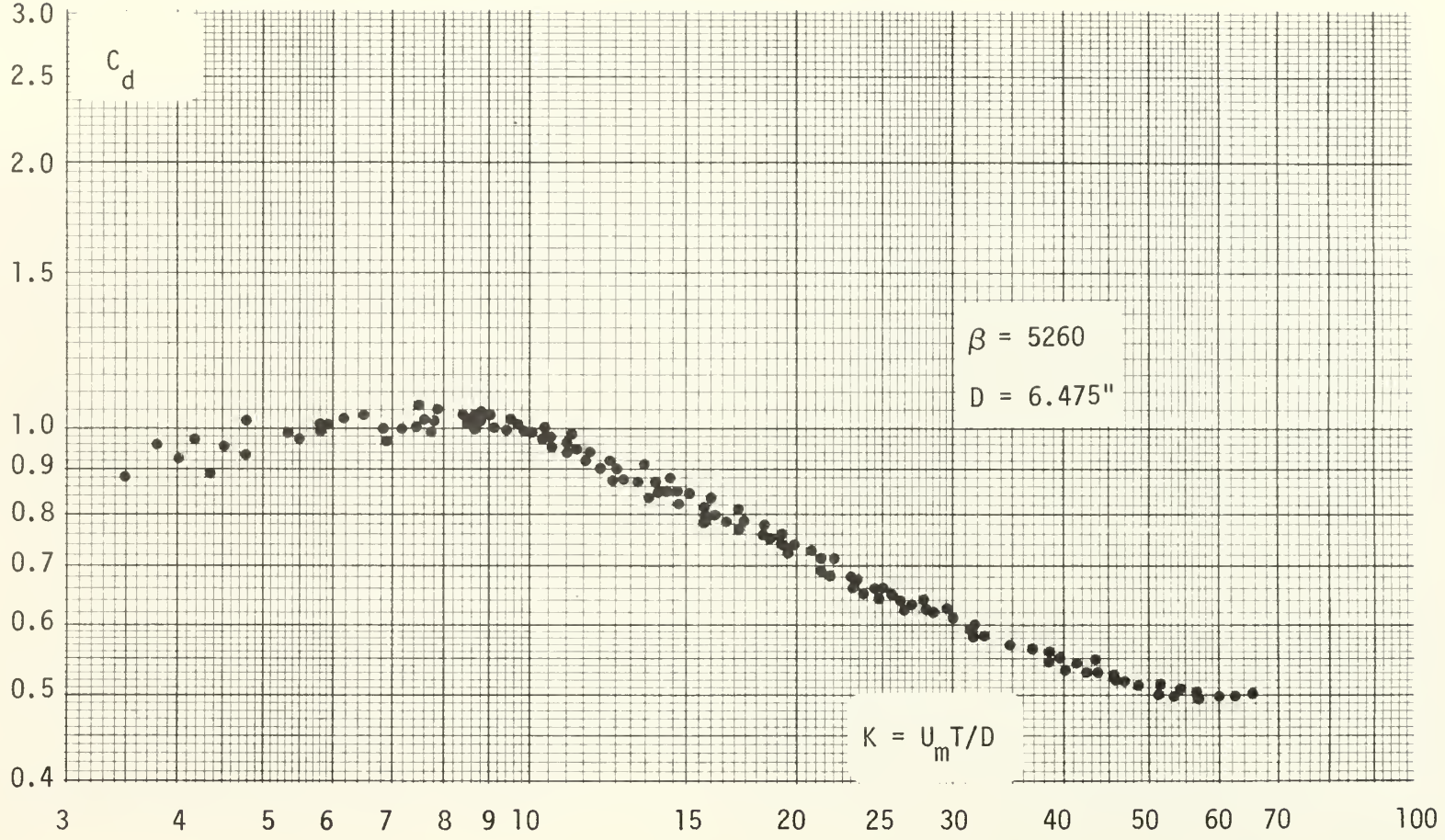

Fig. 19 C_d versus K for β = 5260

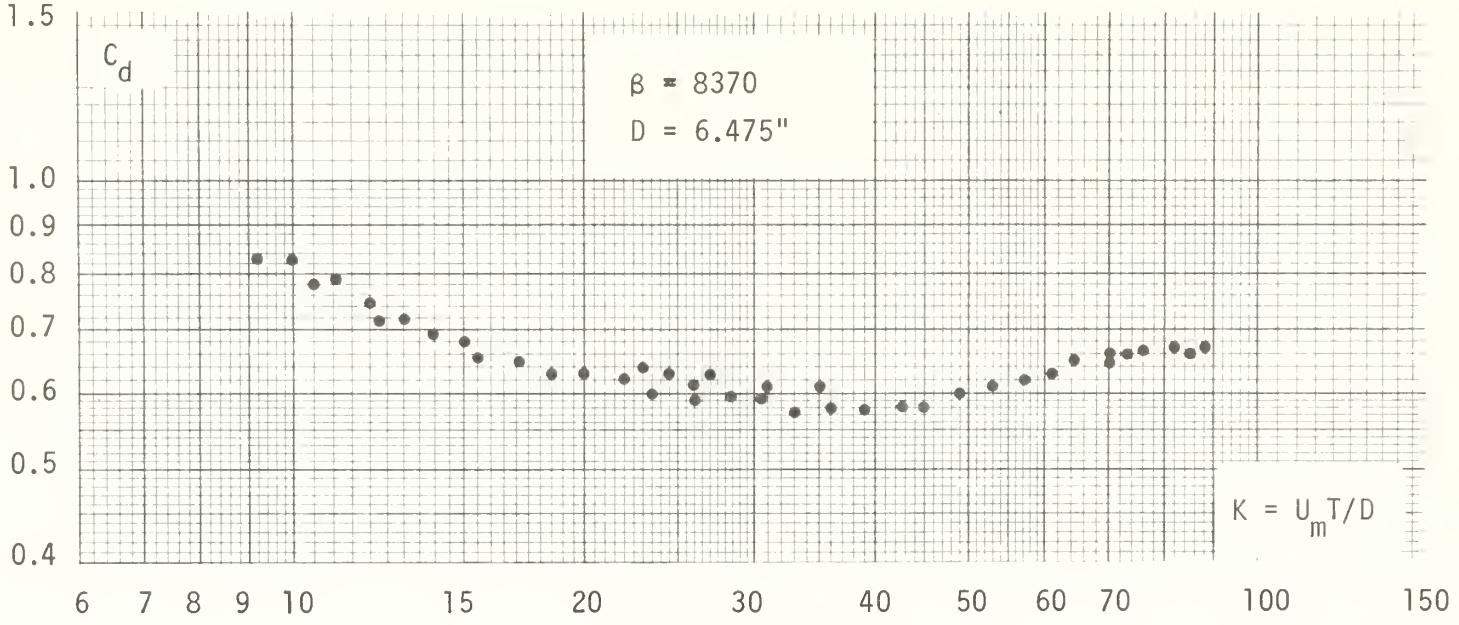

Fig. 20 C_d versus K for β = 8370

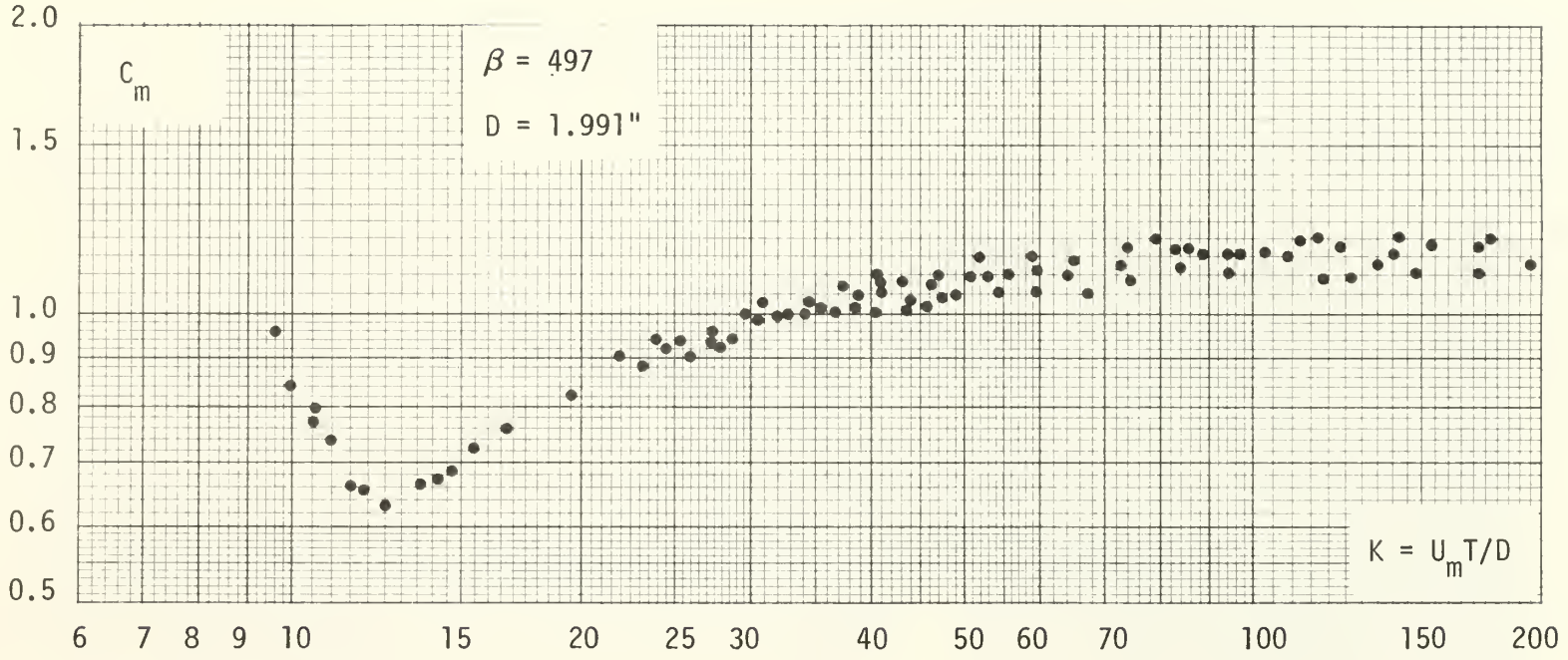

Fig. 21 C_m versus K for β = 497

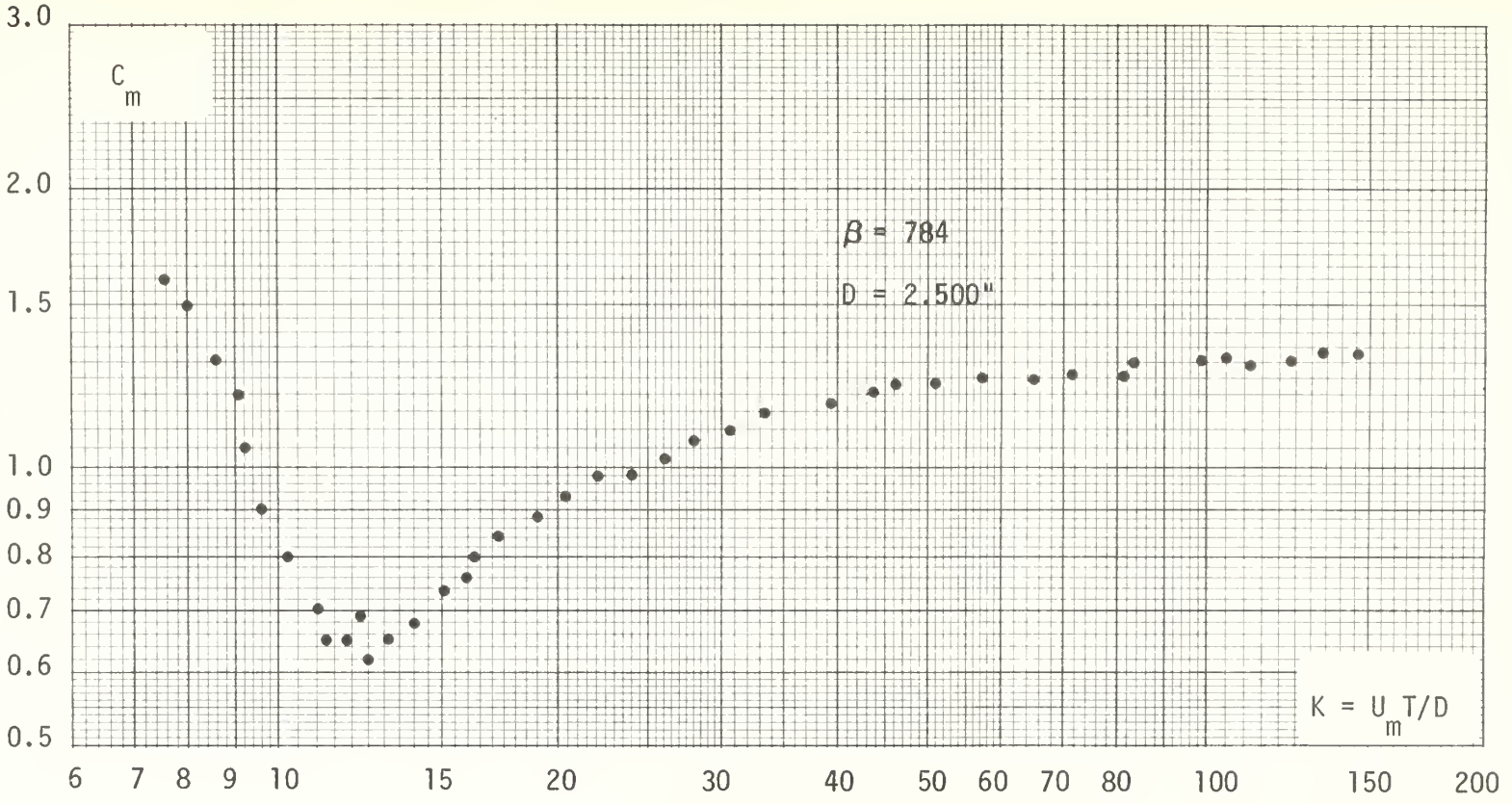

Fig. 22 C_m versus K for $\beta = 784$

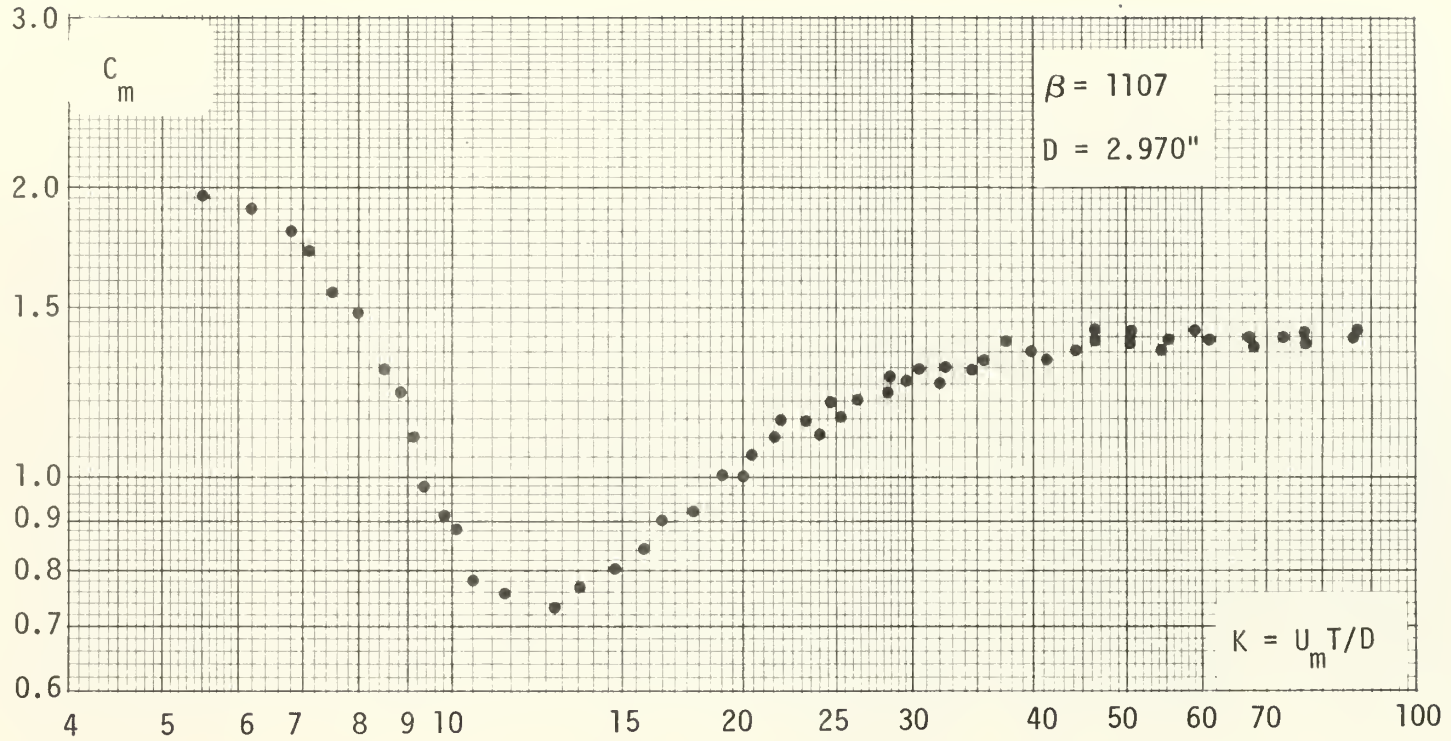

Fig. 23 C_m versus K for β = 1107

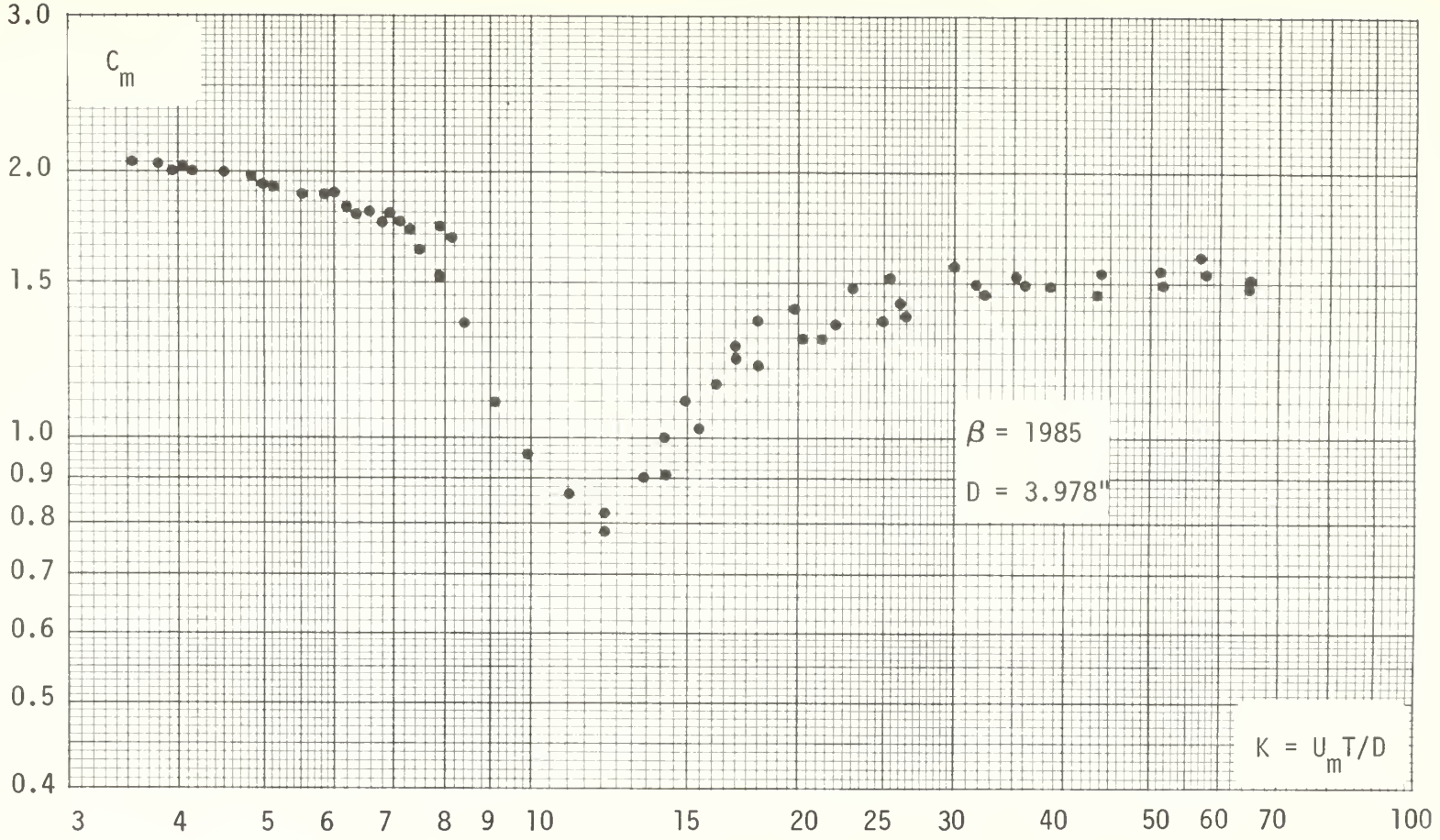

Fig. 24 C_m versus K for β = 1985

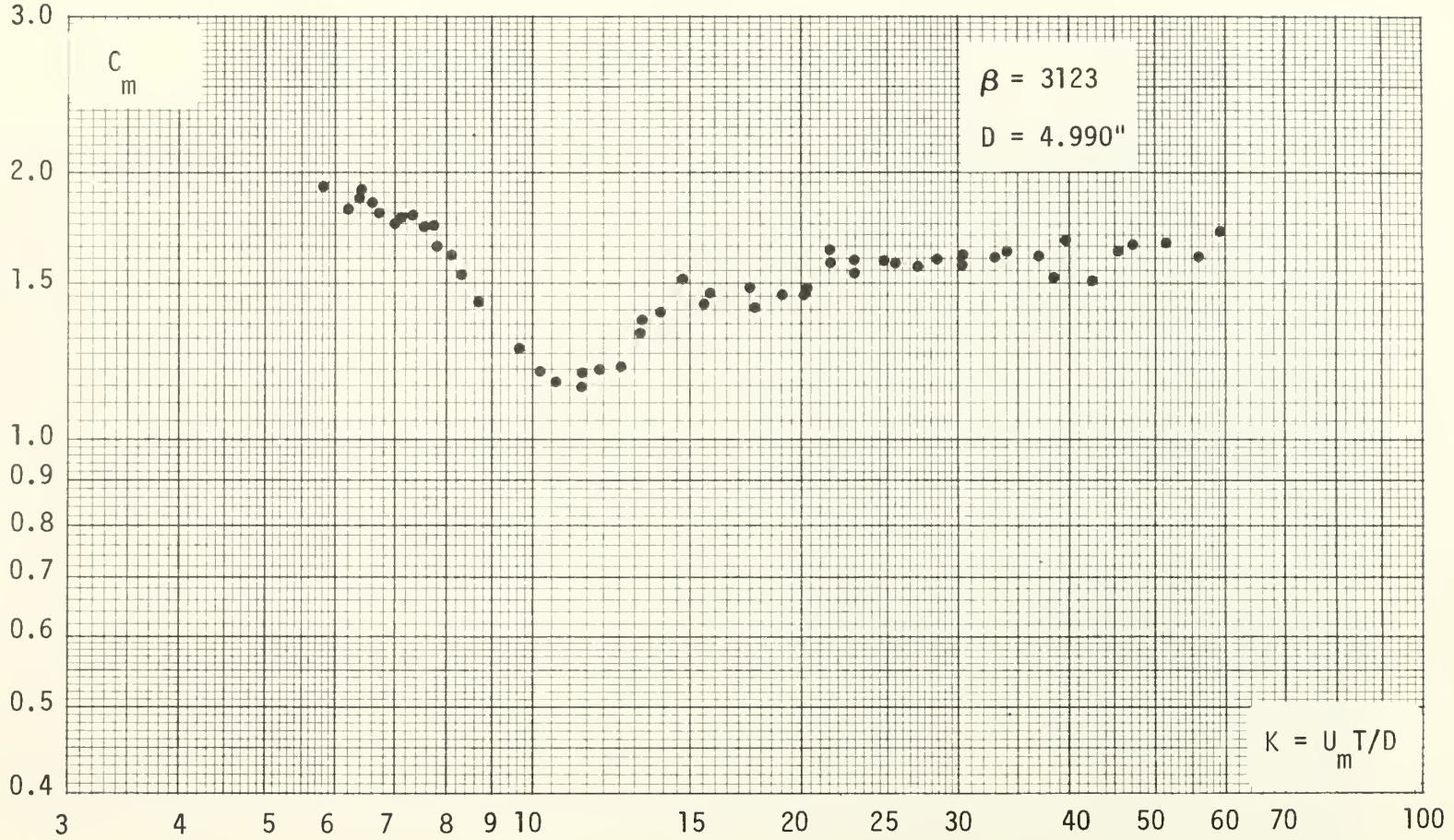

Fig. 25 C_m versus K for β = 3123

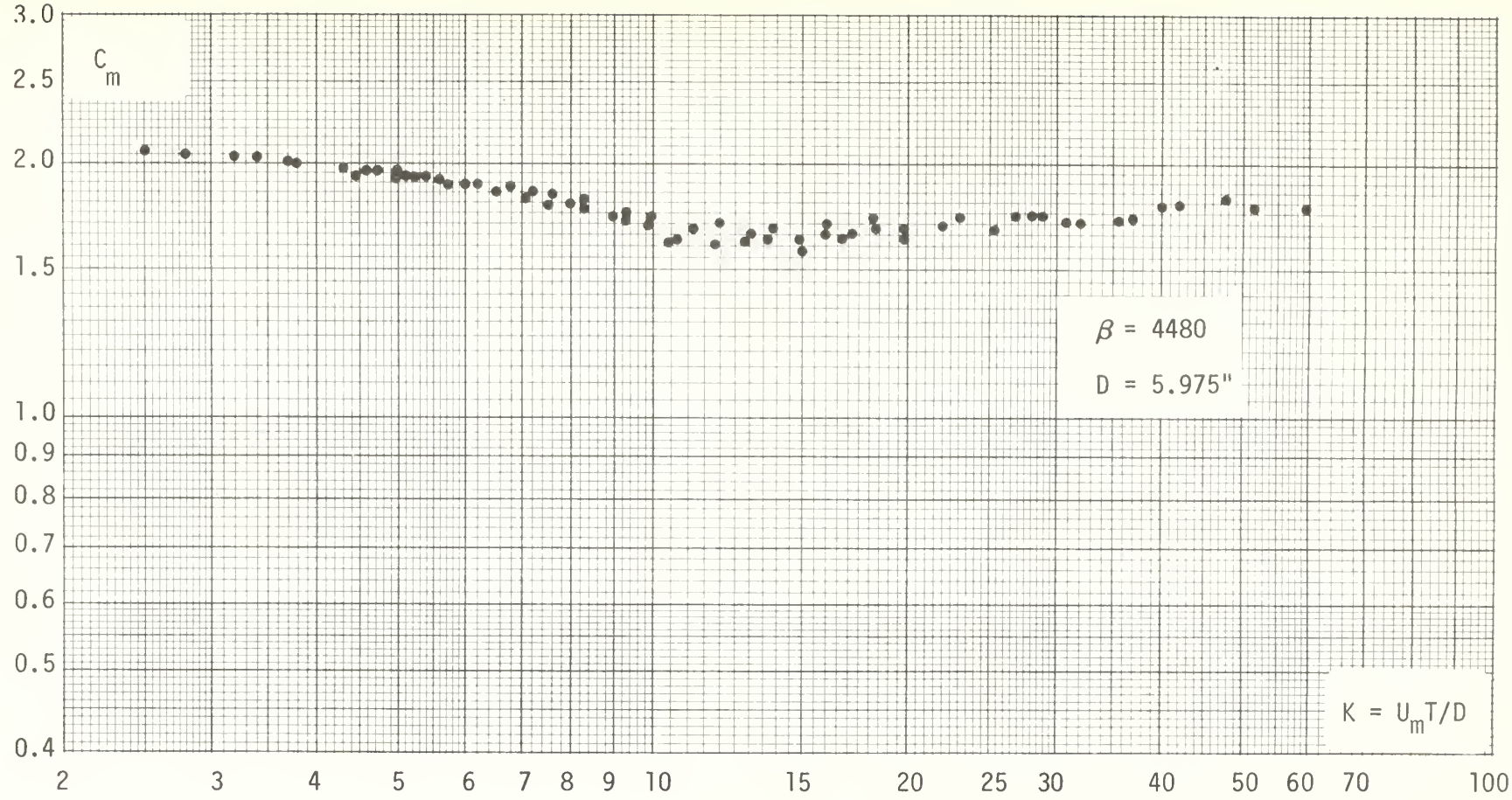

Fig. 26 C_m versus K for β = 4480

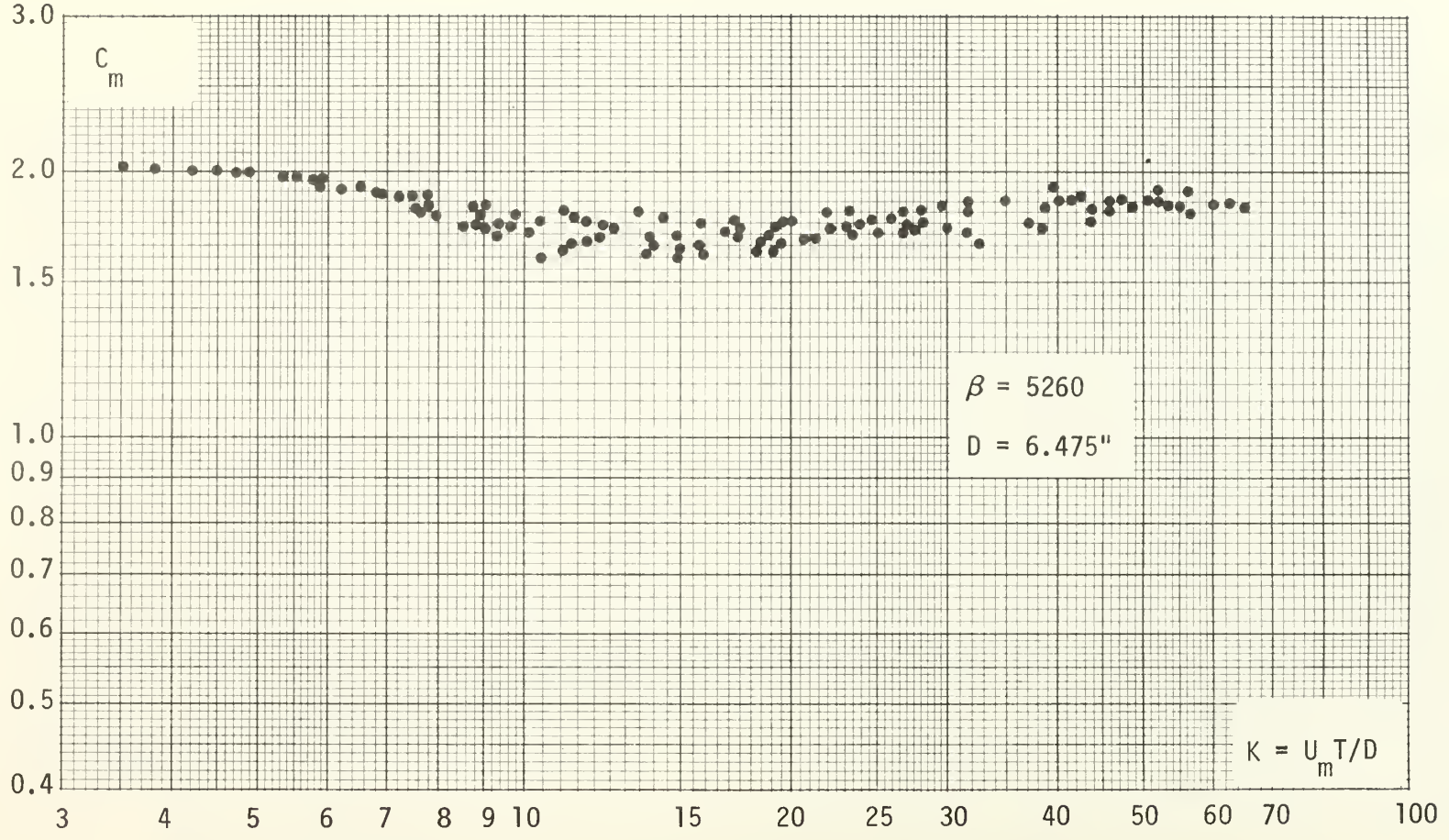

Fig. 27 C_m versus K for β = 5260

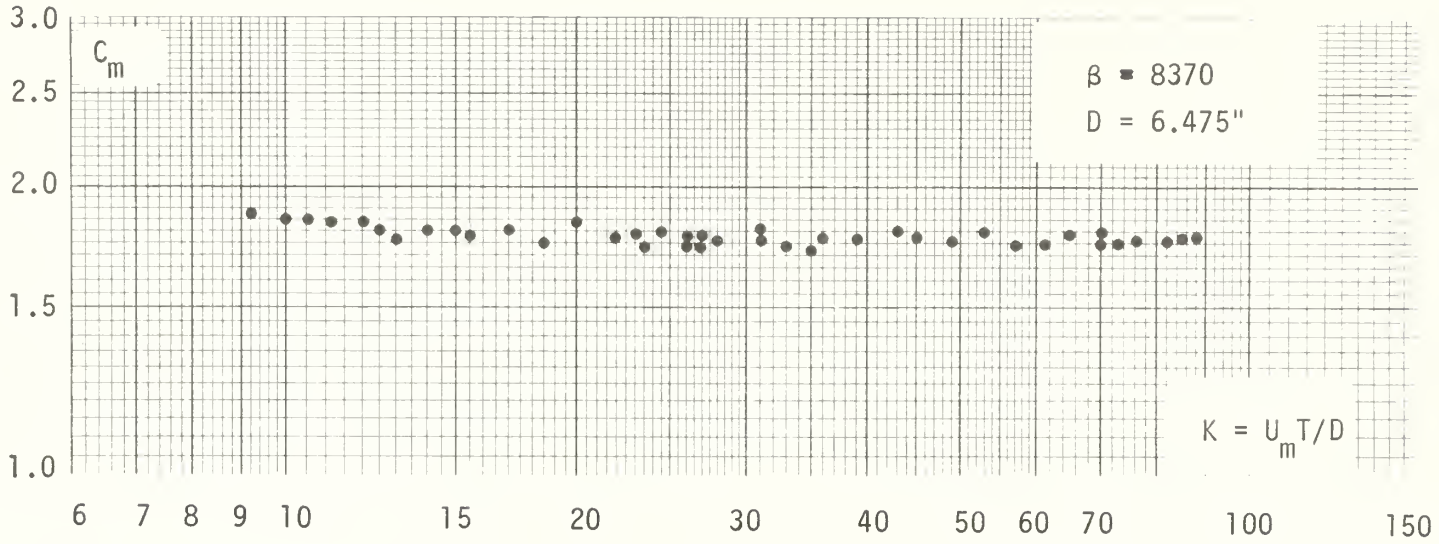

Fig. 28 C_m versus K for β = 8370

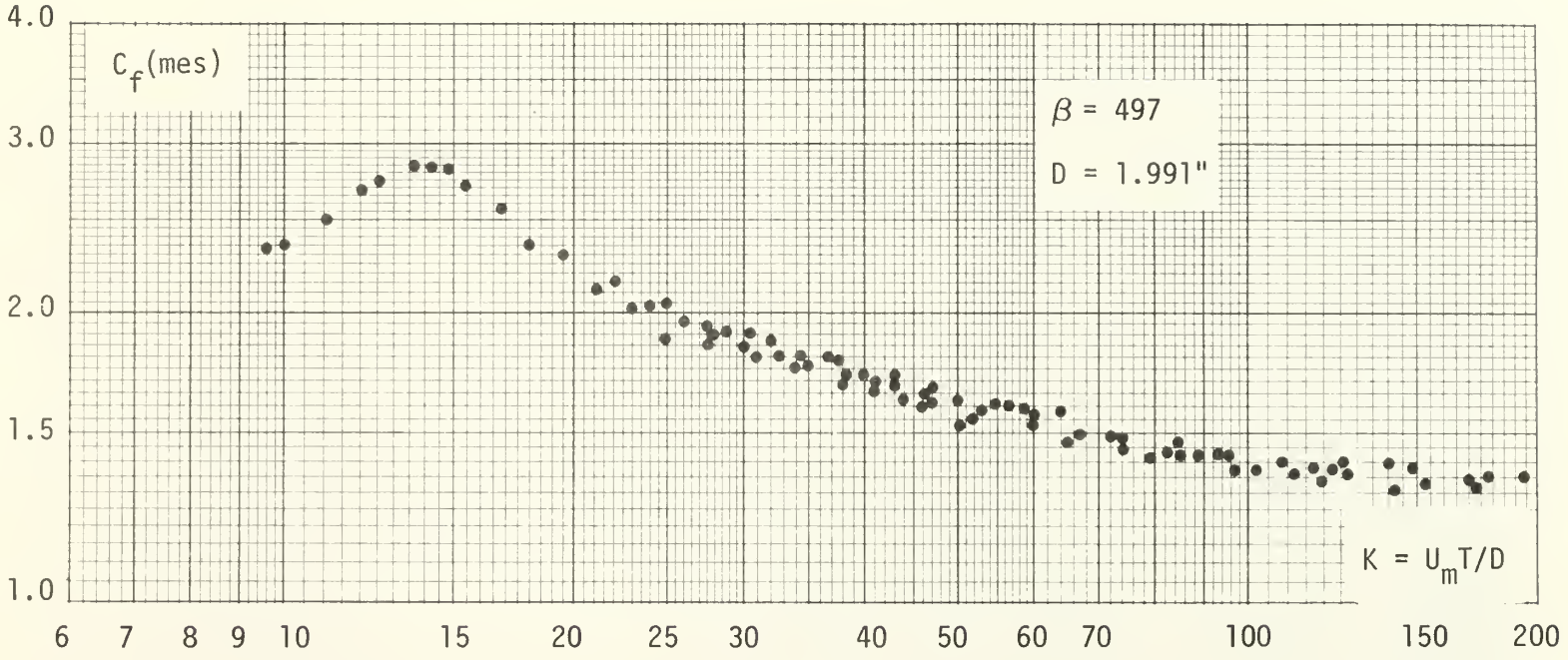

Fig. 29 C_f(mes) versus K for β = 497

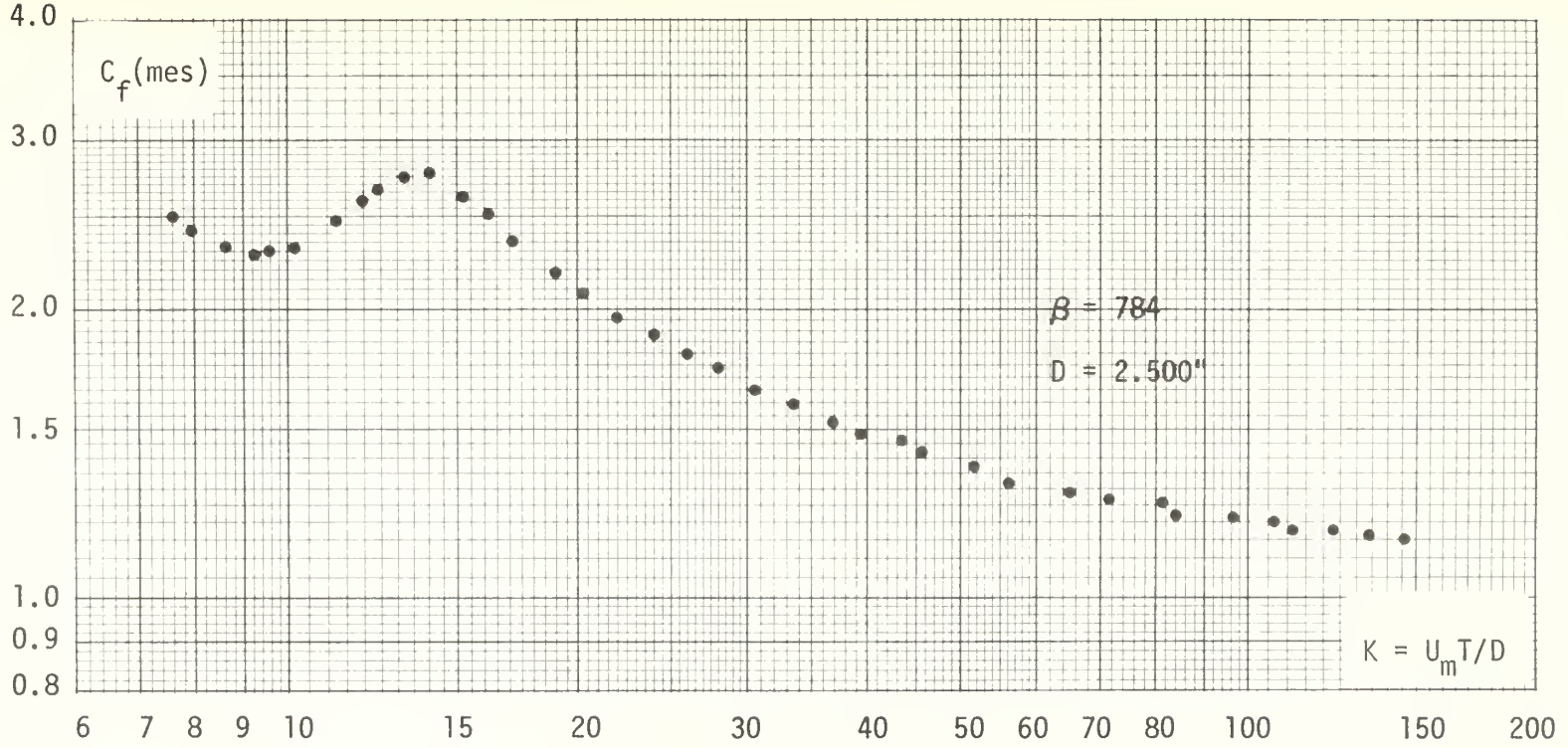

Fig. 30 C_f(mes) versus K for β = 784

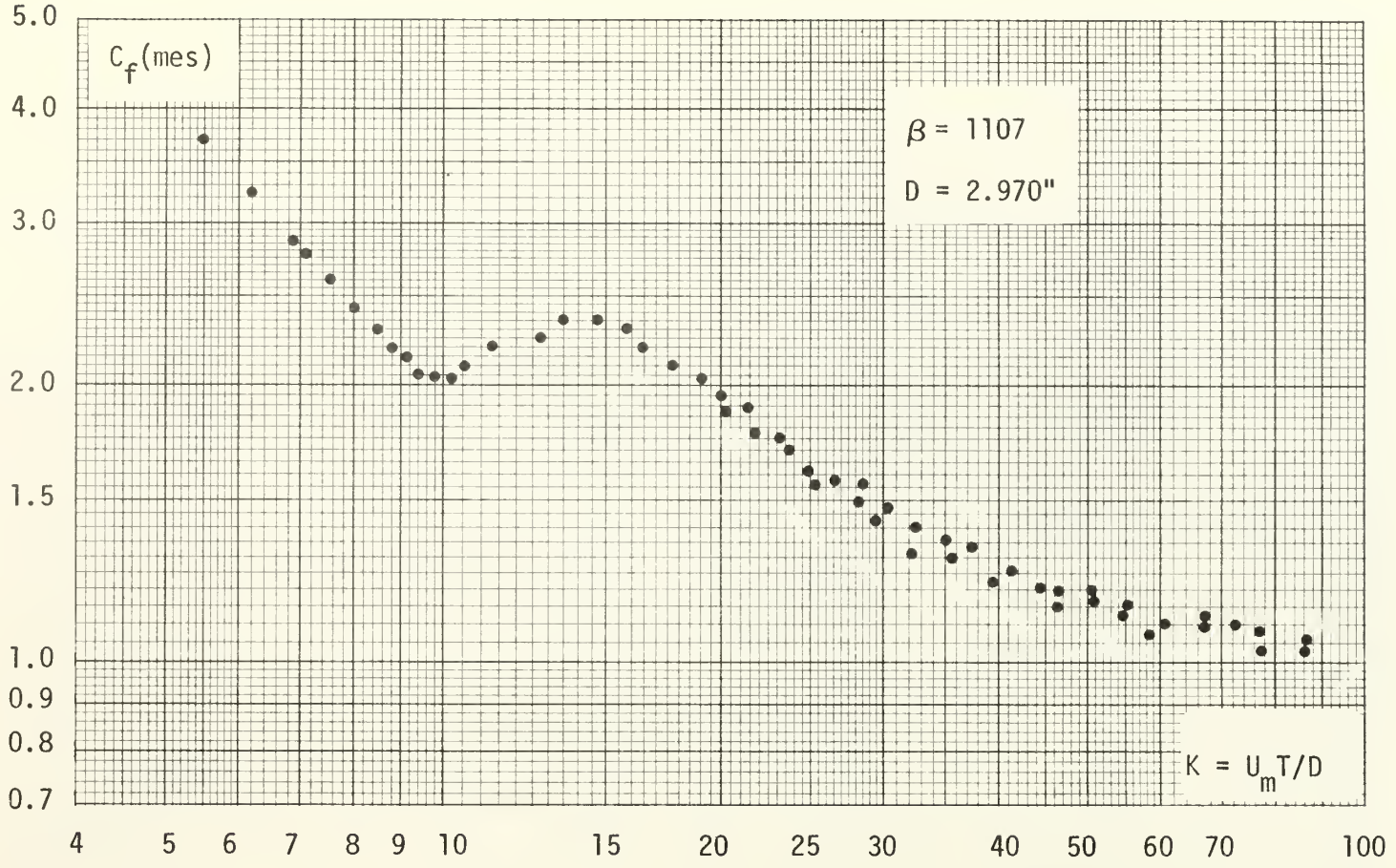

Fig. 31 C_f(mes) versus K for β = 1107

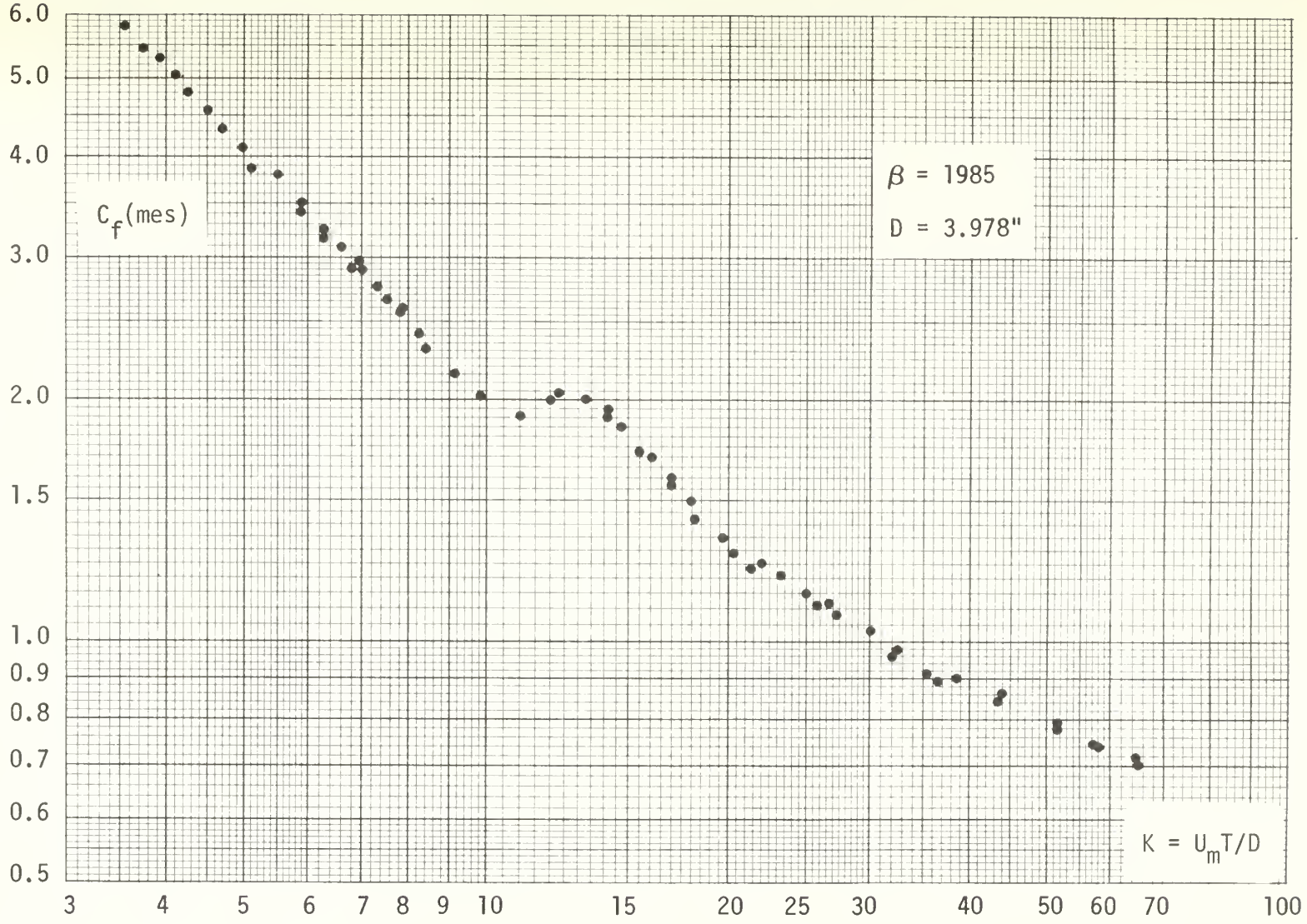

Fig. 32 C_f(mes) versus K for β = 1985

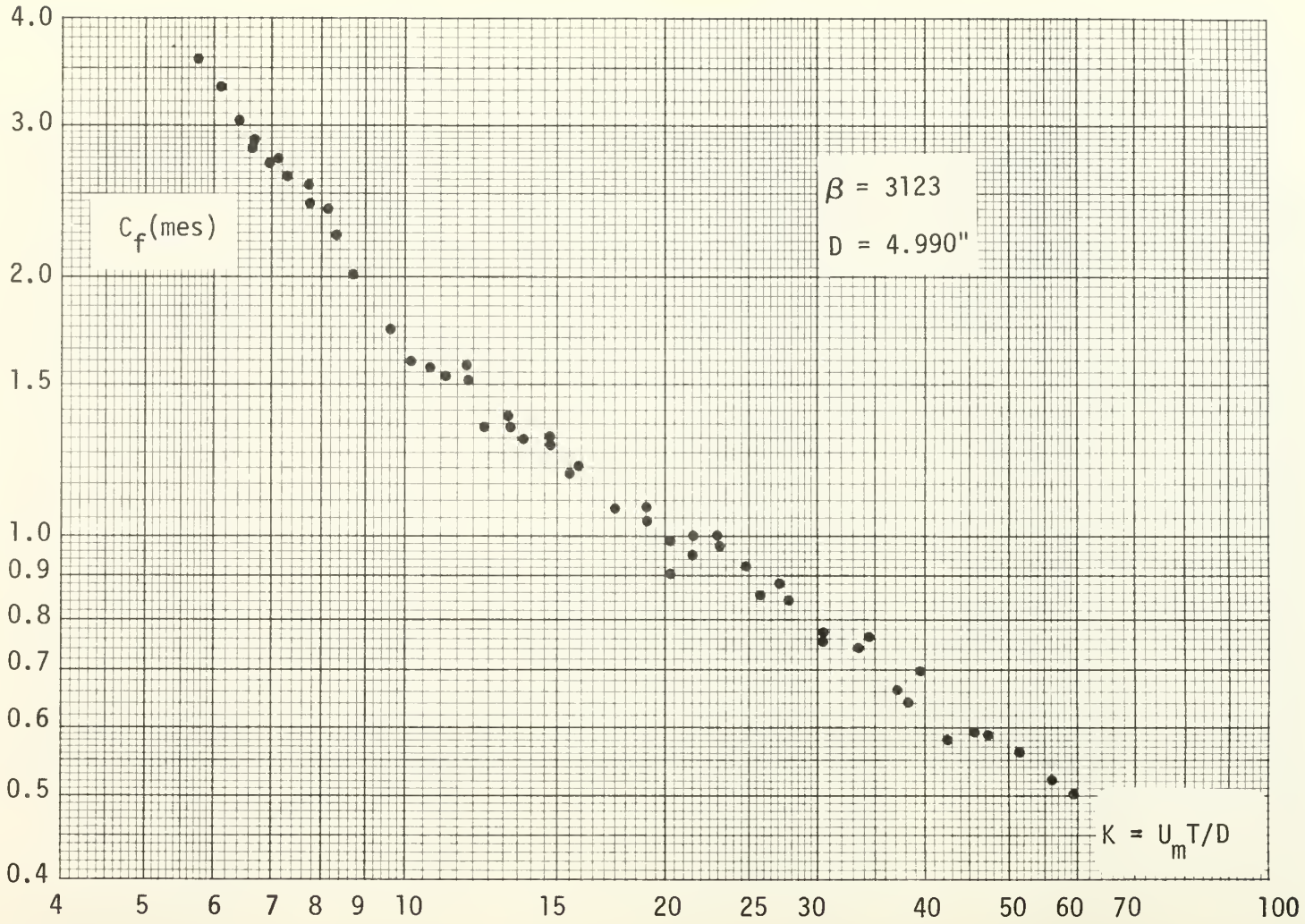

Fig. 33 C_f(mes) versus K for β = 3123

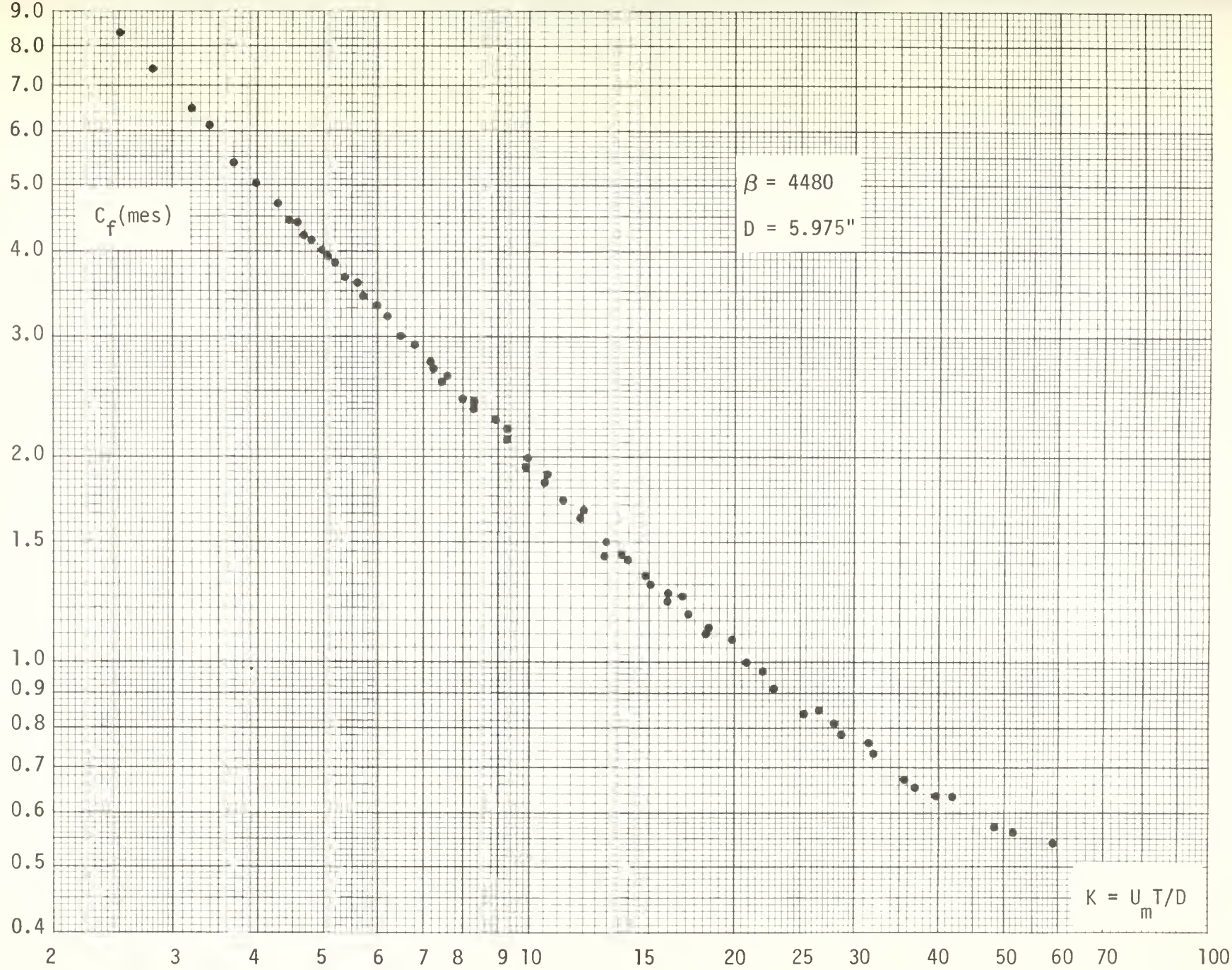

Fig. 34 C_f(mes) versus K for β = 4480

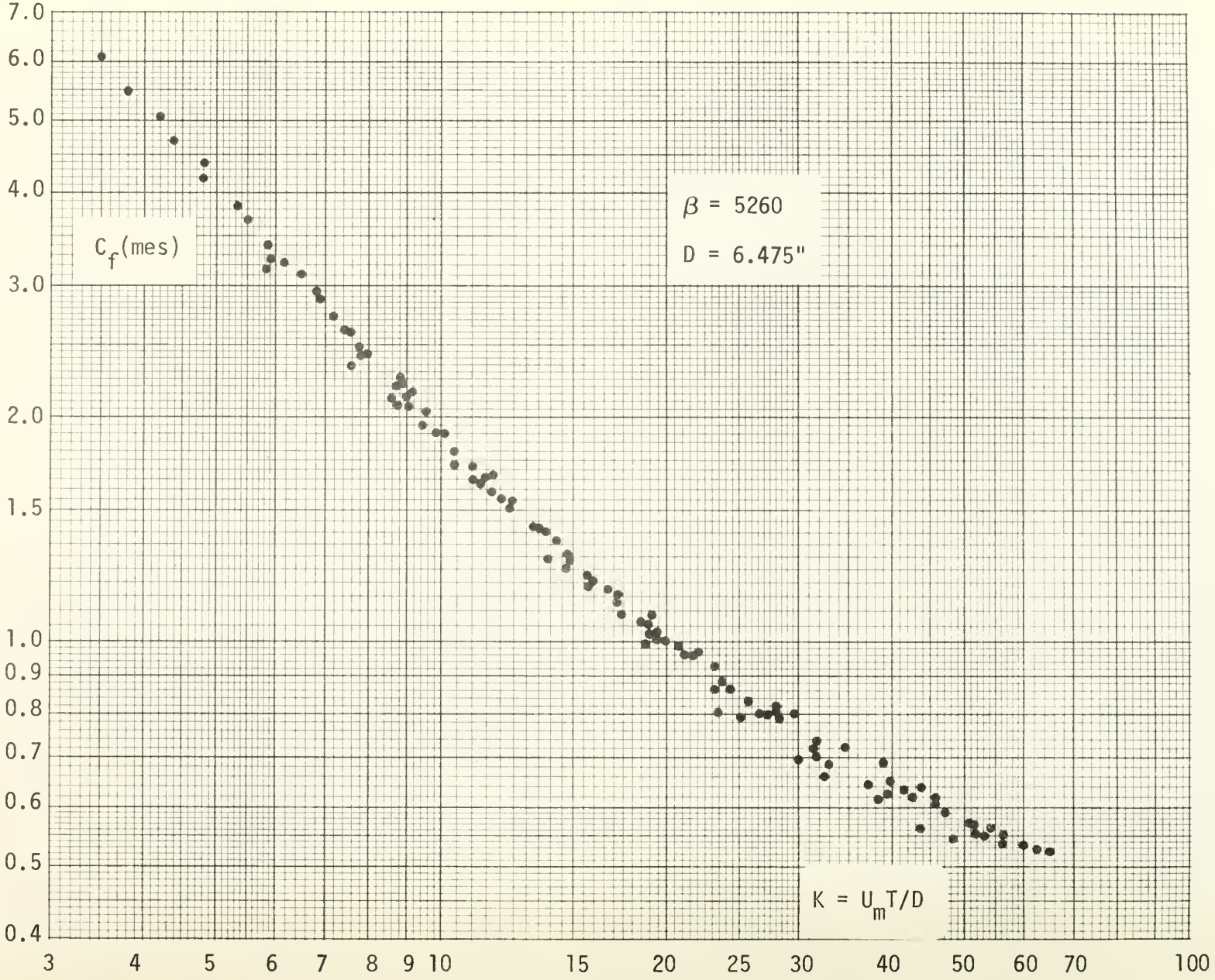

Fig. 35 C_f(mes) versus K for β = 5260

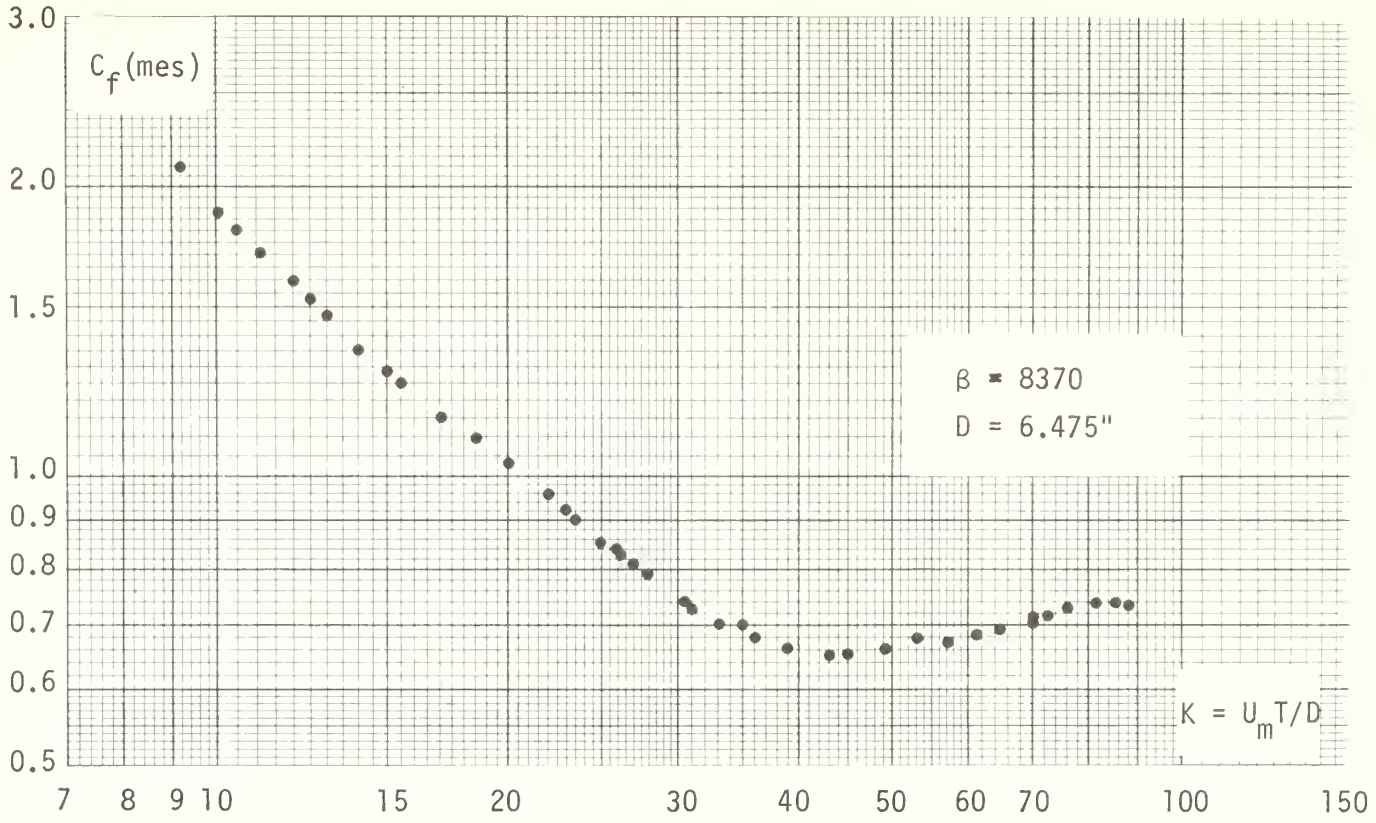

Fig. 36 C_f(mes) versus K for β = 8370

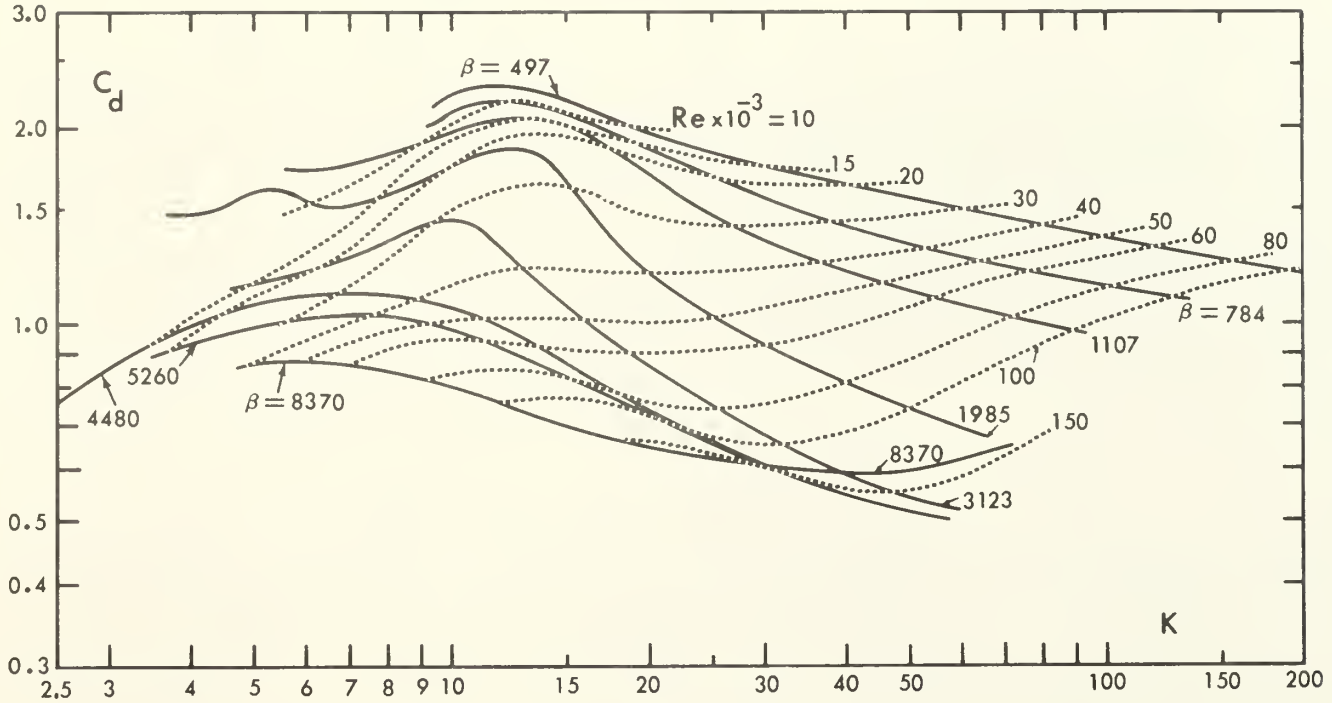

Fig. 37 C_d versus K for particular values of Re and β

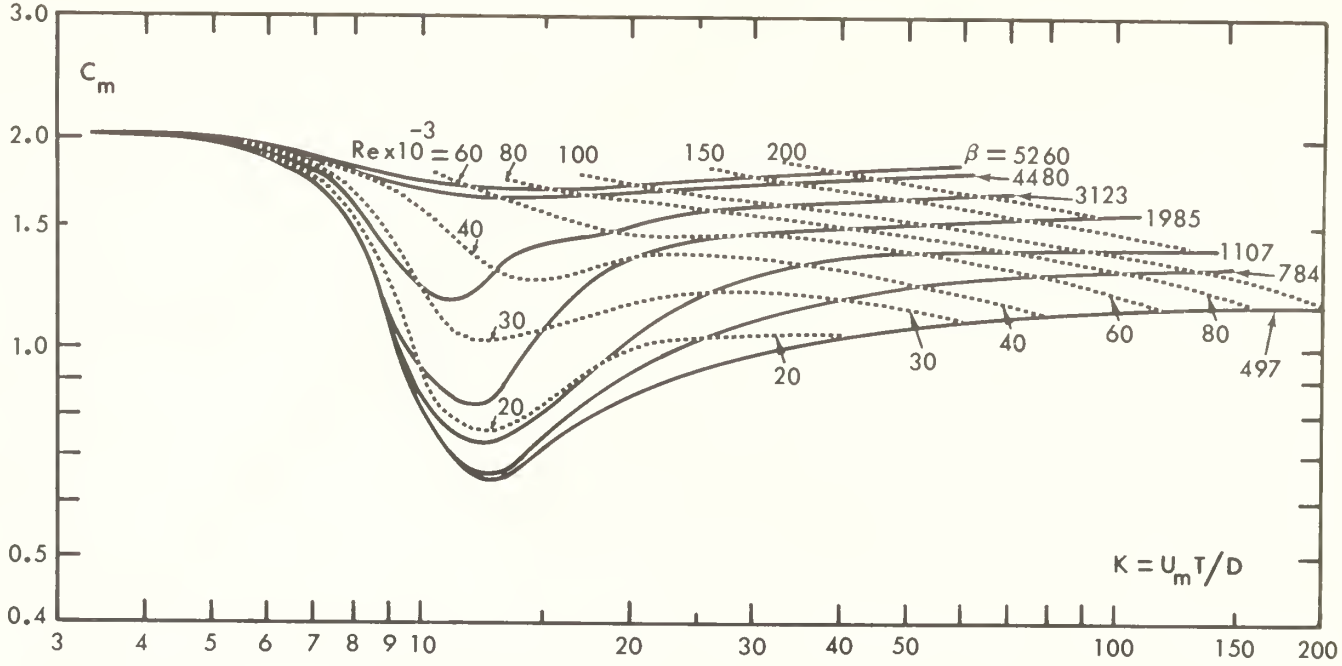

Fig. 38 C_m versus K for particular values of Re and β.

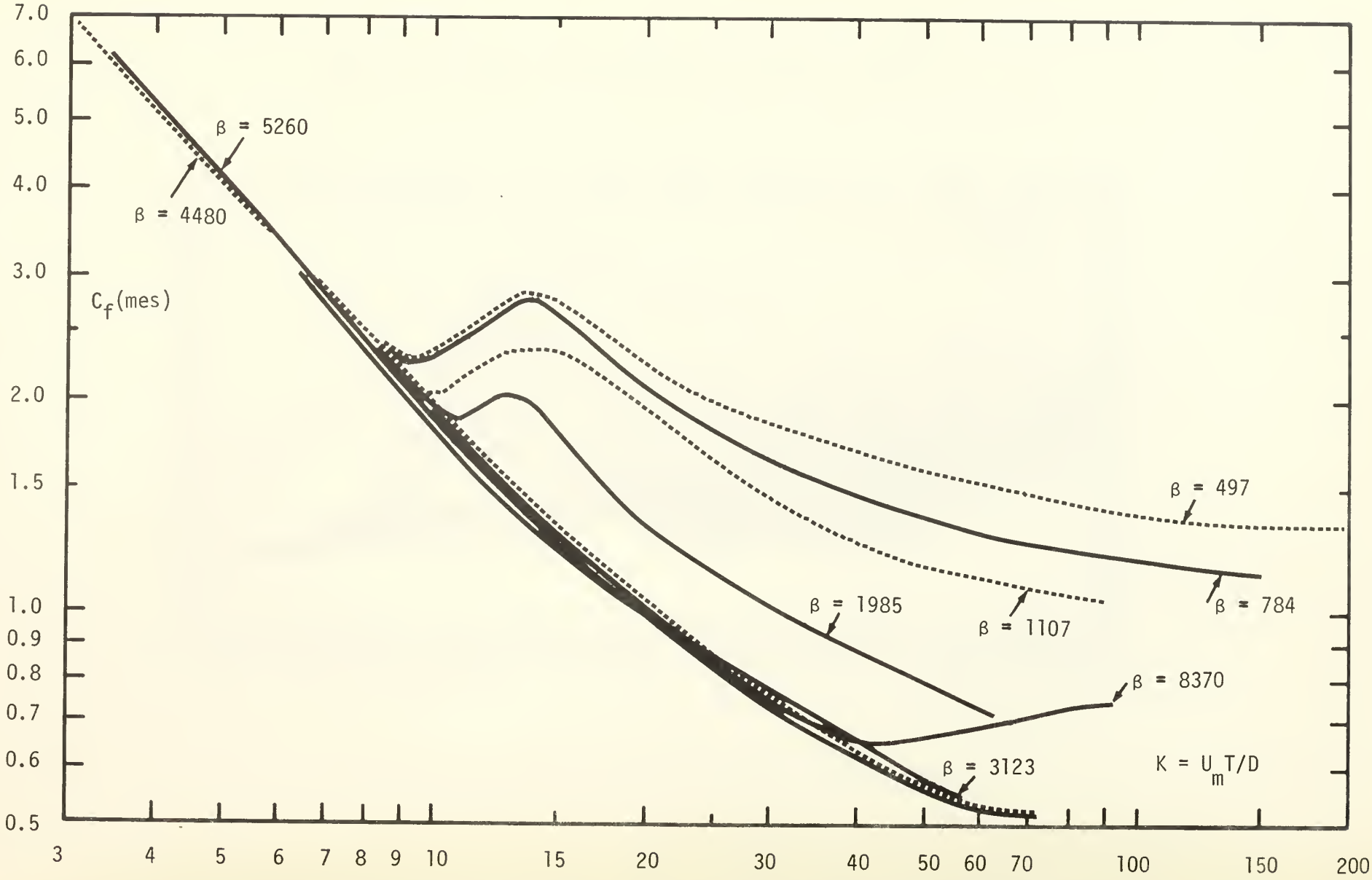

Fig. 39 C_f(mes) versus K for particular values of β.

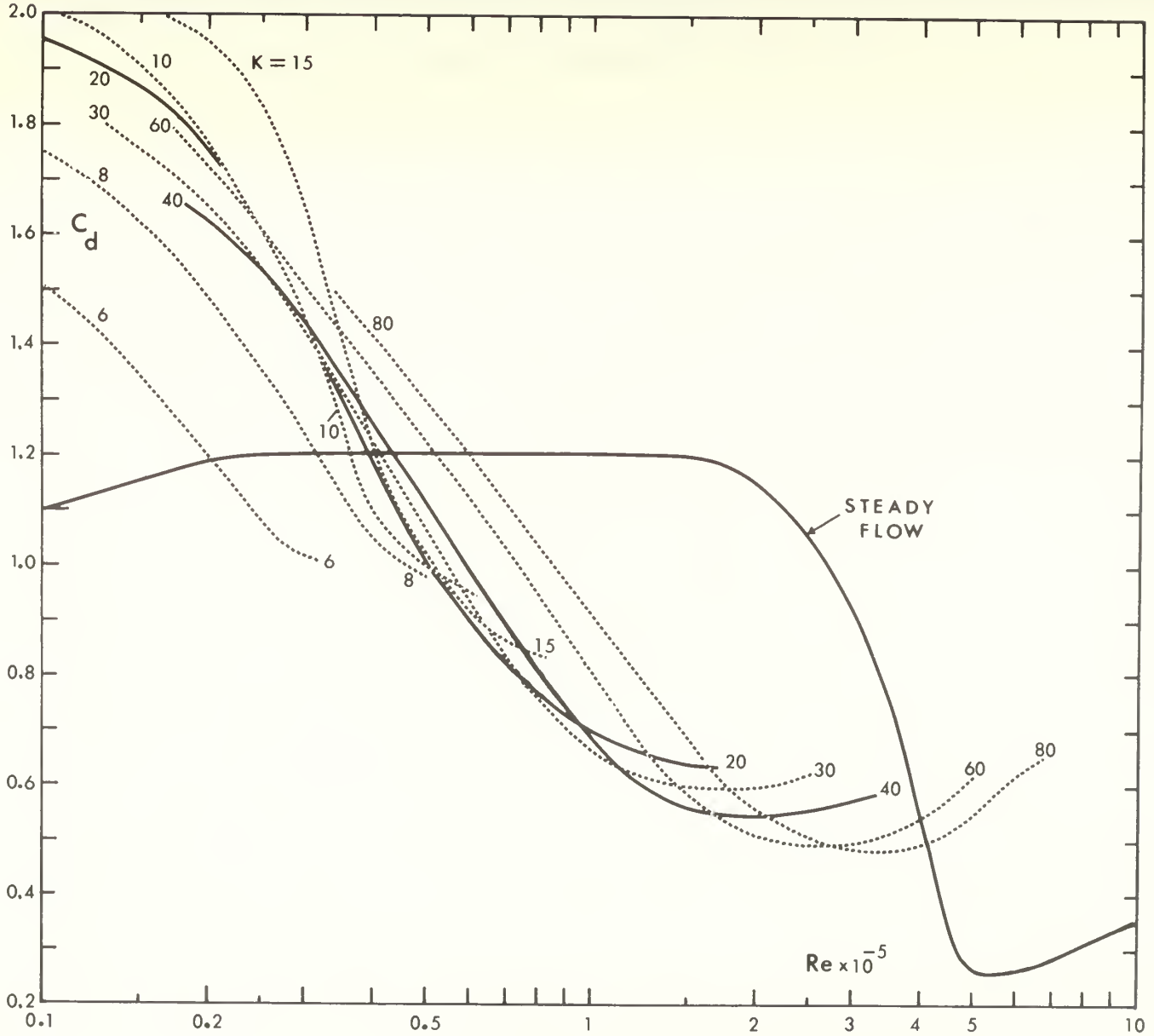

Fig. 40 C_d versus Re for constant values of K.

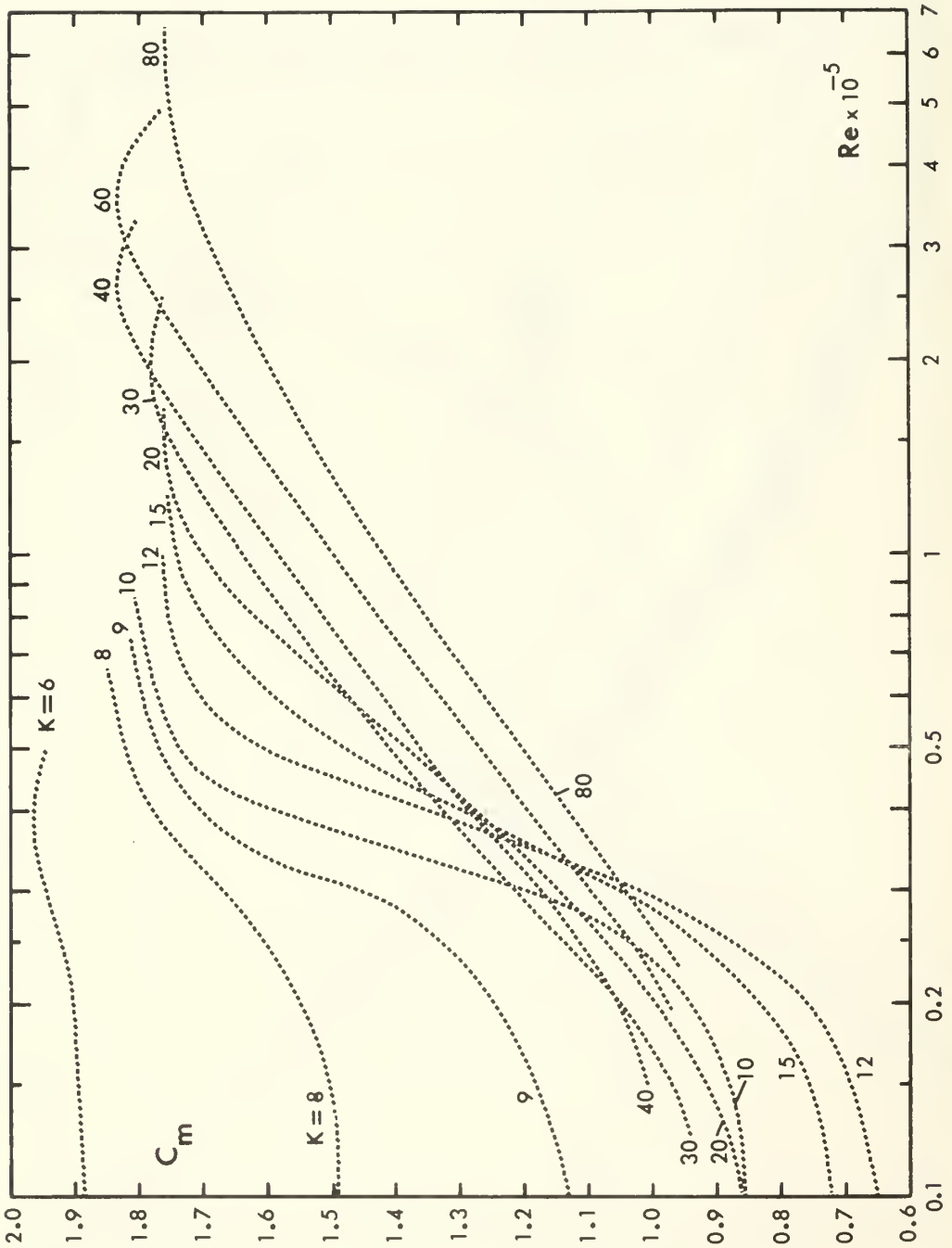

Fig. 41 C_m versus Re for constant values of K.

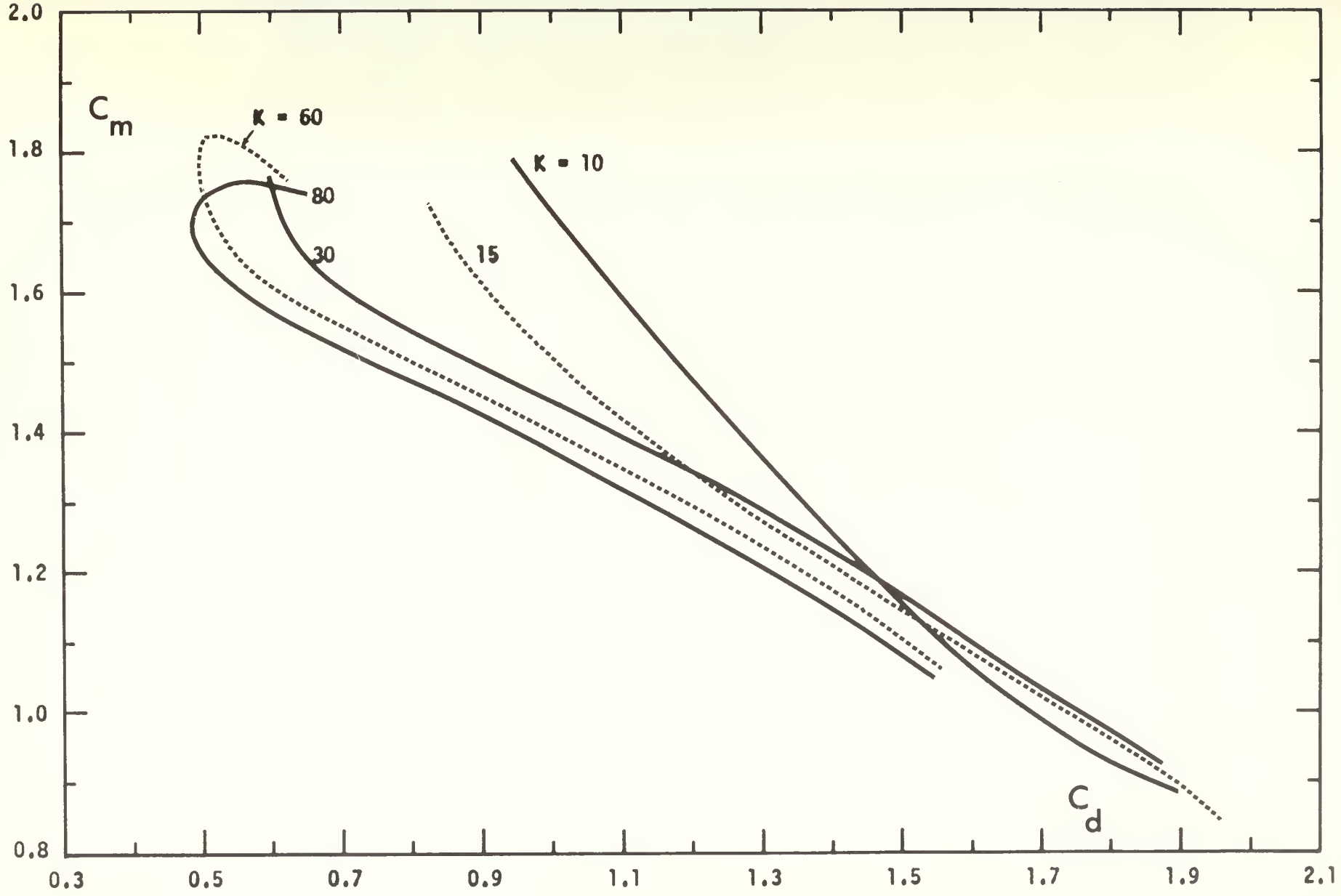

Fig. 42 C_m versus C_d for various values of K.

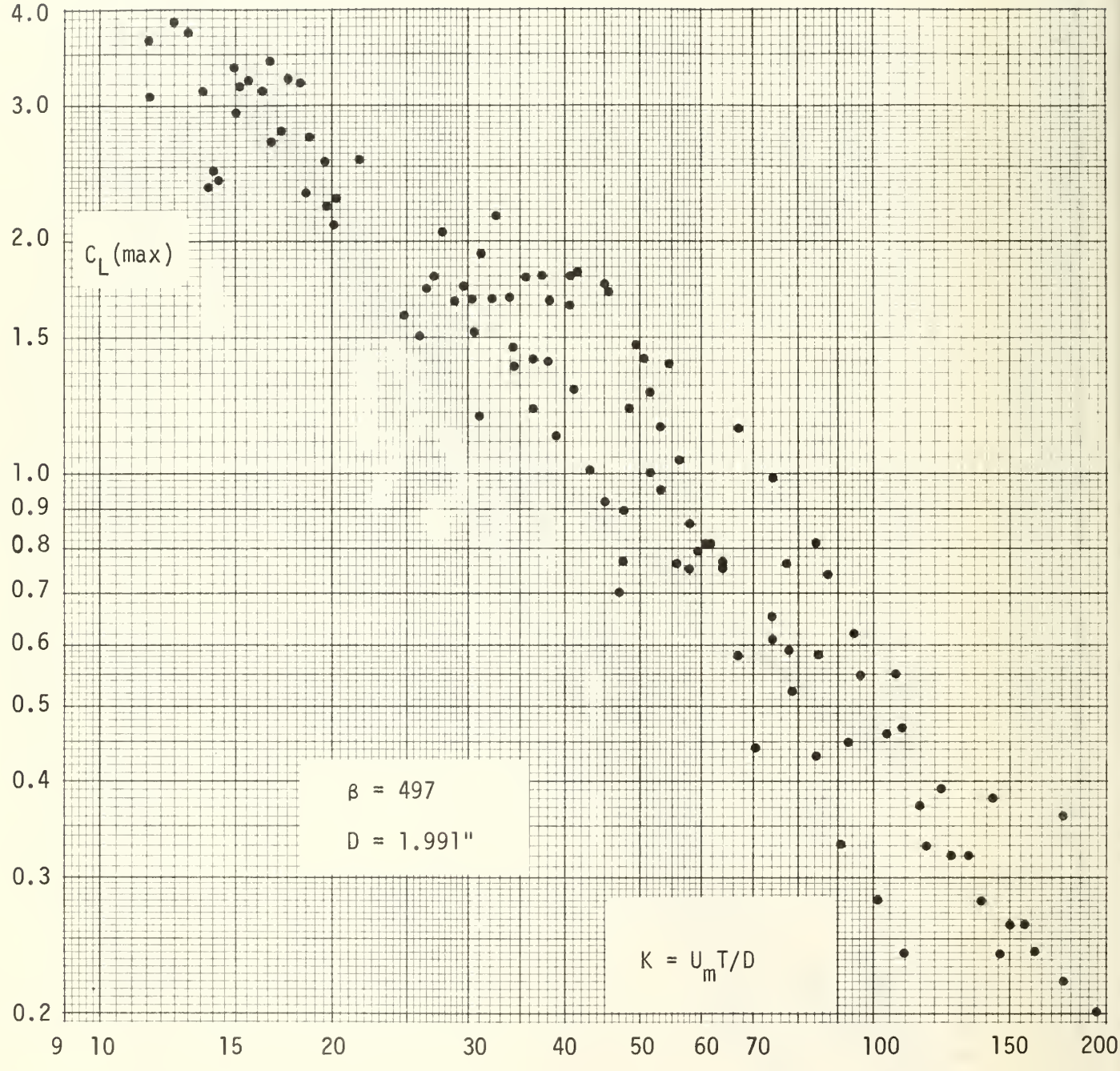

Fig. 43 C_L(max) versus K for β = 497.

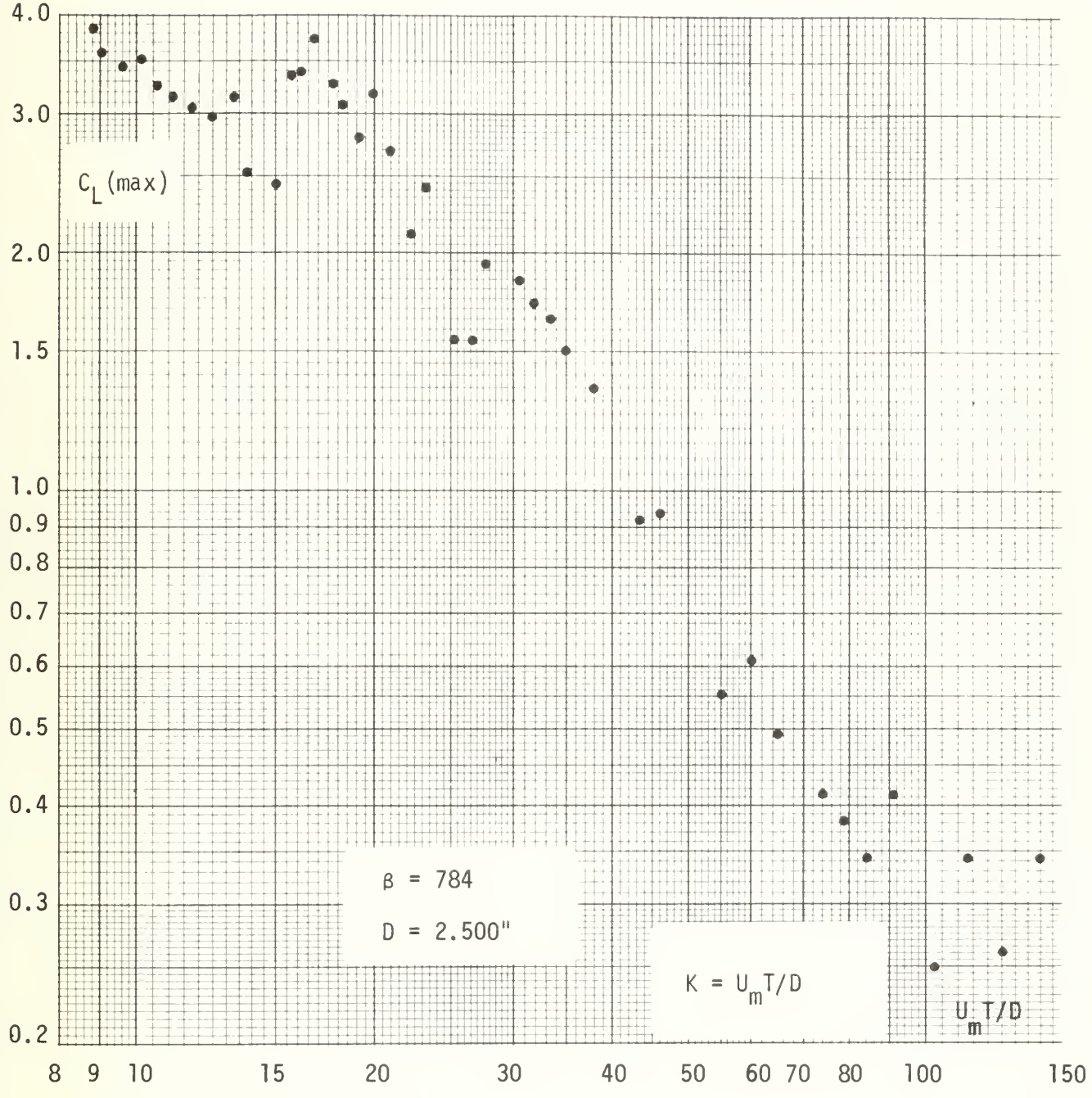

Fig. 44 C_L (max) versus K for β = 784.

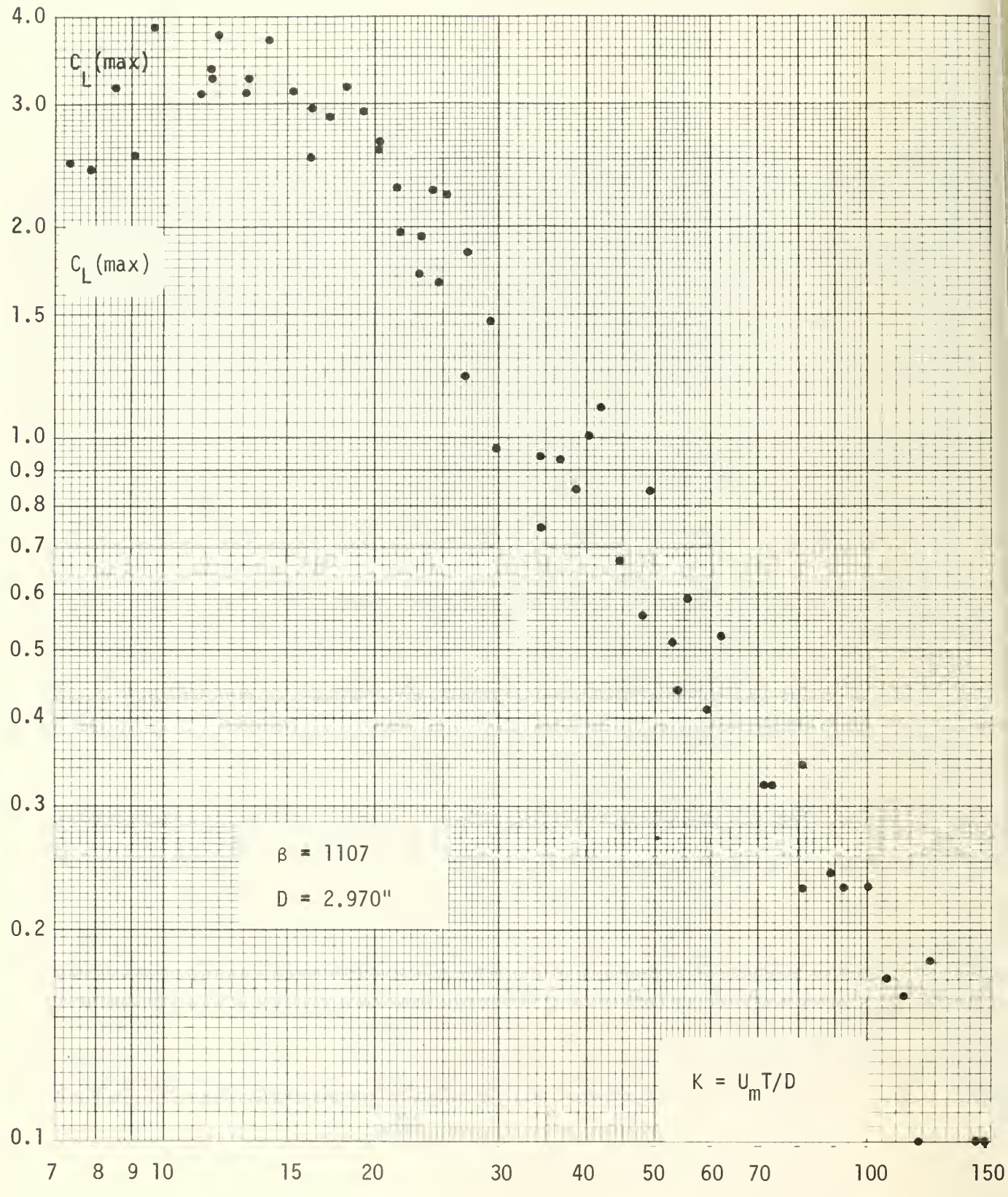

Fig. 45 C_L(max) versus K for β = 1107.

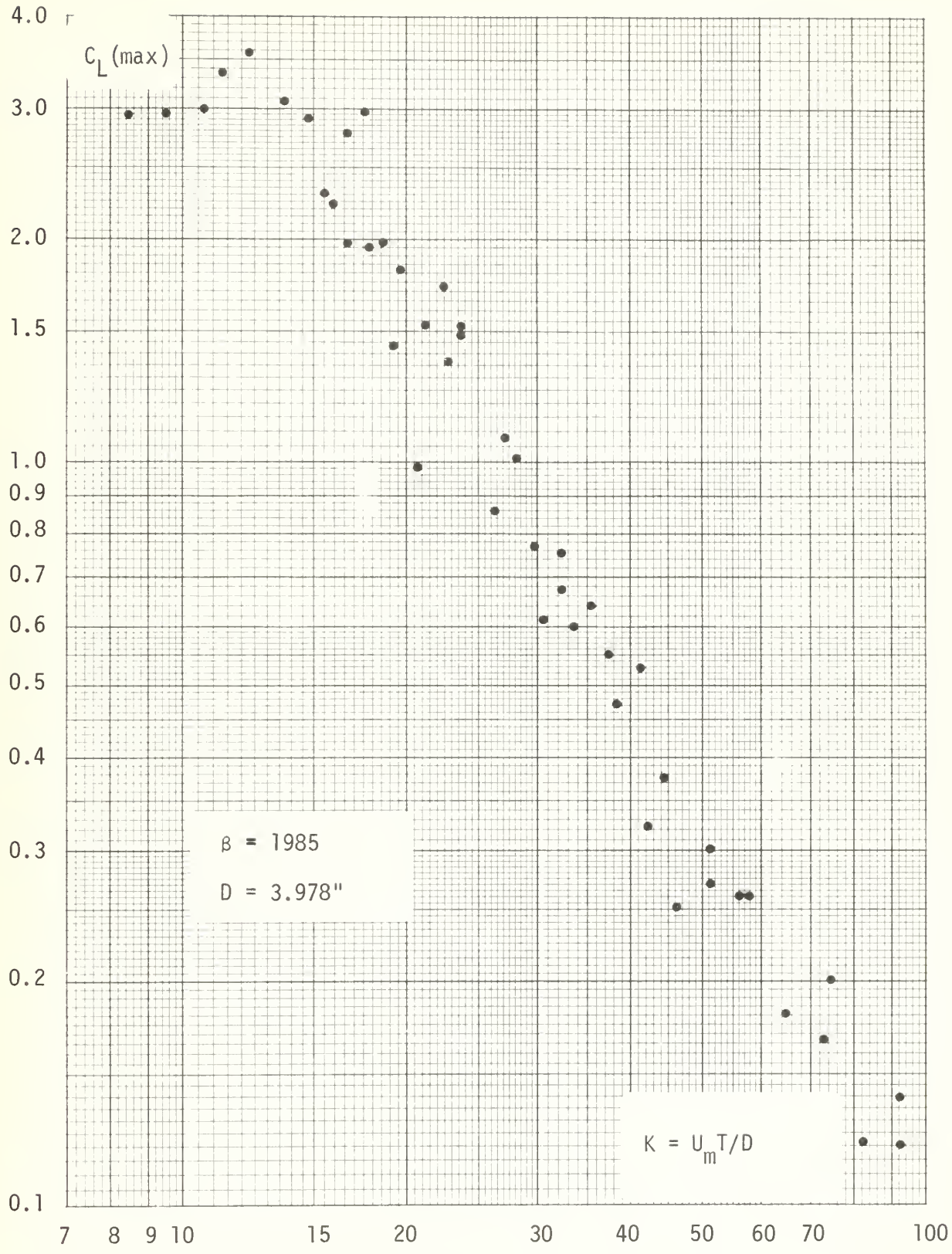

Fig. 46 C_L(max) versus K for β = 1985.

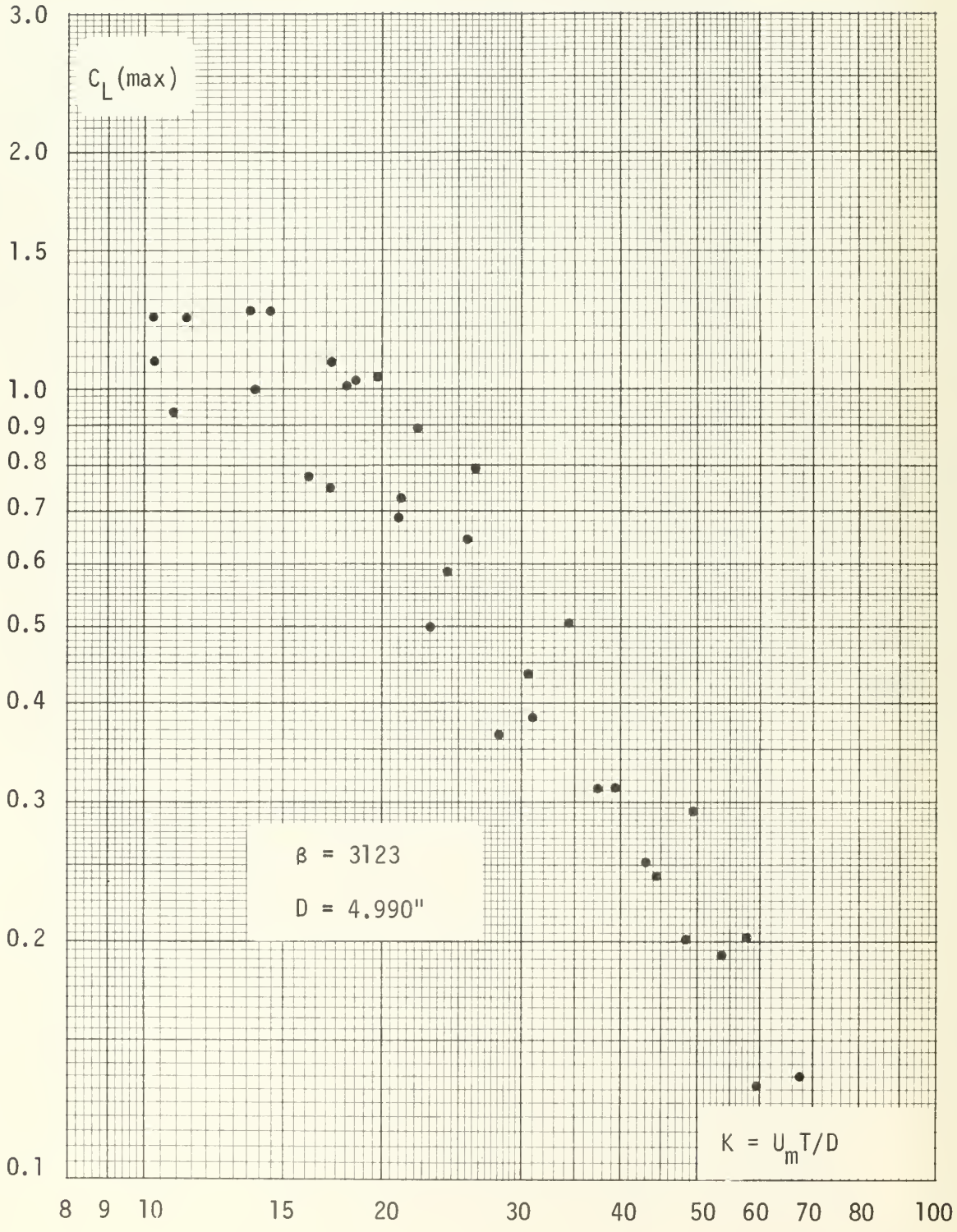

Fig. 47 C_L(max) versus K for β = 3123.

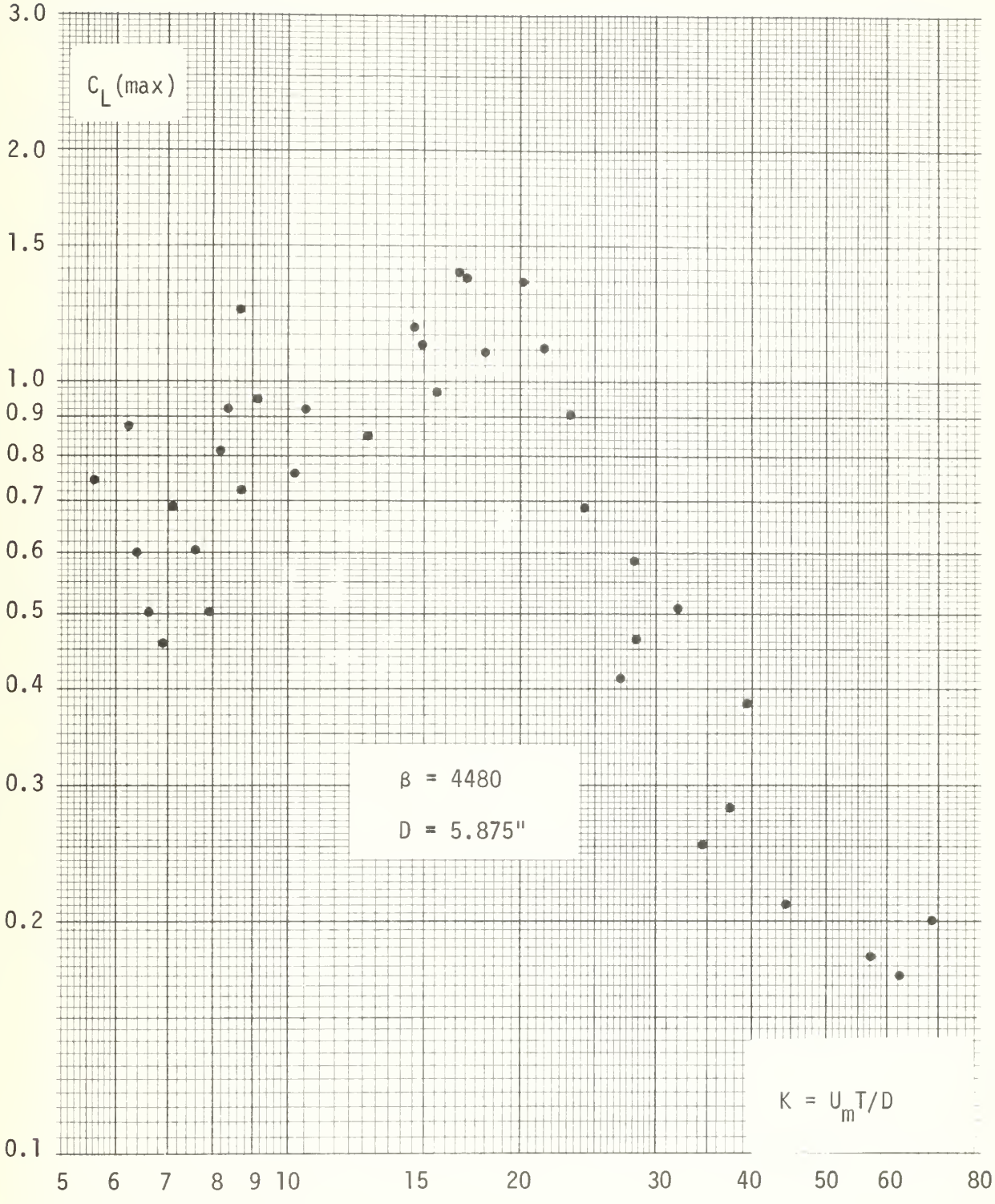

Fig. 48 C_L(max) versus K for β = 4480.

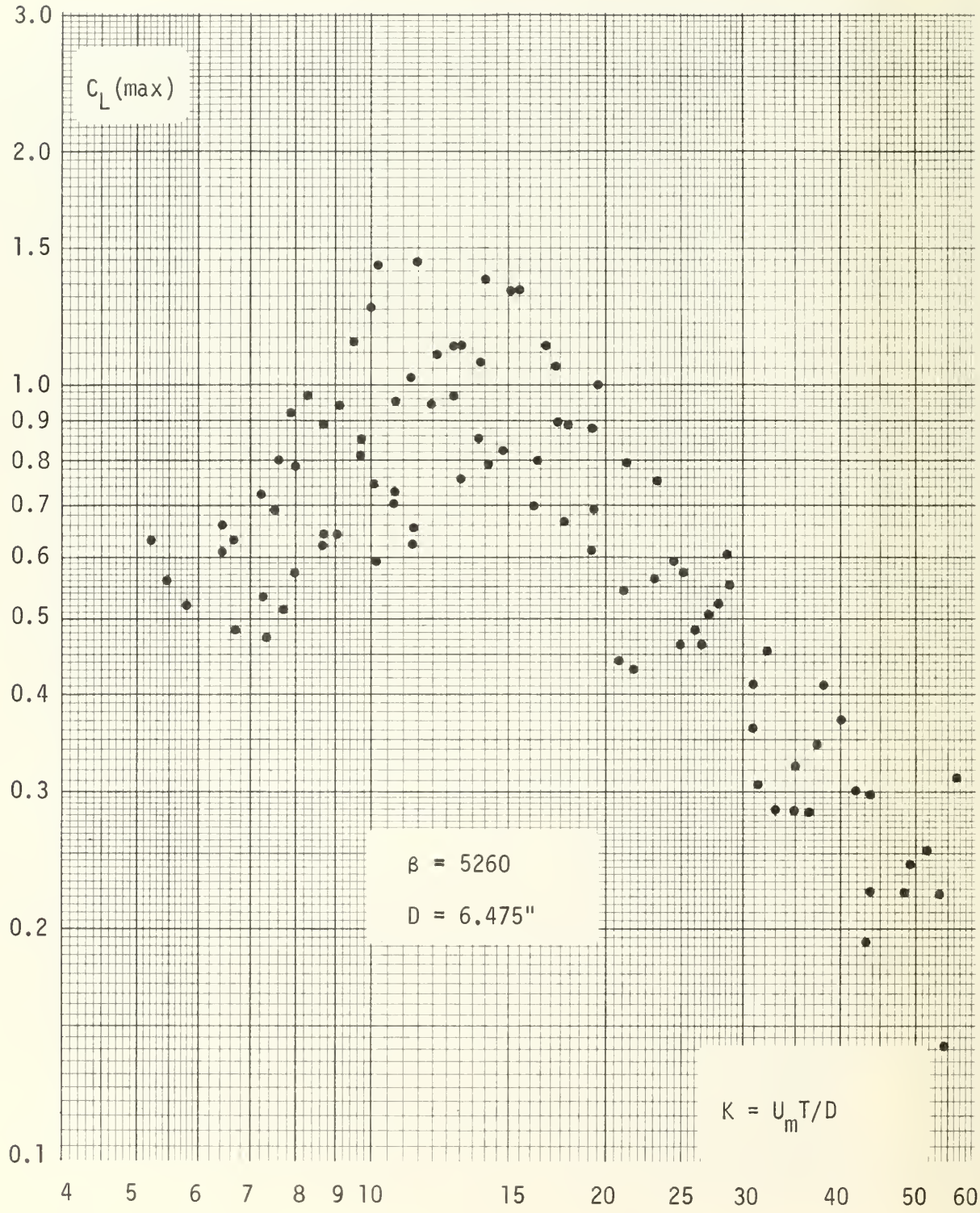

Fig. 49 C_L(max) versus K for β = 5260.

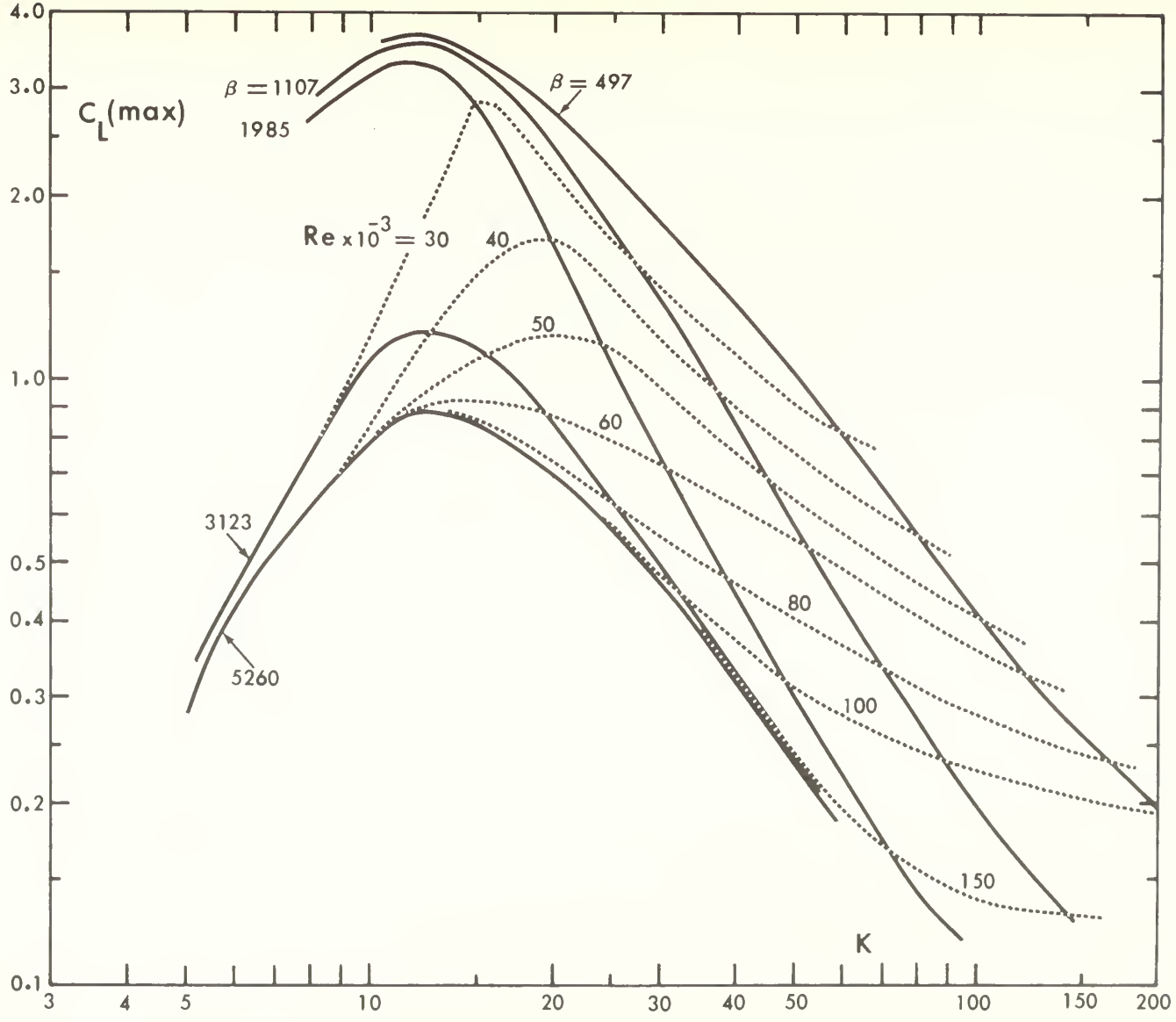

Fig. 50 C_L(max) versus K for various values of K and β.

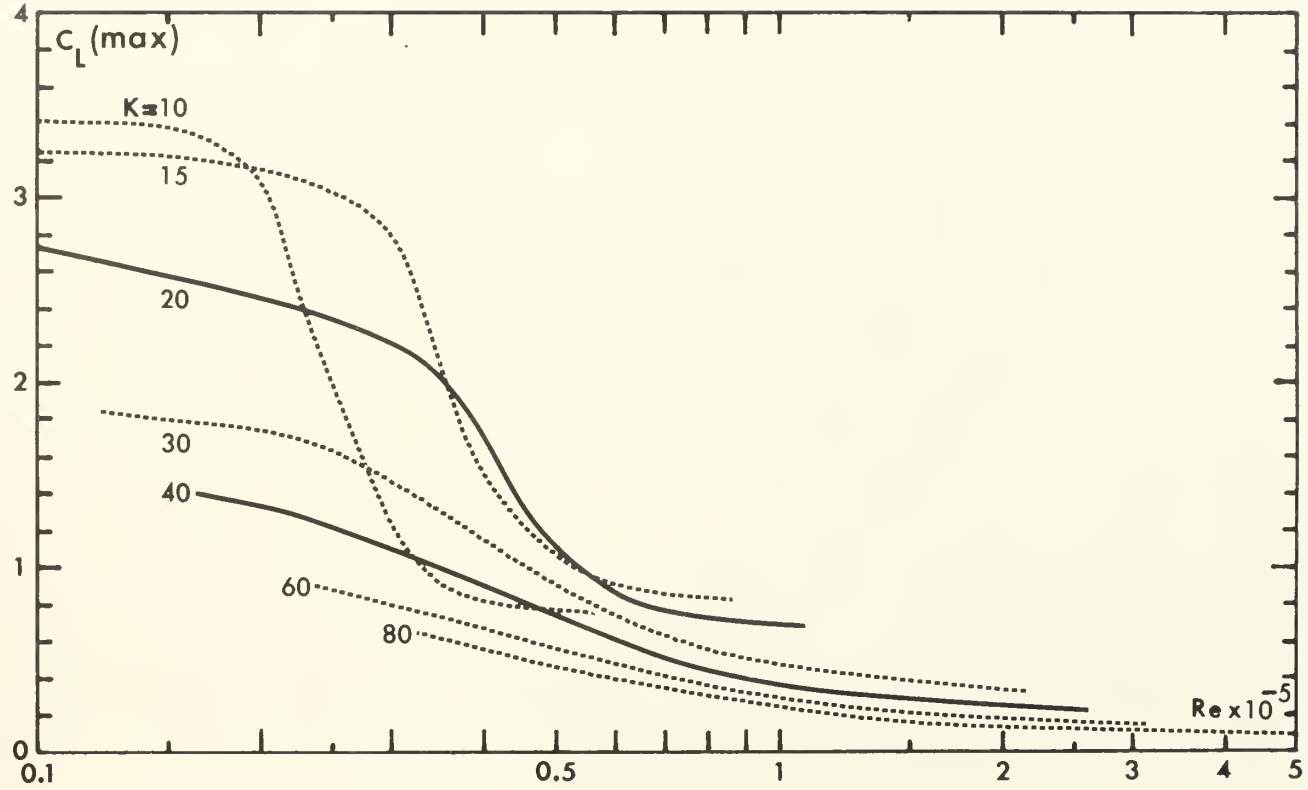

Fig. 51 C_L(max) versus Re for various values of K.

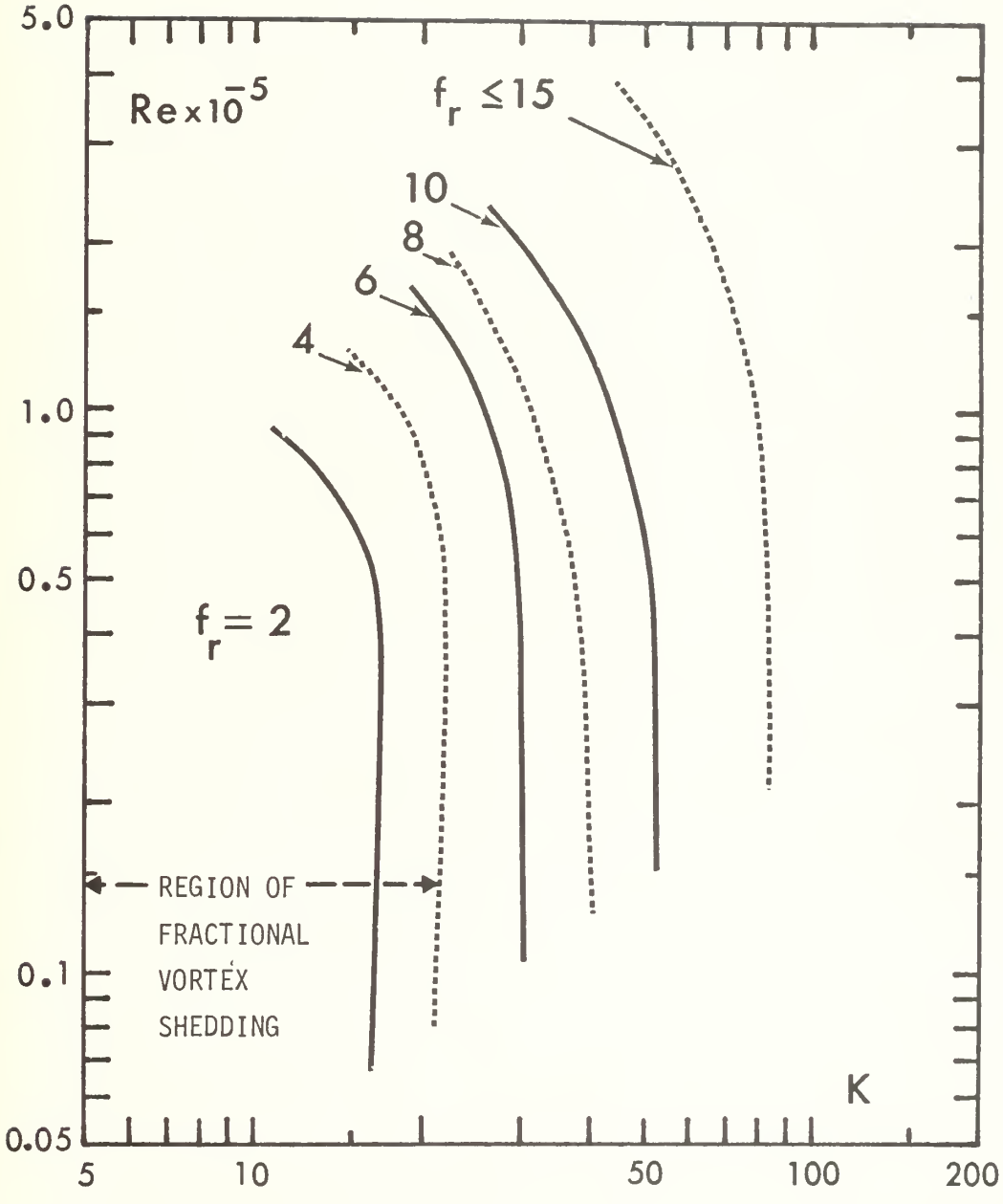

Fig. 52 Relative frequency of vortex shedding as a function of the Reynolds and Keulegan-Carpenter numbers.

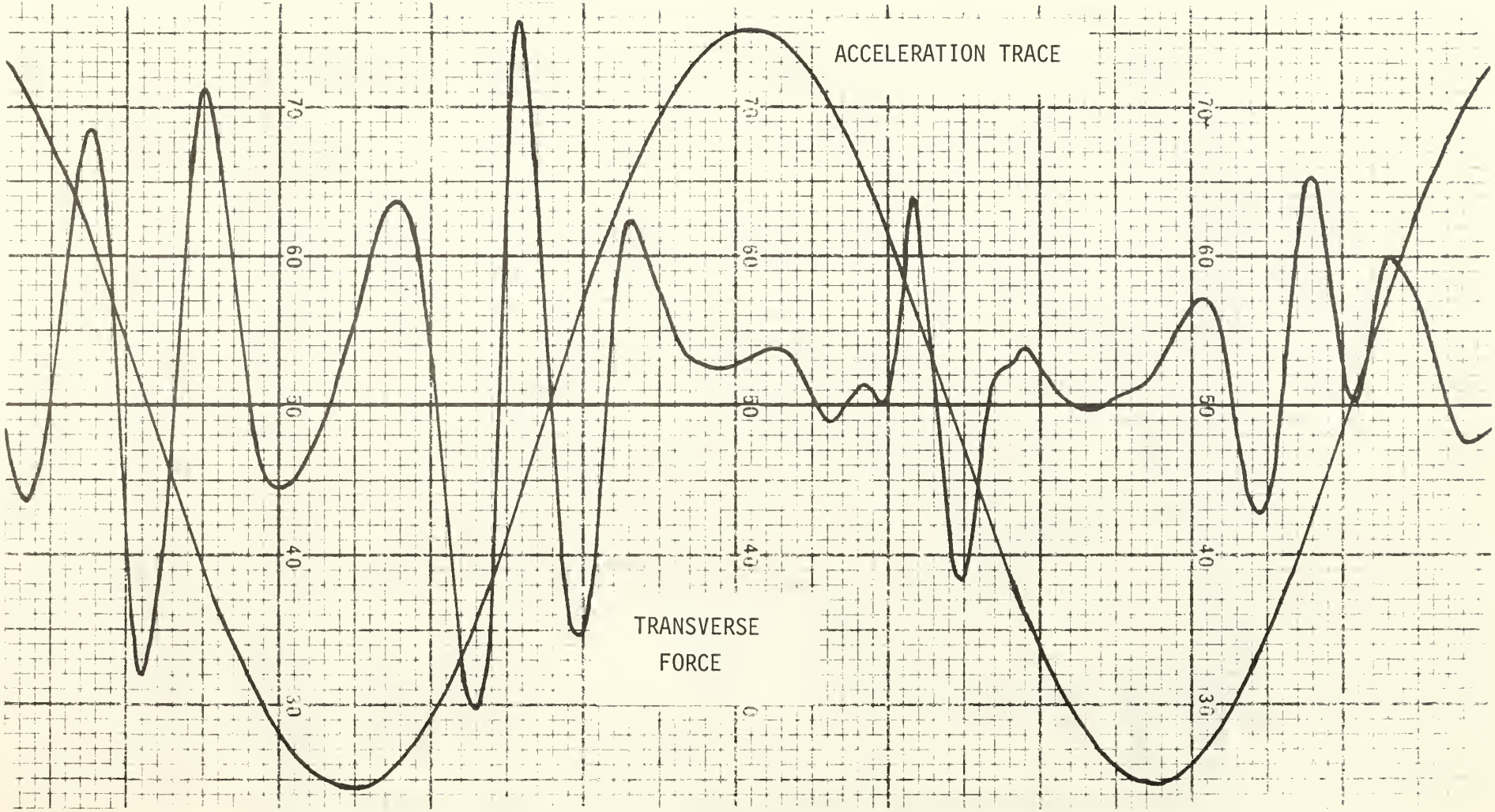

Fig. 53 Transverse force and acceleration traces showing the irregularity of the transverse force at relatively high Keulegan-Carpenter numbers.

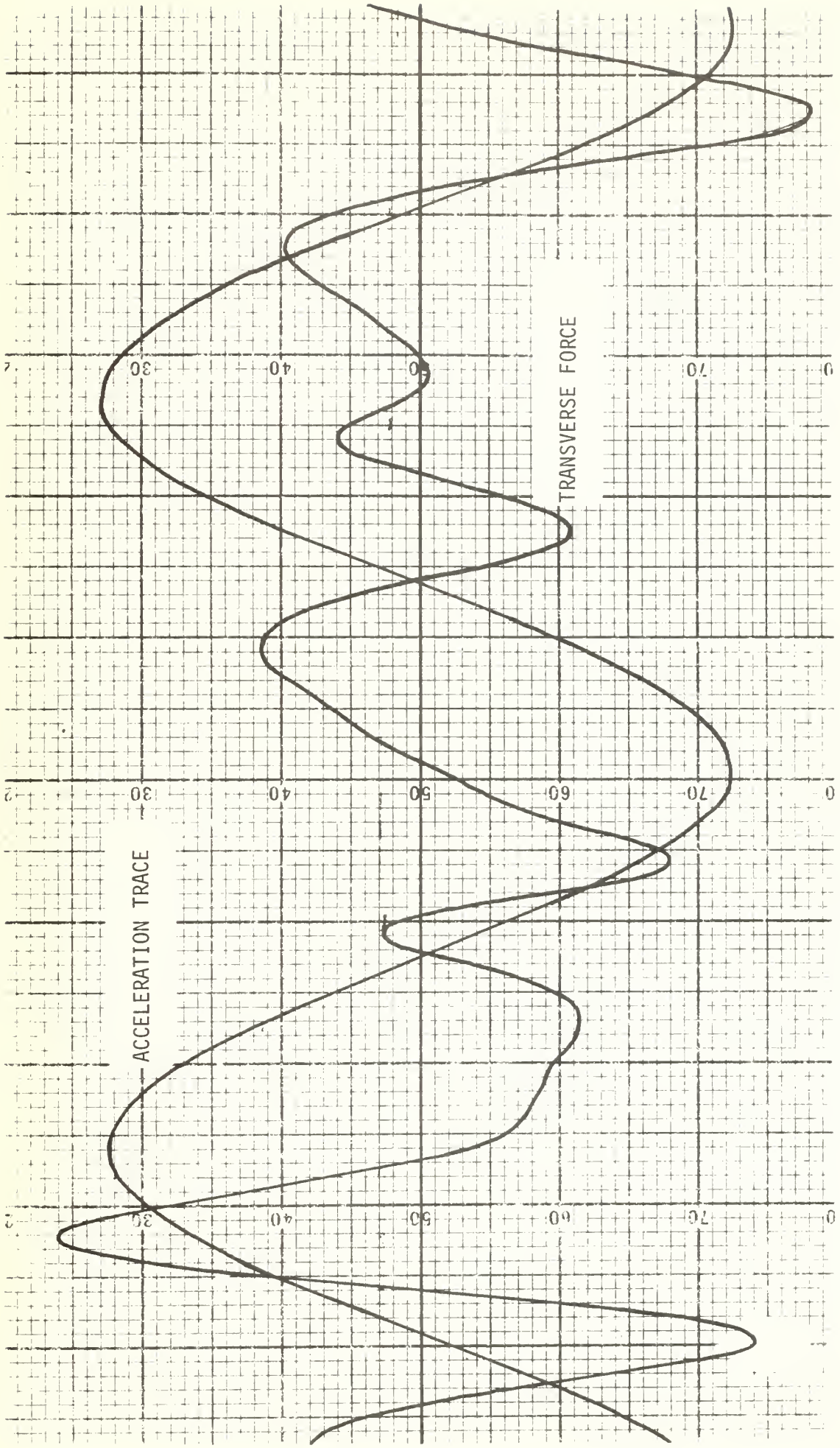

Fig. 54 Transverse force and acceleration traces and fractional sheding of vortices at K ≈ 13.

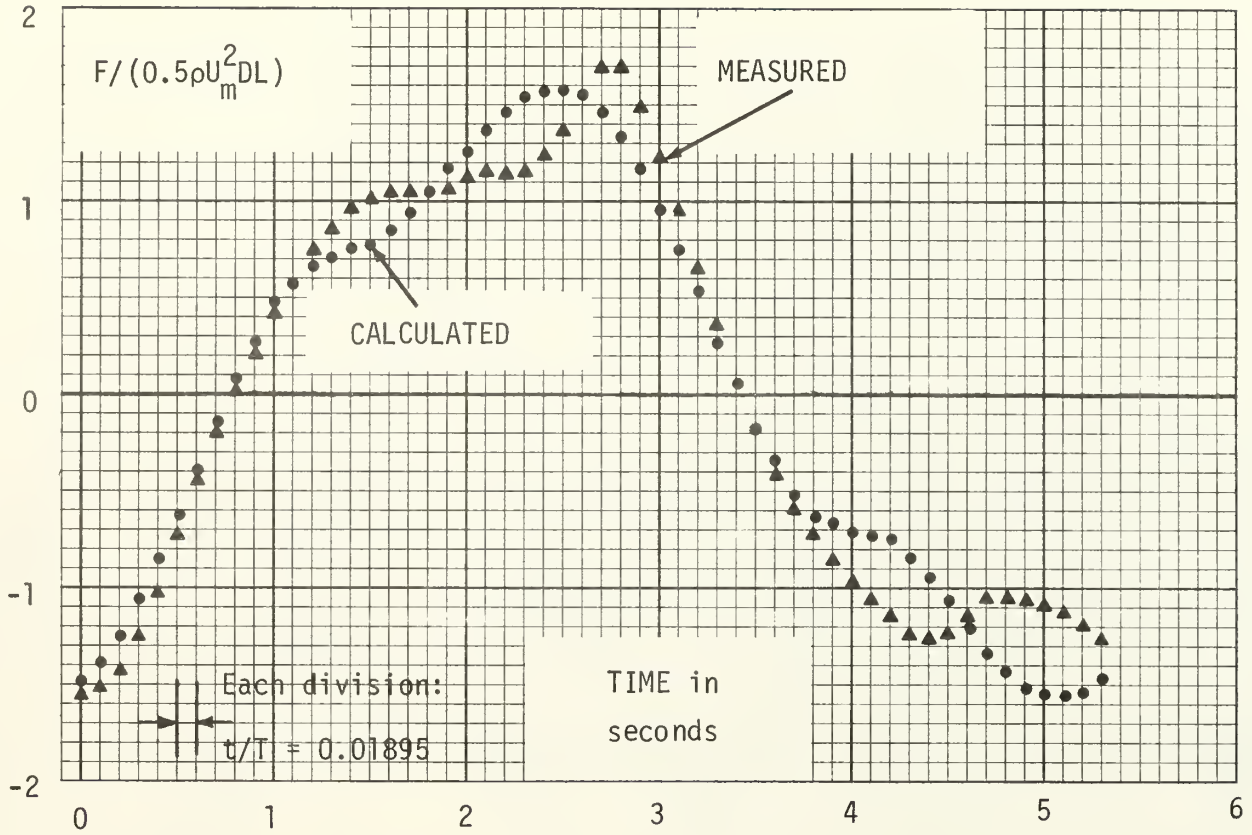

Fig. 55 Asymmetry in the in-line force and the comparison of measured and calculated forces. K = 16.1297, Re = 32045, C_d = 1.4953, C_m = 1.154, C_f(mes) = 1.7198, D = 0.3315 ft, A = 0.851, U_m = 1.015, T = 5.272. Data and additional details are given in the next three pages.

SPECIAL COMMENTS ABOUT FIG. 55.

The computer output for the data plotted in Fig. 55 is presented in the next two pages. The nomeclature is listed below:

DIA = Diameter in feet

AMP = Amplitude at the test section in feet

PER = Period of oscillations in seconds

UMX = Maximum velocity in the cycle, U_m in ft/sec.

TIME = Time/period

F = Normalized measured force

F1 = Normalized calculated force with the Fourier-averaged drag and inertia coefficients.

REMF = $(|F| - |F1|)/|FMAX|$

FMAX = Normalized maximum force in the cycle.

FLS = Normalized calculated force with the Least-squares averaged drag and inertia coefficients.

RLS = $(|F| - |FLS|)/|FMAX|$

CM = Fourier-averaged inertia coefficient

CD = Fourier-averaged drag coefficient

BETA = Keulegan-Carpenter number, K, U_mT/D.

REYNO = Reynolds number x 10^{-3}

CMLS = Least-squares averaged inertia coefficient.

CDLS = Least-squares averaged drag coefficient.

CFSPP = Normalized semi-peak-to-peak maximum force coefficient.

CFRMS = Root-mean-square, normalized force coefficient calculated through the use of Eq. (13).

CFMAX = Normalized maximum force coefficient, C_f(mes).

CARMS = Normalized root-mean-square force coefficient calculated through the use of Eq. (14).

COMPUTER OUTPUT OF THE DATA PLOTTED IN Fig. 55

OFF= 0.3315 AMP= 0.8510 PER= 5.2720 UMX= 1.0150

TIME	F	F1	REMF	FLS	RLS
0.0	-1.5225	-1.4953	0.0158	-1.4796	0.0250
0.0190	-1.5157	-1.3910	0.0725	-1.3754	0.0816
0.0379	-1.4207	-1.2471	0.1010	-1.2322	0.1096
0.0569	-1.2579	-1.0683	0.1102	-1.0545	0.1183
0.0759	-1.0137	-0.8613	0.0886	-0.8489	0.0959
0.0948	-0.7289	-0.6345	0.0549	-0.6236	0.0612
0.1138	-0.4575	-0.3974	0.0349	-0.3884	0.0402
0.1328	-0.1998	-0.1607	0.0227	-0.1535	0.0269
0.1517	0.0037	0.0651	-0.0357	0.0704	-0.0388
0.1707	0.2072	0.2594	-0.0361	0.2736	-0.0383
0.1897	0.4107	0.4427	-0.0186	0.4449	-0.0199
0.2086	0.5667	0.5767	-0.0058	0.5778	-0.0065
0.2276	0.7363	0.6653	0.0413	0.6656	0.0411
0.2466	0.8448	0.7040	0.0819	0.7040	0.0819
0.2656	0.9533	0.7146	0.1388	0.7145	0.1389
0.2845	1.0008	0.7539	0.1436	0.7532	0.1446
0.3035	1.0212	0.8218	0.1159	0.8202	0.1169
0.3225	1.0212	0.9136	0.0626	0.9107	0.0643
0.3414	1.0212	1.0228	-0.0069	1.0183	0.0017
0.3604	1.0619	1.1416	-0.0463	1.1353	-0.0427
0.3794	1.1229	1.2613	-0.0805	1.2532	-0.0757
0.3983	1.1568	1.3729	-0.1256	1.3629	-0.1198
0.4173	1.1365	1.4674	-0.1924	1.4557	-0.1856
0.4363	1.1365	1.5368	-0.2327	1.5236	-0.2251
0.4552	1.2247	1.5738	-0.2030	1.5594	-0.1947
0.4742	1.3693	1.5733	-0.1239	1.5581	-0.1150
0.4932	1.5299	1.5319	-0.0012	1.5162	0.0080
0.5121	1.6995	1.4483	0.1461	1.4326	0.1552
0.5311	1.6995	1.3237	0.2185	1.3095	0.2274
0.5501	1.4960	1.1617	0.1944	1.1473	0.2027
0.5690	1.2247	0.9679	0.1493	0.9547	0.1576
0.5880	0.9533	0.7498	0.1183	0.7381	0.1251
0.6070	0.6481	0.5166	0.0765	0.5066	0.0823
0.6259	0.3429	0.2783	0.0375	0.2702	0.0422
0.6449	0.0715	0.0458	0.0150	0.0395	0.0186

TIME	F	F1	REMF	FLS	RLS
0.6639	-0.1794	-0.1705	0.0052	-0.1750	0.0026
0.6828	-0.4033	-0.3604	0.0249	-0.3633	0.0232
0.7018	-0.5864	-0.5150	0.0415	-0.5167	0.0406
0.7208	-0.7424	-0.6270	0.0671	-0.6277	0.0667
0.7398	-0.8781	-0.6916	0.1088	-0.6911	0.1087
0.7587	-0.9798	-0.7066	0.1589	-0.7066	0.1589
0.7777	-1.0683	-0.7304	0.1963	-0.7301	0.1965
0.7967	-1.1494	-0.7845	0.2122	-0.7834	0.2128
0.8156	-1.2172	-0.8650	0.2048	-0.8628	0.2061
0.8346	-1.2511	-0.9664	0.1656	-0.9627	0.1677
0.8536	-1.2376	-1.0815	0.0908	-1.0761	0.0939
0.8725	-1.1697	-1.2018	-0.0187	-1.1947	-0.0145
0.8915	-1.0816	-1.3186	-0.1378	-1.3096	-0.1326
0.9105	-1.0816	-1.4228	-0.1984	-1.4110	-0.1921
0.9294	-1.0816	-1.5057	-0.2466	-1.4932	-0.2394
0.9484	-1.1019	-1.5597	-0.2662	-1.5458	-0.2581
0.9674	-1.1223	-1.5786	-0.2653	-1.5637	-0.2567
0.9863	-1.2037	-1.5579	-0.2060	-1.5423	-0.1969

CM=	CD=	BETA=	REYNO=	CMLS=	CDLS=
1.1540	1.4953	16.1297	32.0450	1.1540	1.4796

CFSPP=	CFRMS=	CFMAX=	CARMS=
1.5787	1.0430	1.7198	1.0504

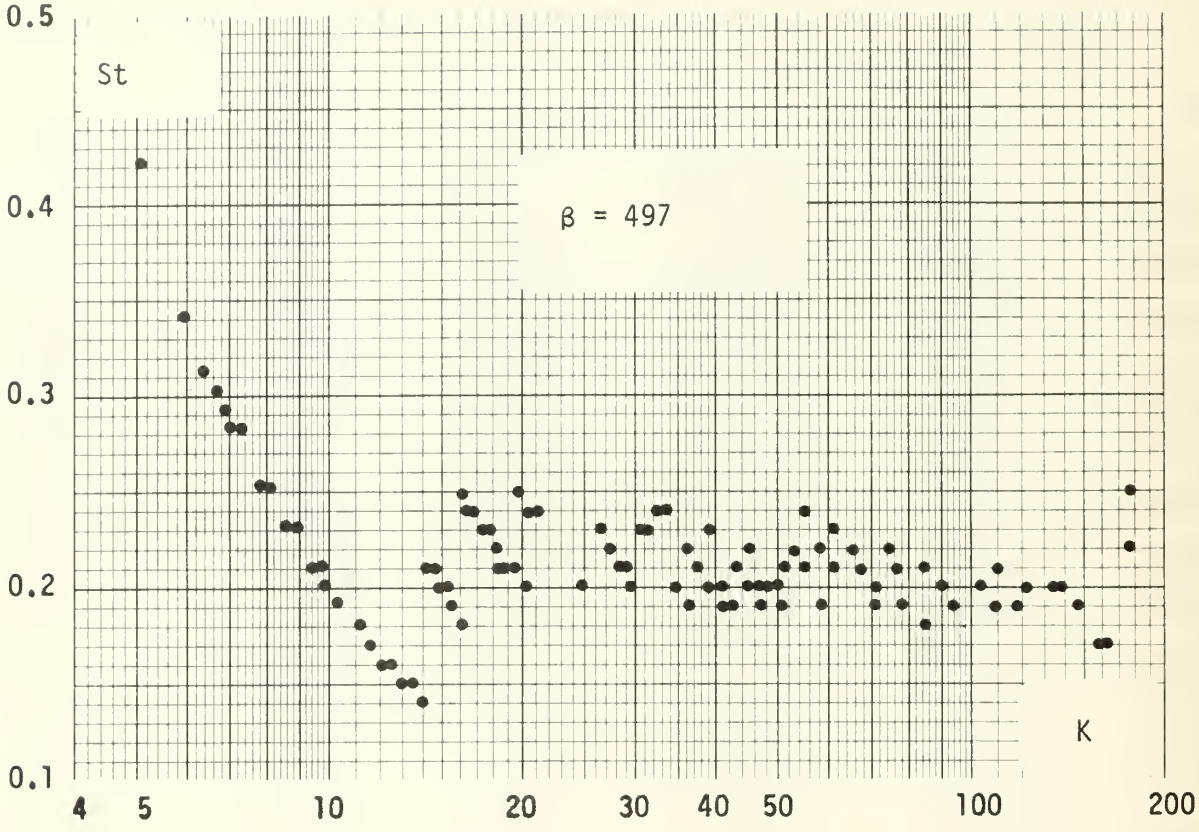

Fig. 56a Strouhal number versus K for β = 497.

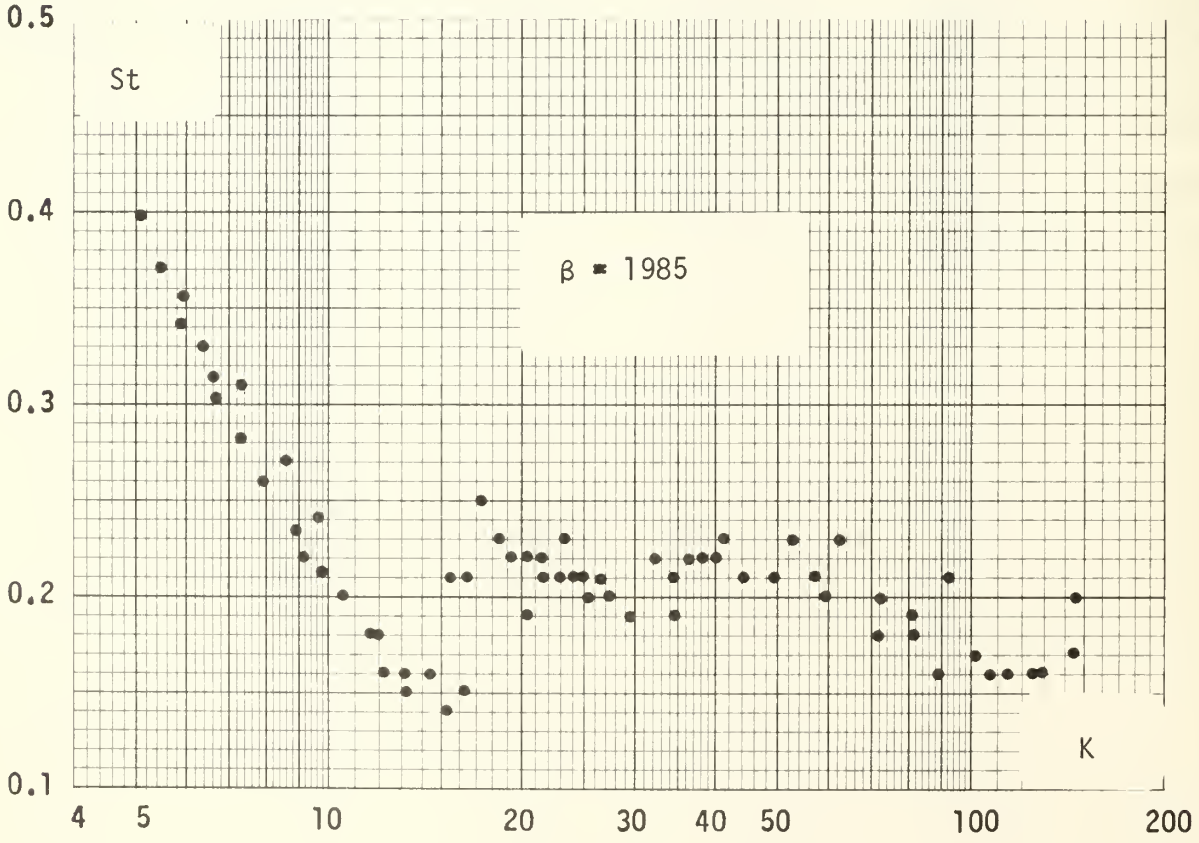

Fig. 56b Strouhal number versus K for β = 1985.

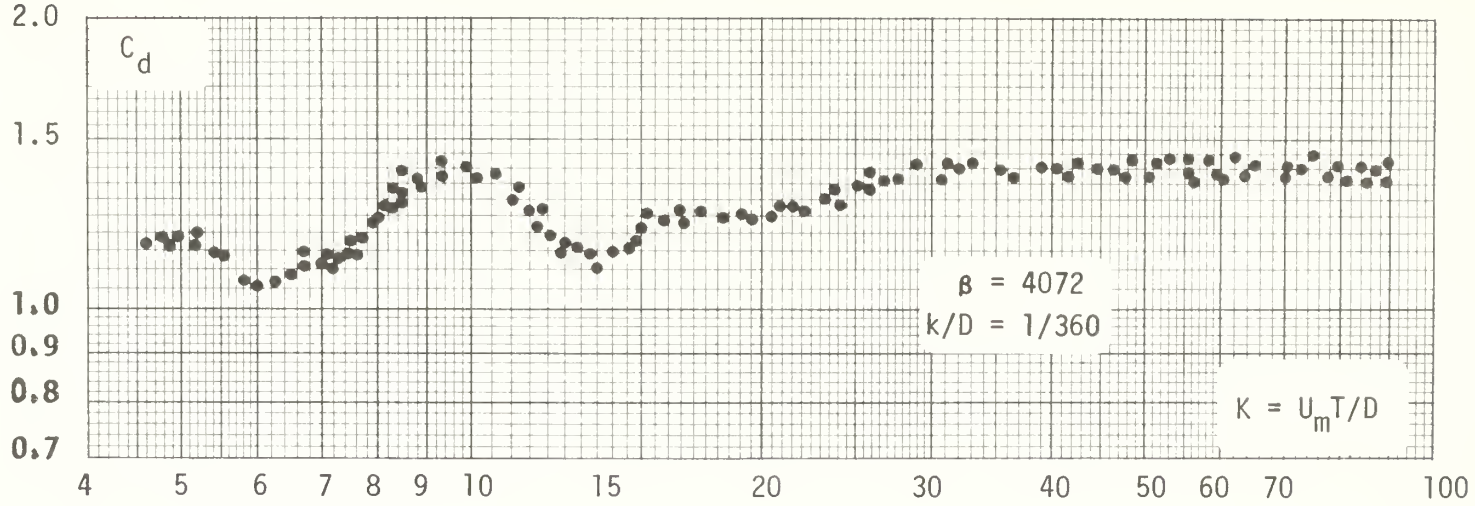

Fig. 57 C_d versus K for β = 4072 and k/D = 1/360.

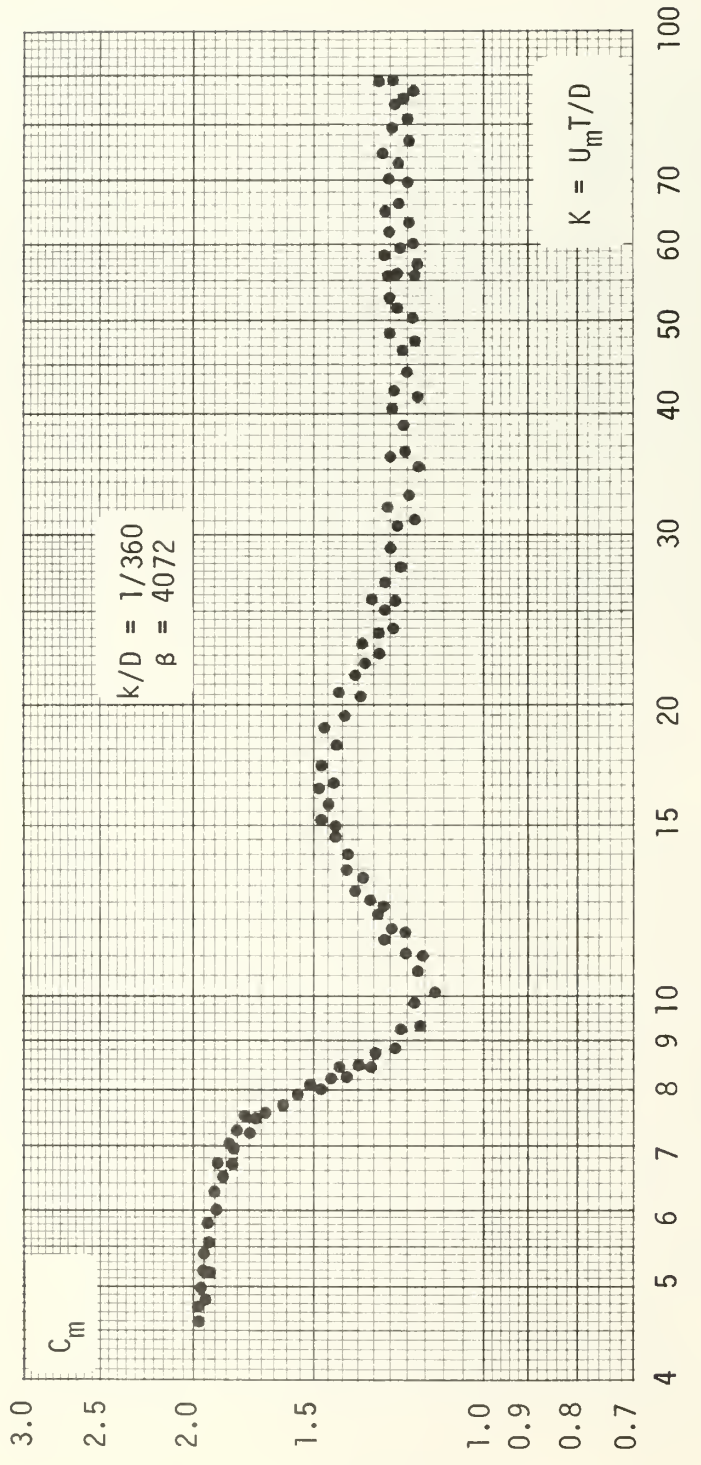

Fig. 58 C_m versus K for β = 4072 and k/D = 1/360.

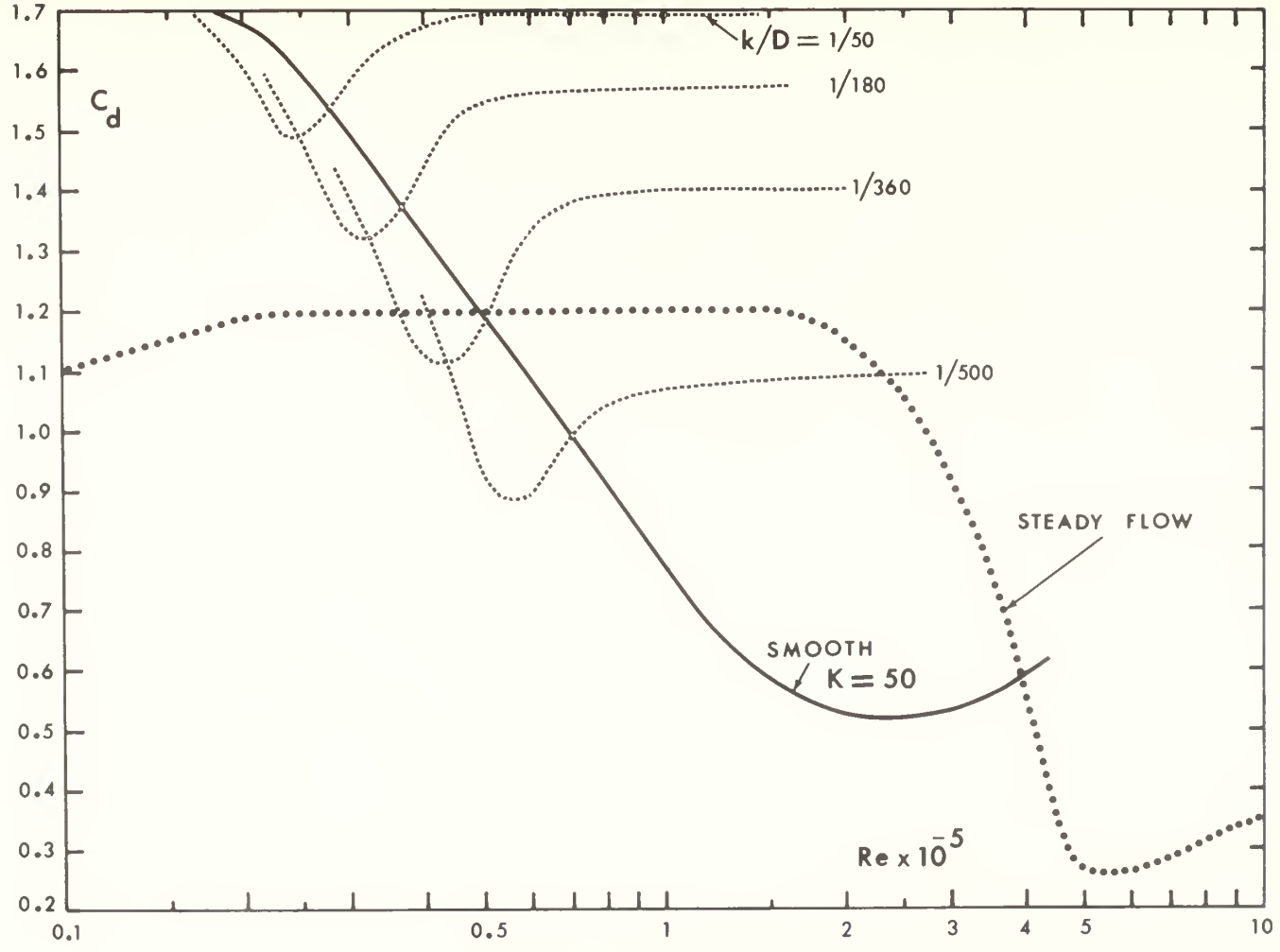

Fig. 59 C_d versus Re for various relative roughnesses, (K = 50).

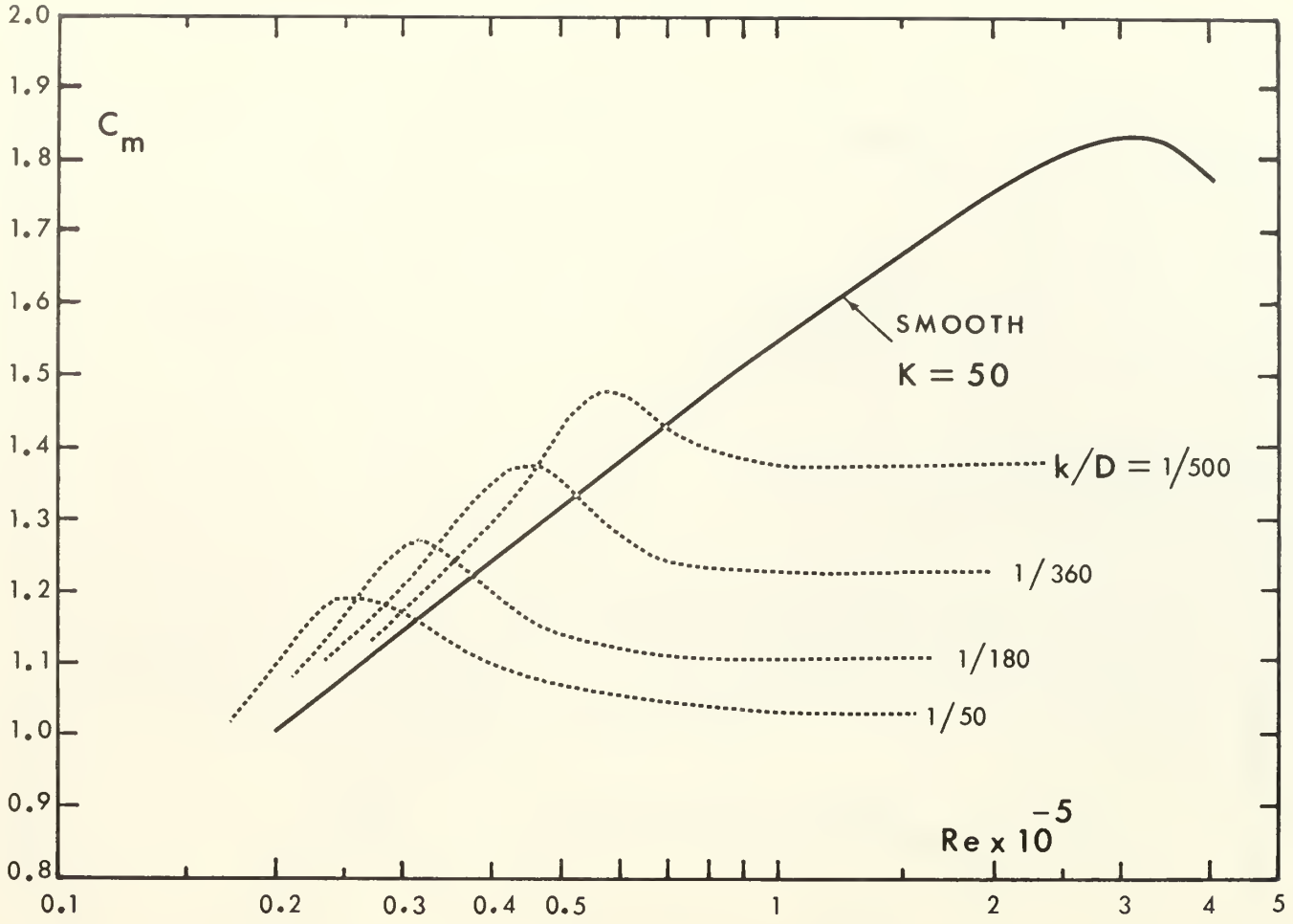

Fig. 60 C_m versus Re for various relative roughnesses, (K = 50).

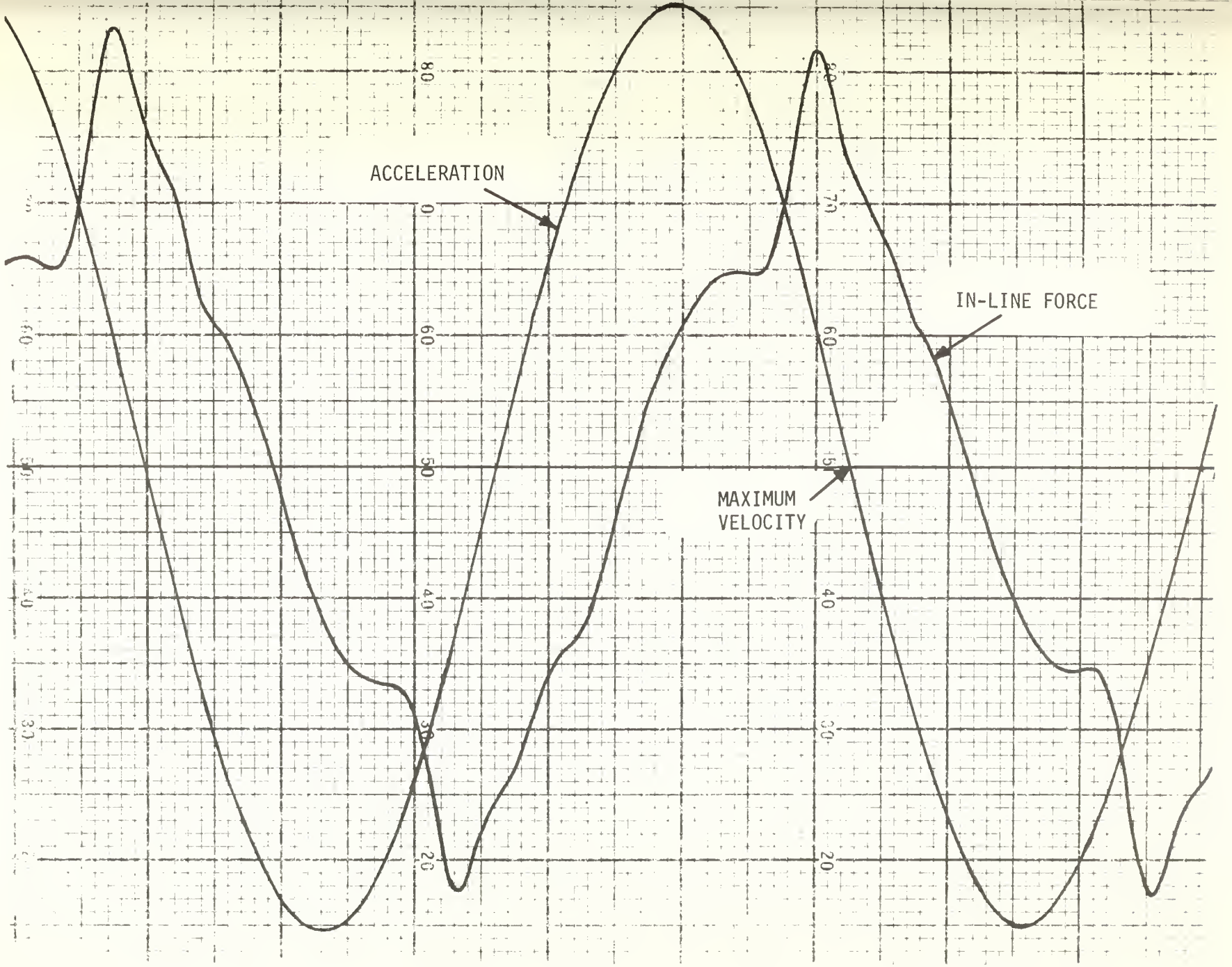

Fig. 61 In-line force and acceleration traces for harmonic flow over a rough cylinder. Note the occurrence of maximum force just before the maximum velocity.

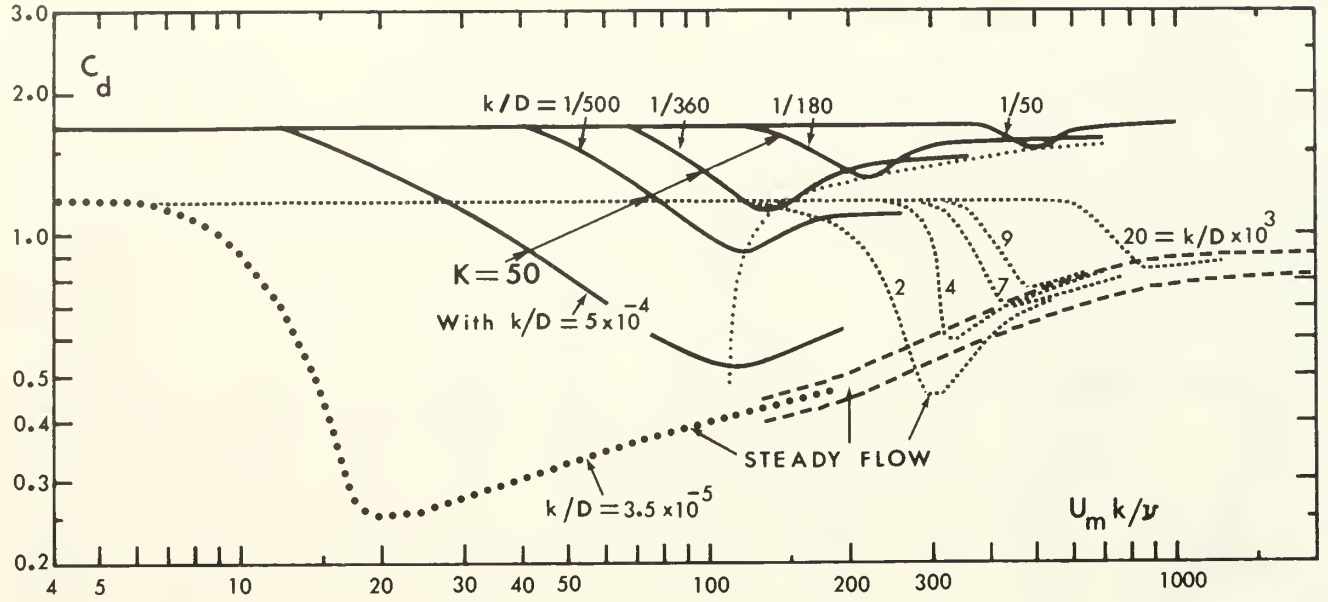

Fig. 62 C_d versus $U_m k/\nu$ for various relative roughnesses.
Dotted lines are for steady flow over rough cylinders.

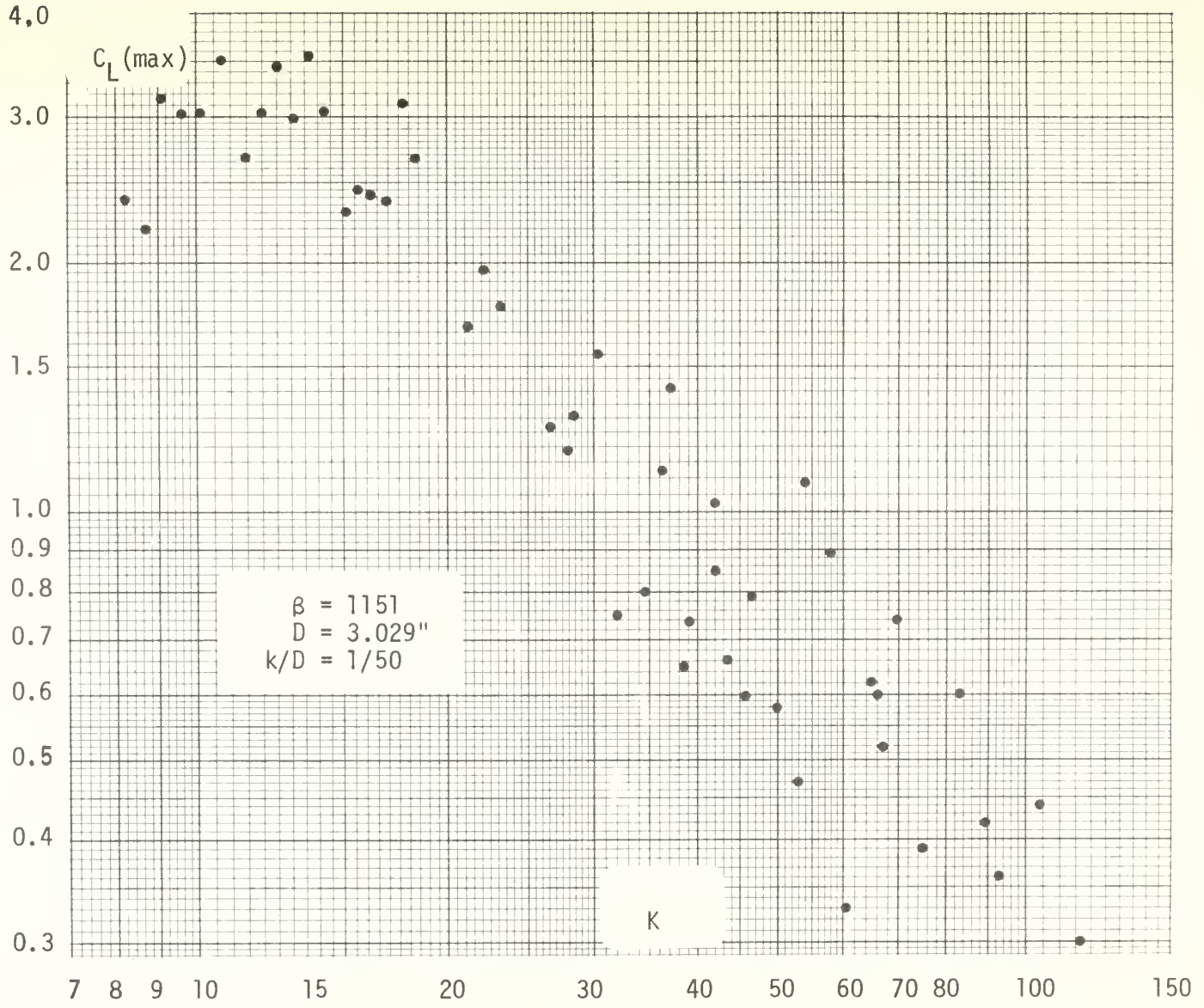

Fig. 63 C_L (max) versus K

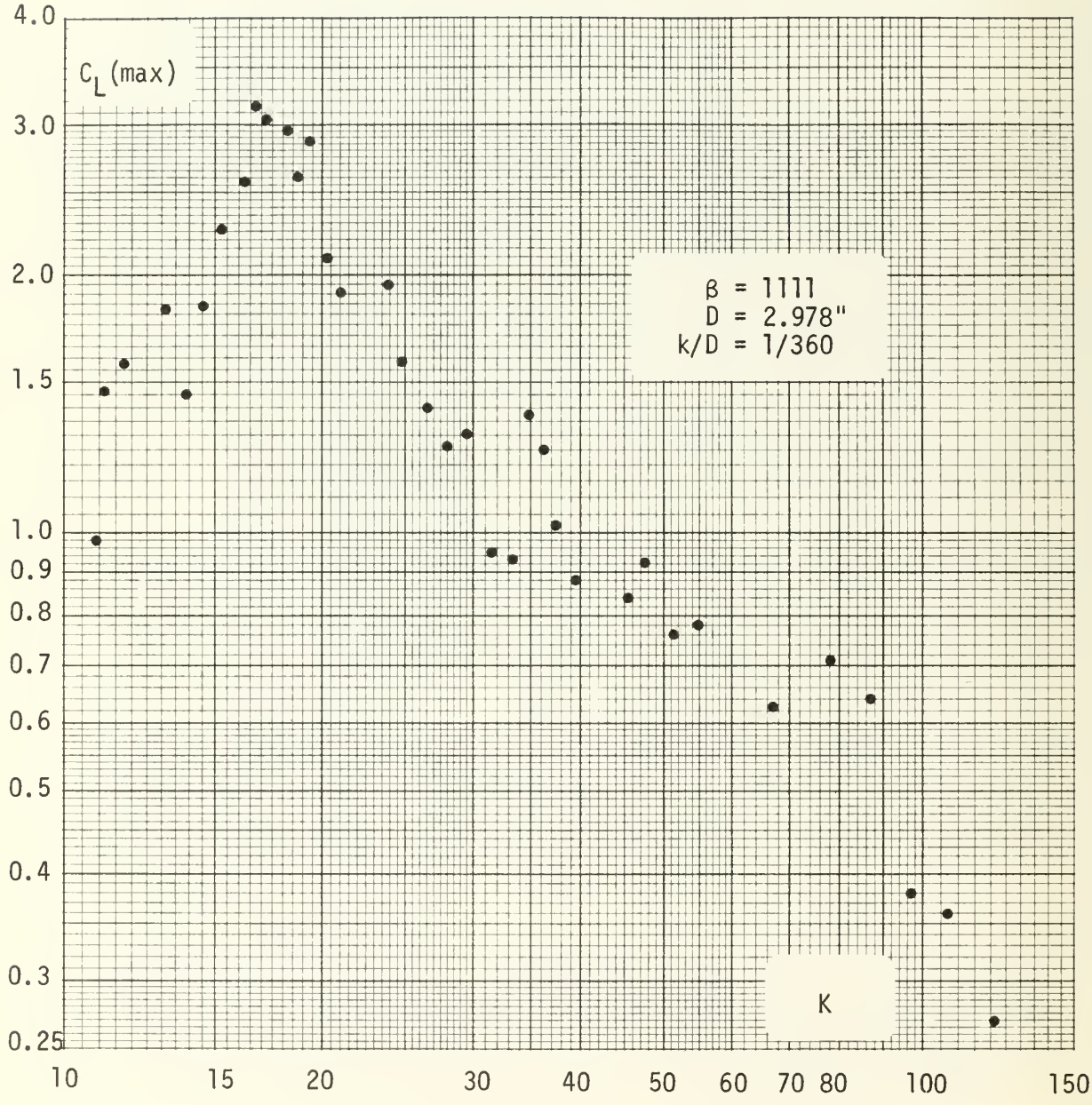

Fig. 64 C_L(max) versus K.

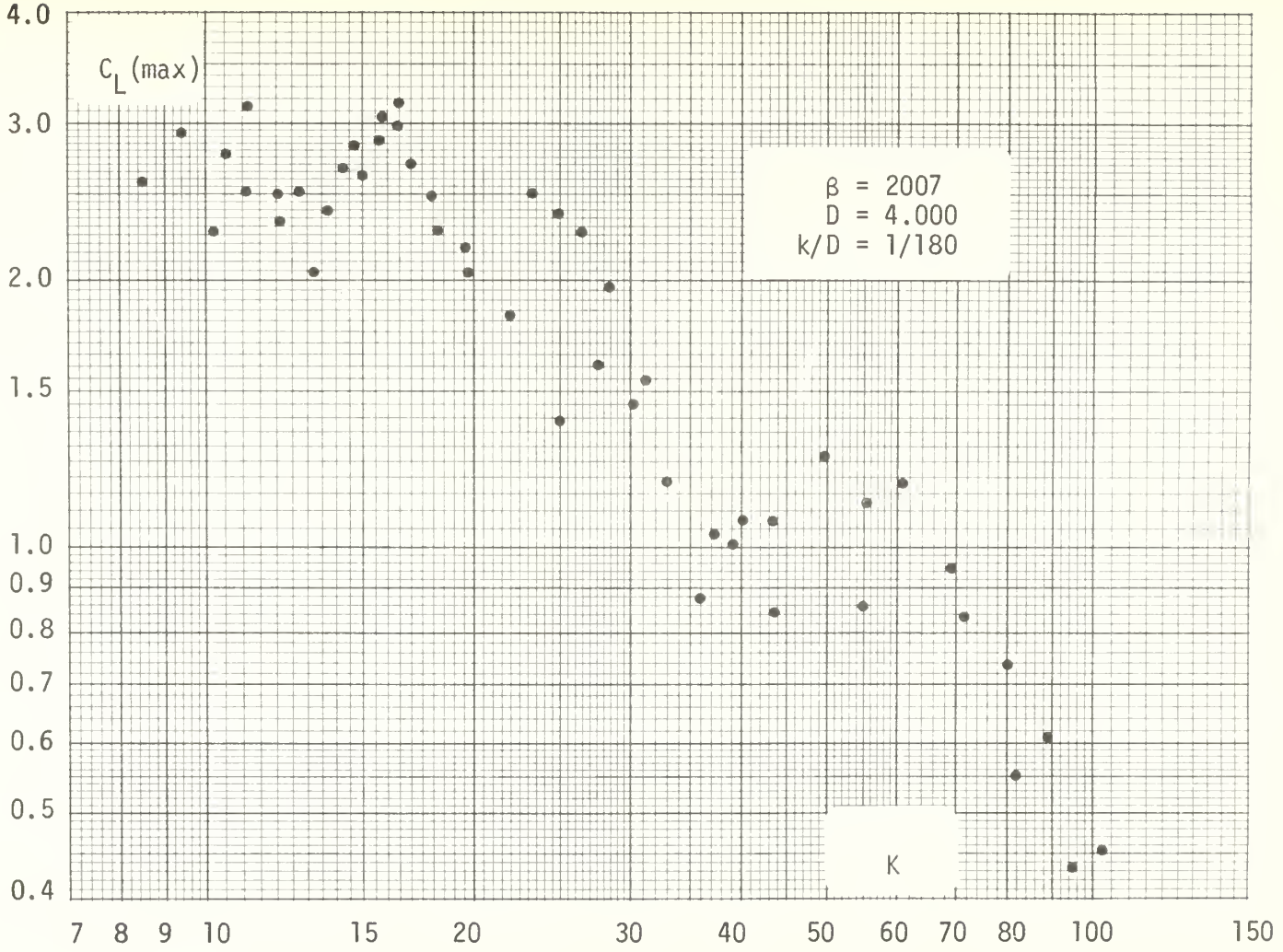

Fig. 65 C_L(max) versus K.

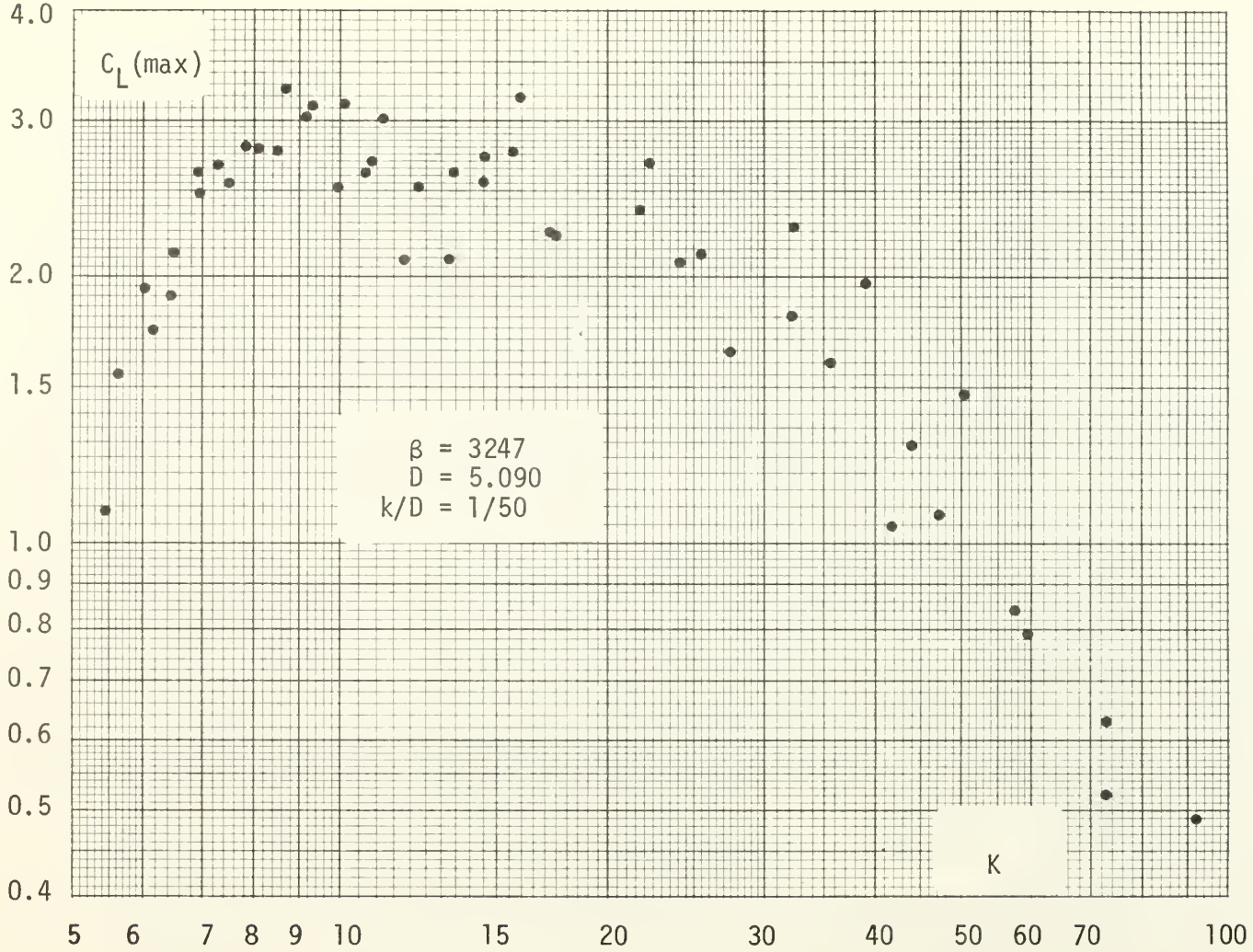

Fig. 66 C_L(max) versus K.

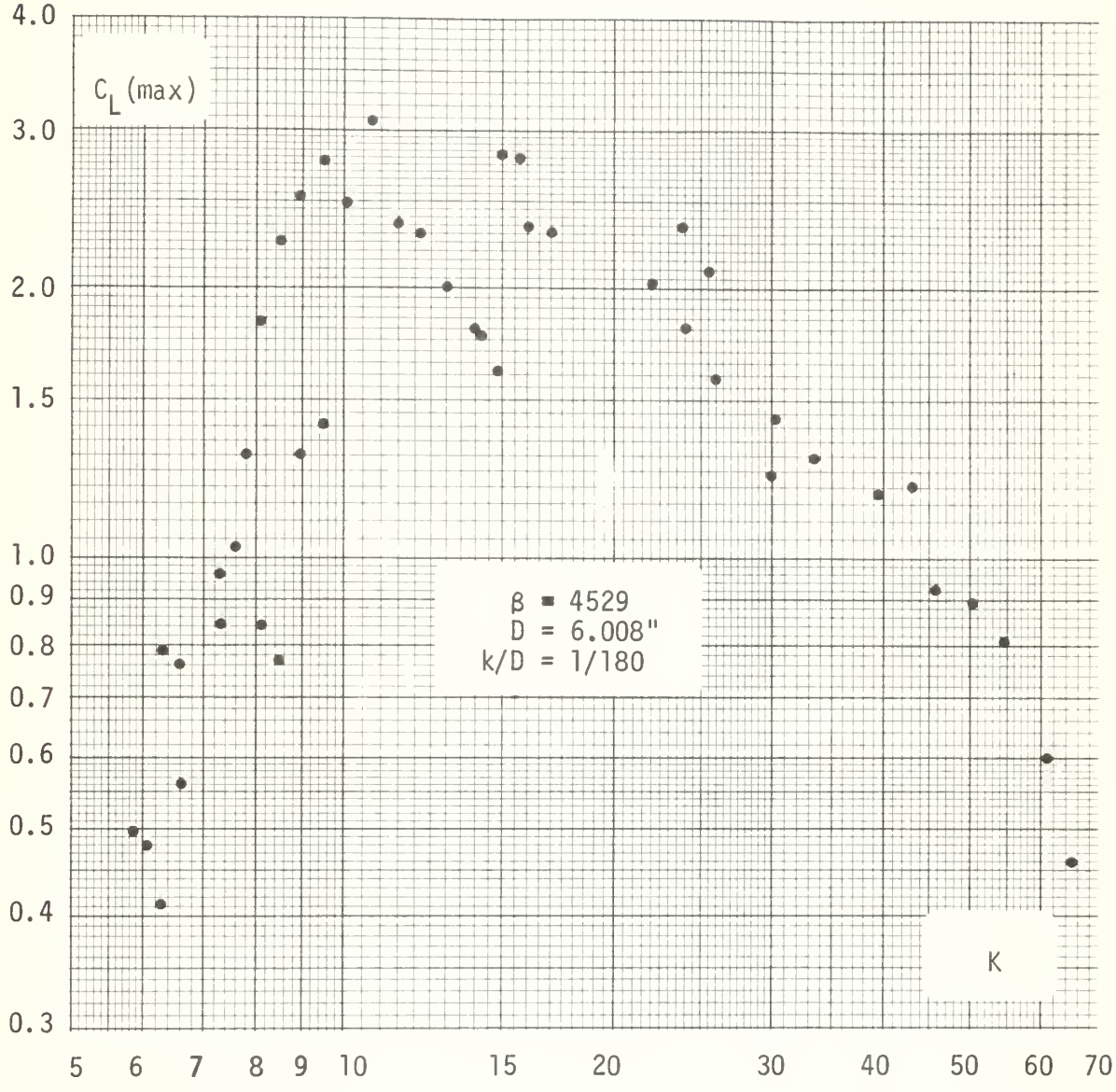

Fig. 67 C_L (max) versus K.

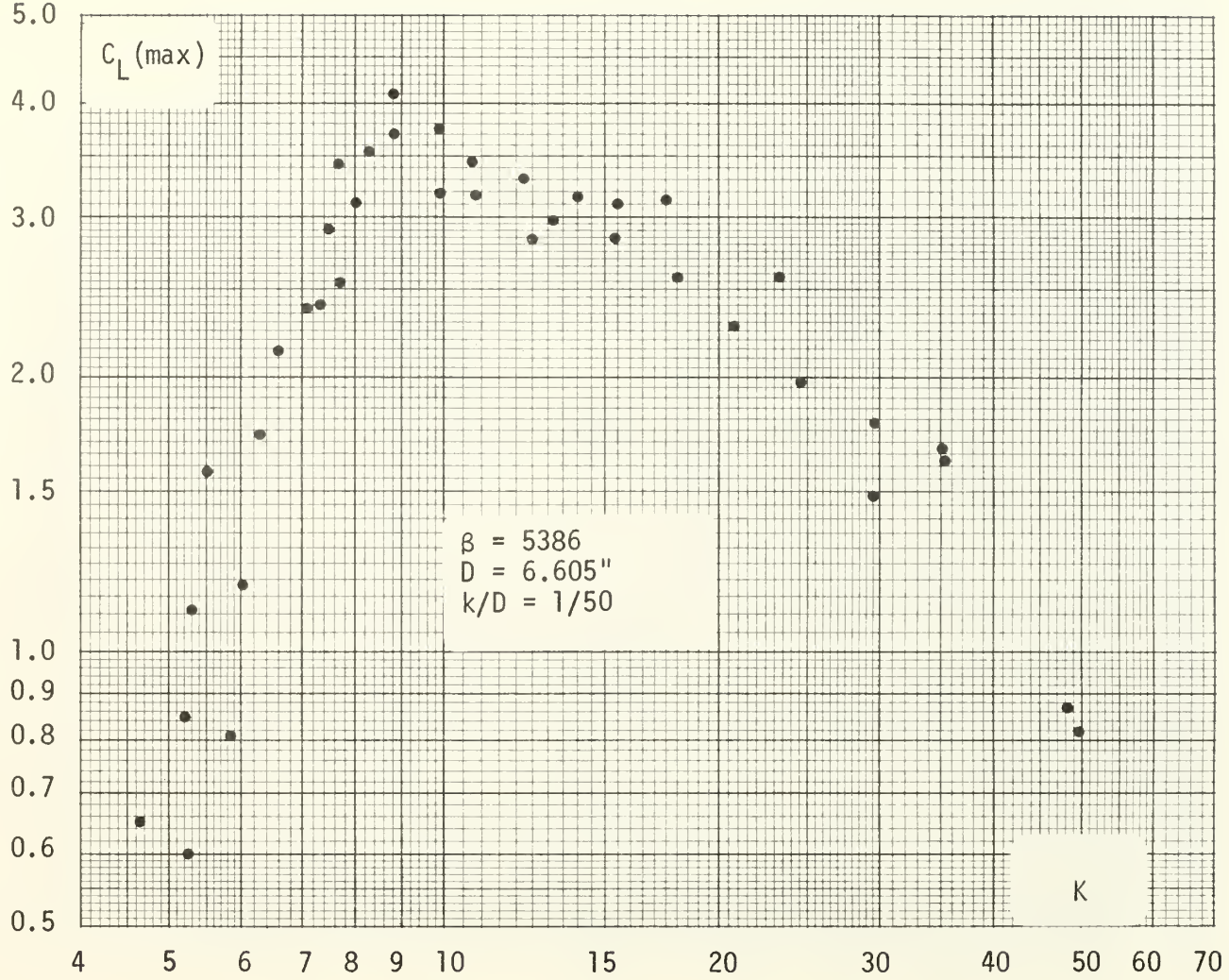

Fig. 68 C_L(max) versus K.

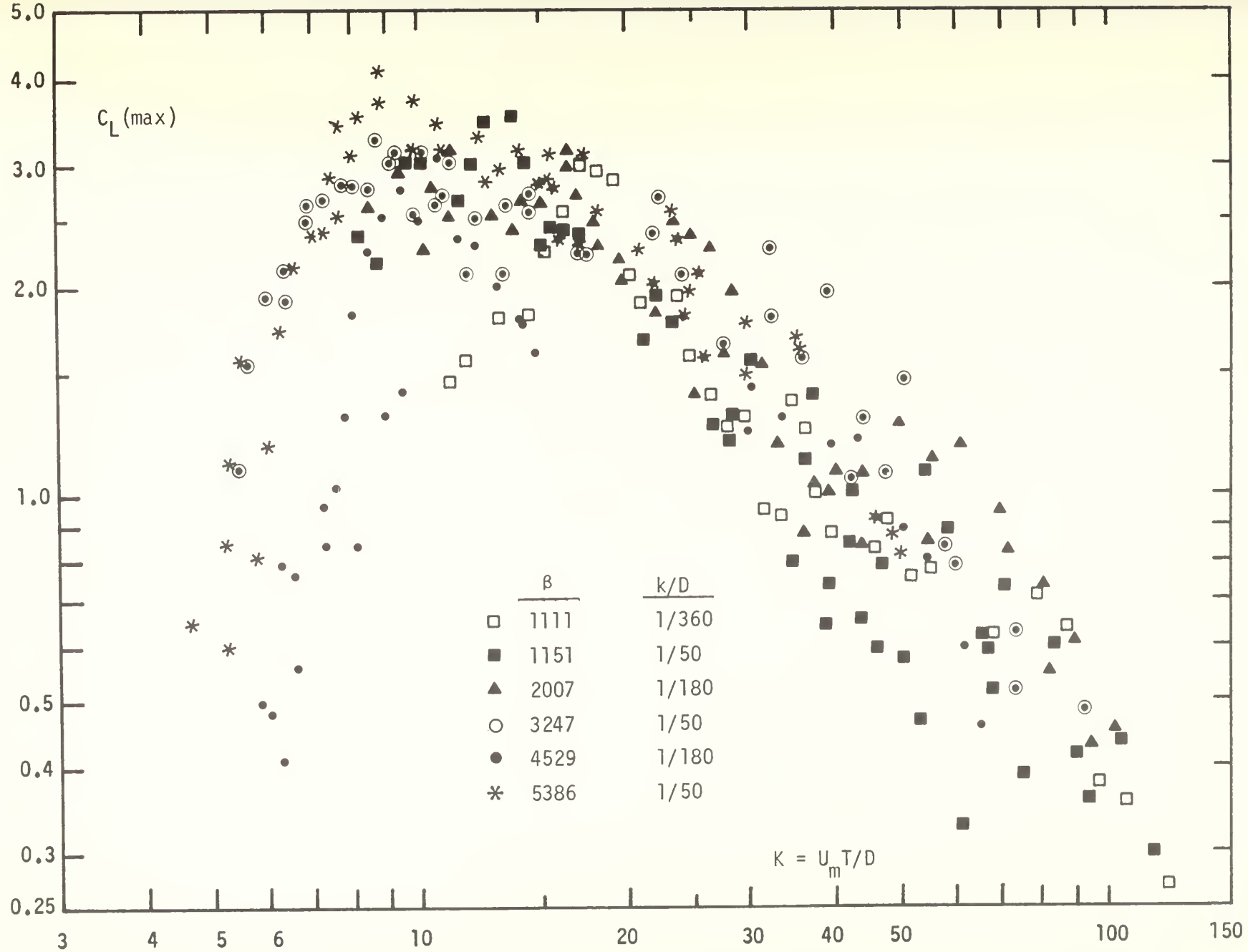

Fig. 69 C_L(max) versus K for various values of k/D and β.

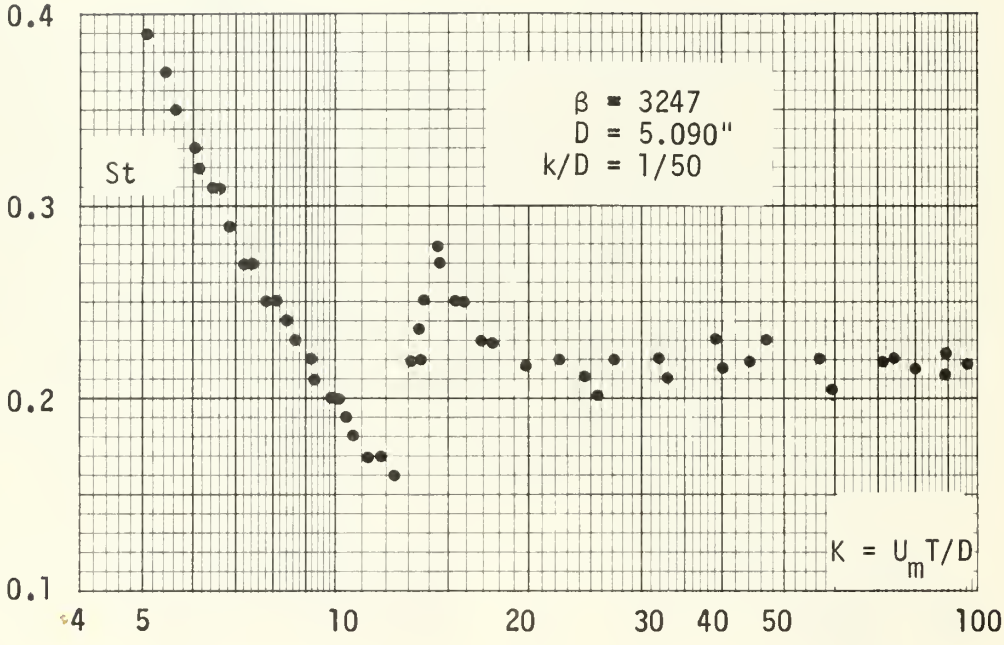

Fig. 70 Strouhal number versus K for a particular rough cylinder.

APPENDIX A

SPECIAL NOTES:

1. $\beta = D^2/\nu T$ and cylinder diameter D, given on top of each page, identify the data set;

2. $K = U_m T/D$ is the Keulegan-Carpenter number;

3. C_m represents the inertia coefficient calculated through the use of the Fourier analysis;

4. C_d represents the drag coefficient calculated through the use of the Fourier analysis;

5. $C_f(mes)$ represents the maximum measured-force coefficient;

6. σ represents a measure of goodness-of-fit, see Eq, (17);

7. λ^* represents the error coefficient, see Eq. (16);

8. All of the data given in Appendix A are for smooth cylinders.

APPENDIX A - IN-LINE FORCE DATA FOR SMOOTH CYLINDERS

β = 497 D = 1.991"

K	Re x 10^{-3}	C_m	C_d	C_f(mes)	σ	λ^*
194.78	96.87	1.12	1.20	1.35	11	8
175.50	87.28	1.20	1.25	1.35	9	0
149.33	74.24	1.10	1.29	1.38	7	0
142.63	70.93	1.20	1.24	1.30	8	1
126.69	62.99	1.09	1.31	1.37	8	0
116.20	57.78	1.20	1.33	1.36	6	2
107.94	53.67	1.15	1.37	1.40	8	3
100.55	50.00	1.16	1.35	1.36	8	4
94.27	46.88	1.10	1.39	1.42	6	-1
88.70	44.11	1.15	1.36	1.42	9	2
84.04	41.79	1.12	1.39	1.47	8	-1
79.15	39.36	1.20	1.38	1.41	7	3
74.27	36.92	1.07	1.45	1.47	8	0
64.08	31.87	1.10	1.53	1.60	7	3
59.73	29.70	1.05	1.52	1.51	10	1
56.24	27.98	1.10	1.54	1.60	6	0
53.02	26.34	1.10	1.55	1.59	6	2
49.69	24.71	1.05	1.59	1.61	6	0
47.00	23.37	1.10	1.55	1.66	8	9
45.41	22.59	1.02	1.66	1.63	9	-1
42.95	21.36	1.17	1.64	1.69	8	3
40.41	20.10	1.00	1.63	1.72	7	2
38.44	19.12	1.05	1.68	1.73	9	1
36.47	18.14	1.00	1.70	1.80	9	9
34.35	17.09	1.03	1.74	1.80	9	3
32.50	16.16	1.01	1.63	1.80	8	2
30.37	15.10	0.98	1.73	1.92	8	8
28.82	14.33	0.94	1.79	1.90	10	8
27.42	13.63	0.96	1.85	1.95	14	12
25.83	12.85	0.90	1.71	1.96	9	4
24.47	12.18	0.92	1.86	1.87	11	6
171.11	85.08	1.10	1.17	1.39	8	0
153.65	76.41	1.17	1.25	1.31	6	0
135.1	67.18	1.12	1.24	1.40	5	1
119.0	59.20	1.08	1.30	1.34	5	2
94.3	46.9	1.15	1.35	1.42	7	1
85.4	42.5	1.17	1.39	1.43	8	3
73.9	36.8	1.16	1.42	1.45	6	1
65.5	32.6	1.13	1.44	1.46	6	1
58.6	29.1	1.15	1.56	1.57	10	3
51.9	25.8	1.15	1.51	1.55	8	2
46.1	22.9	1.07	1.62	1.65	9	-2
44.0	21.9	1.04	1.61	1.64	8	-1
40.5	20.2	1.10	1.61	1.70	9	2
37.6	18.7	1.06	1.65	1.79	12	-3
35.0	17.4	1.02	1.63	1.75	8	2
32.0	15.9	0.99	1.70	1.89	7	1

		β = 497 D = 1.991"				
K	Re x 10^{-3}	C_m	C_d	C_f(mes)	σ	λ^*
29.8	14.9	1.00	1.73	1.85	9	1
27.8	13.8	0.92	1.74	1.90	7	1
25.3	12.6	0.94	1.80	2.05	11	2
23.1	11.5	0.89	1.86	2.02	12	3
21.8	10.8	0.90	1.92	2.15	12	3
19.5	9.7	0.82	1.92	2.30	12	5
16.7	8.3	0.76	2.05	2.67	11	4
14.9	7.4	0.68	2.18	2.80	18	6
13.7	6.8	0.66	2.30	2.88	16	4
12.0	6.0	0.66	2.36	2.67	12	4
10.0	5.0	0.84	2.23	2.35	9	2
171.1	85.1	1.16	1.23	1.31	7	-2
139.8	69.5	1.15	1.30	1.40	7	-1
123.2	61.3	1.18	1.29	1.37	5	0
110.7	55.1	1.19	1.30	1.37	5	0
96.9	48.2	1.15	1.37	1.37	7	1
83.2	41.4	1.17	1.43	1.43	6	2
72.6	36.1	1.12	1.44	1.49	8	3
66.9	33.3	1.05	1.45	1.50	6	2
59.9	29.8	1.10	1.55	1.56	6	2
54.2	26.9	1.05	1.54	1.61	7	-3
51.1	25.4	1.09	1.50	1.53	7	-2
47.2	23.5	1.03	1.62	1.61	9	-4
43.3	21.5	1.00	1.65	1.72	11	-4
41.0	20.4	1.08	1.59	1.63	8	2
38.1	19.0	1.01	1.70	1.68	10	4
33.9	16.9	1.00	1.71	1.75	9	2
30.7	15.3	1.03	1.65	1.80	9	3
27.4	13.6	0.93	1.75	1.85	8	2
24.0	12.0	0.94	1.86	2.08	13	5
15.5	7.7	0.72	2.13	2.70	14	6
14.2	7.1	0.67	2.23	2.84	20	8
12.5	6.2	0.63	2.32	2.75	18	7
11.0	5.5	0.74	2.32	2.50	16	8
9.6	4.8	0.96	2.20	2.35	8	4

β = 784 D = 2.500"

K	Rex10^{-3}	C_m	C_d	C_f(mes)	Sigma	λ^*
144.2	113.1	1.31	1.08	1.15	10	2
123.5	96.8	1.30	1.12	1.18	13	3
65.1	51.1	1.24	1.27	1.29	7	5
43.7	34.2	1.20	1.38	1.47	11	-2
33.5	26.2	1.15	1.50	1.59	9	1
28.1	22.0	1.06	1.65	1.63	12	5
26.0	20.4	1.02	1.68	1.80	11	7
21.8	17.1	0.98	1.77	1.95	10	6
20.3	15.9	0.93	1.82	2.07	13	8
19.0	14.9	0.88	1.90	2.17	14	7
17.2	13.5	0.84	2.10	2.33	13	6
16.2	12.7	0.80	2.07	2.50	14	6
15.1	11.9	0.74	2.02	1.60	16	8
14.1	11.1	0.78	2.14	2.74	12	4
13.2	10.4	0.65	2.20	2.74	18	10
11.8	9.2	0.65	2.20	2.57	16	8
12.4	9.8	0.69	2.21	2.65	20	11
11.3	8.8	0.65	2.22	2.49	19	9
10.2	8.0	0.80	2.12	2.30	16	6
9.6	7.5	0.91	2.05	2.30	12	4
9.2	7.2	1.05	2.00	2.31	11	-3
8.6	6.7	1.30	1.95	2.32	8	-2
8.0	6.3	1.50	1.92	2.40	6	-1
7.6	6.0	1.60	1.85	2.50	4	0
97.7	76.6	1.30	1.15	1.22	7	2
71.6	56.1	1.26	1.21	1.27	9	3
56.7	44.5	1.25	1.31	1.32	9	3
46.4	36.4	1.23	1.36	1.42	7	-2
39.6	31.1	1.16	1.40	1.49	10	2
30.7	24.1	1.10	1.54	1.65	11	4
24.0	18.8	0.98	1.70	1.87	8	3

β = 1107 D = 2.970"

K	Re x 10^{-3}	C_m	C_d	C_f(mes)	σ	λ^*
85.91	95.09	1.39	1.00	1.03	13	14
76.46	84.62	1.42	1.02	1.08	10	7
72.53	80.26	1.41	1.01	1.10	14	9
66.94	74.09	1.42	1.04	1.11	12	4
61.05	67.58	1.37	1.05	1.10	11	2
55.19	61.07	1.36	1.10	1.16	10	10
50.42	55.82	1.38	1.18	1.20	8	2
46.41	51.36	1.39	1.17	1.16	8	-3
39.86	44.13	1.35	1.24	1.22	9	-3
35.69	39.51	1.32	1.20	1.30	15	3
32.47	35.92	1.30	1.25	1.40	12	-6
29.80	32.98	1.25	1.37	1.43	15	4
28.28	31.30	1.22	1.35	1.49	12	-2
26.68	29.54	1.20	1.43	1.59	16	10
25.21	27.89	1.15	1.48	1.56	12	5
23.36	25.83	1.15	1.51	1.75	11	13
21.50	23.78	1.10	1.57	1.89	18	14
20.46	22.65	1.06	1.66	1.86	13	3
16.50	14.90	0.90	1.95	2.20	15	8
13.50	12.19	0.77	2.02	2.35	11	9
10.50	9.48	0.78	2.00	2.10	12	6
10.20	9.21	0.88	1.95	2.02	9	3
9.30	8.40	0.98	1.90	2.05	8	2
8.80	7.95	1.22	1.85	2.20	7	1
7.50	6.77	1.55	1.77	2.60	5	1
6.80	6.14	1.80	1.75	2.86	2	0
86.29	95.51	1.42	0.97	1.06	11	9
76.46	84.62	1.38	0.99	1.02	10	6
67.73	74.96	1.36	1.06	1.13	7	3
58.77	65.03	1.42	1.07	1.17	9	-4
54.30	60.11	1.37	1.12	1.13	12	-5
50.57	55.98	1.41	1.12	1.07	10	-4
46.64	51.62	1.43	1.16	1.20	9	2
44.25	48.98	1.36	1.15	1.21	11	4
41.20	45.61	1.32	1.16	1.26	9	3
37.34	41.32	1.39	1.26	1.34	10	5
34.96	38.70	1.30	1.24	1.32	12	6
32.06	35.48	1.26	1.32	1.31	14	7
30.21	33.42	1.30	1.36	1.48	11	5
28.53	31.59	1.27	1.44	1.57	9	2
24.83	27.48	1.20	1.49	1.63	10	3
23.63	26.16	1.11	1.45	1.70	12	-4
21.68	24.00	1.15	1.60	1.77	14	-6
20.00	22.16	1.00	1.69	1.95	15	-5
19.09	21.12	1.00	1.78	2.04	16	-5
17.80	19.68	0.92	1.88	2.10	16	1

β = 1107 D = 2.970"

K	Re x 10^{-3}	C_m	C_d	C_f(mes)	σ	λ^*
15.84	17.54	0.86	1.97	2.30	16	9
14.83	16.41	0.80	1.99	2.35	15	8
12.79	14.14	0.73	2.07	2.25	13	9
11.40	12.61	0.76	2.05	2.20	15	10
9.80	8.85	0.91	1.95	2.05	14	9
9.10	8.22	1.10	1.85	2.15	10	7
8.50	7.68	1.30	1.87	2.30	9	5
8.00	7.23	1.47	1.82	2.45	6	3
7.10	6.41	1.71	1.75	2.77	4	1
6.20	5.60	1.90	1.70	3.22	2	1
5.51	4.97	1.95	1.70	3.70	2	0

β = 1985 D = 3.978"

K	Re x 10^{-3}	C_m	C_d	C_f(mes)	σ	λ^*
65.13	129.28	1.51	0.66	0.71	12	0
57.51	114.16	1.60	0.72	0.75	11	-2
51.69	102.61	1.49	0.76	0.79	11	6
43.76	86.88	1.54	0.83	0.86	10	-7
38.47	76.40	1.48	0.86	0.90	10	-1
35.27	70.03	1.52	0.89	0.91	10	-6
32.37	64.28	1.45	0.94	0.98	11	-5
30.10	59.76	1.58	0.96	1.03	10	1
26.65	52.91	1.36	1.00	1.13	12	1
25.04	49.73	1.35	1.05	1.15	13	10
22.00	43.66	1.34	1.12	1.25	16	0
20.20	40.10	1.28	1.22	1.27	12	-1
18.00	35.77	1.21	1.32	1.50	11	6
17.02	33.78	1.27	1.40	1.49	12	-2
15.58	30.94	1.02	1.60	1.72	10	10
14.18	28.13	0.92	1.80	1.94	16	10
12.07	23.96	0.78	1.85	2.00	16	15
9.86	19.57	0.95	1.75	2.02	18	12
9.10	18.10	1.08	1.68	2.15	17	5
8.43	16.76	1.35	1.62	2.30	14	16
7.87	15.60	1.52	1.60	2.57	14	-5
7.47	14.84	1.63	1.50	2.67	12	2
6.94	13.80	1.81	1.54	2.95	11	10
6.58	13.04	1.82	1.54	3.10	11	8
6.16	12.22	1.83	1.56	3.22	9	12
5.91	11.74	1.88	1.52	3.40	9	11
65.26	129.57	1.48	0.67	0.72	14	0
58.19	115.56	1.53	0.70	0.74	14	-6
51.53	102.32	1.56	0.73	0.78	14	-9
43.59	86.57	1.46	0.79	0.84	14	6
36.26	72.01	1.49	0.86	0.89	11	-1
31.88	63.30	1.43	0.99	0.96	10	0
27.33	54.24	1.43	1.02	1.08	11	0
25.72	51.05	1.53	1.02	1.11	11	-1
23.33	46.32	1.48	1.06	1.22	10	1
21.25	42.21	1.29	1.13	1.23	13	1
19.67	39.05	1.41	1.21	1.35	14	9
18.10	35.93	1.36	1.25	1.41	10	7
17.02	33.78	1.23	1.35	1.56	15	-9
16.13	32.05	1.15	1.50	1.70	17	8
14.80	29.39	1.12	1.70	1.85	17	-2
14.14	28.07	1.00	1.76	1.90	13	-3
13.40	26.58	0.90	1.87	2.00	14	-7
12.32	24.44	0.82	1.82	2.05	11	-1
11.00	21.85	0.86	1.80	1.90	14	-3
8.24	16.39	1.68	1.54	2.43	10	9
7.87	15.60	1.74	1.56	2.60	9	10

		β = 1985 D = 3.978"				
K	Re x 10^{-3}	C_m	C_d	C_f(mes)	σ	λ^*
7.34	14.55	1.72	1.64	2.75	10	9
7.09	14.08	1.76	1.55	2.90	11	8
6.80	13.51	1.80	1.46	2.90	9	5
6.33	12.57	1.79	1.51	3.08	9	5
5.93	11.77	1.89	1.50	3.49	9	9
5.53	10.99	1.87	1.61	3.80	11	7
5.21	10.35	1.92	1.59	3.86	8	5
5.00	9.95	1.93	1.60	4.12	8	5
4.70	9.34	1.97	1.53	4.37	6	4
4.53	9.00	1.99	1.51	4.55	6	2
4.28	8.49	2.00	1.48	4.80	5	2
4.11	8.18	2.03	1.45	5.08	5	1
3.92	7.80	2.01	1.49	5.31	4	1
3.77	7.51	2.04	1.50	5.47	3	1
3.56	7.07	2.06	1.47	5.81	2	0

β = 3123 D = 4.990"

K	Re x 10^{-3}	C_m	C_d	C_f(mes)	σ	λ^*
59.10	184.62	1.73	0.55	0.50	13	-1
51.59	161.13	1.67	0.56	0.56	12	0
45.29	141.45	1.63	0.57	0.59	11	-2
42.64	133.17	1.50	0.59	0.58	14	-4
37.00	115.47	1.61	0.61	0.66	11	-3
33.43	104.43	1.60	0.66	0.74	12	0
30.29	94.60	1.60	0.68	0.76	10	-4
27.10	84.63	1.56	0.72	0.88	11	4
24.93	77.85	1.59	0.76	0.92	10	1
23.03	71.91	1.59	0.82	1.00	9	2
21.56	67.36	1.64	0.81	0.95	9	-4
20.10	62.81	1.46	0.88	0.99	12	0
17.94	56.03	1.41	0.97	1.03	14	0
15.84	49.46	1.47	1.05	1.21	12	3
14.72	45.98	1.54	1.12	1.30	11	3
13.87	43.36	1.38	1.13	1.30	10	5
13.21	41.26	1.36	1.25	1.34	10	-3
12.47	38.92	1.29	1.30	1.33	15	-9
11.80	36.87	1.17	1.36	1.60	16	8
11.17	34.85	1.24	1.37	1.52	14	-6
10.59	33.07	1.16	1.42	1.57	12	-7
10.12	31.64	1.19	1.40	1.59	10	-5
9.60	30.00	1.26	1.45	1.74	8	4
8.72	27.24	1.42	1.44	2.01	8	9
8.34	26.06	1.54	1.40	2.23	6	12
7.63	23.84	1.68	1.34	2.38	4	11
7.28	22.73	1.69	1.34	2.61	4	11
7.01	21.90	1.75	1.32	2.74	4	8
6.71	20.95	1.78	1.27	2.84	4	3
6.44	20.08	1.79	1.25	3.02	3	2
6.18	19.29	1.81	1.26	3.17	2	1
5.77	18.02	1.91	1.25	3.36	2	1
56.11	175.27	1.52	0.55	0.56	15	-5
47.16	147.35	1.65	0.57	0.59	13	0
39.77	124.23	1.69	0.65	0.70	11	0
38.29	119.63	1.51	0.62	0.64	12	-6
34.10	106.48	1.62	0.66	0.77	11	2
30.51	95.28	1.57	0.70	0.75	10	5
27.90	87.12	1.60	0.72	0.84	10	1
25.58	79.95	1.56	0.75	0.85	11	-5
23.10	72.19	1.52	0.81	0.98	12	4
21.47	67.08	1.57	0.84	1.00	13	0
20.37	63.60	1.46	0.88	0.90	12	-3
19.00	59.28	1.45	0.90	1.09	12	-9
17.54	54.81	1.48	0.96	1.07	10	0
15.49	48.39	1.41	1.02	1.18	9	0

β = 3123 D = 4.990"

K	Re x 10^{-3}	C_m	C_d	C_f(mes)	σ	λ^*
14.73	46.06	1.52	1.10	1.28	13	1
13.18	41.14	1.31	1.16	1.38	11	7
11.95	37.34	1.14	1.38	1.54	12	3
8.13	25.38	1.62	1.36	2.40	14	1
7.72	24.12	1.70	1.36	2.55	9	6
7.06	22.06	1.72	1.30	2.74	8	-2
6.62	20.67	1.75	1.30	2.87	6	0

β = 4480 D = 5.975"

K	Re x 10^{-3}	C_m	C_d	C_f(mes)	σ	λ^*
59.30	265.74	1.79	0.51	0.54	10	-5
48.23	216.13	1.83	0.51	0.57	11	1
39.84	178.52	1.77	0.55	0.63	10	0
35.71	160.02	1.70	0.58	0.67	12	2
30.76	137.83	1.71	0.62	0.76	11	4
28.65	128.39	1.74	0.61	0.78	11	-2
26.68	119.61	1.73	0.65	0.85	10	5
23.03	103.20	1.74	0.66	0.91	10	2
20.70	92.77	1.62	0.78	0.99	10	2
18.22	81.67	1.72	0.78	1.10	8	4
16.70	74.89	1.63	0.84	1.25	13	8
16.09	72.04	1.65	0.84	1.24	10	10
14.82	66.45	1.61	0.94	1.34	13	8
13.63	61.09	1.63	0.92	1.43	12	8
12.91	57.86	1.62	0.90	1.41	10	7
11.90	53.31	1.60	1.02	1.62	14	9
10.50	47.05	1.60	1.09	1.83	13	6
9.94	44.58	1.70	1.03	1.94	11	9
9.29	41.59	1.73	1.10	2.19	12	9
8.30	37.23	1.80	1.08	2.40	10	11
8.04	36.00	1.77	1.15	2.44	11	10
7.56	33.86	1.84	1.05	2.63	11	9
7.21	32.35	1.83	1.11	2.74	12	9
6.81	30.54	1.87	1.04	2.94	10	8
6.17	27.65	1.88	1.08	3.20	9	7
5.60	25.09	1.90	1.05	3.60	8	4
5.11	22.91	1.93	1.05	3.95	7	3
4.72	21.15	1.95	1.04	4.23	6	3
4.32	19.35	1.97	0.99	4.69	5	3
3.97	17.83	2.00	1.01	5.14	5	3
3.70	16.69	2.00	0.95	5.45	4	2
3.37	15.08	2.02	0.94	6.11	3	2
3.18	14.23	2.03	0.90	6.46	2	1
2.81	12.62	2.05	0.83	7.35	2	1
2.54	11.33	2.07	0.74	8.27	1	0
51.65	231.45	1.77	0.51	0.56	11	1
42.15	188.86	1.77	0.55	0.64	11	1
37.26	166.95	1.71	0.57	0.65	10	2
32.16	144.09	1.71	0.61	0.73	9	0
28.02	125.54	1.71	0.63	0.81	11	-1
25.44	113.97	1.66	0.67	0.83	10	1
22.03	98.70	1.69	0.71	0.98	11	0
19.71	88.26	1.67	0.75	1.08	9	1
18.41	82.48	1.68	0.76	1.12	9	2
17.15	76.83	1.65	0.83	1.17	8	0

β = 4480 D = 5.975"

K	Re x 10^{-3}	C_m	C_d	C_f(mes)	σ	λ^*
15.91	71.29	1.69	0.85	1.26	10	8
14.93	66.87	1.56	0.91	1.29	10	4
13.82	61.89	1.67	0.86	1.41	10	10
12.94	58.00	1.66	0.99	1.50	11	6
12.06	54.07	1.71	0.98	1.66	11	10
11.34	50.84	1.66	1.05	1.73	12	7
10.66	47.81	1.62	1.04	1.90	17	9
9.88	44.25	1.70	1.07	1.99	14	11
9.36	41.93	1.75	1.05	2.13	11	12
8.77	39.27	1.74	1.11	2.26	10	13
8.33	37.33	1.82	1.04	2.38	10	10
7.66	34.34	1.78	1.14	2.59	12	10
7.18	32.20	1.86	1.03	2.75	9	9
6,57	29.45	1.84	1.15	3.00	9	8
5.96	26.65	1.88	1.13	3.35	8	9
5.72	25.56	1.88	1.14	3.46	6	6
5.40	24.24	1.91	1.06	3.68	4	3
5.20	23.33	1.92	1.10	3.82	2	2
5.02	22.48	1.93	1.14	4.02	2	0
4.79	21.44	1.93	1.02	4.19	2	1
4.58	20.54	1.95	1.07	4.40	2	0
4.45	19.92	1.93	1.00	4.46	1	0

β = 5260 D = 6.475"

K	Re x 10^{-3}	C_m	C_d	C_f(mes)	σ	λ^*
48.1	253.0	1.81	0.52	0.54	12	2
38.3	201.5	1.72	0.54	0.61	10	6
31.5	166.0	1.70	0.58	0.70	12	4
26.3	138.4	1.86	0.62	0.81	11	1
25.0	131.4	1.69	0.66	0.79	8	6
19.8	104.2	1.75	0.74	1.00	9	0
19.0	100.0	1.61	0.75	1.02	6	11
15.6	82.2	1.72	0.80	1.22	7	9
13.9	73.1	1.65	0.85	1.19	8	8
11.6	61.1	1.65	0.94	1.58	7	10
10.5	55.0	1.74	0.96	1.73	6	7
9.4	49.4	1.68	1.00	1.89	3	4
8.6	45.0	1.72	1.02	2.11	6	6
7.6	39.9	1.76	1.02	2.34	3	2
5.9	31.1	1.89	1.02	3.27	2	1
5.8	30.4	1.92	1.01	3.19	1	0
56.2	295.6	1.90	0.49	0.55	13	10
47.1	247.7	1.86	0.52	0.59	11	7
38.8	204.1	1.82	0.56	0.69	11	6
34.7	182.7	1.85	0.57	0.72	9	10
31.8	167.5	1.80	0.60	0.73	8	8
29.4	155.0	1.83	0.62	0.80	7	9
24.7	129.8	1.66	0.66	0.88	10	10
23.1	121.7	1.81	0.68	0.86	9	6
21.2	111.3	1.66	0.69	0.95	8	12
19.4	102.1	1.75	0.73	1.00	7	8
17.4	91.5	1.72	0.78	1.08	6	9
16.2	85.3	1.70	0.80	1.21	4	10
14.7	77.2	1.68	0.85	1.25	1	9
13.3	70.2	1.78	0.87	1.42	8	8
12.6	66.4	1.73	0.88	1.49	9	10
11.1	58.2	1.80	0.94	1.71	10	6
10.4	54.7	1.74	0.99	1.80	11	6
9.8	51.3	1.76	1.00	1.90	13	5
9.4	49.2	1.74	1.01	1.95	10	4
8.7	45.6	1.81	1.03	2.19	9	2
51.5	270.7	1.84	0.51	0.55	12	4
43.9	230.7	1.75	0.53	0.56	10	3
37.0	194.8	1.75	0.56	0.64	12	7
30.0	157.6	1.71	0.61	0.69	11	7
25.6	134.5	1.75	0.65	0.83	8	7
23.4	122.9	1.70	0.67	0.80	9	6
21.2	111.3	1.70	0.71	0.88	6	8
18.7	98.4	1.68	0.75	0.99	7	9
16.0	84.3	1.62	0.83	1.11	6	3

β = 5260 D = 6.475"

K	Re x 10^{-3}	C_m	C_d	C_f(mes)	σ	$\overset{*}{\lambda}$
15.2	79.8	1.59	0.84	1.22	9	12
13.8	72.7	1.62	0.87	1.20	8	0
12.5	65.6	1.62	0.90	1.34	6	3
11.0	57.9	1.63	0.96	1.65	6	6
10.2	53.8	1.68	0.97	1.72	6	5
8.7	45.8	1.73	1.00	2.06	8	3
45.7	240.5	1.85	0.53	0.62	12	9
39.6	208.2	1.91	0.55	0.62	10	3
31.5	165.7	1.85	0.59	0.71	10	4
28.2	148.3	1.80	0.62	0.78	8	6
24.6	129.3	1.75	0.64	0.86	11	10
21.7	114.0	1.80	0.68	0.94	9	10
19.1	100.5	1.74	0.76	1.09	8	9
17.2	90.7	1.75	0.76	1.13	11	10
15.6	82.0	1.73	0.78	1.18	10	8
14.3	75.0	1.76	0.85	1.36	11	7
12.1	63.5	1.69	0.90	1.55	13	9
11.2	58.7	1.65	0.98	1.64	9	8
10.4	54.6	1.56	1.00	1.73	8	5
9.5	50.1	1.73	1.03	2.09	6	-2
9.0	47.6	1.83	1.04	2.18	4	-1
8.4	44.2	1.79	1.04	2.41	4	-1
7.8	41.2	1.86	1.02	2.44	4	-2
7.4	38.9	1.85	1.00	2.62	3	0
56.2	295.5	1.76	0.51	0.55	9	4
53.1	279.4	1.83	0.50	0.55	11	3
42.5	223.5	1.86	0.53	0.62	9	7
32.9	173.2	1.62	0.58	0.68	11	9
28.0	147.5	1.70	0.64	0.80	10	9
27.1	142.7	1.72	0.63	0.80	9	8
23.8	125.3	1.72	0.66	0.88	10	9
19.4	102.3	1.64	0.74	1.02	10	7
17.3	91.2	1.68	0.81	1.15	10	7
15.8	83.3	1.60	0.81	1.20	13	9
14.9	78.2	1.57	0.88	1.27	14	11
13.6	71.4	1.60	0.91	1.41	15	11
12.5	66.0	1.73	0.87	1.55	11	9
11.7	61.4	1.75	0.92	1.66	9	7
10.2	53.9	1.70	0.99	1.90	8	6
8.8	46.5	1.79	1.03	2.23	6	4
7.8	41.2	1.80	0.97	2.48	5	2
6.9	36.2	1.88	0.97	2.88	4	-1
6.2	32.8	1.89	1.02	3.21	4	-1
5.5	28.8	1.95	0.97	3.67	2	0
4.8	25.5	1.96	1.02	4.10	0	0
4.4	22.9	1.99	0.89	4.67	2	0

β = 5260 D = 6.475"

K	Re x 10^{-3}	C_m	C_d	C_f(mes)	σ	λ^*
3.8	20.0	2.01	0.96	5.42	4	2
54.9	288.8	1.81	0.51	0.57	10	9
51.9	273.1	1.87	0.49	0.57	11	9
43.7	229.7	1.79	0.55	0.64	9	8
41.7	219.4	1.85	0.54	0.63	9	7
32.8	172.3	1.65	0.53	0.66	9	5
26.7	140.4	1.69	0.64	0.80	9	3
23.2	122.1	1.72	0.66	0.93	9	-1
20.9	109.8	1.68	0.73	0.99	8	-3
18.5	97.4	1.67	0.78	1.06	8	12
16.7	87.9	1.71	0.78	1.18	9	10
14.8	77.8	1.63	0.82	1.31	10	11
13.6	71.5	1.67	0.83	1.41	11	10
12.4	65.1	1.73	0.92	1.50	9	9
11.4	59.9	1.78	0.95	1.65	8	6
9.2	48.4	1.66	1.00	2.17	8	6
8.8	46.5	1.75	1.04	2.27	6	5
7.9	41.6	1.79	1.05	2.45	6	3
7.2	38.1	1.86	0.98	2.74	5	3
6.5	34.1	1.90	1.04	3.11	4	2
5.9	30.8	1.90	0.98	3.41	4	0
5.3	28.1	1.96	0.92	3.82	4	1
4.8	25.0	1.98	0.93	4.40	4	1
4.2	21.9	1.99	0.97	5.07	3	1
3.5	18.6	2.01	0.88	6.07	2	2

β = 8370 D = 6.475"

K	Re x 10^{-3}	C_m	C_d	C_f(mes)	σ	λ^*
88.20	738.32	1.76	0.67	0.73	8	2
85.15	712.79	1.76	0.66	0.74	9	3
82.10	687.26	1.75	0.67	0.74	7	4
76.00	636.20	1.76	0.67	0.73	8	3
73.25	613.18	1.74	0.66	0.71	9	4
70.05	586.37	1.75	0.66	0.71	8	4
69.86	584.82	1.80	0.65	0.70	7	3
64.65	541.14	1.78	0.65	0.69	7	3
60.55	506.88	1.75	0.63	0.68	8	4
57.05	477.57	1.74	0.62	0.67	8	5
53.10	444.44	1.80	0.61	0.68	8	4
49.11	411.10	1.75	0.60	0.66	6	4
44.99	376.60	1.76	0.58	0.65	8	5
42.85	358.71	1.80	0.58	0.65	9	4
39.20	328.14	1.75	0.58	0.66	8	5
36.12	302.36	1.76	0.58	0.68	7	5
34.47	291.04	1.72	0.61	0.70	9	5
33.21	278.00	1.73	0.57	0.70	8	6
31.08	260.12	1.76	0.61	0.74	9	5
31.15	260.72	1.81	0.59	0.73	9	6
28.14	235.56	1.75	0.60	0.79	8	6
27.08	226.72	1.73	0.63	0.81	9	6
26.11	218.57	1.77	0.59	0.83	7	4
26.05	217.98	1.74	0.61	0.84	8	5
24.63	206.16	1.80	0.63	0.85	9	6
23.50	196.72	1.72	0.60	0.90	9	6
23.03	192.80	1.78	0.64	0.92	8	6
22.20	185.84	1.76	0.62	0.96	9	7
20.12	168.40	1.84	0.63	1.03	7	7
18.50	154.86	1.75	0.63	1.09	8	7
17.21	144.07	1.80	0.65	1.15	9	8
15.51	129.83	1.77	0.65	1.25	10	10
15.08	126.23	1.80	0.68	1.27	11	12
13.97	117.00	1.80	0.60	1.35	9	14
13.05	109.24	1.75	0.72	1.46	10	15
12.48	104.49	1.80	0.71	1.52	11	16
12.07	101.04	1.85	0.75	1.60	12	18
11.20	93.70	1.84	0.79	1.70	11	14
10.55	88.31	1.85	0.78	1.80	10	13
10.10	84.54	1.85	0.82	1.87	9	10
9.22	77.17	1.87	0.83	2.10	8	7

APPENDIX B

SPECIAL NOTES:

1. $\beta = D^2/\nu T$ and cylinder diameter D, given on top of each page, identify the data set;

2. K represents the Keulegan-Carpenter number, $U_m T/D$;

3. Re represents the Reynolds number based on diameter, $U_m D/\nu$;

4. C_L(max) represents the maximum transverse force coefficient;

5. C_L(rms) represents the root-mean-square normalized value of the transverse force, (it has not been evaluated for all runs);

6. f_r represents the ratio of the frequency of the transverse force to frequency of flow oscillation (f = 1/T);

7. $St = f_v D/U_m = f_r/K$ represents the Strouhal number;

8. All of the data given in Appendix B are for smooth cylinders;

9. Second and higher harmonics of the transverse force have not been analysed.

APPENDIX B - TRANSVERSE FORCE DATA FOR SMOOTH CYLINDERS

β = 497

D = 1.991"

K	Re x 10^{-3}	C_L (max)	f_r	St
175.55	87.28	0.22	35	0.20
158.93	79.02	0.26	27	0.17
137.64	68.43	0.28	27	0.20
121.84	60.58	0.39	25	0.20
110.75	55.06	0.24	23	0.21
103.79	51.60	0.46	21	0.20
93.11	46.29	0.50	18	0.19
84.34	41.93	0.43	18	0.21
77.48	38.52	0.76	16	0.21
71.82	35.71	0.99	14	0.19
66.61	33.12	1.14	14	0.21
61.72	30.68	0.81	13	0.21
58.16	28.91	0.86	13	0.22
54.72	27.21	1.39	13	0.24
51.61	25.66	1.00	11	0.21
47.35	23.54	0.89	9	0.19
45.03	22.39	1.75	10	0.22
43.09	21.43	1.01	9	0.21
41.03	20.40	1.29	8	0.19
38.93	19.36	1.39	8	0.20
37.21	18.50	1.80	8	0.21
35.78	17.80	1.79	8	0.22
33.85	16.83	1.68	8	0.24
32.64	16.23	1.67	8	0.24
30.70	15.26	1.51	7	0.23
29.49	14.66	1.73	6	0.20
27.87	13.86	2.05	6	0.21
26.54	13.19	1.73	6	0.23
20.53	10.21	2.10	5	0.24
19.64	9.76	2.21	5	0.25
18.59	9.24	2.30	4	0.21
17.61	8.75	3.24	4	0.23
16.72	8.31	3.41	4	0.24
16.05	8.00	3.16	4	0.25
15.19	7.55	3.34	3	0.20
14.36	7.14	2.46	3	0.21

β = 497

D = 1.991"

K	Re x 10^{-3}	C_L(max)	f_r	St
177.49	88.24	0.15	44	0.25
161.16	80.12	0.24	27	0.17
146.76	72.96	0.24	28	0.19
133.76	66.50	0.32	27	0.20
118.51	58.92	0.33	22	0.19
109.93	54.65	0.47	21	0.19
96.45	47.95	0.55	17	0.18
90.22	44.86	0.33	18	0.20
84.92	42.22	0.58	15	0.18
78.24	38.90	0.59	15	0.19
74.02	36.80	0.61	16	0.22
70.14	34.87	0.44	14	0,20
67.37	33.50	0.58	14	0.21
64.93	32.28	0.76	14	0.22
61.05	30.35	0.81	14	0.23
58.28	28.98'	0.75	11	0.19
55.93	27.81	0.76	12	0.21
53.71	26.70	0.95	12	0.22
51.83	25.77	1.27	10	0.19
50.50	25.11	1.41	10	0.20
48.85	24.29	1.21	10	0.20
47.13	23.43	0.77	13	0.28
45.57	22.66	1.71	9	0.20
41.82	20.79	1.83	8	0.19
40.49	20.13	1.79	8	0.20
39.09	19.43	1.12	9	0.23
36.32	18.06	1.21	7	0.19
34.89	17.35	1.38	7	0.20
30.95	15.39	1.19	7	0.23
31.13	14.98	1.93	7	0.22
28.60	14.22	1.66	6	0.21
27.33	13.59	1.80	6	0.22
24.66	12.26	1.60	5	0.20
21.16	10.52	2.55	5	0.24
20.34	10.11	2.21	4	0.20
19.45	9.67	2.52	4	0.21
18.81	9.35	2.73	4	0.21
18.11	9.00	3.20	4	0.22
17.32	8.61	2.78	4	0.23
16.68	8.30	2.86	4	0.24
16.21	8.06	3.17	3	0.18
15.48	7.70	3.25	3	0.19
14.94	7.42	2.92	3	0.20
14.36	7.14	2.39	3	0.21
13.89	6.90	2.35	2	0.14
13.57	6.75	3.15	2	0.15
13.00	6.46	3.71	2	0.15
12.49	6.21	3.83	2	0.16
12.14	6.03	3.07	2	0.16
11.76	5.85	3.64	2	0.17

β = 784

D = 2.500"

K	Re x 10^{-3}	C_L(max)	f_r	St
139.81	109.60	0.34	27	0.19
125.71	98.54	0.26	27	0.21
113.57	89.03	0.34	21	0.18
103.44	81.09	0.25	21	0.20
91.52	71.74	0.41	21	0.23
84.46	66.21	0.34	18	0.21
79.83	62.58	0.38	13	0.16
72.03	56.46	0.41	11	0.15
65.93	51.68	0.49	13	0.20
60.54	47.46	0.61	12	0.20
55.25	43.31	0.55	11	0.20
46.77	36.66	0.93	10	0.21
43.84	34.36	0.92	10	0.23
38.72	30.36	1.34	9	0.23
34.93	27.38	1.50	7	0.20
33.48	26.25	1.63	7	0.21
31.94	25.04	1.71	7	0.22
30.65	24.03	1.83	6	0.20
27.89	21.86	1.93	6	0.22
26.60	20.85	1.54	6	0,23
25.16	19.72	1.50	6	0.24
23.31	18.27	2.42	5	0.21
22.12	17.34	2.09	5	0.23
21.01	16.47	2.69	4	0.19
20.04	15.71	3.19	5	0.25
19.16	15.02	2.79	4	0.21
18.43	14.44	3.07	4	0.22
17.62	13.81	3.27	4	0.23
16.83	13.19	3.71	3	0.18
16.22	12.72	3.39	3	0.18
15.64	12.26	3.36	3	0.19
14.98	11.75	2.44	2	0.13
13.77	10.79	2.51	2	0.15
13.16	10.32	3.17	2	0.15
12.55	9.84	2.94	2	0.16
11.84	9.28	3.05	2	0.17
11.19	8.77	3.13	2	0.18
10.60	8. 31	3.25	2	0.19
10.12	7.94	3.50	2	0.20
9.59	7.52	3.42	2	0.21
9.06	7.10	3.56	2	0.22
8.81	6.90	3.87	2	0.23

β = 1107

D = 2.970"

K	Re x 10^{-3}	C_L(max)	C_L(rms)	f_r	St
146.61	162.26	0.08	0.04	29	0.20
124.70	138.00	0.18	0.06	20	0.16
106.70	118.10	0.17	0.07	17	0.16
92.23	102.10	0.23	0.10	19	0.21
80.73	89.34	0.23	0.11	13	0.18
71.77	79.44	0.32	0.17	13	0.18
59.05	65.36	0.41	0.19	12	0.20
53.51	59.28	0.44	0.14	12	0.23
48.00	53.10	0.56	0.18	9	0.19
41.89	46.34	1.10	0.37	10	0.23
40.16	44.46	1.00	0.49	9	0.22
36.66	40.59	0.93	0.38	8	0.22
34.22	37.88	0.74	0.32	7	0.21
31.02	34.32	0.71	0.22	7	0.22
29.35	32.48	1.46	0.67	6	0.19
27.06	29.94	1.84	0.81	5	0.20
25.21	27.89	2.22	0.74	5	0.20
24.02	26.59	2.25	0.91	5	0.21
22.97	25.43	1.71	0.68	5	0.21
21.60	23.93	1.98	0.87	5	0.22
20.46	22.65	2.59	1.02	5	0.22
19.27	21.33	2.92	1.18	4	0.22
18.43	20.39	3.16	1.29	4	0.23
17.31	19.16	2.87	1.16	4	0.25
16.35	18.08	2.95	1.18	4	0.21
15.49	17.14	2.87	1.21	3	0.21
13.15	14.51	3.10	1.50	2	0.15
12.34	13.65	3.10	1.65	2	0.16
11.73	13.00	3.24	1.67	2	0.18
7.87	8.72	2.40	1.45	2	0.26
143.48	158.78	0.08	0.03	24	0.17
129.55	143.36	0.10	0.04	20	0.16
113.41	125.49	0.16	0.05	18	0.16
100.97	111.73	0.23	0.07	17	0.17
89.08	98.58	0.24	0.10	14	0.16
80.37	88.94	0.34	0.13	15	0.19
72.38	80.10	0.32	0.12	14	0.20
62.37	69.02	0.52	0.19	14	0.23
56.68	62.72	0.69	0.24	12	0.21
53.27	58.95	0.51	0.17	12	0.23
49.25	54.50	0.84	0.38	10	0.21
44.65	49.41	0.66	0.27	9	0.21
38.68	42.81	0.84	0.35	9	0.22
34.38	38.04	0.94	0.42	7	0.19
29.76	32.93	0.96	0.33	6	0.19
26.73	29.58	1.22	0.51	6	0.21
24.84	27.48	1.67	0.74	6	0.21
23.18	25.65	1.94	0.93	5	0.23

β = 1107

D = 2.970"

K	Re x 10^{-3}	C_L(max)	C_L(rms)	f_r	St
21.54	23.83	2.27	1.06	5	0.21
20.39	22.56	2.63	1.35	4	0.19
16.32	18.06	2.51	1.45	2	0.15
15.32	16.95	3.15	1.55	2	0.14
14.12	15.63	3.72	1.72	2	0.16
13.16	14.57	3.26	1.73	2	0.16
11.95	13.22	3.76	1.83	2	0.18
10.63	11.76	3.33	1.72	2	0.20
9.67	10.70	3.86	1.58	2	0.24
8.56	9.48	3.19	1.55	2	0.27
7.35	8.13	2.48	1.54	2	0.31

β = 1985

D = 3.978"

K	Re x 10^{-3}	C_L (max)	C_L (rms)	f_r	St
92.84	184.31	0.12	0.04	24	0.26
83.14	165.06	0.12	0.05	22	0.28
73.03	144.96	0.17	0.05	20	0.28
56.54	112.24	0.26	0.11	14	0.25
51.27	101.79	0.30	0.12	12	0.23
44.16	87.67	0.38	0.14	10	0.23
41.54	82.46	0.53	0.16	10	0.25
37.77	74.98	0.55	0.19	9	0.24
33.76	67.03	0.60	0.24	8	0.23
32.35	64.22	0.75	0.31	7	0.22
29.61	58.79	0.76	0.28	7	0.23
27.32	54.24	1.07	0.45	6	0.21
23.89	47.42	1.50	0.66	5	0.23
22.93	45.53	1.36	0.59	5	0.23
21.37	42.43	1.52	0.68	4	0.19
19.10	37.92	1.45	0.51	4	0.23
17.72	35.17	1.95	0.88	2	0.14
16.67	33.09	2.78	1.06	2	0.14
15.51	30.78	2.31	1.12	2	0.13
14.66	29.11	2.90	1.38	2	0.14
13.57	26.93	3.03	1.57	2	0.15
12.26	24.34	3.59	1.81	2	0.16
11.36	22.54	3.36	1.73	2	0.19
10.69	21.22	2.98	1.75	2	0.19
9.41	18.69	2.94	1.75	2	0.22
8.44	16.76	2.95	1.80	2	0.24
92.55	183.78	0.14	0.05	19	0.20
75.12	149.36	0.20	0.07	21	0.28
65.81	130.67	0.18	0.08	19	0.30
58.19	115.55	0.26	0.10	13	0.23
51.54	102.32	0.27	0.09	16	0.32
46.76	92.85	0.25	0.11	11	0.23
42.76	84.90	0.32	0.15	12	0.28
38.82	77.07	0.47	0.16	12	0.30
35.42	70.34	0.62	0.24	9	0.25
32.77	65.07	0.67	0.24	9	0.28
30.44	60.43	0.61	0.22	8	0.27
28.32	56.23	1.01	0.43	6	0.22
26.27	52.16	0.85	0.34	6	0.23
23.52	46.69	1.51	0.65	5	0.21
22.00	43.69	1.70	0.67	4	0.23
20.75	41.20	0.98	0.48	5	0.22
19.69	39.12	1.82	0.65	5	0.22
18.54	36.81	1.96	0.87	4	0.22
16.79	33.34	1.98	0.90	4	0.22
15.86	31.48	2.23	1.03	4	0.22

β = 3123

D = 4.990"

K	Re x 10^{-3}	C_L(max)	C_L(rms)	f_r	St
59.44	185.64	0.13	0.06	18	0.30
53.91	168.38	0.19	0.07	19	0.35
49.27	153.89	0.29	0.09	18	0.36
44.74	139.75	0.24	0.09	16	0.36
39.22	122.48	0.31	0.12	12	0.31
34.59	108.03	0.50	0.22	9	0.25
30.56	95.44	0.43	0.19	7	0.22
28.03	87.56	0.36	0.17	8	0.28
25.78	80.51	0.64	0.28	7	0.27
23.03	71.91	0.49	0.18	6	0.25
21.03	65.70	0.69	0.25	3	0.16
19.93	62.25	1.03	0.42	5	0.25
18.51	57.82	1.02	0.42	4	0.23
17.38	54.29	1.07	0.37	3	0.18
16.06	50.17	0.67	0.30	2	0.14
13.90	43.40	0.99	0.52	3	0.21
10.21	31.88	1.08	0.60	2	0.21
67.38	210.47	0.15	0.05	16	0.24
58.00	181.17	0.20	0.07	19	0.32
48.39	151.15	0.20	0.08	19	0.39
43.08	134.56	0.25	0.10	14	0.32
37.81	118.13	0.31	0.14	12	0.31
34.18	106.76	0.27	0.12	11	0.31
31.00	96.82	0.38	0.15	8	0.24
26.34	82.29	0.79	0.25	7	0.26
24.27	75.80	0.58	0.24	6	0.23
22.36	69.85	0.88	0.36	5	0.22
21.03	65.70	0.72	0.30	6	0.31
18.31	57.18	1.00	0.45	4	0.23
17.21	53.74	0.74	0.38	4	0.22
14.49	45.26	1.25	0.66	4	0.27
13.52	42.25	1.25	0.66	4	0.27
11.36	35.48	1.22	0.72	2	0.19
10.88	33.98	0.93	0.51	2	0.18
10.32	32.23	1.22	0.76	2	0.20

β = 4480

D = 5.975"

K	Re x 10^{-3}	C_L(max)	C_L(rms)	f_r	St
68.52	307.05	0.20	0.08	23	0.33
57.18	256.21	0.18	0.08	15	0.26
48.88	219.07	0.14	0.07	14	0.29
44.27	198.35	0.21	0.08	17	0.38
39.65	177.71	0.38	0.14	14	0.35
34.57	154.85	0.25	0.08	11	0.32
28.83	129.20	0.46	0.18	10	0.35
28.01	113.78	0.58	0.25	9	0.23
23.29	104.34	0.90	0.38	7	0.28
21.44	96.09	1.11	0.40	6	0.26
19.37	86.79	0.65	0.30	5	0.28
18.04	80.82	1.08	0.47	5	0.28
16.67	74.70	1.38	0.59	5	0.27
15.54	69.67	0.96	0.42	4	0.24
14.50	64.98	1.18	0.59	3	0.22
10.59	47.48	0.92	0.43	3	0.30
9.19	41.17	0.95	0.39	3	0.32
8.68	38.89	1.23	0.57	2	0.26
8.10	36.33	0.81	0.35	2	0.26
7.58	34.01	0.60	0.27	2	0.32
7.09	31.78	0.69	0.29	2	0.28
6.62	29.69	0.50	0.26	2	0.27
6.26	28.03	0.87	0.44	2	0.31
5.60	25.09	0.74	0.31	2	0.39
62.37	279.36	0.17		20	0.32
37.55	168.19	0.28		13	0.35
32.14	143.95	0.51		10	0.31
26.95	120.71	0.41		8	0.30
24.38	109.18	0.68		6	0.25
20.30	90.92	1.34		5	0.25
17.12	76.69	1.37		4	0.23
14.98	67.11	1.12		4	0.27
12.66	56.73	0.85		4	0.31
10.28	46.05	0.76		3	0.29
8.74	39.13	0.72		2	0.23
8.44	37.80	0.92		2	0.24
7.91	35.43	0.50		2	0.25
6.87	30.78	0.46		2	0.29
6.44	28.84	0.60		2	0.31

β = 5260

D = 6.475"

K	Re x 10^{-3}	C_L(max)	C_L(rms)	f_r	St
53.62	282.08	0.22	0,08	14	0.26
43.84	230.33	0.29	0.12	13	0.30
38.30	201.50	0.41	0.13	9	0.23
34.90	183.62	0.28	0.12	11	0.33
31.15	163.88	0.36	0.13	10	0.31
28.32	149.00	0.52	0.20	9	0.31
25.93	136.39	0.48	0.23	8	0.30
21.00	110.39	0.54	0.23	2	0.11
19.27	101.39	0.87	0.33	2	0.11
17.47	91.89	0.89	0.40	2	0.12
16.24	85.41	0.79	0.32	3	0.19
15.11	79.50	1.31	0.64	3	0.21
14.02	73.80	1.36	0.63	2	0.17
13.17	69.33	0.75	0.43	2	0.15
12.24	64.39	0.53	0.21	2	0.18
11.50	60.54	1.44	0.61	3	0.22
10.68	56.17	0.70	0.37	4	0.34
10.03	52.78	1.25	0.46	2	0.16
9.05	47.59	0.64	0.25	3	0.28
8.70	45.79	0.89	0.39	2	0.20
8.00	42.04	0.57	0.29	3	0.31
7.57	39.78	0.69	0.30	2	0.23
5.19	27.29	0.63	0.44	2	0.31
5.45	28.68	0.56	0.40	2	0.28
5.78	30.42	0.52	0.35	2	0.47
7.33	38,54	0.47	0.30	2	0.25
7.86	41.32	0.51	0.26	2	0.29
8.71	45.79	0.62	0.27	3	0.31
9.55	50.62	1.14	0.47	2	0.20
10.29	54.11	1.41	0.58	2	0.18
11.05	58.12	1.02	0.39	3	0.27
12.75	67.06	1.12	0.53	3	0.20
14.24	74.93	0.78	0.43	3	0.21
15.46	81.30	1.33	0.45	3	0.19
17.23	90.65	1.07	0.45	3	0.15
19.11	100.52	0.61	0.23	3	0.17
21.84	114.86	0.43	0.20	7	0.30
25.15	132.28	0.57	0.19	7	0.28
30.99	163.01	0.41	0.15	9	0.28
36.18	190.30	0.28	0.10	8	0.21
42.05	221.18	0.30	0.10	16	0.38
52.61	276.74	0.25	0.09	21	0.40
56.01	294.62	0.31		15	0.27
49.63	261.06	0.24		18	0.36
44.36	233.31	0.22		15	0.34
40.10	210.91	0.37		13	0.32
34.99	184.03	0.32		9	0.26
32.09	168.82	0.45		9	0.28

β = 5260

D = 6.475"

K	Re x 10^{-3}	C_L(max)	C_L(rms)	f_r	St
29.14	153.30	0.55		10	0.34
27.02	142.15	0.51		9	0.33
24.46	128.68	0.59		7	0.29
22.95	120.77	0.56		6	0.26
20.85	109.67	0.44		6	0.29
19.21	101.03	0.69		5	0.26
17.81	93.68	0.66		5	0.28
16.03	84.54	0.69		4	0.25
13.75	72.30	1.06		3	0.22
12.96	68.19	0.96		3	0.23
12.14	63.88	1.09		3	0.25
11.44	60.18	0.65		3	0.26
10.73	56.43	0.71		2	0.19
10.15	53.39	0.59		2	0.20
9.67	50.88	0.85		2	0.21
9.12	47.99	0.94		3	0.33
8.67	45.63	0.63		2	0.23
7.87	41.42	0.92		2	0.25
7.26	38.18	0,53		2	0.27
7.01	36.90	0,61		2	0.28
6.71	35.31	0.48		2	0.30
6.40	33.66	0.61		2	0.31
54.56	287.01	0.14		15	0.27
48.44	254.79	0.22		18	0.37
43.42	228.38	0.19		15	0.34
37.46	197.03	0.34		12	0.32
33.03	173.75	0.28		10	0.30
30.88	162.44	0.31		9	0.29
28.69	150.93	0.60		9	0.31
26.61	139.98	0.46		7	0.26
24.81	130.48	0.46		7	0.28
23.20	122.05	0.75		8	0.34
21.22	111.62	0.79		6	0.28
19.59	103.04	1.00		6	0.31
17.95	94.40	0.88		5	0.28
16.72	87.30	1.11		3	0.18
15.73	82.74	1.59		4	0.25
14.65	77.09	0.81		4	0.27
13.77	72.46	0.83		3	0.22
13.02	68.50	1.13		4	0.31
11.97	62.95	0.94		4	0.33
11.37	59.82	0.62		3	0.26
10.70	56.27	0.95		4	0.37
10.15	53.39	0.74		3	0.30
9.67	50.88	0.81		4	0.41
8.34	43.88	0.97		2	0.24
7.99	42.04	0.78		2	0.25
7.60	39.98	0.80		2	0.26
7.23	38.03	0.72		2	0.28

APPENDIX C

SPECIAL NOTES:

1. This appendix represents sample calculations through the use of the discrete vortex model for K = 9.2. Analysis and complete results will be presented separately;

2. There are four types of discrete vortices: + and * represent the vortices shed from the separation points as flow speed increases from left to right; X and . represent the vortices shed from the additional separation points as the flow reverses its direction;

3. Normalized time t/T is given on each figure.

APPENDIX C - SAMPLE DISCRETE VORTEX ANALYSIS FOR K = 9.2.

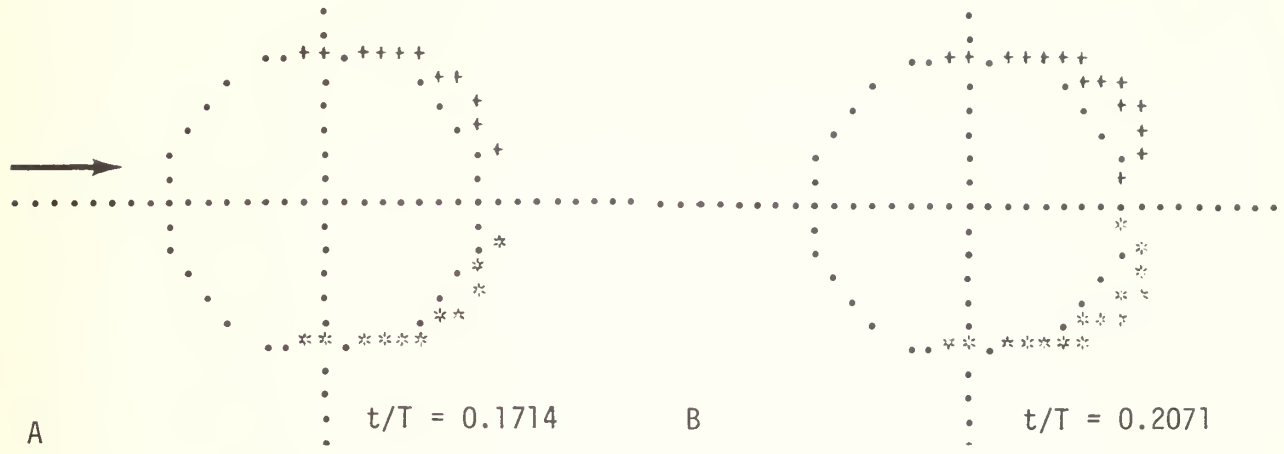

A t/T = 0.1714 B t/T = 0.2071

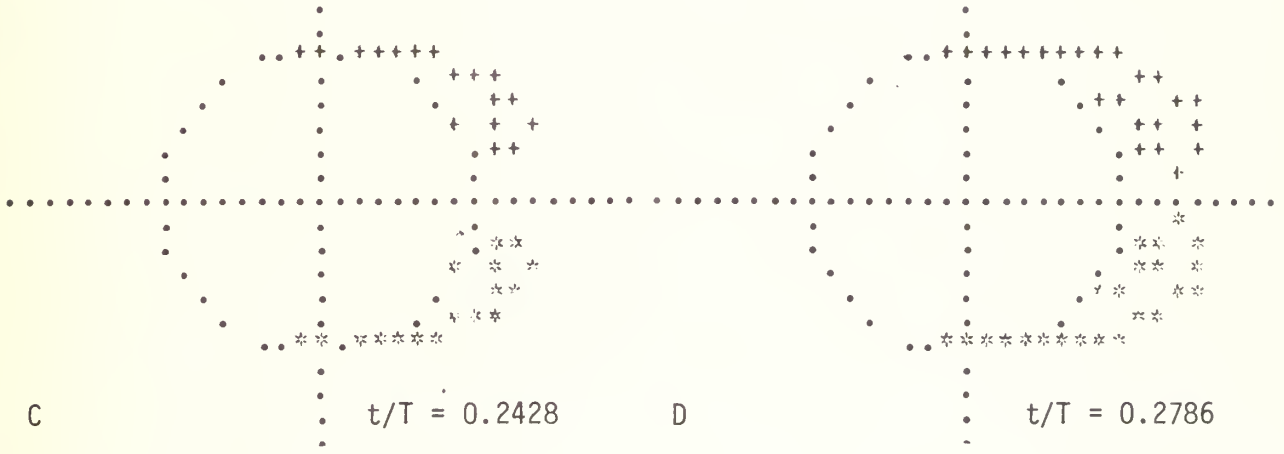

C t/T = 0.2428 D t/T = 0.2786

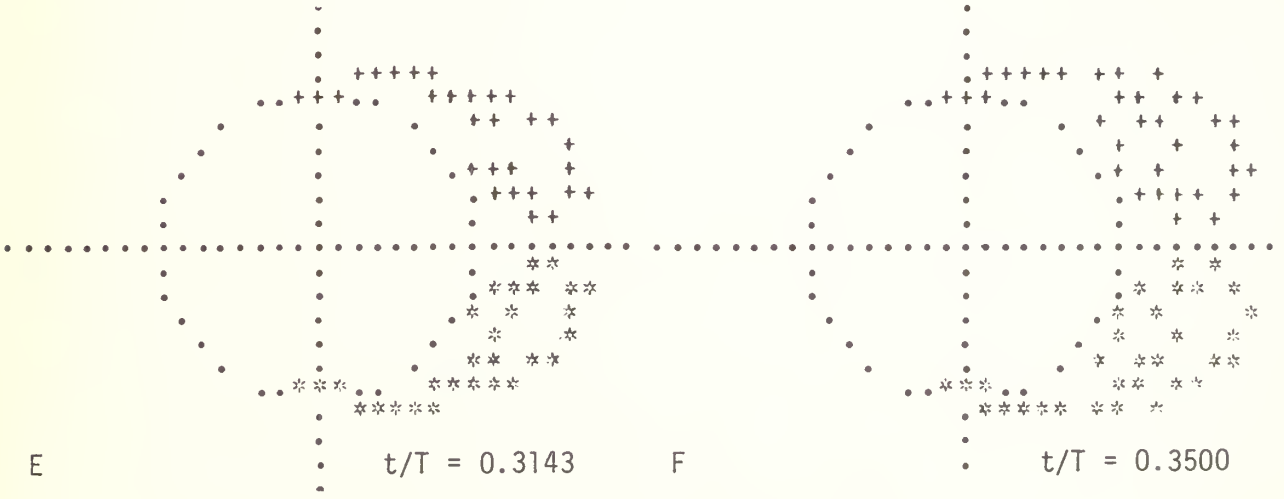

E t/T = 0.3143 F t/T = 0.3500

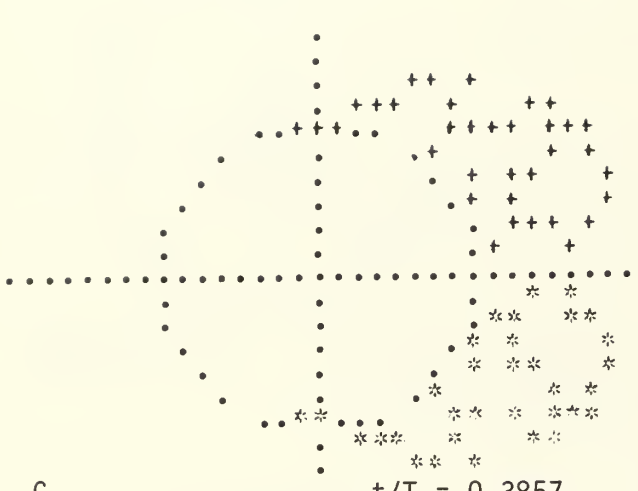

G t/T = 0.3857

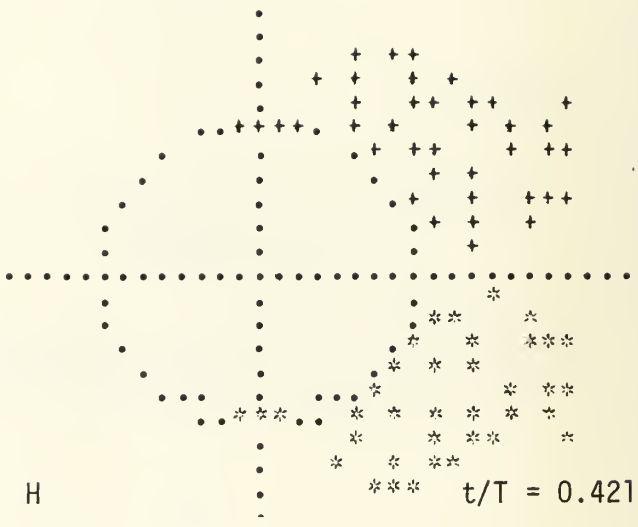

H t/T = 0.421

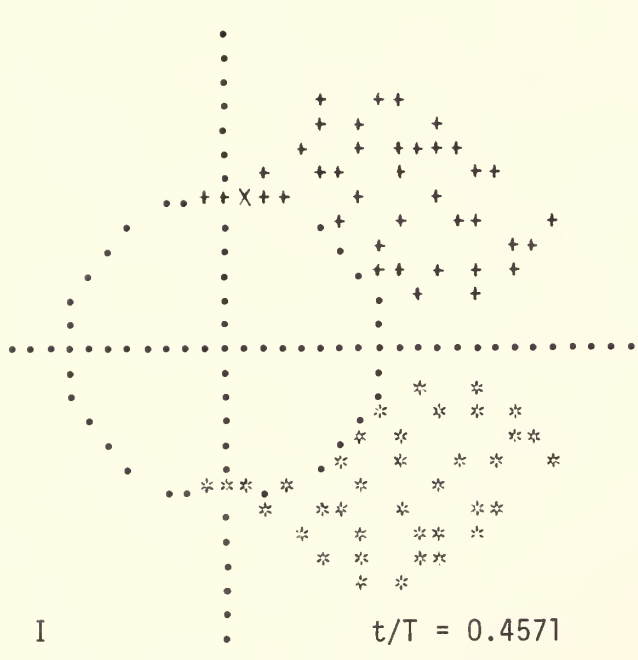

I t/T = 0.4571

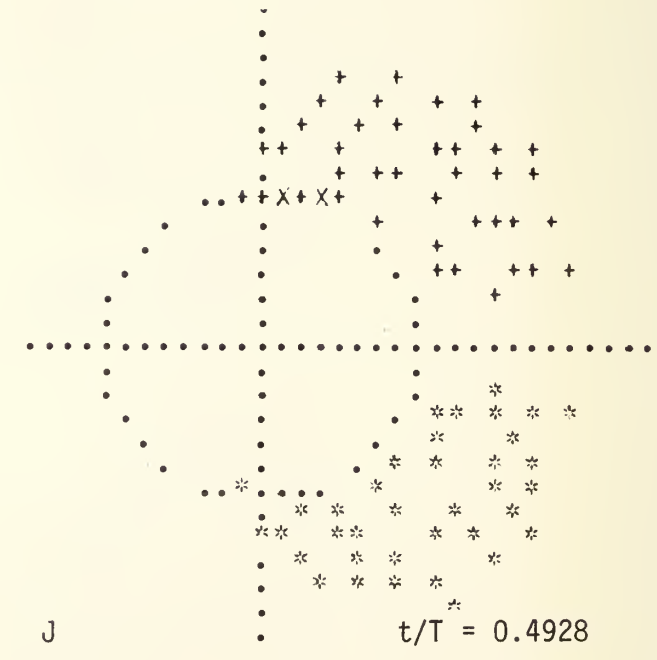

J t/T = 0.4928

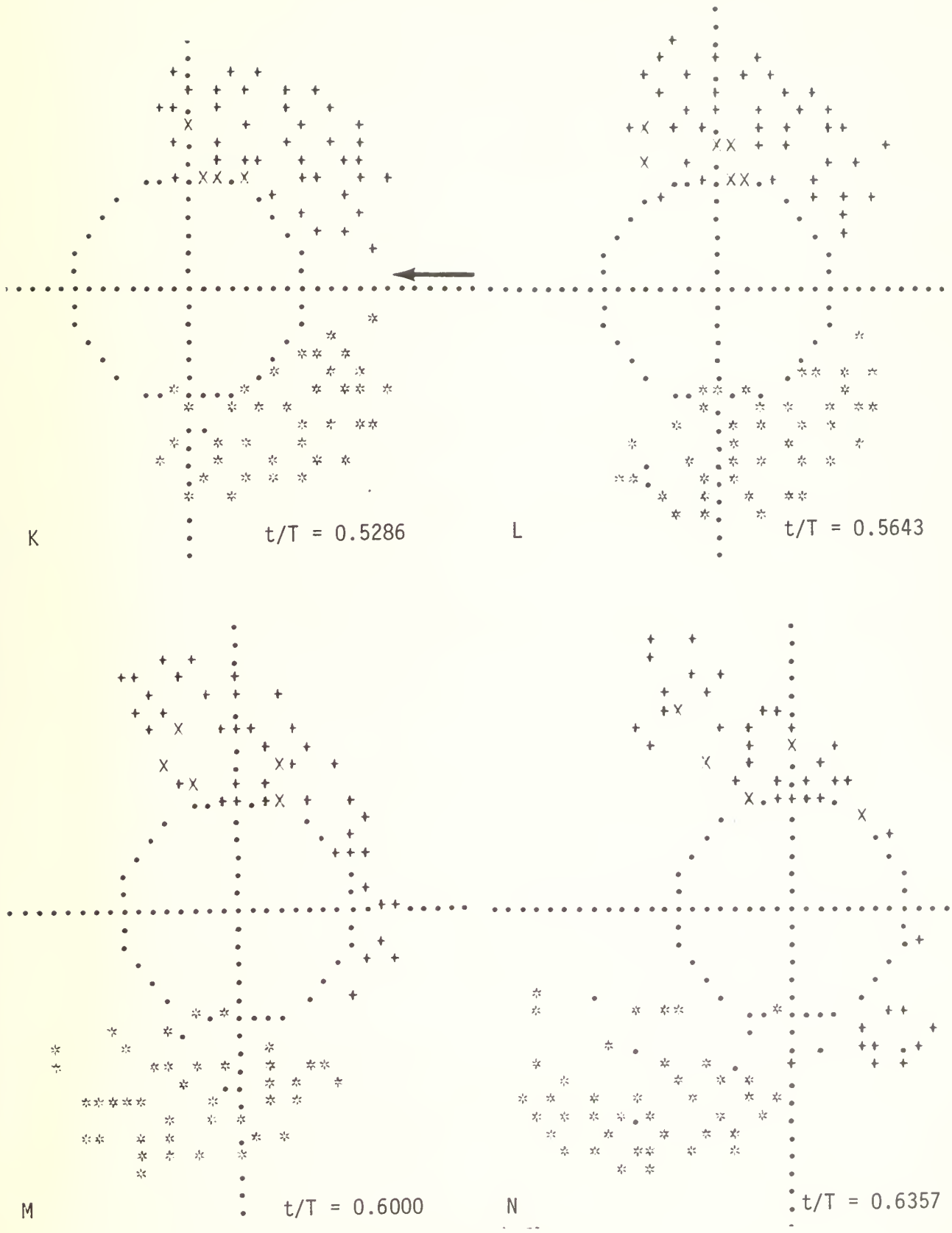
K
t/T = 0.5286
L
t/T = 0.5643
M
t/T = 0.6000
N
t/T = 0.6357

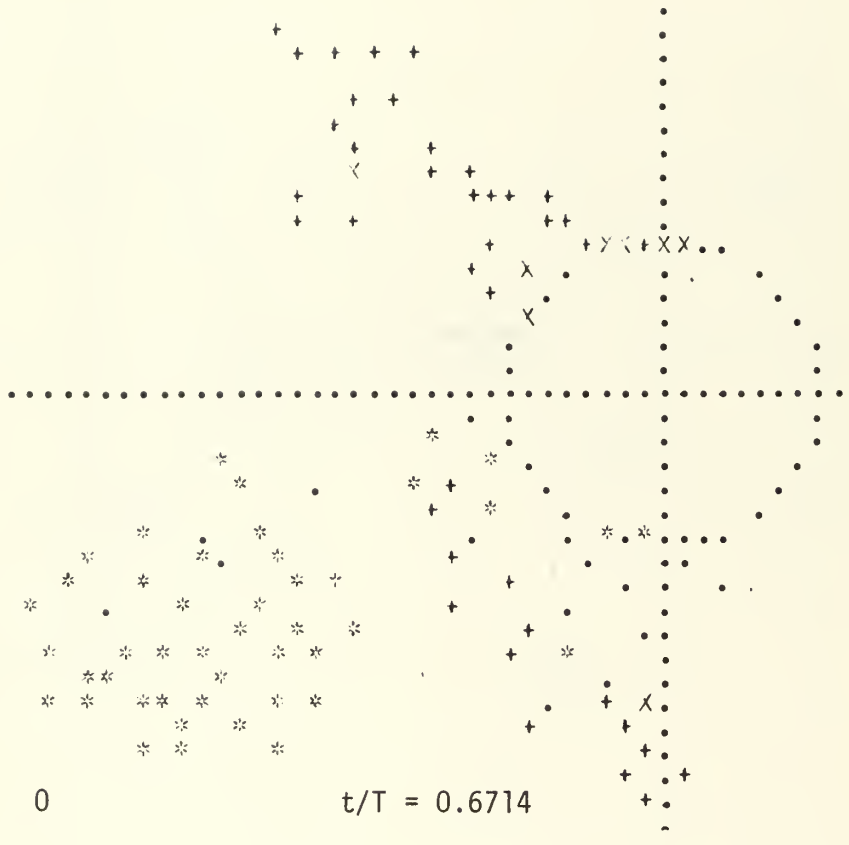
0
t/T = 0.6714

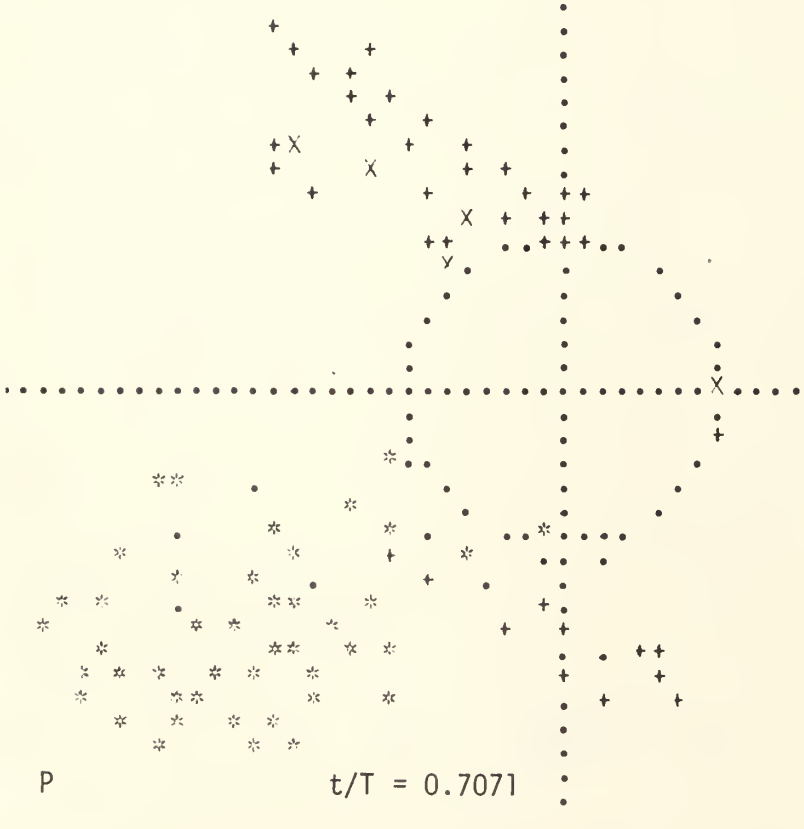
P
t/T = 0.7071

LIST OF REFERENCES

1. Wiegel, R. L., Oceanographical Engineering, Prentice Hall, Inc., Englewood Cliffs, N. J., 1964.

2. Hogben, N., "Fluid Loading on Offshore Structures, A State of Art Appraisal: Wave Loads," Maritime Technology Monograph, No. 1, The Royal Institution of Naval Architects, 1974.

3. Grace, R. A., "Wave Forces on Submerged Objects," Miscellaneous Report No. 10, Univ. of Hawaii Look Lab-M-10, July 1974.

4. Morison, J. R., O'Brien, M. P., Johnson, J. W., and Schaaf, S. A., "The Force Exerted by Surface Waves on Piles," Petroleum Transactions AIME, Vol. 189, 1950.

5. Rott, N., "Theory of Time-Dependent Laminar Flows," in Theory of Laminar Flows, F. K. Moore (Editor), Princeton University Press, Princeton, N. J., 1964, (p. 421).

6. Keulegan, G. H. and Carpenter, L. H., "Forces on Cylinders and Plates in an Oscillating Fluid," Journal of Research of the National Bureau of Standards, Vol. 60, No. 5, May 1958.

7. Sarpkaya, T., "Forces on Cylinders and Spheres in a Sinusoidally Oscillating Fluid," Journal of Applied Mechanics, ASME, Vol. 42 No. 1, March 1975, pp. 32-37.

8. Schlichting, H., Boundary Layer Theory, McGraw-Hill Book Co., New York, 1966.

9. Sarpkaya, T., "Experimental Determination of the Critical Reynolds Number for Pulsating Poiseuille Flow," Journal of Basic Engineering, ASME, Vol. 88, Sept. 1966, pp. 589-598.

10. Thirriot, C., Longree, W. D., and Barthet, H., "Sur la perte de charge due a un obstacle en mouvement periodique," Proceedings of the 14th Congress IAHR, 1971.

11. Isaacson, M. de St. Q., "The Forces on Circular Cylinders in Waves," Ph. D. Dissertation, Univ. of Cambridge, September 1974.

12. Batchelor, G. K., An Introduction to Fluid Dynamics, Cambridge University Press, 1967, (p. 140).

13. Mercier, J. A., "Large Amplitude Oscillations of a Circular Cylinder in a Low-Speed Stream," Ph. D. Dissertation, Stevens Institute of Technology, 1973.

14. Hamman, F. H. and Dalton, C. J., "The Forces on a Cylinder Oscillating Sinusoidally in Water," Trans. ASME, Vol. 93, Series B, No. 4, 1971.

15. Taylor, G. I., "The Instability of Liquid Surfaces when Accelerated in a Direction Perpendicular to Their Planes," Proc. Royal Soc. of London, Ser. A, Pt. I, Vol. 201, 1950, pp. 192-196.

16. Benjamin, T. B. and Ursell, F., "The Stability of the Plane Free Surface of a Liquid in Vertical Periodic Motion," Proc. Royal Soc. of London, Ser. A, Vol. 225, 1954, pp. 505-515.

17. Achenbach, E., "Distribution of Local Pressure and Skin Friction Around a Circular Cylinder in Cross-Flow up to Re = 5 x 10^6," Journal of Fluid Mechanics, Vol. 34, 1968, pp. 625-639.

18. Fage, A. and Falkner, V. M., "Further Experiments on the Flow Around a Circular Cylinder," Aero. Res. Comm., London, Reports and Memoranda No. 1369, 1931.

19. Guven, O., Patel, V. C., and Farell, C., "Surface Roughness Effects on the Mean Flow Past Circular Cylinders," IIHR Report No. 175, Iowa Institute of Hydraulic Research, May 1975.

20. Fage, A. and Warsap, J. H., "The Effects of Turbulence and Surface Roughness on the Drag of a Circular Cylinder," Aero. Res. Comm., London, Reports and Memoranda No. 1283, 1929.

21. Morsbach, M., "Über die Bedingungen für eine Wirbelstrassenbildung hinter Kreiszylindern," Dissertation, T. H. Aachen, 1967.

22. Sarpkaya, T., "Lift, Drag, and Added-Mass Coefficients for a Circular Cylinder Immersed in a Time-Dependent Flow," Journal of Applied Mechanics, Trans, ASME, Vol. 30, Ser. E., No. 1, March 1963, pp. 13-15.

23. Sarpkaya, T., "Separated Flow About Lifting Bodies and Impulsive Flow About Cylinders," AIAA Journal, Vol. 4, No. 3, 1966.

24. Bearman, P. W., "On Vortex Shedding from a Circular Cylinder in the Critical Reynolds Number Regime," Journal of Fluid Mechanics, Vol. 37, Pt. 3, 1969, pp. 577-585.

25. Milne-Thomson, L. M., Theoretical Hydrodynamics, (4th Ed.), The Macmillan Co., New York, 1960, (p. 237).

26. Sarpkaya, T. and Tuter, O., "Periodic Flow About Bluff Bodies, Part-I: Forces on Cylinders and Spheres in a Sinusoidally Oscillating Fluid," Naval Postgraduate School Technical Report NPS-59SL74091, September 1974, Monterey, California.

27. Chang, K. S., "Transverse Forces on Cylinders due to Vortex Shedding in Waves," M.S. Thesis, M.I.T., 1964.

28. Bidde, D. D., "Wave Forces on a Circular Pile due to Eddy Shedding," Ph. D. Thesis, Univ. of California, Berkeley, Calif. Tech. Report No. HEL-9-16, 1970. See also: "Laboratory Study of Lift Forces on Circular Piles," Proc. ASCE, Vol. 97, No. WW4, 1971.

29. Wiegel, R. L. and Delmonte, R. C., "Wave-Induced Eddies and 'Lift' Forces on Circular Cylinders," Univ. of Calif., Berkeley, Tech. Report No. HEL 9-19, 1972.

30. Sarpkaya, T., "Forces on Cylinders Near a Plane Boundary in a Sinusoidally Oscillating Fluid," Fluid Mechanics in the Petroleum Industry, ASME, 1975, pp. 43-47.

31. Sarpkaya, T., "An Inviscid Model of Two-Dimensional Vortex Shedding for Transient and Asymptotically Steady Separated Flow Over an Inclined Plate," Journal of Fluid Mechanics, Vol. 68, Pt. 1, 1975, pp. 109-128.

32. Namork, J. E., "Cylinder Subjected to an Ocean Wave," M.S. Thesis, University of Salford, Mechanical Engineering, June 1975.

33. Rance, P. J., "Wave Forces on Cylindrical Members of Structures," Hydraulic Research Station Ann. Report, 1969.

34. Roshko, A., "Experiments on the Mean Flow Past a Circular Cylinder at Very High Reynolds Number," Journal of Fluid Mechanics, Vol. 10, 1961, pp. 345-356.

35. Szechenyi, E., "Supercritical Reynolds Number Simulation for Two-Dimensional Flow Over Circular Cylinders," Journal of Fluid Mechanics, Vol.70, Pt. 3, 1975, pp. 529-542.

		No. Copies
1.	Defense Documentation Center Cameron Station Alexandria, Virginia 22314	2
2.	National Science Foundation Washington, D. C. 20550 ATTN: Dr. George K. Lea	2
3.	Dean of Research Naval Postgraduate School Monterey, Calif. 93940	1
4.	Chairman, Department of Mechanical Engineering, Code: 59 Naval Postgraduate School Monterey, Calif. 93940	2
5.	Library, Code 0212 Naval Postgraduate School Monterey, Calif. 93940	2
6.	Prof. T. Sarpkaya, Code: 59SL Mechanical Engineering Naval Postgraduate School Monterey, Calif. 93940	20
7.	National Physical Laboratory Division of Maritime Science Teddington, Middlesex England ATTN: Superintendent N. Hogben B. L. P. Miller	3
8.	Prof. Robert A. Grace Department of Ocean Engineering University of Hawaii Honolulu, Hawaii	1
9.	Prof. R. L. Wiegel Hydraulic Engineering Lab. University of California Berkeley, California	1
10.	Prof. Charles Dalton Mechanical Engineering University of Houston Houston, Texas	1

		No. Copies
11.	Dr. Yoshimi Goda Marine Hydrodynamics Division Port and Harbour Institute Ministry of Transport Nagase, Yokosuka, Japan	1
12.	Prof. Yuichi Iwagaki Civil Engineering Kyoto University Kyoto, Japan	1
13.	Prof. John H. Nath Mechanical Engineering/Oceanography Oregon State University Corvallis, Oregon	1
14.	Prof. Yoshito Tsuchiya Disaster Prevention Research Institute Kyoto University Kyoto, Japan	1
15.	Prof. Robert G. Dean Ocean Engineering University of Delaware Newark, Delaware	1
16.	Prof. John S. McNown College of Engineering University of Kansas Lawrence, Kansas	1
17.	Dr. D. J. Maull Engineering Department University of Cambridge Trumpington Street Cambridge, England	1
18.	British Hydromechanics Research Association Cranfield, Bedford England	1
19.	Dr. John A. Mercier CONACO P. O. Box 2197 Houston, Texas 77001	1
20.	Dr. M. M. Zdravkovich Mechanical Engineering University of Salford Salford M5 4WT, England	1

		No. Copies
21.	National Science Foundation Engineering Division Library 1800 G Street, N.W. Washington, D.C. 20550	20
22.	Commanding Officer (L31) Naval Civil Engineering Lab. Port Hueneme, California 93043	1
23.	Commander Naval Undersea Research and Development Center San Diego, California 92132 ATTN: Dr. A. Fabula	1
24.	Officer-in-Charge Naval Undersea Research and Development Center Pasadena, California 91107 ATTN: Library (13111)	1
25.	Research Center Library Waterways Experiment Station Corp. of Engineers P.O. Box 631 Vicksburg, Mississippi 39180	1
26.	National Bureau of Standards Washington, D.C. ATTN: G. Kulin Fluid Mechanics Hydraulic Section	1
27.	Assistant Chief Design Eng. for Naval Architecture Code 250 Mare Island Naval Shipyard Vallejo, California 94592	1
28.	U. S. Merchant Marine Academy Kings Point, L.I., New York 11204 ATTN: Academy Library	1
29.	Hydronautics, Inc. Pindell School Road Howard County Laurel, Maryland 20810 ATTN: Library	1
30.	Oceanics, Inc. Technical Industrial Park Plainview, L.I., New York 11803	1

		No. Copies
31.	Commander Naval Ship Research and Development Center Bethesda, Maryland 20034 ATTN: Code 1505	1
32.	Officer-in-Charge Annapolis Laboratory Naval Ship Research and Development Center Annapolis, Maryland 21402 ATTN: Code 5642 (Library)	1
33.	Commander Naval Sea Systems Command Washington, D.C. 20362 ATTN: SEA 033	1
34.	Director Defense Documentation Center 5010 Duke Street Alexandria, Virginia 22314	1
35.	Office of Naval Research 800 North Quincy Street Arlington, Virginia 22217 ATTN: Mr. R. D. Cooper Code 438	1
36.	Chief Scientist Office of Naval Research Branch Office 1030 E. Green Street Pasadena, California 91106	1
37.	Office of Naval Research San Francisco Area Office Room 447 760 Market Street San Francisco, California 94102	1
38.	Director Naval Research Laboratory Washington, D.C. 20390 ATTN: Code 2027	1
39.	Commander Naval Facilities Engineering Command (Code 032C) Washington, D.C. 20390	1
40.	Library of Congress Science & Technology Division Washington, D.C. 20540	1

		No. Copies
41.	Society of Naval Architects and Marine Engineers 74 Trinity Place New York, New York 10006 ATTN: Technical Library	1
42.	Stevens Institute of Technology Davidson Laboratory 711 Hudson Street Hoboken, New Jersey 07030 ATTN: Prof. J. Breslin, Director	1
43.	Stanford University Department of Civil Engineering Stanford, California 94305 ATTN: Prof. R. L. Street	1
44.	Southwest Research Institute P.O. Drawer 28510 San Antonio, Texas 78284 ATTN: Applied Mech. Review Dr. H. Abramson	1
45.	Ocean Engineering Department Woods Hole Oceanographic Institute Woods Hole, Massachusetts 02543	1
46.	University of California College of Engineering Berkeley, California 94720 ATTN: Library Prof. J. Wehausen	1
47.	Harvard University Pierce Hall Cambridge, Massachusetts 02138 ATTN: Gordon McKay Library	1
48.	University of Hawaii Department of Ocean Engineering 2565 The Mall Honolulu, Hawaii 96822 ATTN: Dr. C. Bretschneider	1
49.	University of Illinois Urbana, Illinois 61801 ATTN: Dr. J. Robertson	1
50.	Department of Ocean Engineering Massachusetts Institute of Technology Cambridge, Massachusetts 02139 ATTN: Department Library	1

No. Copies

51. Webb Institute of Naval Architecture
Crescent Beach Road
Glenn Cover, L.I., New York 11542
ATTN: Library 1

52. St. Anthony Falls Hydraulic Lab
University of Minnesota
Mississippi River at 3rd Avenue, S.E.
Minneapolis, Minnesota 55414
ATTN: Library 1

53. Department of Naval Architecture and Marine Engineering
Ann Arbor, Michigan 48104
ATTN: Library 1

54. Davidson Laboratory
Stevens Institute of Technology
711 Hudson Street
Hoboken, New Jersey 07030
ATTN: Library 1

55. Department of Ocean Engineering
Massachusetts Institute of Technology
Cambridge, Massachusetts 02139
ATTN: Prof. J. N. Newman 1

56. Hydronautics, Inc.
Laurel, Maryland 20810
ATTN: Dr. M. P. Tulin 1

57. Library (Code 1640)
Naval Oceanographic Office
Washington, D.C. 20390 1

U175162

DUDLEY KNOX LIBRARY - RESEARCH REPORTS
5 6853 01071043 7